ON TISSUE ENGINEERING AND REGENERATIVE MEDICINE OF SKIN AND ITS APPENDAGES

EDITED BY: Marianna Bei and Basak E. Uygun
PUBLISHED IN: Frontiers in Physiology

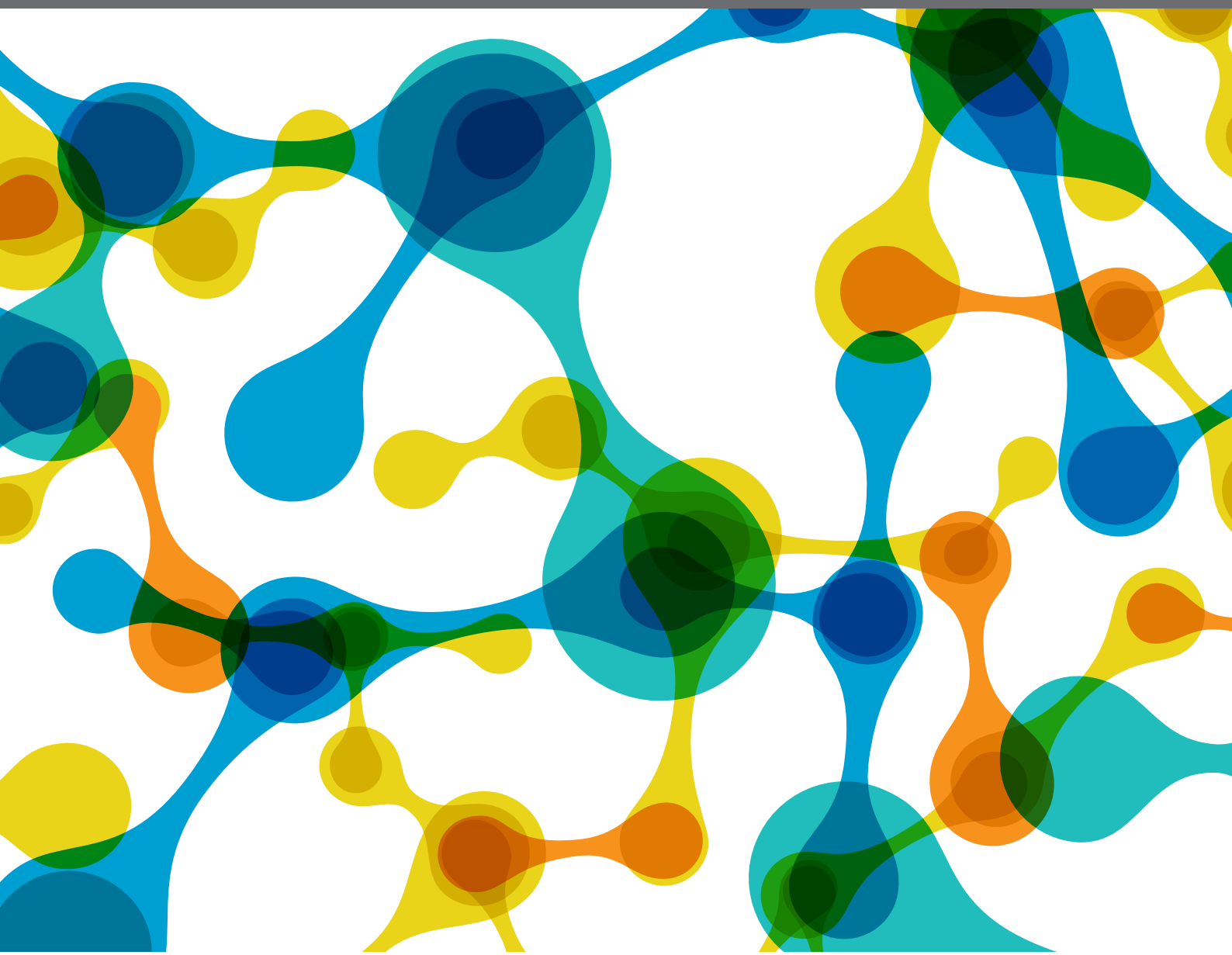

frontiers Research Topics

ISSN 1664-8714
ISBN 978-2-88963-107-0
DOI 10.3389/978-2-88963-107-0

About Frontiers

Frontiers is more than just an open-access publisher of scholarly articles: it is a pioneering approach to the world of academia, radically improving the way scholarly research is managed. The grand vision of Frontiers is a world where all people have an equal opportunity to seek, share and generate knowledge. Frontiers provides immediate and permanent online open access to all its publications, but this alone is not enough to realize our grand goals.

Frontiers Journal Series

The Frontiers Journal Series is a multi-tier and interdisciplinary set of open-access, online journals, promising a paradigm shift from the current review, selection and dissemination processes in academic publishing. All Frontiers journals are driven by researchers for researchers; therefore, they constitute a service to the scholarly community. At the same time, the Frontiers Journal Series operates on a revolutionary invention, the tiered publishing system, initially addressing specific communities of scholars, and gradually climbing up to broader public understanding, thus serving the interests of the lay society, too.

Dedication to Quality

Each Frontiers article is a landmark of the highest quality, thanks to genuinely collaborative interactions between authors and review editors, who include some of the world's best academicians. Research must be certified by peers before entering a stream of knowledge that may eventually reach the public - and shape society; therefore, Frontiers only applies the most rigorous and unbiased reviews.
Frontiers revolutionizes research publishing by freely delivering the most outstanding research, evaluated with no bias from both the academic and social point of view. By applying the most advanced information technologies, Frontiers is catapulting scholarly publishing into a new generation.

What are Frontiers Research Topics?

Frontiers Research Topics are very popular trademarks of the Frontiers Journals Series: they are collections of at least ten articles, all centered on a particular subject. With their unique mix of varied contributions from Original Research to Review Articles, Frontiers Research Topics unify the most influential researchers, the latest key findings and historical advances in a hot research area! Find out more on how to host your own Frontiers Research Topic or contribute to one as an author by contacting the Frontiers Editorial Office: researchtopics@frontiersin.org

ON TISSUE ENGINEERING AND REGENERATIVE MEDICINE OF SKIN AND ITS APPENDAGES

Topic Editors:
Marianna Bei, Massachusetts General Hospital and Harvard Medical School, United States
Basak E. Uygun, Massachusetts General Hospital and Harvard Medical School, United States

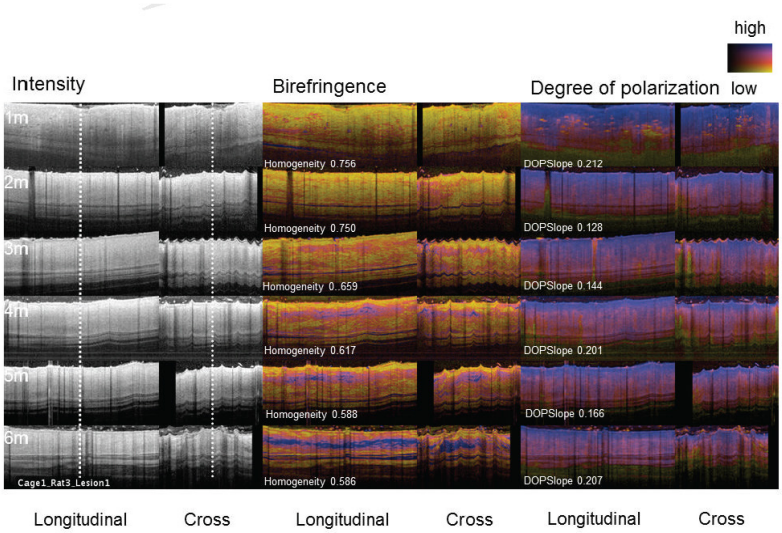

Prediction of scar size after burns based on early post injury polarization-sensitive optical frequency domain imaging.
Image: Alex Golberg.

Skin is the largest organ of the body and is necessary for survival, since it performs many functions such as providing a physical barrier to the external environment, sensation, retention of normal hydration and thermal regulation. Significant skin loss is associated with high mortality and morbidity in the acute phase, and with physically and cosmetically drastic scarring in the long term. Although there are a number of tissue-engineered products in the clinic that are used as skin substitutes to promote healing of traumatic burn and diabetic wounds, yet they lack several important functions including those provided by the appendages such as the hair follicles, sebaceous and sweat glands. The understanding of cellular, molecular and engineering aspects of the pathology, repair and/or regeneration of skin after wound induction is of paramount importance in order to develop the next generation of tissue engineered products with gene-enhanced capacity.

In that context, we brought together scientists from basic research, translational and bioengineering fields, whose work focus on cutting-edge research associated with the acquisition of new therapeutic approaches towards skin regeneration.

Citation: Bei, M., Uygun, B. E., eds. (2019). On Tissue Engineering and Regenerative Medicine of Skin and Its Appendages. Lausanne: Frontiers Media.
doi: 10.3389/978-2-88963-107-0

Table of Contents

ARTICLES

REVIEWS

frontiers in Physiology

EDITORIAL
published: 11 June 2019
doi: 10.3389/fphys.2019.00712

Editorial: On Tissue Engineering and Regenerative Medicine of Skin and Its Appendages

Marianna Bei[1,2,3]* *and Basak E. Uygun*[1,2,3]

[1] Department of Surgery, Harvard Medical School, Boston, MA, United States, [2] Center for Engineering in Medicine, Massachusetts General Hospital, Boston, MA, United States, [3] Research Department, Shriners Hospitals for Children, Boston, MA, United States

Keywords: skin, stem cells, wound healing, skin substitutes, inflammation, biomateials

Editorial on the Research Topic

On Tissue Engineering and Regenerative Medicine of Skin and Its Appendages

This Frontiers research topic, on tissue engineering and regenerative medicine of skin and its appendages, covers mainly cellular, molecular, and engineering aspects of the pathology, repair, and/or regeneration of skin after wound induction. Chronic or non-healing wounds represent a growing health problem worldwide. The underlying pathogenesis of chronic wounds is further complicated by factors such as advanced age, poor nutrition, and immunosuppression which put additional cellular and systemic stress and thus, delaying wound healing. The current treatments do not allow the skin tissue to fully regenerate and the recurrence rate of chronic wounds is extremely high. Thus, there is a significant need for improved understanding of the biology occurring during wound healing process and identify targeted therapies that can yield satisfactory clinical outcomes.

The topic presents 7 manuscripts and 2 reviews from different countries that together convey important aspects of skin wound healing research. As it is impossible, in this short editorial, to highlight all aspects of each of the papers and reviews submitted to this topic, we have chosen to present an overview of the main findings for each paper and an overall perspective of the two state of the art reviews included in this digital collection. Specifically:

The study on the reparative abilities of menstrual stem cells (MenSCs) to modulate the wound matrix signals and improve cutaneous regeneration by Cuenca et al. compares the biological functions and the transcriptomic pattern of MenSCs with umbilical cord MSCs. Their findings provide evidence, for the first time, about the superior clonogenicity, immunosuppressive, migration, and enhanced wound healing potential of MenSCs compared to that of MSCs. A valuable source of MSCs is the gelatinous material of the umbilical cord called Wharton's jelly. WJ-derived MSCs have been the subject of extensive research, while very little is known about the de-cellularized jelly material of the umbilical cord, a native niche of stem cells. Bakhtyar et al. explore the role of acellular Wharton's jelly. They isolate Wharton's jelly from umbilical cords and then fractionate acellular gelatinous Wharton's jelly (AGWJ) providing evidence on the role of AGWJ in enhancing wound healing *in vitro* and *in vivo*. The research paper by Wang et al. on the other hand, highlights the role of a specific neuronal protein, that of P311, in promoting cutaneous wound healing and regeneration. P311 is expressed by the endothelial cells in the dermis of murine and human skin wounds and, when its function is eliminated either *in vitro* or *in vivo*, wound healing is delayed due to reduction of angiogenic factors such as VEGF and TGFβ1. These findings suggest that P311 may play a significant role in angiogenesis during wound healing.

Edited by:
Johannes Van Lieshout, University of Amsterdam, Netherlands

Reviewed by:
Nicola Smart, University of Oxford, United Kingdom

****Correspondence:***
Marianna Bei
mbei@mgh.harvard.edu

Specialty section:
This article was submitted to Clinical and Translational Physiology, a section of the journal Frontiers in Physiology

Received: *07 January 2019*
Accepted: *21 May 2019*
Published: *11 June 2019*

Citation:
Bei M and Uygun BE (2019) Editorial: On Tissue Engineering and Regenerative Medicine of Skin and Its Appendages. Front. Physiol. 10:712. doi: 10.3389/fphys.2019.00712

The study by Kravez et al. opens new possibilities for quantitative and more objective assessment of scar severity. So far, scar size prediction is based on imaging modalities that lack the ability to image individual layers of the scar. The authors develop a predictive model of scar formation based on polarization sensitive optical frequency domain imaging (PS-OFDI), which offers comprehensive subsurface imaging and predicts the size of a scar 6 months after third-degree burn injuries in rats. The importance of accurately predicting scar size comes as an imperative necessity in case of keloid formation after wound induction, a fibrotic skin condition that typically results from abnormal wound healing, and is characterized by the deposition of an excess of extracellular matrix (ECM). The study by Jiao et al. provides a thorough investigation of the histology and biology of keloid lesion at different depths, focusing on the cellular composition, collagen composition and the biological behavior of the fibroblasts at the different levels within the keloid dermis. A key finding of this study is the identification of the superficial dermis layer as the initiator of keloid formation, providing thus a cue in which layer intra-lesional injection of pharmaceuticals and of other treatments should be performed for keloid.

The role of engineering approaches to improve skin wound healing using synthetic, biopolymeric scaffolds loaded with different therapeutic and antimicrobial agents, is very popular. In this topic, Wang et al. introduce the formation of composite nanofibrous membranes using chitosan (CS) and poly (vinyl alcohol) (PVA) loaded with antibiotics at different ratios fabricated by electrospinning. The authors show that there is a specific volumetric ratio of CS/PVA to achieve an optimal nanofibrous structure and that the CS/PVA electrospun scaffold has great potential to be used for infection related wound dressing and thus for skin tissue regeneration. On the other hand, the paper by Chung et al. introduces selenium nanoparticles as novel antibiotic chemical composites to which there is no known bacterial resistance. Using this unique property, they dope selenium nanoparticles to electrospun silk scaffolds to impart antibacterial properties to silk and show for the first time that these scaffolds reduce bacterial growth *in vitro*.

The research findings presented in this topic have as major goal to stimulate our thinking and open new avenues of research. Both, clinicians and researchers will find up-to-date discoveries and perspectives on the etiology, translational, and therapeutic approaches for skin wound healing. The current status of research however is elegantly summarized in the two state of the art reviews that report ongoing efforts to improve the outcomes of chronic wound healing therapies. The review by Krzyszczyk et al. explains different macrophage phenotypes *in vivo* and *in vitro* as described in the literature and discusses the attempts to restore the macrophage function by therapeutic approaches. It summarizes experimental therapies that aim to attenuate endogenous M1 macrophages, supplement exogenous M2 macrophages, or use cells and growth factors that modulate the macrophage transition from M1 to M2 phenotype. The authors emphasize the need to standardize the macrophage phenotype nomenclature and definition to provide consistency in the field and improve the understanding of their roles to promote chronic wound healing. The second review is by Dickinson and Gerecht who provide a comprehensive overview of skin substitutes that are in clinical use. A challenge in using engineered skin substitutes for treatment of chronic wounds is that there is no consensus of one significantly outperforming the others. Recent research efforts aim to develop innovative materials that have the ability modulate the endogenous cellular processes to promote wound healing. The review summarizes these efforts focusing on synthetic and polymeric materials as scaffolds that have the advantage of tunable mechanical and biological characteristics for enhanced wound healing.

Space precludes a more detailed description of the articles and reviews published in this topic but readers are urged to visit the on line content list to quickly access the full papers. We would like to thank the team at Frontiers for allowing open access to the papers as soon as they are accepted for publication following full peer review. We also thank the contributors whose dedication to their science brought this research topic to fruition. We hope that the research presented here continues to develop and advances our understanding of skin regeneration and wound healing research.

AUTHOR CONTRIBUTIONS

All authors listed have made a substantial, direct and intellectual contribution to the work, and approved it for publication.

FUNDING

This work was supported by the NIH 3R01DE027255-01S1; NIH 1R21DE028091-01 to MB; Shriners Hospitals for Research Grant #85105 to BU.

Conflict of Interest Statement: The authors declare that the research was conducted in the absence of any commercial or financial relationships that could be construed as a potential conflict of interest.

frontiers in Physiology

ORIGINAL RESEARCH
published: 14 May 2018
doi: 10.3389/fphys.2018.00464

The Reparative Abilities of Menstrual Stem Cells Modulate the Wound Matrix Signals and Improve Cutaneous Regeneration

Jimena Cuenca[1,2,3], Alice Le-Gatt[1], Valentina Castillo[1], Jose Belletti[4], Macarena Díaz[1], Mónica Kurte G[5], Paz L. Gonzalez[2], Francisca Alcayaga-Miranda[2,3], Christina M. A. P. Schuh[2], Fernando Ezquer[6], Marcelo Ezquer[6] and Maroun Khoury[1,2,3]**

[1] Consorcio Regenero, Chilean Consortium for Regenerative Medicine, Santiago, Chile, [2] Laboratory of Nano-Regenerative Medicine, Faculty of Medicine, Universidad de los Andes, Santiago, Chile, [3] Cells for Cells, Santiago, Chile, [4] Laboratory of Pathological Anatomy, Hospital DIPRECA, Las Condes, Chile, [5] Laboratory of Immunology, Faculty of Medicine, Universidad de los Andes, Santiago, Chile, [6] Centro de Medicina Regenerativa, Facultad de Medicina Clínica Alemana-Universidad del Desarrollo, Santiago, Chile

OPEN ACCESS

Edited by:
Marianna Bei,
Harvard Medical School,
United States

Reviewed by:
Riikka Kivelä,
University of Helsinki, Finland
Yvonne Alexander,
Manchester Metropolitan University,
United Kingdom

***Correspondence:**
Jimena Cuenca
jcuenca@uandes.cl
Maroun Khoury
mkhoury@uandes.cl

Specialty section:
This article was submitted to Clinical and Translational Physiology, a section of the journal Frontiers in Physiology

Received: 15 January 2018
Accepted: 13 April 2018
Published: 14 May 2018

Citation:
Cuenca J, Le-Gatt A, Castillo V, Belletti J, Díaz M, Kurte G M, Gonzalez PL, Alcayaga-Miranda F, Schuh CMAP, Ezquer F, Ezquer M and Khoury M (2018) The Reparative Abilities of Menstrual Stem Cells Modulate the Wound Matrix Signals and Improve Cutaneous Regeneration. Front. Physiol. 9:464. doi: 10.3389/fphys.2018.00464

Considerable advances have been made toward understanding the cellular and molecular mechanism of wound healing, however, treatments for chronic wounds remain elusive. Emerging concepts utilizing mesenchymal stem cells (MSCs) from umbilical cord, adipose tissue and bone marrow have shown therapeutical advantages for wound healing. Based on this positive outcome, efforts to determine the optimal sources for MSCs are required in order to improve their migratory, angiogenic, immunomodulatory, and reparative abilities. An alternative source suitable for repetitive, non-invasive collection of MSCs is from the menstrual fluid (MenSCs), displaying a major practical advantage over other sources. This study aims to compare the biological functions and the transcriptomic pattern of MenSCs with umbilical cord MSCs in conditions resembling the wound microenvironment. Consequently, we correlate the specific gene expression signature from MenSCs with changes of the wound matrix signals *in vivo*. The direct comparison revealed a superior clonogenic and migratory potential of MenSCs as well as a beneficial effect of their secretome on human dermal fibroblast migration *in vitro*. Furthermore, MenSCs showed increased immunomodulatory properties, inhibiting T-cell proliferation in co-culture. We further, investigated the expression of selected genes involved in wound repair (growth factors, cytokines, chemokines, AMPs, MMPs) and found considerably higher expression levels in MenSCs (ANGPT1 1.5-fold; PDGFA 1.8-fold; PDGFB 791-fold; MMP3 21.6-fold; ELN 13.4-fold; and MMP10 9.2-fold). This difference became more pronounced under a pro-inflammatory stimulation, resembling wound bed conditions. Locally applied in a murine excisional wound splinting model, MenSCs showed a significantly improved wound closure after 14 days, as well as enhanced neovascularization, compared to the untreated group. Interestingly, analysis of excised wound tissue revealed a significantly higher expression of VEGF (1.42-fold) among other factors, translating an important conversion of the matrix signals in the wound site. Furthermore, histological analysis of the wound tissue from MenSCs-treated group displayed a more mature

robust vascular network and a genuinely higher collagen content confirming the pro-angiogenic and reparative effect of MenSCs treatment. In conclusion, the superior clonogenicity, immunosuppressive and migration potential in combination with specific paracrine signature of MenSCs, resulted in an enhanced wound healing and cutaneous regeneration process.

Keywords: menstrual stem cells, mesenchymal stem cells, wound healing, angiogenesis, regeneration, cell therapy

INTRODUCTION

Although considerable advances have been made concerning understanding the process of wound healing, as well as cellular and molecular responses involved, treatment of chronic wounds remains elusive. Especially, patients with comorbidities such as diabetes are prone to face complications within the triad of ischemia, neuropathy, and infection (Eldor et al., 2004). This results in frequent and prolonged hospitalization and displays a major burden to patients and the social health-care systems. Traditional approaches to initiate regeneration include sterile wound dressings, repeated debridement of necrotic material and administration of antibiotics to decrease the bacterial load (Werdin et al., 2008). Among the various factors contributing to non-healing wounds play a key factor the reduced angiogenesis and the dysregulation in the production of cytokines by local immune cells and fibroblast (Otero-Viñas and Falanga, 2016).

Over the last decades, novel approaches using therapeutic cells have become increasingly popular and proven to be promising in tissue regeneration. In particular, mesenchymal stem cells (MSCs) have been shown to express a number of beneficial characteristics for wound healing. MSCs are tissue resident progenitor cells with self-renewable, immune-modulatory, anti-inflammatory characteristics as well as the capability of differentiating into a number of cell types. Sources for MSCs are abundant in the human bodies, as they can be found in virtually every tissue (bone marrow, adipose tissue, dental pulp, umbilical cord, amniotic membrane. . .). However, increasing evidence suggests that MSCs are prone to explant site-dependent differences, ranging from secretion of growth factors, differentiation potential, immunosuppressive properties, migration or expression of specific cell surface markers (Hass et al., 2011; Nombela-Arrieta et al., 2011; Al-Nbaheen et al., 2013; Wegmeyer et al., 2013). Depending on the intended application, these differences can be utilized to maximize the effect of transplanted cells.

The gold standard in clinical trials so far have been bone marrow derived MSCs (BM-MSCs), but also adipose derived MSCs (ADSCs), as well as umbilical cord derived MSCs (UC-MSCs) (Squillaro et al., 2016; Wang et al., 2016). All of these sources, however, show distinct disadvantages as they are obtained by either painful and invasive procedures or single donations.

Based on the positive outcome of the use of MSCs in wound healing, efforts to determine the optimal sources for MSCs are still needed to improve their migratory, angiogenic, immunomodulatory, and reparative abilities. An alternative source for repetitive, non-invasive collection and without ethical concerns are menstrual blood-derived mesenchymal stem cells (MenSCs) (Meng et al., 2007). These characteristics are potentially what makes MenSCs an attractive MSCs source for cell therapy. Aside from the classic MSCs traits, MenSCs compared with BM-MSCs exhibit characteristics such as increased migration and angiogenesis making them favorable for application in wound healing (Alcayaga-Miranda et al., 2015a). Our group and others have described the therapeutic potential of allogenic MenSCs derived from healthy donors in different preclinical studies such as sepsis (Alcayaga-Miranda et al., 2015b), Graft-Vs.-Host-Disease (Luz-Crawford et al., 2016b), acute lung injury (Xiang et al., 2017), ischemic stroke (Rodrigues et al., 2012), Duchenne muscular dystrophy (Cui et al., 2007) or liver fibrosis (Chen et al., 2017), supporting the promising use for clinical applications. While the capacity of MenSCs to differentiate *in vitro* to epidermal lineage and keratinocytes has been described (Faramarzi et al., 2016; Akhavan-Tavakoli et al., 2017), their contribution *in vivo* to wound healing treatment remains unclear. Besides, UC-MSCs have been shown to exhibit enhanced therapeutic abilities in terms of angiogenesis and cell migration when compared to BM-MSCs, suggesting that UC-MSCs might be a better source of MSCs for tissue repair (Hsieh et al., 2013). Therefore, this study aims to compare first the biological functions and the specific transcriptomic pattern of different secreted factors from MenSCs with UC-MSCs, in conditions resembling the wound microenvironment. Consequently, we correlate the specific gene expression signature from MenSCs with the changes occurred in the wound healing milieu *in vivo*.

MATERIALS AND METHODS

Ethics Statement

This work was revised and approved by the Ethics Committee of the Universidad de los Andes. Menstrual fluids and umbilical cord were collected from healthy donors after written informed consent following institutional guidelines (Alcayaga-Miranda et al., 2015a; González et al., 2015). All animal studies were performed at the Cells for Cells Animal Facility in accordance with protocols revised and approved by the Institutional Animal Care and Use Committee of Universidad de los Andes.

Cell Culture

Umbilical cord derived MSCs and MenSCs were isolated, characterized, cultured and expanded as previously described

(Alcayaga-Miranda et al., 2015a; González et al., 2015). Briefly, menstrual blood samples from healthy donors were collected using a silicone menstrual cup (Mialuna®, Santiago, Chile). Menstrual blood mononuclear cells were separated by Ficoll-Paque Plus (GE Healthcare, Amersham, United Kingdom) (1.077 g/ml) density gradient according to the manufacturer's instructions. Cells were collected and cultured in a T25 flask (Falcon®, Becton Dickinson, United States) containing Dulbecco's modified Eagle's medium (DMEM) high glucose supplemented with 1% penicillin/streptomycin solution (10,000 U/ml / 10,000 μg/ml), 1% amphotericin B (250 μg/ml), 1% L-glutamine (200 mM) (all from Gibco, Paisley, United Kingdom) and 15% fetal bovine serum (FBS) (Lonza, Walkersville, MD, United States) at 37°C, 5% CO_2 to obtain adherent cells. All MSCs were evaluated in their capacity to differentiate into adipocytes, osteocytes, and chondrocytes by using the StemPro Differentiation Kits (Gibco) in accordance with manufacturer's instructions. Normal human dermal fibroblast- adult (NHDF-Ad CC-2511) were purchased from Lonza and cultured according manufacture's protocols.

Immunophenotyping of MSCs was performed by flow cytometry using a FACSCanto II cytometer (BD Biosciences, San Jose, CA, United States) after staining with monoclonal antibodies CD105, CD90, CD73, CD44, HLA-DR, CD34, HLA-ABC, CD19, CD14, and CD45 (all from BD Pharmingen) using standard protocol. The data acquired was analyzed using the FlowJo software V10 (Tree Star, Ashland, OR, United States).

MSCs Stimulation With Pro-inflammatory Cytokines or Deferoxamine (DFX)

Mesenchymal stem cells at 70% confluency was incubated with IL1β and TNFα (10 ng/ml each) (Peprotech, Rocky Hill, NJ, United States) or 150 μM DFX (Sigma-Aldrich, St. Louis, MO, United States) for 24 h in serum-free DMEM supplemented with 1% penicillin/streptomycin and 1% L-glutamine (all from Gibco) at 37°C with 5% CO_2. Viability of MSCs was determined by trypan blue solution dye (Gibco) under a phase contrast microscope.

Conditioned Medium

Mesenchymal stem cells were cultured in the absence (control group) or presence of 10 ng/ml IL1β and 10 ng/ml TNFα (Peprotech) in serum-free DMEM supplemented with 1% penicillin-streptomycin and 1% L-glutamine (all from Gibco). After 48 h, the supernatant was collected and the cellular debris were removed by centrifugation at 500 × *g* for 5 min at room temperature. For negative controls, equal volumes of serum- free DMEM were used. The conditioned medium (CM) was stored at −80°C until use.

Quantification of Secreted Factors by ELISA

Levels of VEGF, bFGF, IL8, PDGFBB, TGFb1, HGF, and IL6 in MSCs-CM, were detected using duo set ELISA (R&D Systems, Minneapolis, MN, United States) according to the manufacturer's protocol. Hypoxia inducible factor 1 alpha (HIF-1α) abundance was evaluated in cell lysates using the human HIF-1α ELISA kit (Abcam, Cambridge, United Kingdom) as previously described (Oses et al., 2017).

Proliferation

Quick Cell Proliferation Assay Kit (BioVision, Milpitas, CA, United States) was used to assess proliferation of MSCs and NHDF-Ad, following manufacturer's instructions. Briefly, MSCs or NHDF-Ad were cultured (1×10^3/well) in a 96-well plate (Falcon) in a final volume of 200 μl/well of DMEM supplemented with 10% FBS or with CM, respectively. Cell proliferation was quantified by measuring the absorbance (Tecan Reader) of the dye solution at 450 nm at different time points.

Colony Forming Units

Mesenchymal stem cells were evaluated for frequency of fibroblast colony-forming units (CFU-F) as previously described (Alcayaga-Miranda et al., 2015a; González et al., 2015). CFU-F were evaluated in a serial dilution assay: 25 to 250 cells per well were seeded in a six-well plate (Falcon®) and cultivated for 14 days. Cells were fixed in 70% methanol and stained with 0.5% crystal violet (Sigma-Aldrich) in 10% methanol for 20 min. After several washes, colonies formed by more than 50 fibroblast-like cells were counted under a light microscope at low magnification. Results were expressed as CFU/initial number of cells plated.

T Cell Proliferation Assay

Immunosuppressive capacity of MenSCs in comparison to UC-MSCs was assessed in a T-cell proliferation assay. MSCs, pre-stimulated with 10 ng/ml IL1β and TNFα (Peprotech) (control: no stimulation) were seeded in defined cell numbers in 48 well plates (Falcon) and left to adhere. Peripheral blood mononuclear cells (PBMCs) were isolated from heparinized human peripheral blood samples (healthy donors) using density gradient centrifugation. PBMCs were stained with Cell Trace™ Violet (CTV) (Molecular Probes, Springfield, MA, United States) following manufacturer's instructions and co-cultured with MSCs (MSC:T-cell ratios 1:5 and 1:10) in RPMI 1640 medium supplemented with 10% FBS, 1% L-glutamine, 1% penicillin/streptomycin (all from Gibco). Proliferation of T-cells was stimulated with phytohemagglutinin (PHA; 15 μg/ml, Sigma-Aldrich). After 72 h, cells were harvested and stained for CD3 and CD4 (BD Biosciences). Samples were analyzed by flow cytometry, and the percentage of CD3+CD4+ proliferative T-cells was determined using FlowJo software V10 (Tree Star, Ashland, OR, United States). PBMCs cultured in medium containing PHA without MSCs and PBMCs cultured in absence of PHA and in presence of MSCs served as controls.

Real-Time Quantitative Polymerase Chain Reaction (RT-qPCR)

Total RNA was extracted by using the RNeasy kit (Qiagen, Marseille, France) from cultured MSCs (without or stimulated with IL1β and TNFα or DFX) or from harvested wound tissue (mouse). RNA (500 ng) was reverse-transcribed by using superscript II kit (Invitrogen) and qPCR was performed at

Stratagene Mx3000P (Agilent Technologies, Santa Clara, CA, United States) with the primers listed in Supplementary Table S1 (Supplementary Information). All values were normalized to GAPDH or b-actin as housekeeping genes and expressed as fold change or relative expression using the $2^{-\Delta\Delta C_T}$ formula (Livak and Schmittgen, 2001). Gene ontology analysis, gene functional classification and gene ID conversions were performed using PANTHER version 11: Expanded annotation data from Gene Ontology and Reactome pathways, and data analysis tool enhancements (Mi et al., 2017) using Homo sapiens as reference List and Fisher's Exact with FDR multiple test correction. The 10 most important biological process were selected according to lowest *p*-value. For this analysis were used the differentially expressed genes obtained from the MSCs, stimulated in absence and presence of pro-inflammatory cytokines, according to the Mann–Whitney *U* test to filter the data by an adjusted *p*-value ≤ 0.05 with a $\geq$1.5-fold difference.

Cell Migration Assay

Cell migration capacity of MSCs and NHDF-Ad was evaluated using a Transwell two-chamber cell culture method and Transwell inserts (Corning, Cambridge, MA, United States) with an 8 μm pore size polycarbonate membrane. The upper side of the inserts membrane was coated with 0.1% gelatin (Sigma) in PBS for 2 h at 37°C. The MSCs or the NHDF-Ad at a density of 10,000 or 15,000 cells/100 μl, were seeded in the upper compartment and incubated for 5 and 20 h, respectively. The lower compartment contained 500 μl of MSCs-CM or medium alone as chemoattractant factor or control, respectively. After incubation, non-migrating cells were carefully removed from the upper surface of the insert and washed with PBS. The membrane was fixed and stained with crystal violet as described above. The inserts (lower side) were photographed in five random fields under an inverted bright-field microscope at 10× magnification and percentage of area of migrated cells was determined using Image J analysis software (NIH).

Mouse Wound Healing Model

C57BL/6 were obtained from Jackson Laboratories (8–10-week-old male/female). Animals were randomly assigned to groups according to experimental design and mouse excisional wound splinting model was generated as described previously (Galiano et al., 2004; Wang et al., 2013). Briefly, under anesthesia (Sevoflurane, Baxter SA, Lessines, Belgium) a 6-mm-diameter sterile biopsy punch (Premier medical, Plymouth, PA, United States) was used on shaved and depilated dorsum to create two full-thickness excisional wounds besides the midline. Subsequently mice received intradermal injections at four different sites around each wound using a 30-G syringe (BD Biosciences) containing a total number of 1.0×10^6 MenSCs in 100 μl saline (MenSCs group) or 100 μl saline only (Control group). A donut-shaped silicone splint (Grace Bio-Labs, Sigma) with a 15 mm diameter was centered on the wound and fixed to the skin using a topical adhesive (Histoacryl®, B. Braun, Germany) and interrupted 5/0 poliamide sutures (Dafilon®, B. Braun). Finally, the wounds were dressed with Tegaderm (3M, St. Paul, MN, United States) and self-adhering elastic bandage (Coban®, 3M). Following surgery, mice received saline and analgesic treatment, and were placed under a warming lamp to recover from the anesthesia. The animals were monitoring daily to assess recovery and to ensure wound area remains covered and sterile. Skin tissue samples were harvested using an 8-mm biopsy punch (Premier medical) at different time points for the following analyses.

Wound Closure and Angiogenesis Analysis

Individual wounds were recorded using a digital camera at 0, 3, 6, 10, and 14 days after treatment, and the wound areas were measured using Image J software (NIH). The percentage of wound closure was calculated as follows: *(area of original wound − area of actual wound)/area of original wound × 100*. For angiogenesis, photos of skin biopsies were taken above a transillumination device and pictures were processed with the software VesSeg-Tool[1] (Schenck et al., 2014). After the digital segmentation of the blood vessels, quantitative data were obtained with the option Image Statistics. The percentage of white coverage was picked up, and the percentage of vessels coverage compared to healthy skin (intern control made for each animal) was calculated as follows: (% white coverage of the wound/% white coverage of healthy skin) × 100.

Histological Analysis

For histological evaluation, mice were euthanized 14 days after treatment. Wound tissues were harvested, fixed in 10% formalin solution (Sigma-Aldrich), and subsequently embedded in paraffin using standard protocols. Samples were cut into 5-μm sections and stained with hematoxylin-eosin (HE, Sigma-Aldrich) to compare re-epithelization rate and the amount of inflammatory infiltration. The total collagen and collagen III content was determined by Van Gieson (Diapath S.p.A, Bergamo, Italy) and Gomori reticular fiber stain (Sigma-Aldrich). Sample pictures were taken with Olympus CX41 microscope and the quantification was determined using ImageJ software (NIH). Immunohistochemistry was performed to detect CD31 (Rabbit polyclonal 1:50, Abcam, Cambridge, MA, United States) using Dako Envision system (Dako, Carpinteria, CA, United States) according to manufacturer's recommendations. Immunoreactive sections were visualized with diaminobenzidine (DAB) solution (Dako) and counterstained with hematoxylin. Vascular density was evaluated counting the number of $CD31^+$ microvessels per mm^2 using microscope under 100× magnification. Counting was performed in five different fields per each wound using the Image J software. Histological scoring was performed in a blinded fashion. In **Table 1**, were summarized the criteria for semi-quantitative histological scores, modified from previous reports (Wu et al., 2007; Yew et al., 2011; Pelizzo et al., 2015). Briefly, each slide was given a histological score ranging from 0 to 3 according to the following parameters: re-epithelialization, collagen content, angiogenesis and cell infiltration.

[1] http://www.isip.uni-luebeck.de/index.php?id=150&L=2%255

TABLE 1 | Criteria for semi-quantitative histological scores.

Score	0	1	2	3
Re-epithelialization	None	Regenerated mono-layered epithelium	Regenerated multi-layered epithelium	Differentiated multi-layered epithelium (stratum corneum)
Collagen content	None	Poor	Moderate	High
Angiogenesis	None	Capillary density poor	Capillary density moderate	Capillary density high
Cell infiltration (inflammatory cells)	None	Few	Fair	Rich

MenSCs Engraftment and Tracking

Menstrual fluids were labeled with PKH26 Red Fluorescent Cell Linker kit (Sigma-Aldrich) according to manufacturer's instructions. Labeling efficiency was determined by flow cytometry (>97%), as previously described (Alcayaga-Miranda et al., 2015b). Labeled MenSCs (1×10^6 cells/wound) were resuspended in 100 μl of saline solution and injected intradermally. Animals were euthanized at different time points (Days 0, 3, 6, 10, and 14) and the skin wound samples were recovered. Skin samples were digested 1 h at 37°C with 5 mg/ml of Collagenase type IV (Gibco) and 5 μg/ml of DNase I (Roche, Mannheim, Germany). All samples were passed through a 70-μm nylon cell strainer (BD Falcon) and centrifuged. Skin samples were resuspended in flow cytometry buffer (PBS 1x, 0.5% BSA, 0.01% sodium azide). Percentage of PKH26-positive cells was determined by flow cytometry and data obtained were analyzed using the FlowJo data analysis software. A single-cell suspension of saline or control wounds was used each time for negative controls and gate setting in flow cytometry analysis.

Statistical Analysis

Data are expressed as mean ± standard error. Mann–Whitney *U* test was used to evaluate the differences between groups. One-way analysis of variance followed by Tukey's post-test was used for analysis of multiple comparison groups. The number of samples per group (*n*) are specified in the figure legends. Probability value, $p \leq 0.05$ was considered statistically significant.

RESULTS

MenSCs Display a Superior Clonogenic Potential in Comparison With UC-MSCs

All the *in vitro* experiments have been conducted with three different donors of MSCs from the menstrual fluid and umbilical cord tissue, characterized according to their expression of MSCs markers and differentiation potential. Both MSCs showed strong positive expression for CD105, CD90, CD73, CD44 and were negative for hematopoietic cell surface markers including CD34, CD45, CD14, and CD19. Additionally, both MSC sources expressed major histocompatibility complex (MHC) class I antigen HLA-ABC, but not class II HLA-DR (**Figure 1A**). The evaluation of the mesodermal tri-differentiation capacity to osteoblasts, adipocytes, and chondroblasts, showed no differences among cell types (**Figure 1B**). Analysis of proliferative rate over time revealed similar patterns between the different donor tissues, except on day 6 where MenSCs showed an increased proliferation rate (**Figure 1C**). Notably, evaluating the colony forming unit-fibroblast (CFU-F) assay, which reflects the ability of a cell to grow in a density-insensitive fashion (Kurt Yüksel et al., 2010), MenSCs exhibited a notable higher CFU-F potential compared to UC-MSCs. MenSCs initially seeded at ratios 25, 50, 100, 150, 200, and 250 showed an increase of 8-; 6.63-; 6.18-; 4.96-; 4.4-; and 4.2-folds, respectively, compared to UC-MSCs (**Figure 1D**).

MenSCs Exhibit Higher Immunosuppressive Effects Compared to UC-MSCs Independently of the MSCs Activation State

The immunosuppressive properties of MenSCs and UC-MSCs were studied by determining their capacity to modulate the proliferative response of CTV-labeled PBMCs upon PHA stimulation. As shown in **Figure 2**, both sources displayed significant immunosuppressive properties in all tested conditions. Interestingly, MenSCs showed an increased effect inhibiting CD4+ T-cell proliferation compared to UC-MSCs at both ratios 1:5 ($p \leq 0.001$) and 1:10 ($p \leq 0.05$). We also observed that the inhibitory effect of MenSCs was higher at ratio 1:5 ($p \leq 0.001$) on the contrary no dose dependent effect was observed for UC-MSCs. To determine if the immunosuppressive effect is maintained in a pro-inflammatory context (as it occurs in injured skin), MSCs were pre-stimulated for 24 h with IL1β and TNFα before co-culture with T-cells. Stimulation with pro-inflammatory cytokines did not affect the ability of MSCs to abrogate T-cell proliferation at the mentioned ratios, and similar as occurred in non-treated cells, MenSCs exhibited a higher inhibition at both ratios (1:5 $p \leq 0.001$; 1:10 $p \leq 0.05$) compare to UC-MSCs.

MenSCs and MenSCs-CM Exhibit Higher Migratory Capacity

In addition to the immunomodulatory activity, the migratory capacity is an important biological function allowing MSCs to reach and integrate the site of injury and exert their therapeutic effects. Analysis of the migratory capacity revealed significantly increased migration of MenSCs compared to UC-MSCs in both, control conditions and challenged with pro-inflammatory cytokines ($p \leq 0.001$) (**Figure 3A**). There is several evidence that MSCs secrete paracrine factors that can modulate components of different stages of the wound healing process (Otero-Viñas and Falanga, 2016). Paracrine effects of MSCs on NHD

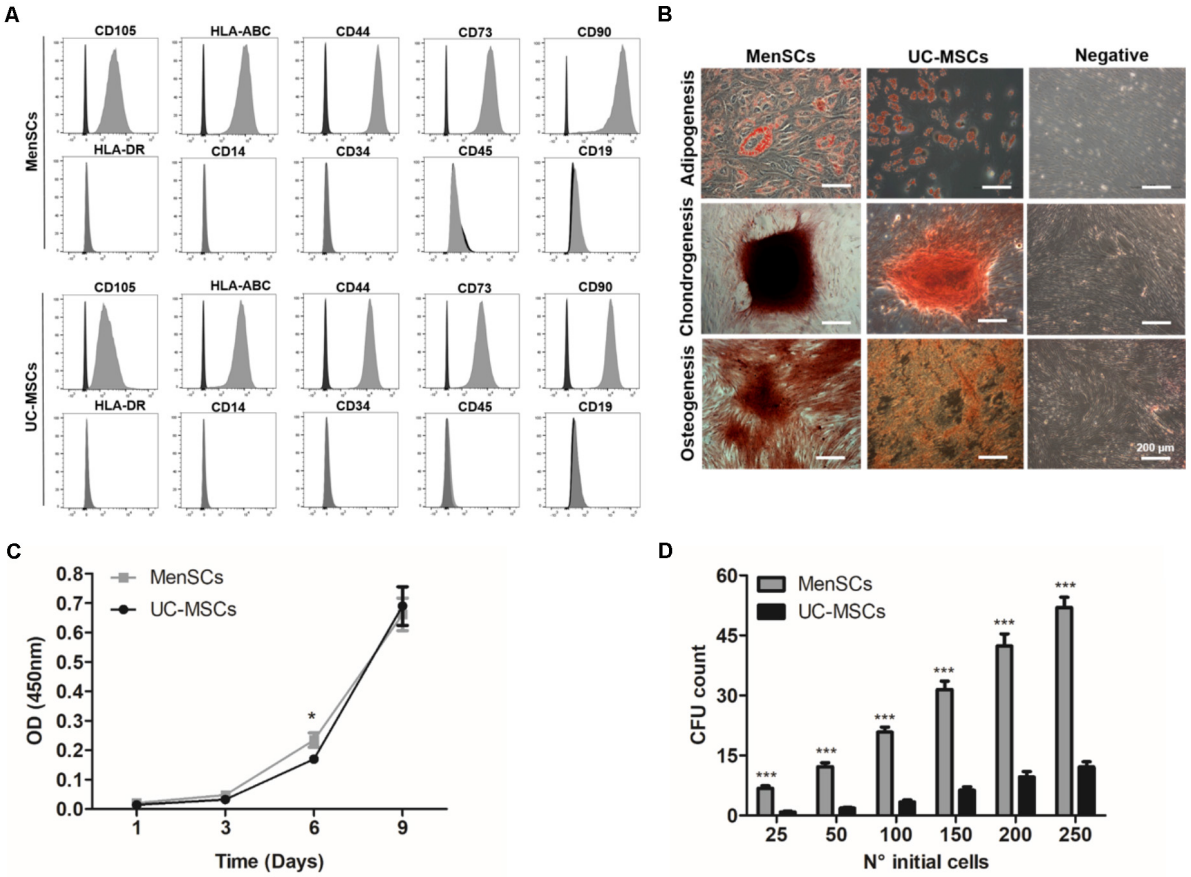

FIGURE 1 | Characterization of MenSCs and UC-MSCs. **(A)** Flow cytometric analysis of MenSCs and UC-MSCs markers. Representative histograms of MSCs surface markers (gray) and their respective isotypes (black). **(B)** MenSCs and UC-MSCs displayed mesodermal tri-differentiation capacity. Representative images of MSCs differentiation after specific inductions and staining to adipocytes (Oil Red O), chondrocytes (safranin O), and osteocytes (alizarin red). Scale bar = 200 µm. **(C)** Proliferation assay of MenSCs and UC-MSCs on days 1, 3, 6, and 9. **(D)** Colony Forming Unit-F assay of MenSCs and UC-MSCs, evaluated until day 14 after cell seeding. Values are expressed as the mean ± SE of at least three independent experiments in triplicates. MenSCs vs. UC-MSCs, $*p \leq 0.05$, $***p \leq 0.001$. MenSCs, menstrual derived mesenchymal stem cells; UC-MSCs, umbilical cord mesenchymal stem cells; CFU, colony forming unit; OD, optical density.

fibroblast (skin cells which play a key role in the ECM production and wound repair) proliferation and migration were investigated, using serum-free CM from respective MSCs cultures (**Figures 3B,C**). Both, MenSCs-CM and UC-MSC-CM enhanced NHDF proliferation at day 1 compared to serum free control medium. However, only MenSCs-CM revealed a persisting stimulatory effect for several days. Interestingly, the CM from stimulated MenSCs showed an increased cell proliferation at day 3 vs. their control medium (**Figure 3B**). Furthermore, both MSCs-CM exhibited a significantly higher chemoattractive effect than their respective control medium on the migration of dermal fibroblast as shown by transwell assay (**Figure 3C**). However, MenSCs-CM showed a greater effect compared to UC-MSCs and this effect is retained with CM obtained from stimulated cells with pro-inflammatory cytokines. Surprisingly, in this case UC-MSCs-CM lost the ability to favor cell migration of dermal fibroblast compared to control medium (**Figure 3C**).

MenSCs Showed a Differential Transcription Pattern of Genes Associated With Wound Healing

An analysis of selected genes involved in wound repair, such as growth factors, cytokines, chemokines, antimicrobial peptides, metalloproteinases (among others), was performed to investigate the relative mRNA expression levels, in both, basal and in pro-inflammatory conditions. As shown in **Figure 4**, we analyzed 30 genes and compared four groups of data: Group 1: MenSCs vs. UC-MSCs; Group 2: IL1β+TNFα MenSCs vs. IL1β+TNFα UC-MSCs; Group 3: IL1β+TNFα MenSCs vs. MenSCs, and Group 4: IL1β+TNFα UC-MSCs vs. UC-MSCs.

Our results indicated that in basal conditions, the expression levels of several genes were considerably different between MSCs, and these differences became more pronounced when the cells were treated with pro-inflammatory cytokines IL1β+TNFα (**Figures 4A,B** and Supplementary Table S2).

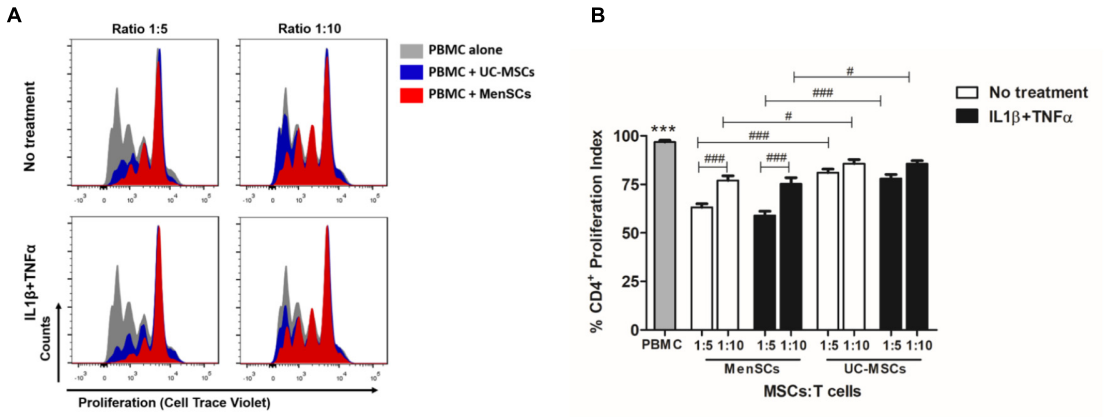

FIGURE 2 | MenSCs display higher immunosuppressive properties resulting in an increased inhibition of T cell proliferation. To study the immunosuppressive capacity of MSCs on T-cell response, we performed an *in vitro* T-cell proliferation assay at different ratios of MSCs:T-cell, as described in Section "Materials and Methods." MSCs were either unstimulated or were stimulated with IL1β+TNFα (10 ng/ml each) for 24 h before T cells co-culture in complete RPMI medium. Previously, PBMC were labeled with CTV and stimulated with PHA, 15 μg/ml for 3 days. T-cell proliferation was evaluated by flow cytometry, gating on CD3+CD4+ cells. **(A)** Representative histograms of T-cell proliferation in presence and absence of MenSCs and UC-MSCs. **(B)** Graphical presentation of the quantified data. Values are expressed as the mean ± SE of at least 3 independent experiments in triplicates. PBMC alone vs. with MSCs, $^{***}p \leq 0.001$. MSCs vs. each reciprocal condition, $^{\#}p \leq 0.05$, $^{\#\#\#}p \leq 0.001$. MSCs, mesenchymal stem cells; IL1 β, interleukin-1 beta; TNFα, tumor necrosis factor alpha; MenSCs, menstrual derived mesenchymal stem cells; UC-MSCs, umbilical cord mesenchymal stem cells; PBMC, peripheral blood mononuclear cells: PHA, phytohaemagglutinin, CTV, Cell trace violet.

In particular, without treatment, a significant up-regulation of 43% and a down-regulation of 27% of genes in MenSCs was observed in comparison with UC-MSCs (**Figure 4A**, Group 1). More in detail, genes involved in angiogenesis and neovascularization ANGPT1 (1.5-fold), PDGFA (1.8-fold), PDGFB (791-fold), and MMP3 (21.6-fold), ECM components ELN (13.4-fold) and MMP10 (9.2-fold) which helps to control degradation of collagen in the wound during tissue remodeling (Wang et al., 2012; Yolanda, 2014), showed a significantly up-regulation in MenSCs compared to UC-MSCs. Furthermore, genes implicated with anti-apoptotic and anti-fibrotic properties, and immunomodulation, anti-microbial effects and transcriptional pathways like GM-CSF (5.2-fold) and TIMP2 (2.5-fold), TSG6 (1.8-fold), LCN2 (5.6-fold) and NFkB1 (1.9-fold), respectively, were also increased in MenSCs compared to UC-MSCs. By contrast, a down-regulation of TGFB2 (0.47-fold) was observed, factor which higher activity was related to keloids (Xia et al., 2006). Interestingly, MenSCs compared to UC-MSCs expressed lower but significant levels of SERPINE2 (0.19-fold) and IL1β (0.09-fold), the former encoding a protein that inhibit serine proteases and displays anti-angiogenic function (Bhakuni et al., 2016) and the second the pro-inflammatory IL1β (**Figure 4A**, Group 1). The pro-inflammatory condition significantly regulated differentially the mRNA expression of 53% of the genes in MenSCs (**Figure 4B**, Group 3) while only 33% in UC-MSCs (**Figure 4B**, Group 4). Collectively these results suggest that MenSCs are more sensitive to an inflammatory environment. Among the genes identified as responding to the stimuli (73.3%) in MenSCs vs. UC-MSCs (**Figure 4A**, Group 2), it can be found that PDGFB (523-fold), MMP3 (274-fold), ELN (261-fold), and MMP10 (51-fold) displayed the highest increase. Other genes that displayed a significant expression increase were IL8 (4.9-fold), a potent angiogenic and inflammatory chemokine that up-regulates VEGF expression (Martin et al., 2009); bFGF (2-fold), also a pro-angiogenic factor that influences granulation tissue formation, epithelialization, and tissue remodeling (Eming et al., 2014); and IL6 (2.9-fold), a pro-inflammatory cytokine that has notable effects in immunomodulation and on angiogenic processes as promoting endothelial progenitor cell migration and proliferation, regulation of bFGF, induction of PDGF as well as stimulation of vascular smooth muscle cell migration (Kang et al., 2015). GO analysis were used to identify at least the 10 most important biological processes in which the differentially expressed genes in stimulated MSCs were involved (**Figure 4C**). This data suggests that in pro-inflammatory conditions MenSCs will be associated with tissue remodeling and UC-MSCs with activators of the immune system.

Hypoxia Condition Increases the Expression of Pro-angiogenic Factors

Hypoxia, inflammation, infection, arterial and venous insufficiency are part of the non-healing wound microenvironment (Chae et al., 2017). Therefore, we decided to evaluate in both MSCs the differential expression of pro-angiogenic genes during hypoxia induced by deferoxamine (DFX), a hypoxia mimetic agent. A concentration of 150 μM of DFX was selected since it has been previously reported that this dose improves their therapeutic potential with no toxic effects detected on MSCs (Oses et al., 2017). The treatment with DFX revealed no changes in morphology or viability of both, MenSCs and UC-MSCs as shown in **Figure 5A**. DFX induced an increase of HIF-1α levels in MenSCs (6.82-fold) and UC-MSCs (7.5-fold). HIF-1α is a factor known for activating

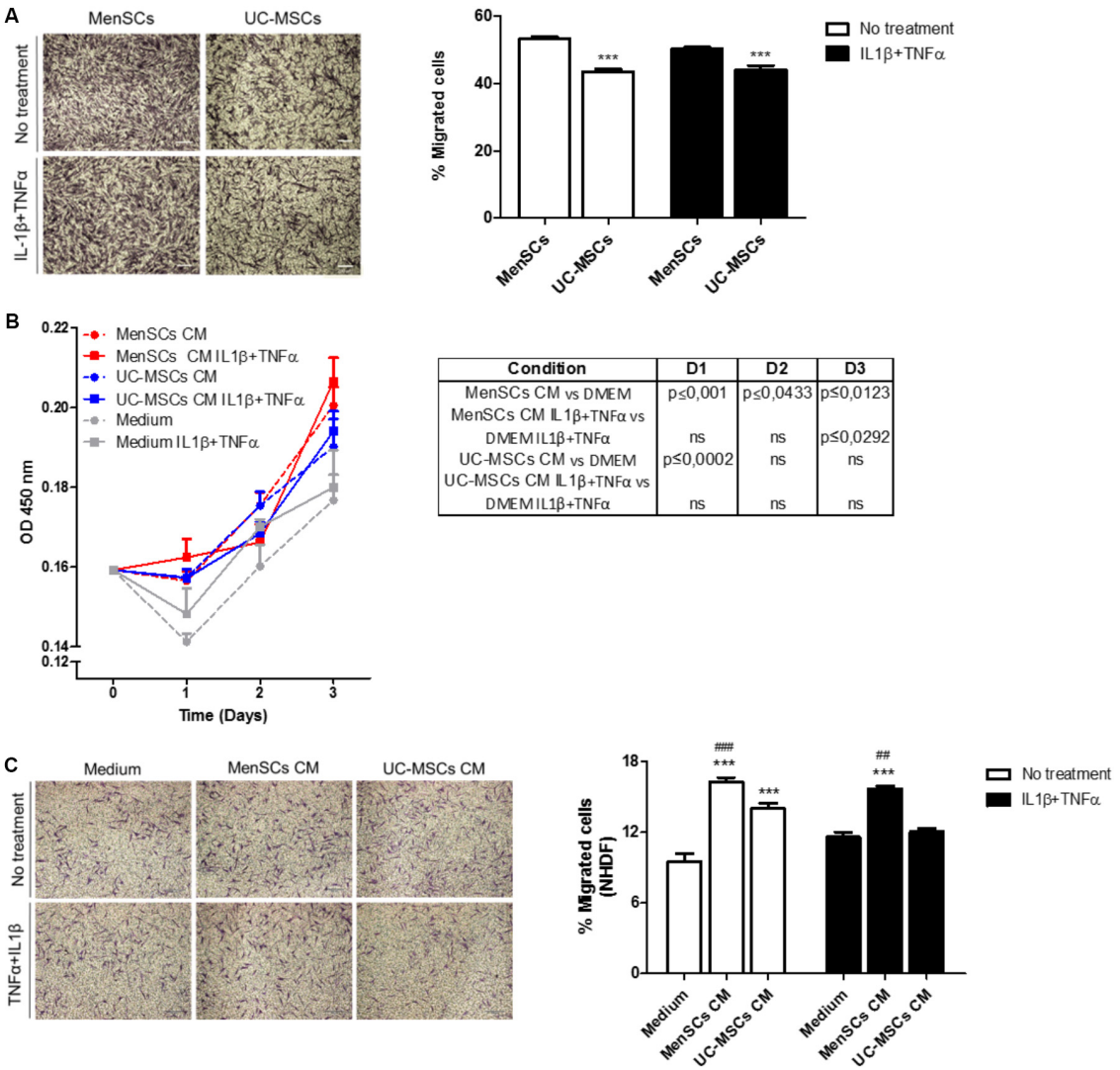

FIGURE 3 | MenSCs and MenSCs-secretome exhibits increased migratory effects. **(A)** Migration of MenSCs and UC-MSCs with and without proinflammatory stimuli. Migration was evaluated by the Transwell assay system. Left panel, representative images of migrated cells. Right panel, quantification of the area of migrated cells per photographic field using Image J software. **(B)** Effect of MSCs-CM on NHDF proliferation. MSCs-CM was prepared by incubating MSCs (2 × 105/well) in serum-free medium or with IL1β and TNFα (10 ng/ml each). Right, table with statistical analysis comparing MSCs-CM vs. Medium. **(C)** Effect of MSCs-CM on NHDF migration. Migration was evaluated by Transwell assay system. MSCs-CM was prepared by incubating MSCs (2 × 105/well) in serum-free medium or with IL1β and TNFα (10 ng/ml each). Left panel, representative images of migrated cells. Right panel, quantification of the area of migrated cells per photographic field using Image J software. Values are expressed as the mean ± SE of at least 3 independent experiments in triplicates. For **(A)** UC-MSCs vs. MenSCs $^{***}p \leq 0.001$ and for **(C)** MSCs-CM vs. Medium, $^{***}p \leq 0.001$; MenSCs-CM vs. UC-MSCs CM, $^{###}p \leq 0.001$, $^{##}p \leq 0.01$. CM, conditioned medium; MenSCs, menstrual derived mesenchymal stem cells; UC-MSCs, umbilical cord mesenchymal stem cells; NHDF, normal human dermal fibroblast; TNFα, tumor necrosis factor alpha; IL1β, interleukin 1 beta.

the transcription of pro-angiogenic genes (**Figure 5B**). Under DFX culture condition, MenSCs showed a significant increase of VEGF (9.96-fold), PDGF (2.22-fold), and bFGF (1.95-fold) mRNA expression levels. In contrast, among factors expressed by UC-MSCs only VEGF experienced a 5.35-fold increase. Comparing differences in the expression levels of factors between the two cell sources under hypoxic conditions, only ANGPT1 and PDGF secreted by MenSCs showed an increased expression of 5.58 and 3.07-fold, respectively (**Figure 5C**).

MenSCs on the Healing Milieu Promotes Changes in the Matrix Signal and Enhance the Angiogenic Process *in Vivo*

MenSCs were directly injected into the 6-mm diameter wound sites of animals from the mouse excisional wound-splitting model. As shown in **Figure 6A**, macroscopical changes started to be perceived at day 6 in the field surrounding the open wound. There were significant differences in the percentage of wound closure among the groups during the 14-day follow-up period.

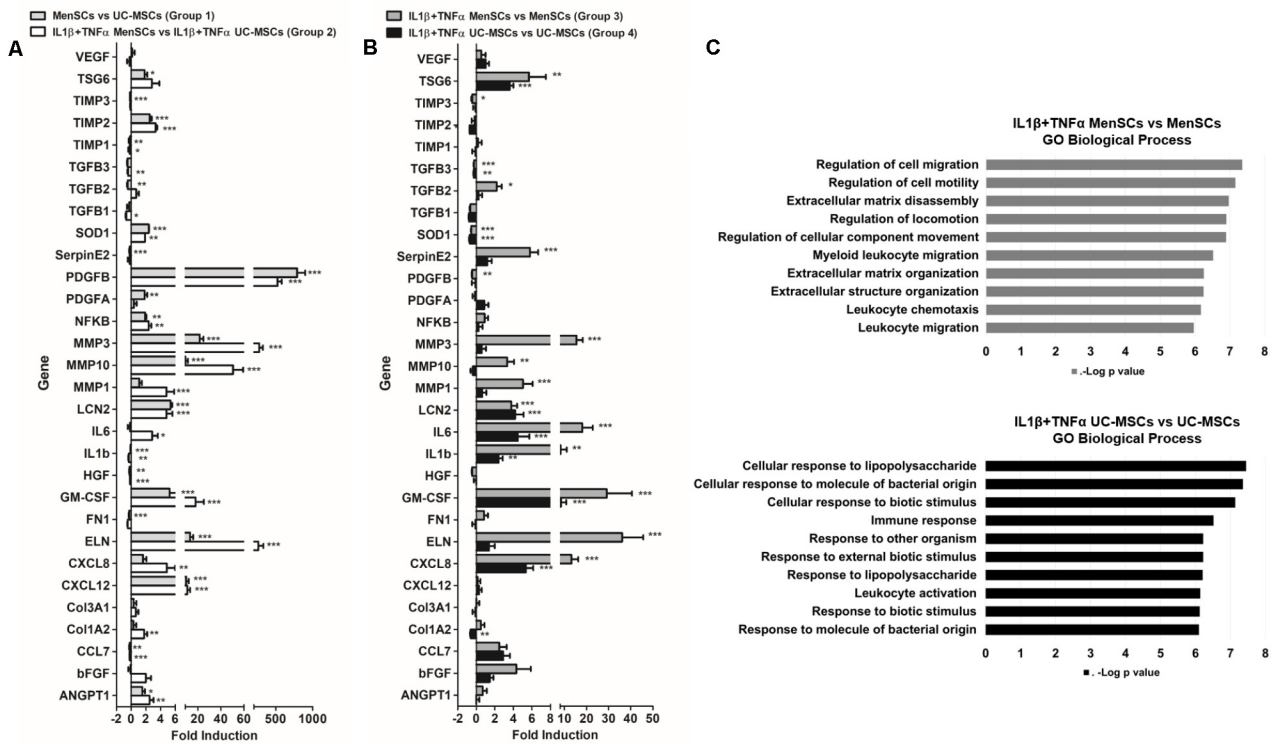

FIGURE 4 | MenSCs exhibited a robust wound healing transcriptomic pattern. MSCs were cultured in basal conditions (medium serum free) and with pro-inflammatory cytokines, IL1β and TNFα (10 ng/ml each) during 24 h. The cells were recovered and total mRNA was extracted, reverse-transcribed and RT-qPCR was performed using Stratagene Mx3000P. The quantitative data from the RT-PCR was normalized by the expression of GAPDH. Expression of different genes involved in wound healing process, **(A)** fold induction of MenSCs vs. UC-MSCs and IL1β+TNFα MenSCs vs. IL1β+TNFα UC-MSCs and **(B)** fold induction of IL1β+TNFα MenSCs vs. MenSCs and IL1β+TNFα UC-MSCs vs. UC-MSCs. Values are expressed as the mean ± SE of at least 3 independent experiments in triplicates. $*p \leq 0.05$, $**p \leq 0.01$, $***p \leq 0.001$ compared to their corresponding MSCs condition. **(C)** GO analysis showing the 10 most important biological process of IL1β+TNFα MenSCs vs. MenSCs and IL1β+TNFα UC-MSCs vs. UC-MSCs. MSCs, mesenchymal stem cells; MenSCs, menstrual derived mesenchymal stem cells; UC-MSCs, umbilical cord-derived mesenchymal stem cells; TNFα, tumor necrosis factor alpha; IL1β, interleukin 1 beta.

Quantitative analysis showed that the measured wound closure significantly increased in mice treated with MenSCs starting from day 6 and persisted until the 10- and 14-day post-injection (**Figure 6B**), indicating an acceleration of the wound closure. The vascularization of skin biopsies was detected by direct blood vessel visualization and digital segmentation. At the end point, MenSCs promote an increased formation of a well-defined vascular network when compared to control group (**Figure 6C**). The vascularization reached values of 41.8% significantly higher than in control group. Notably, the quantification of the vascularization analyzed at different time points indicated an enhanced network by MenSCs statistically significant starting at day 6 with a 53.42% increase over the control. That was maintained, but at lower rates until day 14, suggesting a faster neovascularization with MenSCs treatment (**Figure 6D**). To determine the specificity of the MenSCs effect, human dermal fibroblasts were administered in an additional experimental group. As expected, the fibroblast injection showed no effect on the wound closure rate and angiogenesis (Supplementary Figure S1).

To gain insight on the factors involved in the enhanced reparative effect of MenSCs and their induction by the wound site milieu, the relative mRNA expression of endogenous VEGF, IL8 and Serpine2 were measured in skin biopsies at day 14 (**Figure 6E**). The data showed a significant up-regulation of VEGF levels in the MenSCs treated tissues compared to the control, IL8 showed a tendency to increase while Serpine2 remained unchanged. These results were consistent with the histological findings by IHC staining, where higher significant differences in the CD31 angiogenesis marker were observed in the treated group with 278.63 $CD31^{+}/mm^{2}$ vs. 163.85 $CD31^{+}/mm^{2}$ in control (**Figure 7**, panels 5,10). In MenSCs group, there was a high quantity of blood vessels lumens of different diameters distributed throughout the dermis in a homogeneous manner and large lymphatic vessels predominantly present in the lower part of the dermis. In contrast, the saline group sections displayed a lower number of blood vessels of diameters mostly smaller (**Figure 7**, panels 5,10). On the other hand, we determined the accumulation of pro-angiogenic factors in MenSCs-CM by ELISA with the presence or absence of the pro-inflammatory stimuli, to address the probable contribution of these factors in the healing process (**Figure 6F**). Detectable levels of VEGF, IL8 and PDGF-BB were found in both conditions. However, in the presence of pro-inflammatory cytokines, a significant

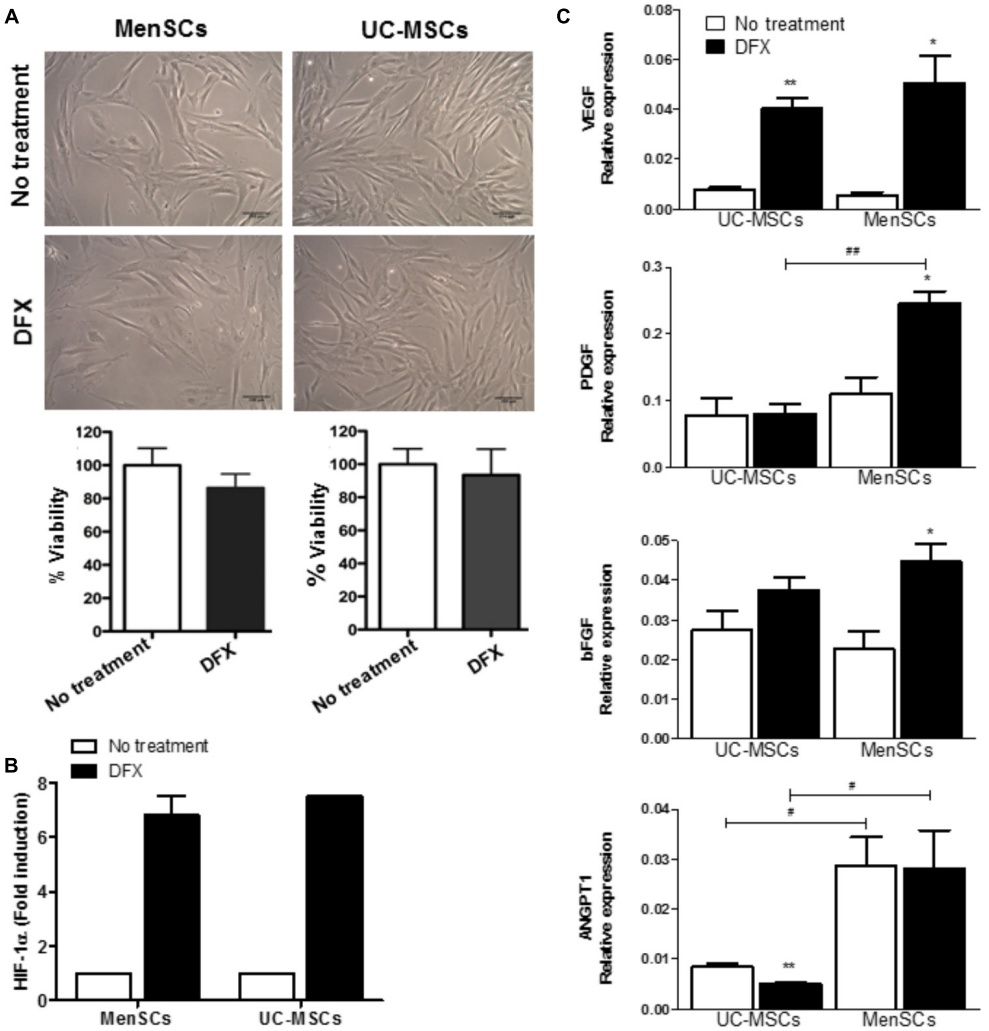

FIGURE 5 | Increased expression levels of pro-angiogenic factors in hypoxia conditions. MSCs were incubated during 24 h with 150 μM of DFX. **(A)** Upper: Representative images showing no changes of morphological characteristics of MSCs comparing to no treated control (without DFX). Lower: Percentage of MSCs viability quantified by trypan blue exclusion assay. **(B)** Levels of HIF-1α determined by ELISA in MSCs lysates. Data were expressed as fold change comparing to non-treated control (without DFX). Values are expressed as the mean ± SE. **(C)** Expression of mRNA levels of the pro-angiogenic factors VEGFα, ANGPT1, PDGF, and bFGF. Values are expressed as the mean ± SE. Treated DFX MSCs vs. non-treated MSCs, $^{*}p \leq 0.05$, $^{**}p \leq 0.01$. MenSCs vs. their respective condition in UC-MSCs, $^{\#}p \leq 0.05$, $^{\#\#}p \leq 0.01$. MSCs, mesenchymal stem cells; MenSCs, menstrual derived mesenchymal stem cells; UC-MSCs, umbilical cord-derived mesenchymal stem cells; DFX, deferoxamine; HIF-1α, hypoxia inducible factor 1 alpha; VEGF, vascular endothelial growth factor; ANGPT1, angiopoietin 1; PDGF, platelet derived growth factor; bFGF, basic fibroblast growth factor.

increase in VEGF secretion was observed, but conversely, the levels of PDGF-BB decreased with the stimuli. Additionally, IL8 although abundant, did not experience significant changes. Also, we determined the accumulation of several growth factors, cytokines or ECM components. Interestingly, IL6 and HGF release were higher in pro-inflammatory conditions while TGFβ1 level remained unchanged.

MenSCs Treatment Improves the Quality of the Repaired Cutaneous Tissue

Consequently, we evaluated the benefit of the treatment with MenSCs on epidermal healing by analyzing the re-epithelialization of the wound site. HE staining showed in most cases that MenSCs-treated wounds had advanced re-epithelization (multi-layered) with presence of keratin formation compared to control, although this observed difference did not become significant (**Figure 7**, panels 1,6). Nonetheless, skin appendages, i.e., hair follicles, sweat glands and sebaceous glands, were not observed in any of the group of animals. Taking into account that the inflammatory phase occurs within the first 3 days of wound healing, low levels of inflammatory cell infiltration were detected in both groups, with a tendency of less infiltration in the treated group (**Figure 7**, panels 2,7). This observation correlates with the immunosuppressive properties described in the *in vitro* setting.

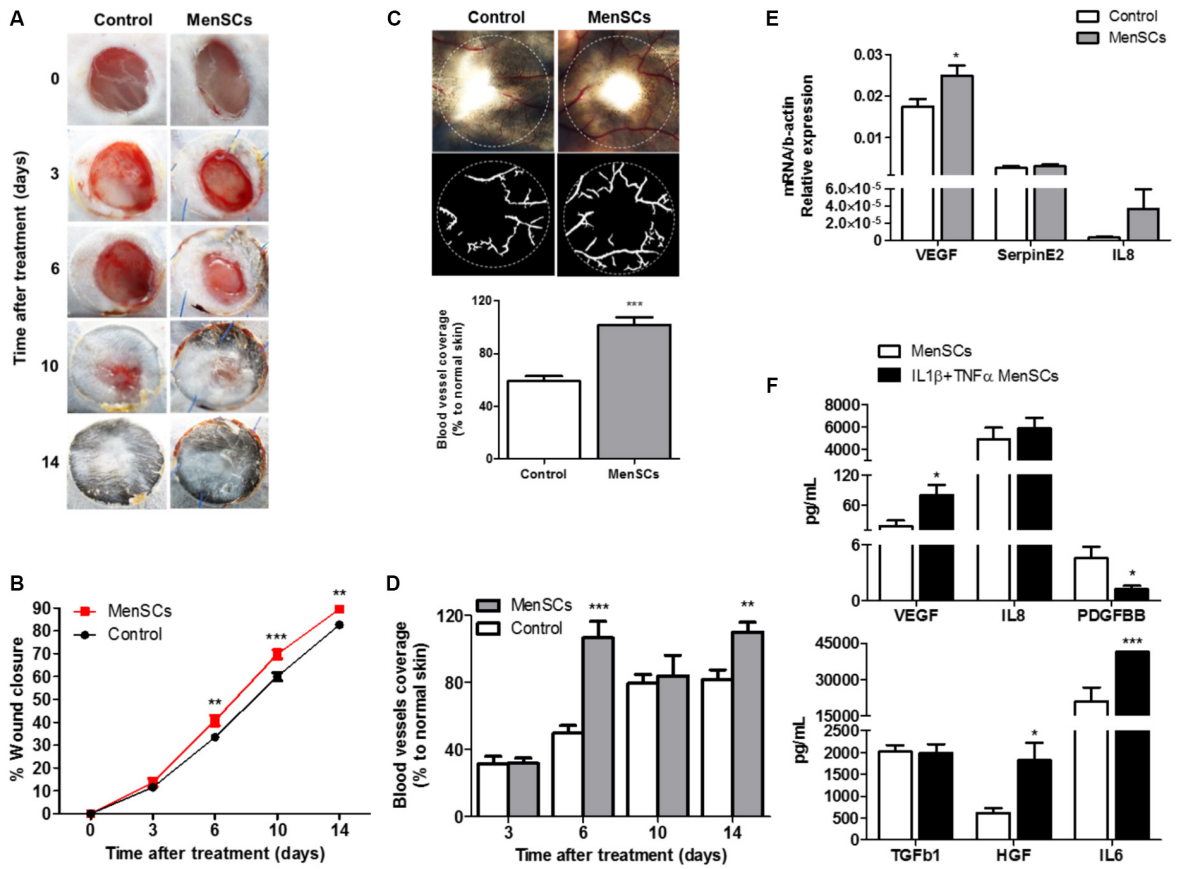

FIGURE 6 | MenSCs injection accelerate the wound healing process in a mouse excisional wound splinting model. Percentage of wound closure and angiogenesis were evaluated after the mice were injected (intradermal) with 1 × 106/100 μl of MenSCs (MenSCs group, $n = 49$) or Saline (Control group, $n = 38$). **(A)** Representative images of the silicone-splinted excisioned wound at different time points. **(B)** Percentage of wound closure at different time points. The percentage of wound closure was calculated using the Image J Software. **(C)** Representative images and quantification of angiogenesis in skin biopsies 14 days after treatment. The photos were taken above a transillumination device (upper photos) and the digital segmentation (lower photos) of the blood vessels and angiogenesis quantification was performed using the VesSeg-Tool software. **(D)** Quantification of angiogenesis in skin biopsies at different time points, analyzed with the software VesSeg-Tool. **(E)** Quantitative RT-PCR to determine expression levels of key genes associated with angiogenesis process in skin biopsies 14 days after injection. Values represent mean ± SE. MenSCs group vs. Control group,*$p \leq 0.05$, **$p \leq 0.01$, ***$p \leq 0.001$. **(F)** Levels of secreted angiogenesis and repair mediated factors measured by ELISA in MenSCs supernatant in the absence or presence of pro-inflammatory stimuli, IL1β+TNFα for 24 h *in vitro*. Values are expressed as the mean ± SE of at least 3 independent experiments in triplicates. IL1β+TNFα MenSCs vs. MenSCs, *$p \leq 0.05$; ***$p \leq 0.001$, menstrual derived mesenchymal stem cells; TNFα, tumor necrosis factor alpha; IL1β, interleukin 1 beta; VEGF, vascular endothelial growth factor; IL8, interleukin 8; PDGFBB, platelet derived growth factor BB; TGFb1, transforming growth factor beta 1; HGF, hepatocyte growth factor; IL6, interleukin 6.

To evaluate the quality of the repair, the deposition and organization of collagen, central component of ECM products, were analyzed. The collagen fibers content was very compact, dense and significantly increased in the reticular dermis of MenSCs-treated wound compared to the control group as showed by Van Gieson's staining (**Figure 7**, panels 3,8). Furthermore, the amount of organized collagen (birefringent), revealed by polarized light microscopy on the same slides was also higher in the treated group (not showed). In the MenSCs injected group, the wound area contains dense thick collagen bundles arranged in diverse directions and parallel to the surface as observed in contiguous normal skin. On the other hand, the control group showed a wound with dense but thinner collagen bundles displayed in a less organized pattern (**Figure 7**, panels 3,8). In addition, with silver staining we determined the reticular fibers made up of thin bundles of fine type III collagen fibrils. As seeing in **Figure 7**, panels 4,9 there is a significant lower content of type III collagen in treated wound compared to controls. Type III collagen represents the firstly formed more disorganized fibers and type I collagen represents later formed and more organized fibers suggesting that the healing process was accelerated in the MenSCs treated wound. The healing index (semi-quantitative score parameters are shown in **Table 1**) of wounds treated with MenSCs was significantly greater than those treated with saline (**Figure 7B**). Interestingly, we also investigated in wound tissues the mRNA expression of several factors and cytokines known to be associated with the wound healing process. The results revealed significant differences in the expression of genes related to ECM remodeling such as Col1, ColA3, ELN, or Icam1, when comparing both groups (**Figure 8**). The general conclusion is

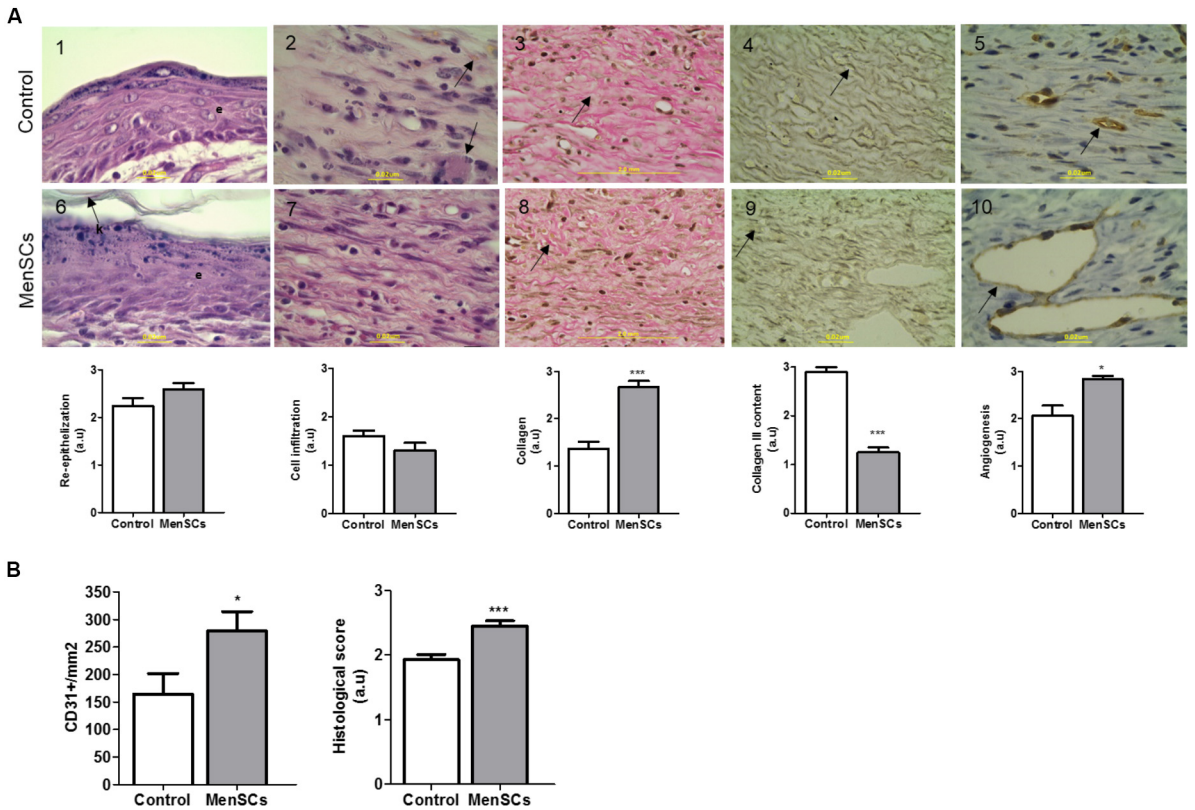

FIGURE 7 | Histologic analysis of wound sections in the wound healing model. For histological evaluation, mice were euthanized 14 days after treatment (Saline or MenSCs) and the wound tissues were harvested. **(A)** Upper panel, representative images of each parameter of Control group (1–5); Lower panel, representative images of each parameter of MenSCs group (6–10). Re-epithelialization evaluated by HE staining (Panels 1,6), arrow indicates keratin layer (k) and e, epithelial layer; Cell infiltration evaluated by HE staining (Panels 2,7), arrow indicates macrophages presence in Control group; Collagen content evaluated by Van gieson stain (Panels 3–8), arrow indicate the collagen bundles, compact in treated group; Collagen III content evaluated by silver stain Gomori (Panels 4,9), arrow indicates collagen III fiber, in treated group fibers are more disorganized, shorter an thinner than control; Angiogenesis evaluated by immunohistochemistry with anti-CD31 (Panels 5,10), arrow indicate the vessel stain with CD31. Quantification of CD31+ was performed using Image J software. (100×, scale bars 2 mm or 0,2 μum as shown in image). Below photos, semi-quantitative score of each parameter. **(B)** Quantification of CD31+ using Image J software (left panel). Semi-quantitative total histological score of MenSCs group (n = 14) comparing to Control (n = 14) (right panel). Values represent mean ± SE, MenSCs group vs. Control, $^{*}p \leq 0.05$, $^{***}p \leq 0.001$. MenSCs, menstrual derived mesenchymal stem cells; HE, hematoxylin-eosin; a.u., arbitrary units.

that the MenSCs treatment increase the rate of wound closure, forming a robust vascular network with dense collagen content promoting proper tissue regeneration.

Fate and Distribution of Engrafted MenSCs

To examine the persistence of intra-dermally administered MenSCs at the wound site, we labeled the cells with PKH26 dye prior to their injection. The labeling efficiency of MenSCs with PKH26 before injection was found to be >97% (**Figure 9A**). At different time point post-injection, the entire wound and skin included in the splint were enzymatically dispersed into a single cell suspension and analyzed by flow cytometry. The absolute number of MenSCs obtained at the same day of the injection (day 0) was set as 100% of the engraftment. The percentages of engrafted MenSCs were obtained at different times of 3, 6, 10, and 14 days after injection. A gradual decrease in the percentage of fluorescent positive cells was observed started at day 3 (73.8%) and persisted throughout the experiment. We were able to detect PKH26+ cells until the endpoint of the experiment, at day 14 with 26.6% of the initial engraftment (**Figure 9B**).

DISCUSSION

Although bone marrow, adipose tissue, and umbilical cord are well established sources of MSCs used in clinical trials to treat skin ulcers[2], they are prone to a number of disadvantages, which MenSCs can easily overcome: non-invasive and repetitive isolation procedure, as well as high frequency of mesenchymal progenitors and proliferative rate that allow a clinical-scale allogeneic transplantation in less time and recurrent applications (; Meng et al., 2007; Alcayaga-Miranda et al., 2015a). The efficacy of MSCs from various sources showed discrepancies, and as a consequence extrapolation of results from one source to other

[2]www.clinicaltrials.gov/

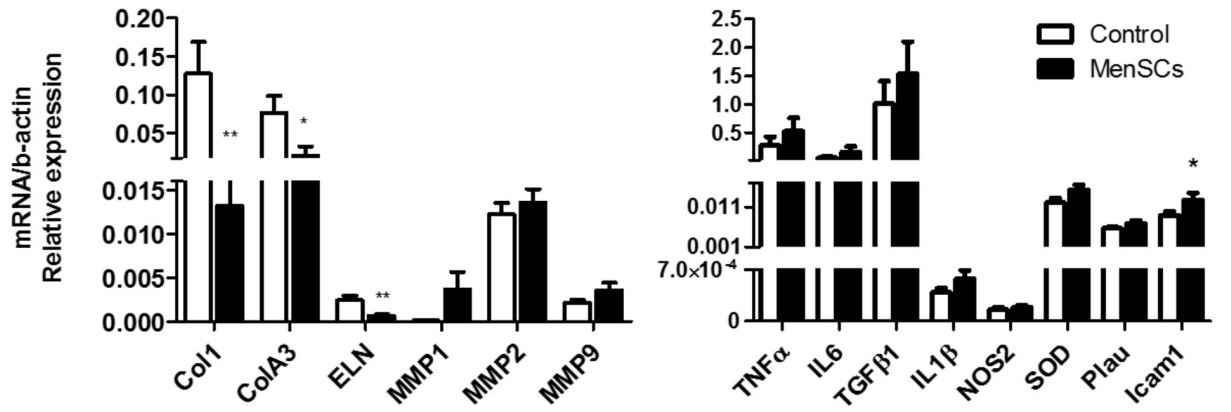

FIGURE 8 | Expression of matrix signal related genes from the wound site. Quantitative RT-PCR analysis was performed in skin biopsies harvested 14 days after treatment (Saline and MenSCs). Expression of genes associated with wound healing was analyzed. The quantitative data from the RT-PCR was normalized by the expression of b-actin. Values are expressed as the mean ± SE. MenSCs vs. control group, $^{*}p \leq 0.05$, $^{**}p \leq 0.01$. MenSCs, menstrual derived mesenchymal stem cells.

MSCs types would suffer from inaccuracy (Akimoto et al., 2013; Lee et al., 2016). In this study we demonstrate for the first time that MenSCs through the enhanced properties presented here, can improve and accelerate the regenerative process in wound healing, promoting MenSCs as strong candidates for the treatment of skin ulcers.

In the *in vitro* comparative study with UC-MSCs, different classical and functional properties related to the repair process were evaluated. While no difference in the immunophenotypic analysis or differentiation capacity was noted, MenSCs showed a superior clonogenic capability compared to UC-MSCs. The relevance of a higher CFU indicate the capacity of cells to grow in a density-insensitive fashion, an important attribute to increase the quality of the newly regenerated skin. One of the mechanism implicated in the repair abilities of MenSCs is their high migration capacity to injury sites in response to signals of cellular damage. In this report, under both basal and pro-inflammatory conditions, MenSCs demonstrated an increased migration ability respect to UC-MSCs. Consistent with this data, it has been shown that in presence of a potent inflammatory stimulus, e.g., bacterial lipopolysaccharide, MenSCs display a strong migration potential, however, further *in vivo* studies are required to fully address this property. In previous reports, MenSCs also outmatched other sources such as ADSCs or BM-MSCs (Alcayaga-Miranda et al., 2015a,b; Chen et al., 2015; Fathi-Kazerooni et al., 2017).

One of the most important challenges for the treatment of non-healing wounds is the presence of sustained inflammation and infections (Zahorec et al., 2015; Otero-Viñas and Falanga, 2016). In this regard, MSCs have been demonstrated to exhibit several antimicrobial and immunomodulatory effects on host immune cells (Luz-Crawford et al., 2016b; Harman et al., 2017; Johnson et al., 2017). Analyzing the immunosuppressive effect of both MSCs, we found that MenSCs exhibit an increased inhibition on CD4+ T cell proliferation than UC-MSCs, at 1:5 and 1:10 cell ratio. Moreover, in contrast to UC-MSCs, MenSCs were more efficient to inhibit T proliferation at ratio 1:5. Interestingly, our group previously demonstrated that MenSCs showed similar immunosuppressive effect as BM-MSCs at 1:10 ratio but fail to match them when diluted to a 1:100 ratio (Luz-Crawford et al., 2016b). In agreement with that, Nikoo et al. (2012) described that MenSCs exert their immunoregulatory activity in a dose-dependent manner. In summary, both MSCs origin and dosis are directly implicated in the changes of immunosuppressive properties of MSCs. These variables are important requisites, which need to be considered for consistent clinical outcomes. In injured sites, the recruited MSCs can be activated by the secretome of activated lymphocytes and monocytes, or by combinations of IFNγ with TNFα, IL1α, or IL1β (Ren et al., 2008). Thus, to functionally define the impact of a pro-inflammatory environment in the suppressive signature of MenSCs, we performed the T cell proliferation assay with MSCs activated with pro-inflammatory cytokines.

Similar to the basal conditions, the experimental outcome pointed at a higher inhibition of T cell proliferation of activated MenSCs when directly compared with UC-MSCs. This suggest that the immunosuppressive potential would be conserved independently of the pro-inflammatory stimuli.

Paracrine factors have been described to play a key role in the mechanisms accounting for tissue regeneration. Multiple angiogenic, growth and trophic factors, as well as chemokines, cytokines, hormones, and extracellular matrix proteins have been identified as constituents of the MSCs secretome (Walter et al., 2010; Figueroa et al., 2014). There are several studies demonstrating the benefit of the conditioned medium derived from MSCs in wound repair (Yew et al., 2011; Akram et al., 2013). To gain insight in the mechanism behind it, we further investigated the selected biological function and identified a specific transcriptomic pattern of relevant factors known to play an essential role in the different pathways involved in wound healing. The recruitment of fibroblasts for instance, is directly involved in the wound healing process, contributing to the deposit of collagen and other ECM proteins and hence, remodeling the immature collagen matrix (Tracy et al., 2016). The experimental results presented here, show that

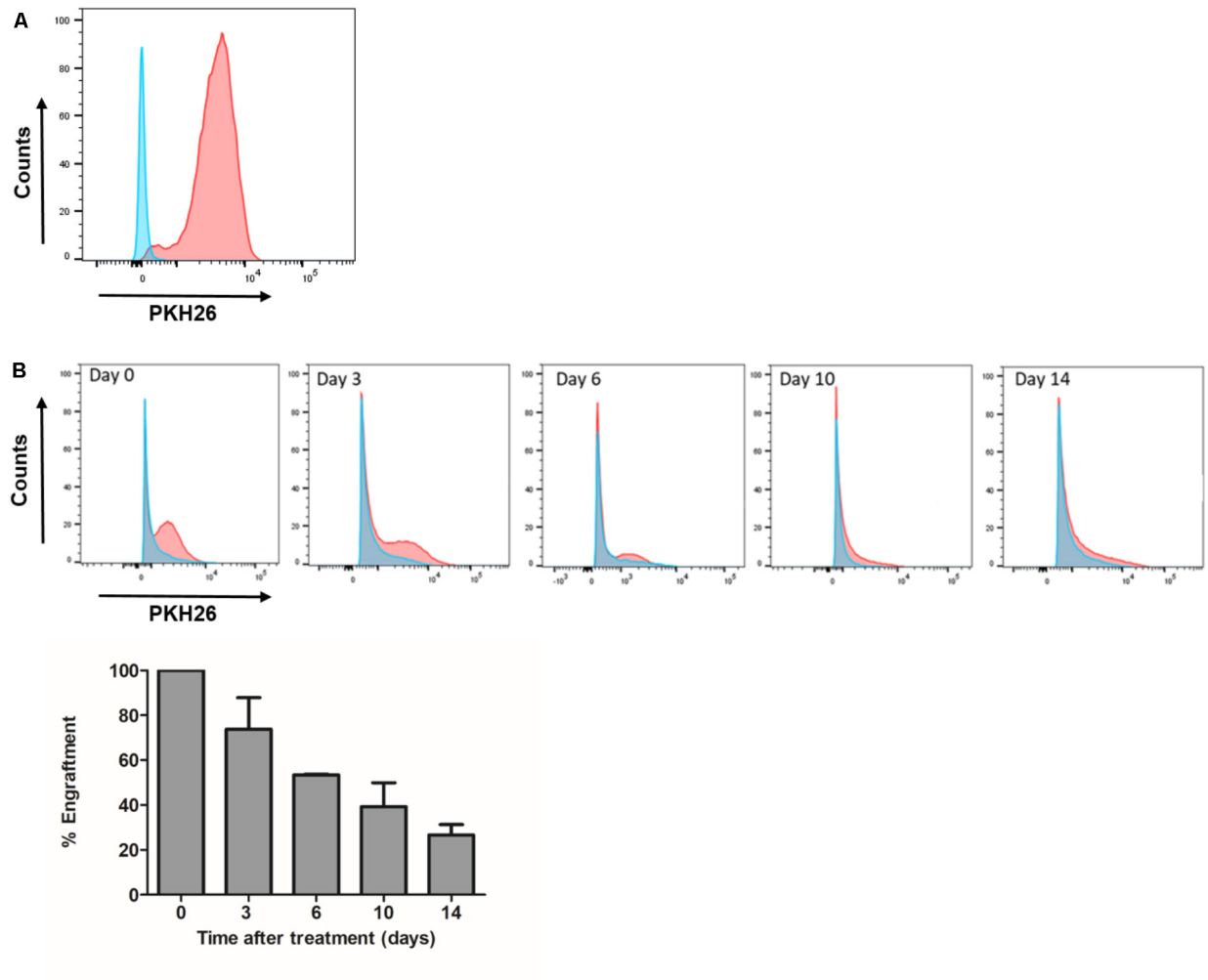

FIGURE 9 | Engraftment of MenSCs into the wound persist for at least 2 weeks of treatment. Each wound received an intradermal injection of one million total MenSCs labeled with PKH26 and an equal volume of saline (Control group). **(A)** Representative plot of labeled MenSCs showing 97% of labeling efficiency (red line). **(B)** The engraftment at different time points was evaluated by FACS analyses of wound digests for PKH26 positive MenSCs. Cells from control wounds were used for negative controls and gate setting (blue line). Percentages of PKH26 positive cells are indicated. Values are expressed as the mean ± SE. MenSCs, menstrual derived mesenchymal stem cells.

MenSCs-CM induced an increased migration of fibroblasts compared to UC-MSCs CM under basal and pro-inflammatory conditions. Moreover, both MSCs-CM showed an induction of the proliferation rate compared to medium alone, and this effect was independent of the pro-inflammatory stimulation of MSCs. Several studies have disclosed similar results, showing an enhanced dermal fibroblast migration and proliferation using conditioned media from UC-MSCs (Walter et al., 2010; Stessuk et al., 2016; Li et al., 2017). Among the factors that stimulate increased cell migration in dermal fibroblasts, TGFb1, and IL6 appears to be essential elements (Postlethwaite et al., 1987; Luckett and Gallucci, 2007). Those factors were both expressed by MenSCs and UC-MSCs as we and others showed by qPCR and ELISA (Luz-Crawford et al., 2016a; Chen et al., 2017). This finding, in addition, with the observed immunosuppressive properties, suggests that the mediators secreted by MenSCs could affect positively the local microenvironment, which would facilitate proliferation, recruitment and migration of resident cells as a response to chemoattractants and may reinforce tissue regeneration and repair.

In an inflammatory environment, MSCs have been shown to display an anti-inflammatory phenotype, characterized by an increased expression of IL6, among other cytokines (Bernardo and Fibbe, 2013). In line with these findings, we analyzed differential expression of genes associated to the wound healing process in MenSCs and UC-MSCS, in basal and pro-inflammatory conditions Overall, 70–73% of the analyzed genes differed in expression between MenSCs vs. UC-MSCs in both conditions. When subjected to pro-inflammatory stimuli, MenSCs altered expression of 53% of analyzed genes, while UC-MSCs only changed 33%. This suggests that MenSCs are more responsive to an inflammatory environment. Notably, within the

stimulated MenSCs, genes as MMPs, ELN, PDGF, IL8, IL6, and IL1β were strongly upregulated in comparison with stimulated UC-MSCs. It is interesting to note that- although there are no differences between MenSCs and UC-MSCs- both increased their expression of LCN2 in response to the pro-inflammatory cytokines. LCN2 is an antimicrobial peptide (AMP), upregulated at sites of inflammation and injury (Alcayaga-Miranda et al., 2017). It has been recently described in mouse BM-MSCs secretome as well as in equine MSCs culture, that it is at least partially responsible for the antimicrobial effects described for MSCs (Gupta et al., 2012; Harman et al., 2017). Additionally, it has been described that LCN2 has a crucial role in promoting epidermal cell migration and wound healing in skin (Miao et al., 2014). To our knowledge, LCN2 has not been reported to be expressed in UC-MSCs or MenSCs, hence, this is the first study to report the expression of this AMP. It would be of high interest to investigate further understand the effect of LCN2 in a wound infection model. Analysis of the biological processes with the Gene Ontology, revealed that the genes differentially expressed in stimulated MenSCs can be associated with tissue remodeling and in UC-MSCs with activators of the immune system. Wegmeyer et al. (2013) using pathway analysis of gene expression data, found that UC-MSCs possess a higher immunomodulatory potential compared to BM-MSCs, demonstrating a functional diversity between MSCs from distinct sources. Non-healing wounds are associated to a hypoxic state. We studied this condition in MenSCs and UC-MSCs, using a hypoxia mimic agent (DFX). The treatment induced an increase in HIF-1α levels, which in turn promoted the overexpression of genes related to pro-angiogenic responses. Indeed, DFX-stimulated MenSCs displayed an enhanced angiogenic potential, paralleled by an increased expression level of factors such as VEGF, PDGF, and bFGF while in UC-MSCs only VEGF augmented. Comparing treated MenSCs with UC-MSCs, VEGF, and PDGF showed the highest up-regulation. These results are in agreement with previous reports obtained with MSCs from adipose tissue or bone marrow (Potier et al., 2008; Oses et al., 2017). Altogether, these data corroborate that MenSCs and UC-MSCs sense the microenvironment and display different pattern of expressed molecules according to the particular need of injured tissue.

Given that MenSCs share features with UC-MSCs that in some cases were found to be superior, and the ample published reports demonstrating the beneficial effect of UC-MSCs on wound healing (Shrestha et al., 2013; Pereira et al., 2016), we investigate the effect of MenSCs on the signal molecules in the wound site and assayed the therapeutical outcome of this treatment in a well described excisional wound splinting mice model (Galiano et al., 2004). Our data indicated that the injection of MenSCs intradermally favored wound healing. The wound closure and angiogenesis of the treated group progressed more rapidly than the control indicating an acceleration in healing process. These results were consistent with those obtained for other MSCs sources such as UC-MSCs or BM-MSCs (Wu et al., 2007; Fong et al., 2014). Revascularization of the wound bed is a crucial step of the normal wound healing process, where new vessels form as granulation tissue develops to supply blood to the wound area, which requires oxygen and nutrients (Nuschke, 2014). The results showed that MenSCs can promote an increased formation of a well-defined vascular network extended in the wound compared to the control group, suggesting that MenSCs promotes angiogenesis. These differences determined by direct blood vessel visualization and confirmed with immunohistological staining with CD31, was notorious from day 6 after treatment showing an increase which correlates with the observed acceleration of wound closure, until the endpoint of 14 days. We determined that MenSCs treatment also increased the mRNA expression levels of endogenous pro-angiogenic factors such as VEGF and IL8 in the mice wounds. These results are consistent with the *in vitro* data of the MenSCs-CM showing high levels of VEGF and IL8. Furthermore, the secreted levels of VEGF were elevated in response to pro-inflammatory stimuli. VEGF, in the wound bed, is known to play a key role in angiogenesis, stimulating endothelial proliferation, migration and increased circulation endothelial progenitor cells (Herrmann et al., 2011; Nuschke, 2014). IL8 stimulates angiogenesis through enhancement of endothelial cell survival, and proliferation (Li et al., 2003). Interestingly, factors that regulate VEGF and IL-8 such as TGFb1, HGF, and IL6 appeared to be highly secreted by MenSCs, and increased following the pro-inflammatory stimulation. Along with a greater maturation of the vascularization of the wound, the MenSCs-treated group displayed a highly increment in density and content of collagen. The collagen fibers in the MenSCs group were well organized in dense thick bundles while in the control group there were thinner and less organized. Moreover, the lower collagen III quantity detected in the treated mice strongly suggest an accelerated and therefore more mature remodeling process in contrast to group injected with saline, since this collagen is the firstly formed in wound healing process (Landén et al., 2016). The main cell type involved in wound remodeling and responsible for collagen deposition are dermal fibroblasts (DF). An increased presence of DF was detected in the MenSCs treated wound niche as revealed by the intense cellularity detected in the histology sections. Our qRT-PCR analysis, showed that MenSCs in pro-inflammatory conditions up-regulate gene expression of fibronectin, elastin, collagen and MMPs, indicating a contribution to the wound remodeling. In previous work it has been demonstrated that MSCs produce MMPs, collagen types I and III providing long term reconstruction of the wound (Fathke et al., 2004; Almalki and Agrawal, 2016). As mentioned before, MenSCs secreted factors such as HGF, IL6, IL8, and TGFb1 which in turn have been shown to prevent apoptosis and promote keratinocyte and fibroblast migration and proliferation (Gallucci et al., 2004; Nishikai-Yan Shen et al., 2017). Therefore, these factors can actively participate in the observed improved wound healing in the treated group. The modulatory effect of MenSCs on different matrix signals was revealed by qRT-PCR on wound biopsies. We observed that the MenSCs treatment up-regulates the expression of mouse ICAM-1 and VEGF compare to control group, suggesting that they may be producing adhesion molecules for the acceleration of wound closure. In contrast, the expression of Col1A,

Col3A and ELN in the treated wounds was down-regulated. This may be explained by a more advanced stage of the wound healing processes in the MenSCs group, in contrast to early stages, where continuous synthesis of collagens and elastin is still required. Finally, using PKH26 labeling technics, we observed a considerable engraftment of MenSCs at days 3 and 6 after treatment with a rapid reduction at day 14. Consistent with our findings, Wu et al. (2007) also observed with GFP-expressing BM-MSCs a diminished percentage over time in a similar wound healing model (Leibacher and Henschler, 2016). MenSCs presence at the wound site for at least 2-week post-transplantation is a good indicator of a persisting beneficial roles covering the different stages of the healing process.

While we report here, a promising potential for the application of MenSCs in wound injuries, it is still necessary to complete their preclinical characterization with further experimental models including chronic wound models related to diabetes and/or infections. Moreover, is still needed a better mechanistic understanding of MenSCs, along with studies to identify the specific interactions between MSCs, their paracrine factors and the other cell types present in the wound microenvironment.

All these results taken together point at enhanced reparative abilities of MenSCs assigned to a combination of biological properties including extensive immunosuppressive and paracrine effects that are highly responsive to the wound environment. These attributes can modulate the wound matrix signals, hence, contributing to an improved cutaneous regeneration. Besides their detailed therapeutical potential, MenSCs have important practical advantages over other MSC origins that convert them into an important alternative source for cell therapy. Indeed, these cells are devoid of ethical problems, have non-invasive isolation and expansion procedures, additionally, they are well tolerated since there have been no reports of toxicity or side effects (Khoury et al., 2014). In fact, the first report of clinical application of MenSCs involved the allogenic injection of four patients with Multiple sclerosis, showing no apparent adverse effects (Zhong et al., 2009). Also, a stem cell company, launched a phase II clinical trial with MenSCs for congestive heart failure, with patients receiving escalating doses up to 200 million cells from a universal donor (Bockeria et al., 2013). Moreover, FDA clearance was obtained for the treatment of critical limb ischemia, an advanced form of peripheral artery disease (Khoury et al., 2014).

CONCLUSION

The study shows that MSCs from different sources display distinct biological properties, which may be relevant for clinical application of different MSCs types for treatment of specific diseases. The different biological functions including, the superior clonogenicity, immunosuppressive and migratory properties in combination with specific gene/paracrine signature of MenSCs resulted in an enhanced wound healing and cutaneous regeneration process *in vivo*. In addition, our findings provide evidence that the interaction of MenSCs with an inflammatory environment could enhance their beneficial properties. Future investigations should be directed toward exploring the specific mechanisms involved in the enhanced effect of MenSCs on wound healing.

AUTHOR CONTRIBUTIONS

AL-G, MD, VC, PG, MKG, CS, FE, ME, FA-M, and JC performed the experiments. JB performed the histological analysis. JC and MK conceived, designed, and analyzed the data. JC, CS, and MK wrote the manuscript text. All authors reviewed the manuscript.

FUNDING

This study was supported by funding from Consorcio Regenero, the Chilean Consortium for Regenerative Medicine.

ACKNOWLEDGMENTS

The authors thank to Maria José Lagos for histology technical assistance. They also thank to Dr. Flavio Carrion for the kind gift murine primers (TGFb1, NOS2, IL1β, TNFα, and IL8). Macarena Ocaña and Claudia Rubi for their assistance in the animal experiments.

SUPPLEMENTARY MATERIAL

The Supplementary Material for this article can be found online at: https://www.frontiersin.org/articles/10.3389/fphys.2018.00464/full#supplementary-material

REFERENCES

Akhavan-Tavakoli, M., Fard, M., Khanjani, S., Zare, S., Edalatkhah, H., Mehrabani, D., et al. (2017). *In vitro* differentiation of menstrual blood stem cells into keratinocytes: a potential approach for management of wound healing. *Biologicals* 48, 66–73. doi: 10.1016/j.biologicals.2017.05.005

Akimoto, K., Kimura, K., Nagano, M., Takano, S., To'a Salazar, G., Yamashita, T., et al. (2013). Umbilical cord blood-derived mesenchymal stem cells inhibit, but adipose tissue-derived mesenchymal stem cells promote, glioblastoma multiforme proliferation. *Stem Cells Dev.* 22, 1370–1386. doi: 10.1089/scd.2012.0486

Akram, K. M., Samad, S., Spiteri, M. A., and Forsyth, N. R. (2013). Mesenchymal stem cells promote alveolar epithelial cell wound repair *in vitro* through distinct migratory and paracrine mechanisms. *Respir. Res.* 14:9. doi: 10.1186/1465-9921-14-9

Alcayaga-Miranda, F., Cuenca, J., and Khoury, M. (2017). Antimicrobial activity of mesenchymal stem cells: current status and new perspectives of antimicrobial peptide-based therapies. *Front. Immunol.* 8:339. doi: 10.3389/fimmu.2017.00339

Alcayaga-Miranda, F., Cuenca, J., Luz-Crawford, P., Aguila-Díaz, C., Fernandez, A., Figueroa, F. E., et al. (2015a). Characterization of menstrual stem cells: angiogenic effect, migration and hematopoietic stem cell support in comparison with bone marrow mesenchymal stem cells. *Stem Cell Res. Ther.* 6:32. doi: 10.1186/s13287-015-0013-5

Alcayaga-Miranda, F., Cuenca, J., Martin, A., Contreras, L., Figueroa, F. E., and Khoury, M. (2015b). Combination therapy of menstrual derived mesenchymal stem cells and antibiotics ameliorates survival in sepsis. *Stem Cell Res. Ther.* 6:199. doi: 10.1186/s13287-015-0192-0

Almalki, S. G., and Agrawal, D. K. (2016). Effects of matrix metalloproteinases on the fate of mesenchymal stem cells. *Stem Cell Res. Ther.* 7:129. doi: 10.1186/s13287-016-0393-1

Al-Nbaheen, M., Vishnubalaji, R., Ali, D., Bouslimi, A., Al-Jassir, F., Megges, M., et al. (2013). Human stromal (mesenchymal) stem cells from bone marrow, adipose tissue and skin exhibit differences in molecular phenotype and differentiation potential. *Stem Cell Rev. Rep.* 9, 32–43. doi: 10.1007/s12015-012-9365-8

Bernardo, M. E., and Fibbe, W. E. (2013). Mesenchymal stromal cells: sensors and switchers of inflammation. *Cell Stem Cell* 13, 392–402. doi: 10.1016/j.stem.2013.09.006

Bhakuni, T., Ali, M. F., Ahmad, I., Bano, S., Ansari, S., and Jairajpuri, M. A. (2016). Role of heparin and non heparin binding serpins in coagulation and angiogenesis: a complex interplay. *Arch. Biochem. Biophys.* 604, 128–142. doi: 10.1016/j.abb.2016.06.018

Bockeria, L., Bogin, V., Bockeria, O., Le, T., Alekyan, B., Woods, E. J., et al. (2013). Endometrial regenerative cells for treatment of heart failure: a new stem cell enters the clinic. *J. Transl. Med.* 11:56. doi: 10.1186/1479-5876-11-56

Chae, D. S., Han, S., Son, M., and Kim, S. W. (2017). Stromal vascular fraction shows robust wound healing through high chemotactic and epithelialization property. *Cytotherapy* 19, 543–554. doi: 10.1016/j.jcyt.2017.01.006

Chen, J.-Y., Mou, X.-Z., Du, X.-C., and Xiang, C. (2015). Comparative analysis of biological characteristics of adult mesenchymal stem cells with different tissue origins. *Asian Pac. J. Trop. Med.* 8, 739–746. doi: 10.1016/j.apjtm.2015.07.022

Chen, L., Zhang, C., Chen, L., Wang, X., Xiang, B., Wu, X., et al. (2017). Human menstrual blood-derived stem cells ameliorate liver fibrosis in mice by targeting hepatic stellate cells via paracrine mediators. *Stem Cells Transl. Med.* 6, 272–284. doi: 10.5966/sctm.2015-0265

Cui, C.-H., Uyama, T., Miyado, K., Terai, M., Kyo, S., Kiyono, T., et al. (2007). Menstrual blood-derived cells confer human dystrophin expression in the murine model of Duchenne muscular dystrophy via cell fusion and myogenic transdifferentiation. *Mol. Biol. Cell* 18, 1586–1594. doi: 10.1091/mbc.E06-09-0872

Eldor, R., Raz, I., Ben Yehuda, A., and Boulton, A. J. (2004). New and experimental approaches to treatment of diabetic foot ulcers: a comprehensive review of emerging treatment strategies. *Diabet. Med.* 21, 1161–1173. doi: 10.1111/j.1464-5491.2004.01358.x

Eming, S. A., Martin, P., and Tomic-Canic, M. (2014). Wound repair and regeneration: mechanisms, signaling, and translation. *Sci. Transl. Med.* 6:265sr6. doi: 10.1126/scitranslmed.3009337

Faramarzi, H., Mehrabani, D., Fard, M., Akhavan, M., Zare, S., Bakhshalizadeh, S., et al. (2016). The potential of menstrual blood-derived stem cells in differentiation to epidermal lineage: a preliminary report. *World J. Plast. Surg.* 5, 26–31.

Fathi-Kazerooni, M., Tavoosidana, G., Taghizadeh-Jahed, M., Khanjani, S., Golshahi, H., Gargett, C. E., et al. (2017). Comparative restoration of acute liver failure by menstrual blood stem cells compared with bone marrow stem cells in mice model. *Cytotherapy* 19, 1474–1490. doi: 10.1016/j.jcyt.2017.08.022

Fathke, C., Wilson, L., Hutter, J., Kapoor, V., Smith, A., Hocking, A., et al. (2004). Contribution of bone marrow-derived cells to skin: collagen deposition and wound repair. *Stem Cells* 22, 812–822. doi: 10.1634/stemcells.22-5-812

Figueroa, F. E., Cuenca Moreno, J., and La Cava, A. (2014). Novel approaches to lupus drug discovery using stem cell therapy. Role of mesenchymal-stem-cell-secreted factors. *Expert Opin. Drug Discov.* 9, 555–566. doi: 10.1517/17460441.2014.897692

Fong, C. Y., Tam, K., Cheyyatraivendran, S., Gan, S. U., Gauthaman, K., Armugam, A., et al. (2014). Human Wharton's jelly stem cells and its conditioned medium enhance healing of excisional and diabetic wounds. *J. Cell. Biochem.* 115, 290–302. doi: 10.1002/jcb.24661

Galiano, R. D., Michaels, J., Dobryansky, M., Levine, J. P., and Gurtner, G. C. (2004). Quantitative and reproducible murine model of excisional wound healing. *Wound Repair Regen.* 12, 485–492. doi: 10.1111/j.1067-1927.2004.12404.x

Gallucci, R. M., Sloan, D. K., Heck, J. M., Murray, A. R., and O'Dell, S. J. (2004). Interleukin 6 indirectly induces keratinocyte migration. *J. Invest. Dermatol.* 122, 764–772. doi: 10.1111/j.0022-202X.2004.22323.x

González, P. L., Carvajal, C., Cuenca, J., Alcayaga-Miranda, F., Figueroa, F. E., Bartolucci, J., et al. (2015). Chorion mesenchymal stem cells show superior differentiation, immunosuppressive, and angiogenic potentials in comparison with haploidentical maternal placental cells. *Stem Cells Transl. Med.* 4, 1109–1121. doi: 10.5966/sctm.2015-0022

Gupta, N., Krasnodembskaya, A., Kapetanaki, M., Mouded, M., Tan, X., Serikov, V., et al. (2012). Mesenchymal stem cells enhance survival and bacterial clearance in murine *Escherichia coli* pneumonia. *Thorax* 67, 533–539. doi: 10.1136/thoraxjnl-2011-201176

Harman, R. M., Yang, S., He, M. K., and Van de Walle, G. R. (2017). Antimicrobial peptides secreted by equine mesenchymal stromal cells inhibit the growth of bacteria commonly found in skin wounds. *Stem Cell Res. Ther.* 8:157. doi: 10.1186/s13287-017-0610-6

Hass, R., Kasper, C., Böhm, S., and Jacobs, R. (2011). Different populations and sources of human mesenchymal stem cells (MSC): a comparison of adult and neonatal tissue-derived MSC. *Cell Commun. Signal.* 9:12. doi: 10.1186/1478-811X-9-12

Herrmann, J. L., Weil, B. R., Abarbanell, A. M., Wang, Y., Poynter, J. A., Manukyan, M. C., et al. (2011). IL-6 and TGF-α costimulate mesenchymal stem cell vascular endothelial growth factor production by ERK-, JNK-, and PI3K-mediated mechanisms. *Shock* 35, 512–516. doi: 10.1097/SHK.0b013e31820b2fb9

Hsieh, J.-Y., Wang, H.-W., Chang, S.-J., Liao, K.-H., Lee, I.-H., Lin, W.-S., et al. (2013). Mesenchymal stem cells from human umbilical cord express preferentially secreted factors related to neuroprotection, neurogenesis, and angiogenesis. *PLoS One* 8:e72604. doi: 10.1371/journal.pone.0072604

Johnson, V., Webb, T., Norman, A., Coy, J., Kurihara, J., Regan, D., et al. (2017). Activated mesenchymal stem cells interact with antibiotics and host innate immune responses to control chronic bacterial infections. *Sci. Rep.* 7:9575. doi: 10.1038/s41598-017-08311-4

Kang, S., Tanaka, T., and Kishimoto, T. (2015). Therapeutic uses of anti-interleukin-6 receptor antibody. *Int. Immunol.* 27, 21–29. doi: 10.1093/intimm/dxu081

Khoury, M., Alcayaga-Miranda, F., Illanes, S. E., and Figueroa, F. E. (2014). The promising potential of menstrual stem cells for antenatal diagnosis and cell therapy. *Front. Immunol.* 5:205. doi: 10.3389/fimmu.2014.00205

Kurt Yüksel, M., Topçuoğlu, P., Kurdal, M., and İlhan, O. (2010). The clonogenic potential of hematopoietic stem cells and mesenchymal stromal cells in various hematologic diseases: a pilot study. *Cytotherapy* 12, 38–44. doi: 10.3109/14653240903313958

Landén, N. X., Li, D., and Ståhle, M. (2016). Transition from inflammation to proliferation: a critical step during wound healing. *Cell. Mol. Life Sci.* 73, 3861–3885. doi: 10.1007/s00018-016-2268-0

Lee, D. E., Ayoub, N., and Agrawal, D. K. (2016). Mesenchymal stem cells and cutaneous wound healing: novel methods to increase cell delivery and therapeutic efficacy. *Stem Cell Res. Ther.* 7:37. doi: 10.1186/s13287-016-0303-6

Leibacher, J., and Henschler, R. (2016). Biodistribution, migration and homing of systemically applied mesenchymal stem/stromal cells. *Stem Cell Res. Ther.* 7:7. doi: 10.1186/s13287-015-0271-2

Li, A., Dubey, S., Varney, M. L., Dave, B. J., and Singh, R. K. (2003). IL-8 directly enhanced endothelial cell survival, proliferation, and matrix metalloproteinases production and regulated angiogenesis. *J. Immunol.* 170, 3369–3376.

Li, M., Zhao, Y., Hao, H., Dong, L., Liu, J., Han, W., et al. (2017). Umbilical cord–derived mesenchymal stromal cell–conditioned medium exerts *in vitro*

antiaging effects in human fibroblasts. *Cytotherapy* 19, 371–383. doi: 10.1016/j.jcyt.2016.12.001

Livak, K. J., and Schmittgen, T. D. (2001). Analysis of relative gene expression data using real-time quantitative PCR and the 2(-Delta Delta C(T)) Method. *Methods* 25, 402–408. doi: 10.1006/meth.2001.1262

Luckett, L. R., and Gallucci, R. M. (2007). Interleukin-6 (IL-6) modulates migration and matrix metalloproteinase function in dermal fibroblasts from IL-6KO mice. *Br. J. Dermatol.* 156, 1163–1171. doi: 10.1111/j.1365-2133.2007.07867.x

Luz-Crawford, P., Djouad, F., Toupet, K., Bony, C., Franquesa, M., Hoogduijn, M. J., et al. (2016a). Mesenchymal stem cell-derived interleukin 1 receptor antagonist promotes macrophage polarization and inhibits B cell differentiation. *Stem Cells* 34, 483–492. doi: 10.1002/stem.2254

Luz-Crawford, P., Torres, M. J., Noël, D., Fernandez, A., Toupet, K., Alcayaga-Miranda, F., et al. (2016b). The immunosuppressive signature of menstrual blood mesenchymal stem cells entails opposite effects on experimental arthritis and graft versus host diseases. *Stem Cells* 34, 456–469. doi: 10.1002/stem.2244

Martin, D., Galisteo, R., and Gutkind, J. S. (2009). CXCL8/IL8 stimulates vascular endothelial growth factor (VEGF) expression and the autocrine activation of VEGFR2 in endothelial cells by activating NFκB through the CBM (Carma3/Bcl10/Malt1) complex. *J. Biol. Chem.* 284, 6038–6042. doi: 10.1074/jbc.C800207200

Meng, X., Ichim, T. E., Zhong, J., Rogers, A., Yin, Z., Jackson, J., et al. (2007). Endometrial regenerative cells: a novel stem cell population. *J. Transl. Med.* 5:57. doi: 10.1186/1479-5876-5-57

Mi, H., Huang, X., Muruganujan, A., Tang, H., Mills, C., Kang, D., et al. (2017). PANTHER version 11: expanded annotation data from Gene Ontology and Reactome pathways, and data analysis tool enhancements. *Nucleic Acids Res.* 45, D183–D189. doi: 10.1093/nar/gkw1138

Miao, Q., Ku, A. T., Nishino, Y., Howard, J. M., Rao, A. S., Shaver, T. M., et al. (2014). Tcf3 promotes cell migration and wound repair through regulation of lipocalin 2. *Nat. Commun.* 5:4088. doi: 10.1038/ncomms5088

Nikoo, S., Ebtekar, M., Jeddi-Tehrani, M., Shervin, A., Bozorgmehr, M., Kazemnejad, S., et al. (2012). Effect of menstrual blood-derived stromal stem cells on proliferative capacity of peripheral blood mononuclear cells in allogeneic mixed lymphocyte reaction. *J. Obstet. Gynaecol. Res.* 38, 804–809. doi: 10.1111/j.1447-0756.2011.01800.x

Nishikai-Yan Shen, T., Kanazawa, S., Kado, M., Okada, K., Luo, L., Hayashi, A., et al. (2017). Interleukin-6 stimulates Akt and p38 MAPK phosphorylation and fibroblast migration in non-diabetic but not diabetic mice. *PLoS One* 12:e0178232. doi: 10.1371/journal.pone.0178232

Nombela-Arrieta, C., Ritz, J., and Silberstein, L. E. (2011). The elusive nature and function of mesenchymal stem cells. *Nat. Rev. Mol. Cell Biol.* 12, 126–131. doi: 10.1038/nrm3049

Nuschke, A. (2014). Activity of mesenchymal stem cells in therapies for chronic skin wound healing. *Organogenesis* 10, 29–37. doi: 10.4161/org.27405

Oses, C., Olivares, B., Ezquer, M., Acosta, C., Bosch, P., Donoso, M., et al. (2017). Preconditioning of adipose tissue-derived mesenchymal stem cells with deferoxamine increases the production of pro-angiogenic, neuroprotective and anti-inflammatory factors: Potential application in the treatment of diabetic neuropathy. *PLoS One* 12:e0178011. doi: 10.1371/journal.pone.0178011

Otero-Viñas, M., and Falanga, V. (2016). Mesenchymal stem cells in chronic wounds: the spectrum from basic to advanced therapy. *Adv. Wound Care (New Rochelle)* 5, 149–163. doi: 10.1089/wound.2015.0627

Pelizzo, G., Avanzini, M. A., Icaro Cornaglia, A., Osti, M., Romano, P., Avolio, L., et al. (2015). Mesenchymal stromal cells for cutaneous wound healing in a rabbit model: pre-clinical study applicable in the pediatric surgical setting. *J. Transl. Med.* 13:219. doi: 10.1186/s12967-015-0580-3

Pereira, A. R., Mendes, T. F., Ministro, A., Teixeira, M., Filipe, M., Santos, J. M., et al. (2016). Therapeutic angiogenesis induced by human umbilical cord tissue-derived mesenchymal stromal cells in a murine model of hindlimb ischemia. *Stem Cell Res. Ther.* 7:145. doi: 10.1186/s13287-016-0410-4

Postlethwaite, A. E., Keski-Oja, J., Moses, H. L., and Kang, A. H. (1987). Stimulation of the chemotactic migration of human fibroblasts by transforming growth factor beta. *J. Exp. Med.* 165, 251–256.

Potier, E., Ferreira, E., Dennler, S., Mauviel, A., Oudina, K., Logeart-Avramoglou, D., et al. (2008). Desferrioxamine-driven upregulation of angiogenic factor expression by human bone marrow stromal cells. *J. Tissue Eng. Regen. Med.* 2, 272–278. doi: 10.1002/term.92

Ren, G., Zhang, L., Zhao, X., Xu, G., Zhang, Y., Roberts, A. I., et al. (2008). Mesenchymal stem cell-mediated immunosuppression occurs via concerted action of chemokines and nitric oxide. *Cell Stem Cell* 2, 141–150. doi: 10.1016/j.stem.2007.11.014

Rodrigues, M. C., Dmitriev, D., Rodrigues, A., Glover, L. E., Sanberg, P. R., Allickson, J. G., et al. (2012). Menstrual blood transplantation for ischemic stroke: therapeutic mechanisms and practical issues. *Interv. Med. Appl. Sci.* 4, 59–68. doi: 10.1556/IMAS.4.2012.2.1

Schenck, T. L., Chavez, M. N., Condurache, A. P., Hopfner, U., Rezaeian, F., Machens, H.-G., et al. (2014). A full skin defect model to evaluate vascularization of biomaterials *in vivo*. *J. Vis. Exp.* 90:e51428. doi: 10.3791/51428

Shrestha, C., Zhao, L., Chen, K., He, H., and Mo, Z. (2013). Enhanced healing of diabetic wounds by subcutaneous administration of human umbilical cord derived stem cells and their conditioned media. *Int. J. Endocrinol.* 2013:592454. doi: 10.1155/2013/592454

Squillaro, T., Peluso, G., and Galderisi, U. (2016). Clinical trials with mesenchymal stem cells: an update. *Cell Transplant.* 25, 829–848. doi: 10.3727/096368915X689622

Stessuk, T., Puzzi, M. B., Chaim, E. A., Alves, P. C., de Paula, E. V., Forte, A., et al. (2016). Platelet-rich plasma (PRP) and adipose-derived mesenchymal stem cells: stimulatory effects on proliferation and migration of fibroblasts and keratinocytes *in vitro*. *Arch. Dermatol. Res.* 308, 511–520. doi: 10.1007/s00403-016-1676-1

Tracy, L. E., Minasian, R. A., and Caterson, E. J. (2016). Extracellular matrix and dermal fibroblast function in the healing wound. *Adv. Wound Care (New Rochelle)* 5, 119–136. doi: 10.1089/wound.2014.0561

Walter, M. N., Wright, K. T., Fuller, H. R., MacNeil, S., and Johnson, W. E. (2010). Mesenchymal stem cell-conditioned medium accelerates skin wound healing: an *in vitro* study of fibroblast and keratinocyte scratch assays. *Exp. Cell Res.* 316, 1271–1281. doi: 10.1016/j.yexcr.2010.02.026

Wang, L.-T., Ting, C.-H., Yen, M.-L., Liu, K.-J., Sytwu, H.-K., Wu, K. K., et al. (2016). Human mesenchymal stem cells (MSCs) for treatment towards immune- and inflammation-mediated diseases: review of current clinical trials. *J. Biomed. Sci.* 23:76. doi: 10.1186/s12929-016-0289-5

Wang, S., Qu, X., and Zhao, R. (2012). Clinical applications of mesenchymal stem cells. *J. Hematol. Oncol.* 5:19. doi: 10.1186/1756-8722-5-19

Wang, X., Ge, J., Tredget, E. E., and Wu, Y. (2013). The mouse excisional wound splinting model, including applications for stem cell transplantation. *Nat. Protoc.* 8, 302–309. doi: 10.1038/nprot.2013.002

Wegmeyer, H., Bröske, A.-M., Leddin, M., Kuentzer, K., Nisslbeck, A. K., Hupfeld, J., et al. (2013). Mesenchymal stromal cell characteristics vary depending on their origin. *Stem Cells Dev.* 22, 2606–2618. doi: 10.1089/scd.2013.0016

Werdin, F., Tenenhaus, M., and Rennekampff, H. O. (2008). Chronic wound care. *Lancet* 372, 1860–1862. doi: 10.1016/S0140-6736(08)61793-6

Wu, Y., Chen, L., Scott, P. G., and Tredget, E. E. (2007). Mesenchymal stem cells enhance wound healing through differentiation and angiogenesis. *Stem Cells* 25, 2648–2659. doi: 10.1634/stemcells.2007-0226

Xia, W., Longaker, M. T., and Yang, G. P. (2006). P38 MAP kinase mediates transforming growth factor-beta2 transcription in human keloid fibroblasts. *Am. J. Physiol. Regul. Integr. Comp. Physiol.* 290, R501–R508. doi: 10.1152/ajpregu.00472.2005

Xiang, B., Chen, L., Wang, X., Zhao, Y., Wang, Y., and Xiang, C. (2017). Transplantation of menstrual blood-derived mesenchymal stem cells promotes

the repair of LPS-induced acute lung injury. *Int. J. Mol. Sci.* 18:689. doi: 10.3390/ijms18040689

Yew, T. L., Hung, Y. T., Li, H. Y., Chen, H. W., Chen, L. L., Tsai, K. S., et al. (2011). Enhancement of wound healing by human multipotent stromal cell conditioned medium: the paracrine factors and p38 MAPK activation. *Cell Transplant.* 20, 693–706. doi: 10.3727/096368910X550198

Yolanda, M.-M. (2014). Adult stem cell therapy in chronic wound healing. *J. Stem Cell Res. Ther.* 4, 1–6. doi: 10.4172/2157-7633.1000162

Zahorec, P., Koller, J., Danisovic, L., and Bohac, M. (2015). Mesenchymal stem cells for chronic wounds therapy. *Cell Tissue Bank.* 16, 19–26. doi: 10.1007/s10561-014-9440-2

Zhong, Z., Patel, A. N., Ichim, T. E., Riordan, N. H., Wang, H., Min, W.-P., et al. (2009). Feasibility investigation of allogeneic endometrial regenerative cells. *J. Transl. Med.* 7:15. doi: 10.1186/1479-5876-7-15

Conflict of Interest Statement: MK is the chief science officer of Cells for Cells and Consorcio Regenero. JC and FA-M received stipends from Cells for Cells.

The other authors declare that the research was conducted in the absence of any commercial or financial relationships that could be construed as a potential conflict of interest.

frontiers in Physiology

ORIGINAL RESEARCH
published: 04 April 2017
doi: 10.3389/fphys.2017.00200

Acellular Gelatinous Material of Human Umbilical Cord Enhances Wound Healing: A Candidate Remedy for Deficient Wound Healing

Nazihah Bakhtyar[1], Marc G. Jeschke[1,2], Laurence Mainville[1], Elaine Herer[3] and Saeid Amini-Nik[1,2,4,]*

[1] Department of Biological Sciences, Sunnybrook Health Sciences Center, Sunnybrook Research Institute, Toronto, ON, Canada, [2] Division of Plastic Surgery, Department of Surgery, University of Toronto, Toronto, ON, Canada, [3] Department of Gynecology and Obstetrics, Sunnybrook Health Sciences Centre, University of Toronto, Toronto, ON, Canada, [4] Department of Laboratory Medicine and Pathobiology, University of Toronto, Toronto, ON, Canada

Impaired wound healing is a severe clinical challenge and research into finding effective wound healing strategies is underway as there is no ideal treatment. Gelatinous material from the umbilical cord called Wharton's jelly is a valuable source of mesenchymal stem cells which have been shown to aid wound healing. While the cellular component of Wharton's jelly has been the subject of extensive research during the last few years, little is known about the de-cellularized jelly material of the umbilical cord. This is important as they are native niche of stem cells. We have isolated Wharton's jelly from umbilical cords and then fractionated acellular gelatinous Wharton's jelly (AGWJ). Here, we show for the first time that AGWJ enhances wound healing *in vitro* as well as *in vivo* for wounds in a murine model. *In vivo* staining of the wounds revealed a smaller wound length in the AGWJ treated wounds in comparison to control treatment by enhancing cell migration and differentiation. AGWJ significantly enhanced fibroblast cell migration *in vitro.* Aside from cell migration, AGWJ changed the cell morphology of fibroblasts to a more elongated phenotype, characteristic of myofibroblasts, confirmed by upregulation of alpha smooth muscle actin using immunoblotting. AGWJ treatment of wounds led to accelerated differentiation of cells into myofibroblasts, shortening the proliferation phase of wound healing. This data provides support for a novel wound healing remedy using AGWJ. AGWJ being native biological, cost effective and abundantly available globally, makes it a highly promising treatment option for wound dressing and skin regeneration.

Keywords: skin, wound healing, deficient healing, umbilical cord, Wharton's jelly, stem cell, regenerative medicine, tissue regeneration

OPEN ACCESS

Edited by:
Marianna Bei,
Harvard Medical School, USA

Reviewed by:
Chia-Hua Kuo,
University of Taipei, Taiwan
Shiang Y. Lim,
St Vincent's Institute of Medical Research, Australia

***Correspondence:**
Saeid Amini-Nik
saeid.amininik@utoronto.ca

Specialty section:
This article was submitted to Clinical and Translational Physiology, a section of the journal Frontiers in Physiology

Received: *07 February 2017*
Accepted: *17 March 2017*
Published: *04 April 2017*

Citation:
Bakhtyar N, Jeschke MG, Mainville L, Herer E and Amini-Nik S (2017) Acellular Gelatinous Material of Human Umbilical Cord Enhances Wound Healing: A Candidate Remedy for Deficient Wound Healing. Front. Physiol. 8:200. doi: 10.3389/fphys.2017.00200

INTRODUCTION

A wound is described as a disruption of the normal healthy anatomical structure and functional integrity of the skin (Atiyeh et al., 2002). The wound healing process involves four integrated and overlapping phases: hemostasis, inflammation, proliferation and tissue remodeling or resolution (Gosain and DiPietro, 2004). These steps allow for the reformation and revascularization of the skin by allowing a functional dermis and epidermis to form. About 1.5 billion people suffer from skin diseases as a consequence of both progressive aging and the lack of adequate health-care (Valacchi et al., 2012). Among these, skin lesions are highly prevalent

and can be divided into acute or chronic wounds (Whitney, 2005). It has been reported that acute wounds generally follow trauma or inflammation and usually heal within 6 weeks (Valacchi et al., 2012). In certain circumstances, chronic wounds, also known as non-healing wounds result which do not progress through the normal wound healing steps and fail to heal within 6 weeks, this type of wound results in an open laceration of varying degrees of severity (Branski et al., 2009). Such wounds often enter a state of pathologic inflammation due to a postponed, incomplete, or uncoordinated healing process. The management of a chronic wound defined as a barrier defect that has not healed in 3 months—has become a major therapeutic challenge throughout the western world, and it is a problem that will only worsen since the incidence of conditions that prevent wound healing, such as diabetes, obesity, vascular disorders are on the rise in addition to burn injuries (Nunan et al., 2014).

The primary goals in the treatment of wounds are rapid wound closure and a functional and esthetically satisfactory scar. In order to do so, wound coverage is one of the cornerstones of wound management (Singer and Clark, 1999). Clinicians may use various materials and techniques, such as antibiotic therapy, surgical debridement, negative pressure devices, wound dressings, hyperbaric oxygen therapy, antimicrobial therapy, bioengineered skin equivalents and growth factors but these have limited success which illustrates the complexities of wound healing. Skin grafts from allogeneic or autologous sources, reconstructive tissue flaps, and engineered skin substitutes can also be useful in the treatment of more extensive or chronic wounds (Valacchi et al., 2012). Although research continues and skin substitutes gain in efficacy, wound healing remains a clinical challenge, particularly with an aging population (Jeschke et al., 2015, 2016). Clinical and pre-clinical studies using cell-based therapies are being gradually introduced into medical care to manage skin wounds because they can repair/replace damaged tissue with a healthy tissue due to their natural ability to produce cytokines and molecules necessary for wound healing (Marfia et al., 2015; Markeson et al., 2015; Nicholas et al., 2016a,b).

In 1991 McElreavey et al. first isolated the mesenchymal stromal cells from the Wharton's jelly portion of the umbilical cord (McElreavey et al., 1991). Wharton's Jelly is a source of perinatal mesenchymal stem cells (WJ-MSC) with unique properties of both embryonic and adult stem cells (Pirjali et al., 2013). Wharton's jelly-derived MSCs have the ability to maintain phenotypic attributes, cell growth kinetics, cell cycle pattern, *in vitro* multilineage differentiation plasticity, apoptotic pattern, normal karyotype-like intrinsic MSC properties in long-term *in vitro* cultures (Sabapathy et al., 2014). Several studies have investigated cellular therapy with WJ-MSCs, alone or within a scaffold (Azari et al., 2011; Shohara et al., 2012; Fong et al., 2014; Ribeiro et al., 2014; Sabapathy et al., 2014). Studies have elucidated the role of WJ-MSCs for various applications, such as for neurological disorders (Shalitin et al., 2003), kidney injury (Du et al., 2013), lung injury (Moodley et al., 2009), liver injury and cancer therapy (Sabapathy et al., 2014). We have recently reported that WJ-MSCs conditioned-medium with its secretome has positive effects on wound healing *in vitro* (Arno et al., 2014).

Mesenchymal stem cells in Wharton's jelly are in close interaction with their extra cellular matrix. Considering that the secretome of WJ-MSCs enhances wound healing *in vitro*, we asked whether the native extracellular matrix of these cells, which is not necessarily secreted by WJ-MSCs, have any effect on skin healing. The Wharton's jelly itself without cells has not been investigated with regards to wound healing. Wharton's jelly contains a significant amount of extracellular matrix components which are composed primarily of collagen, hyaluronic acid, and various sulphated proteoglycans. It is well-known that biosynthesis of extracellular matrix components is enhanced by several peptide growth factors, mainly insulin-like growth factor (IGF) (Edmondson et al., 2003), fibroblast growth factor (FGF) (Yu et al., 2003) and transforming growth factor b (TGF-b) (Shalitin et al., 2003). These growth factors may accumulate within Wharton's jelly to support the cells (e.g., MSCs). We, therefore, hypothesized that acellular gelatinous Wharton's jelly (AGWJ) enhances skin wound healing. Here we report on the effects of AGWJ treatment on fibroblast cells of the dermis through *in vitro* experiments. We then performed wound healing experiments on 8 weeks old male C57/black 6 mice to establish the effect of AGWJ treatment on wounds *in vivo*. The resulting data support the investigation for a novel wound healing treatment using AGWJ.

MATERIALS AND METHODS

Cell Culture

Tissue culture plastic ware were purchased from BD Falcon™ (Bedford, MA, USA), and all tissue culture media and supplements were purchased from Wisent Inc. (St-Jean-Baptiste, QC, Canada), unless otherwise stated. Fibroblast cell culture medium was high-glucose Dulbecco's modified Eagle's medium (DMEM) supplemented with 10% fetal bovine serum (FBS) and 1% antibiotic–antimycotic solution. Primary human normal skin fibroblasts were obtained from skin tissue samples. The skin was dissected to remove any underlying fat from the dermis, cut into small explant pieces of 2 to 4 mm, and cultured in 10 cm dishes. When fibroblast cells had migrated out of the tissue and onto the plate, the tissue pieces were removed. When fibroblasts reached to 70% confluence, approximately within 1 week, they were trypsinized with 0.05% trypsin in preparation for subculture. Fibroblasts were subcultured in 75 cm^2 tissue culture flasks at a density of 5000 cells/cm^2.

Acellularization of Wharton's Jelly

Sterile umbilical cords were obtained from cesarean sections performed by surgeons from the department of Gynecology and Obstetrics at Sunnybrook Health Sciences Center after obtaining consent from the patients. The cords which were on average 20 cm in length were cut in half. The 10 cm half cords were then cut open lengthwise to reveal the Wharton's jelly contents. The cord pieces were then washed by dipping them in a 2% antibiotic/antimycotic PBS solution followed by dipping them in a 1% antibiotic/antimycotic PBS solution. The cord was then opened completely and a sterile scalpel was used to scrape the jelly out of the umbilical cord. The jelly (approximately 5 ml)

was then placed in a 50 ml conical tube with 20 ml of 1× DMEM complete media and resuspended vigorously using a 5 ml pipette to break apart the jelly. The resuspended jelly in media was then centrifuged at 1400 rpm for 10 min. The cells and cord debris were pelleted. The supernatant with AGWJ was collected and frozen at −80°C. The cell pellet was discarded (**Supplemental Figure 1**).

Cell Migration Study: Scratch Assay

Normal human skin fibroblasts were seeded in six well plates at a cell density of 20,000 cells/well. When the wells had reached to 100% cell confluency, two scratches were made with a 1000 μl pipette tip. The media was then aspirated and the cells were washed with PBS. The PBS was aspirated. One well was immediately stained with crystal violet as a 0 h time point. Treatment media of AGWJ in DMEM or complete DMEM control media was added to the cells. After 24 h, the cells were stained with crystal violet. Images were taken on a microscope (Zeiss) with 4× magnification. Eight images were taken per scratch. Quantification was performed using ImageJ software (National Institutes of Health, Bethesda, MD, USA). The cells within the scratch area were counted as the cells in scratch zone.

In Vivo Wound Healing Model

Eight C57/black 6 (8 weeks old, male, body weight 25 to 30 g) were obtained from Jackson Laboratory under the guidelines of the Sunnybrook Research Institute and Sunnybrook Health Sciences Animal Policy and Welfare Committee of the University of Toronto. Animal procedures were reviewed and approved by Sunnybrook Research Institute and Sunnybrook Health Sciences Centre at University of Toronto animal care and use committee. Animals were anesthetized and back cutaneous hair was removed by electrical shaving under anesthesia as stated in the Animal Protocol. 4 wounds of 6 mm diameter full-thickness skin wounds were created on each side of the midline. The animals were randomly divided into two groups: treatment (AGWJ and Matrigel; Corning Matrigel matrix high concentration product#354262 Corning, NY, USA) and control (complete DMEM medium and Matrigel). For the 5 day time point study: 3 mice received control treatment on their wounds and 3 mice received AGWJ treatment. For the 7 day time point study: 6 mice received control treatment and 7 mice received AGWJ treatment. Each wound topically received 100 μl AGWJ treatment or control DMEM in Matrigel mix. The day of the wounding was counted as day 0. For the 7 day time point study, on days 2 and 4 the wounds were redressed. On day 6, 24 h before sacking the mice, the animals received an intraperitoneal injection of bromodeoxyuridine (BrdU) (Calbiochem, San Diego, CA, USA). For the 5 day time point, the wounds were redressed on day 2, BrdU injected on day 4 and the mice were sacrificed on day 5.

Ethical Regulations for Animal Study

The animal experiments were reviewed and approved by, and performed in accordance with the guidelines and regulations set forth by the Sunnybrook Research Institute and Sunnybrook Health Sciences Animal Policy and Welfare Committee of the University of Toronto, Ontario Canada. All procedures using animals were approved by the Sunnybrook animal care committee, approval #15-503(M-1) issued Nov 20, 2015 under the auspices of Canadian Council on Animal care.

Human umbilical cords were obtained from cesarean sections performed by surgeons from the Department of Gynecology and Obstetrics at Sunnybrook Health Sciences Center, University of Toronto, Toronto, Ontario, Canada. All subjects gave written informed consent in accordance with the Declaration of Helsinki Principles. The protocol was approved by Toronto Academic Health Sciences Network (TAHSN) and University of Toronto-affiliated Sunnybrook Research Institute and Sunnybrook Health Sciences Centre Institutional Ethics Review Board approval (REB number: 017-2011 valid until March 1, 2017), and after getting patient signed informed consent.

Wound Analysis

On day 5 and day 7 the mice were sacrificed. The wounds were then excised using a scalpel and surgical scissors. 3 out of the 4 wounds were placed in histology cassettes and fixed in 10% buffered formalin for 24 h at 4° and then switched to a 70% ethanol solution and then embedded in paraffin. Specimens were cut into 5 μm sections. Tissue specimens were cut through the center or midline of the wound, providing a cross section through the wound center. Both halves of the wound were then placed on slides for analysis. The wounds also included some normal intact skin on either side of the wound. The 4th wound was frozen immediately after excision for future analysis purposes. For high power field (HPF) analysis of wounds, granulation tissue was selected from the center of the wound which was the healed area from both the control and AGWJ treated wounds.

Trichrome Stain

Trichrome reagents were from EMS (Hatfield, PA, USA) unless otherwise stated. Paraffin-embedded slides were heated for 30 min at 60°C. Slides were then deparaffinized with citrosol, followed by rehydration through 100% × 2, 95%, 70% and washed in distilled water. Slides were placed in Bouin's solution (26367–01; EMS, Hatfield, PA, USA) overnight at room temperature overnight and rinsed under running tap water for 10 min. Hematoxylin stain (HHS16; Sigma, Saint Louis, MO, USA) and Biebrich scarlet-acid fuchsin solution were applied sequentially for 10 min. Washes were performed after each stain addition. Slides were differentiated in phosphomolybdic–tungstic acid for 15 min, and were transferred to aniline blue for 5 min. Slides were next rinsed and differentiated in 1% acetic acid for 2 min then washed in distilled water. Slides were then dehydrated through 95% ethanol and absolute ethanol followed by clearing in citrosol. Slides were mounted with SHUR/Mount xylene-based liquid mounting media (Triangle Biomedical Sciences, Durham, NC, USA). Images were acquired using a Zeiss Axiovert 200 light microscope at 5×, 10×, 20×, and 40× magnification. Quantification was carried out using merged images to measure the entire wound length.

Immunohistochemistry

Paraffin-embedded skin tissue slides were deparaffinized by heating for 30 min at 60°. Slides were then placed in citrosol (2×), 100% Ethanol (2×), 95% ethanol, 70% ethanol for 3 min each,

followed by water. Antigen retrieval was then performed using antigen decloaker (1×; Biocare Medical, Concord, CA, USA) which was added to the slides in a preheated decloaking chamber for 4 min at 110°C. For BrdU staining, samples were denatured with 1.5 N HCl for 30 min at 37°C and neutralized with 0.1 M borate buffered twice for 5 min. Samples were blocked with 3% H_2O_2 for 10 min, and then washed with washing buffer (0.05 M Tris–HCl, 0.15 M NaCl, 0.05% Tween 20 in deionized water). The primary antibody (mouse monoclonal anti-BrdU, 1:200; Cell Signaling, Beverly, MA, USA) was diluted in PBS and incubated at room temperature for 1 h. For α smooth muscle actin (α SMA) analysis, a different section was probed with αSMA (mouse monoclonal anti-αSMA, 1:200; clone 1A4; ebioscience, Sandiego CA, USA) primary antibody diluted in PBS was incubated at room temperature for 1 h. Slides were then incubated for 15 min with MACH3 mouse probe (Biocare Medical), followed by MACH3 rabbit or mouse horseradish peroxidase polymer, with washes in between. The betazoid diaminobenzidine chromogen kit (Biocare Medical) was mixed and added for 5 min or until brown stain was noticeable. The reaction was terminated with running water. Nuclear staining was carried out with hematoxylin for 30 s, followed by differentiation with three dips in 1.5% acid alcohol and bluing in 0.1% sodium bicarbonate for 10 s. Sections were dehydrated through 95% and absolute ethanol to citrosol and mounted with SHUR/Mount. Images were acquired using a Zeiss Axiovert 200 light microscope at 10× magnification to image the whole section followed by 40× magnification to further focus on the wound margins and the wound center. The 40× magnification images were quantified by positive cells using ImageJ software, and then normalized to the number of total cells in the 40× field.

Immunofluorescence

Cells were washed with phosphate-buffered saline (PBS) and fixed for 15 min in 4% paraformaldehyde (Alfa Aesar, Karlsruhe, Germany). Fixed cells were washed in PBS and permeabilized for 10 min with 0.5% Triton X-100 solution in PBS. Cells were washed again and then blocked for 30 min with 1% bovine serum albumin in 0.5% Triton X-100 in PBS. A mouse monoclonal αSMA (anti-αSMA, 1:200; clone 1A4; ebioscience, Sandiego CA, USA) primary antibody was added and incubated overnight at 4°C. After washing with PBS, the secondary antibody was added in 1% bovine serum albumin in 0.5% Triton X-100 in PBS and incubated for 1 h at room temperature in the dark (Alexa Fluor 488 donkey anti-mouse, 1:500; Life Technologies, Eugene, OR, USA). The cells were then washed three times with PBS, the slides were mounted with Vectashield mounting medium with 4′,6-diamidino-2-phenylindole (DAPI; Vector Laboratories, Burlingame, CA, USA). Cells were examined and photographed using an Apotome Axiovert fluorescent imaging system at 10× magnification (Zeiss, Oberkochen, Germany). Four images were taken per well and two wells were imaged, one well was AGWJ treated cells and one was control treated cells.

Cell Viability Assay

Cell viability was performed using the CellTiter-glo luminescent cell viability assay kit (G7571 Promega, Madison, WI, USA). Briefly, cells were seeded into a 96 well plate and allowed to grow for 24 h at 37°C in a 5% CO2 incubator. After 24 h, the media was aspirated and AGWJ treatment or control media was added to the cells. The plate was again incubated for 24 h in the incubator. After the 24 incubation with treatment, the cell titer glo substrate was added to the buffer and then added to the plate. The cell titer glo solution was added in a 1:1 ratio to the volume of media in the wells. The plate was shaken to mix the solution with the media and then incubated for 10 min at room temperature. After which the luminescence was read using the Synergy H4 hybrid multi-mode microplate reader (100 Tigan Street Winooski, VT, USA).

Cell Lysate Preparation

Cell lysates were prepared on ice. Media was aspirated from the cells. The cells were washed with PBS, the PBS was then aspirated. Next, lysis Buffer (RIPA) with 5 mM EDTA, 1× protease inhibitor, and phosphatase inhibitor was added to the cells. 150 ul of lysis buffer was added to a 10 cm plate of cells. The cells were scraped off the plate with a cell scraper. The solution was placed in an eppendorf tube and incubated on ice for 30 min with vortexing every 10 min. The cell lysate was then centrifuged at 4°C for 30 min at 20,000 × g. The supernatant was collected in an eppendorf tube and stored at −80°C.

Western Blot Analysis

Briefly, cell lysates (15 μg of protein per well) were separated by 10% SDS-PAGE gel, proteins were then transferred to nitrocellulose membrane, after which the blots were blocked with 5% skim milk in TBST buffer. The blots were washed three times in TBST buffer and then blots were probed using the mouse monoclonal αSMA (anti-αSMA, 1:1000; clone 1A4; ebioscience, Sandiego CA, USA), mouse monoclonal vimentin (anti-vimentin, 1:1000; Thermofisher Scientific, Waltham MA, USA). Loading control used was GAPDH (anti-GAPDH, 1:5000, Cell Signaling, Danvers MA, USA). Primary antibody incubated overnight at 4°C. Band intensities were detected, normalized and quantified with the Chemidoc and Image Lab 5.0 software (Bio-Rad Laboratories).

Statistical Analysis

The statistical comparisons between the AGWJ treatment and control groups were performed using a 2-tailed Student's *t*-test for analysis. A P value of <0.05 was considered statistically significant. Data were graphically represented as the mean of the target group ± the 95% confidence interval. Microsoft excel was used for data analysis.

RESULTS

AGWJ Treatment Enhances Wound Healing in Mice

To validate if there are any beneficial effects of AGWJ on promoting wound healing *in vivo*, we performed two wound healing studies on a murine model. We conducted a 5 day and a 7 day time point study. Wound length and hence wound closure were analyzed using trichome staining on excised wounds

after the end of both studies. The results showed that after 5 days, compared with the control treatment (**Figure 1A**), AGWJ treatment led to a significant reduction in the wound size (**Figure 1B**). Wound length was measured from the border of the intact skin on the right side through the wound bed to the intact skin on the left side of the wound. All of the wounds were measured and the average wound length for the control treated wounds was 4184.09 um ± 358.18 and for the AGWJ treated wounds, the average wound length was 2673.53 um ± 379.02. $^{*}P < 0.05$ (**Figure 1C**). For the 7 day treatment time point, the results also display a dramatic reduction in the wound length with AGWJ treatment as compared with controls, however, the data does not show significance (**Figures 1D–F**). These results show that AGWJ treatment promotes enhanced wound healing observed through shorter wound length and hence faster wound closure at the proliferation phase of skin healing in young mice.

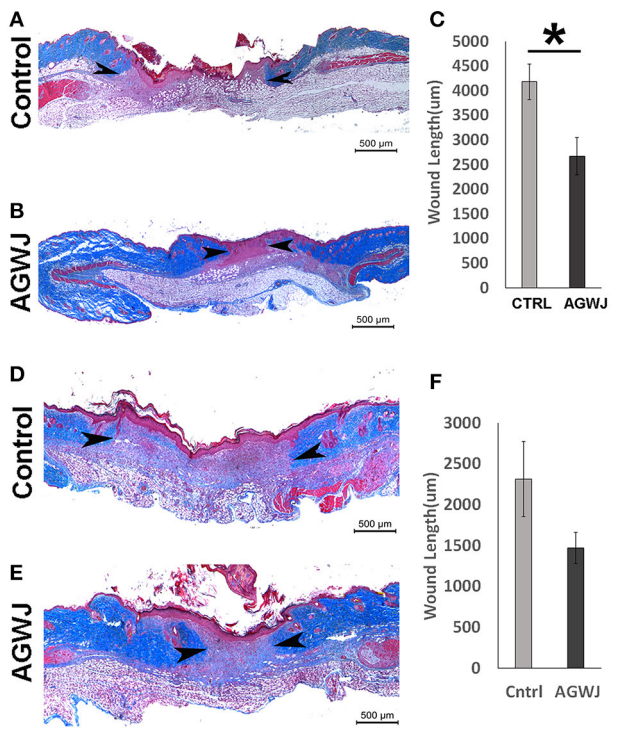

FIGURE 1 | Effect of AGWJ treatment on wound healing *in vivo* after 5 days and 7 days. Wound length was assessed using trichrome staining. **(A)** The representative image displaying the length of a control wound after the 5 day wound healing study. **(B)** A representative AGWJ treated wound displaying the healing at the end of the 5 days. **(C)** Quantitative analysis of the trichrome stain results comparing the wound length between control and AGWJ treated wounds. **(D)** The representative image displaying the length of a control wound after the 7 day wound healing study. **(E)** A representative AGWJ treated wound displaying the healing at the end of the 7 days. **(F)** Quantitative analysis of the trichrome stain results comparing the wound length between control and AGWJ treated wounds. Data shown are mean ± 95% confidence interval. $P<0.05$ compared with control. $N = 3$ for AGWJ and $N = 3$ for control treated mice for the 5 day study. $N = 6$ for control mice for 7 day study, $N = 3$ for treatment mice, each N represents one animal. Black arrow head shows the border of the wound and intact skin. *Indicates the significance of $p < 0.05$ compared to control.

AGWJ Treatment Does Not Affect Cell Proliferation or Cell Viability of Fibroblasts

In an effort to establish the mechanism behind improved wound healing observed in the mice after the treatment of wounds with AGWJ, we aimed to determine if AGWJ treatment affected cell proliferation within the wound. To investigate this, we quantified the total number of cells in the center of the wound bed in high power field (20× magnification). The results did not show a significant difference in cell count between control treated (**Supplemental Figure 2A**) and AGWJ treated wounds (**Supplemental Figure 2B**) for the 5 day (**Supplemental Figure 2C**) time point. For the 7 day time point, the results observed for control treated wounds (**Supplemental Figure 2D**) and AGWJ treated wounds (**Supplemental Figure 2E**) also did not show a significant difference (**Supplemental Figure 2F**) suggesting that AGWJ does not affect cellularity of wounds. Several factors affect cellularity of the tissues including the rate of proliferation. We first measured cell viability *in vitro* in human fibroblasts by exposing the cells to AGWJ and the control media. The results did not show a significant difference in viability between AGWJ and control treated cells (**Supplemental Figure 3**). In order to verify the proliferation state of cells in granulation tissue *in vivo*, we also analyzed BrdU expression through IHC analysis. Positive BrdU protein expression was quantified as a brown stain in the nucleus of fibroblasts in the wound bed at the 5 and 7 day time points. Although the number of BrdU positive cells in the AGWJ treated group (**Figure 2B**) was slightly lower than the control group (**Figure 2A**) at 5 days post wounding (**Figure 2C**) and was higher than the control in 7 days post wounding (**Figure 2F**), the difference in results between AGWJ (**Figures 2B,E**) and controls (**Figures 2A,D**) were not significant. Therefore, collectively our results suggest that AGWJ does not enhance wound healing through modulation of cell proliferation in the wound bed.

Unlike Proliferation, AGWJ Enhances Fibroblast Migration

Since our *in vivo* wound analysis demonstrated that enhanced wound healing post AGWJ treatment was not due to cell proliferation in the wound bed, we investigated the possibility of enhanced cell migration causing faster wound closure. Cellular migration is an essential step during skin healing (Amini-Nik et al., 2011, 2014). To test the effect of AGWJ treatment on cell movement in wound healing, cell migration was analyzed *in vitro* by performing a scratch assay. Human fibroblasts were used as they are the main cellular component of the dermis. Two horizontal scratches were made in a confluent well of fibroblasts and either control media or AGWJ treatment was added. Images were taken at $t = 0$ h and $t = 24$ h (**Figure 3A**). After 24 h we quantified cell infiltration within the scratch zone and observed a significantly higher number of cells in the scratch zone for the AGWJ treated scratches as compared to the controls. For the control treated cells, an average of 58.85 ± 22.95 fibroblasts had migrated into the scratch zone, for AGWJ

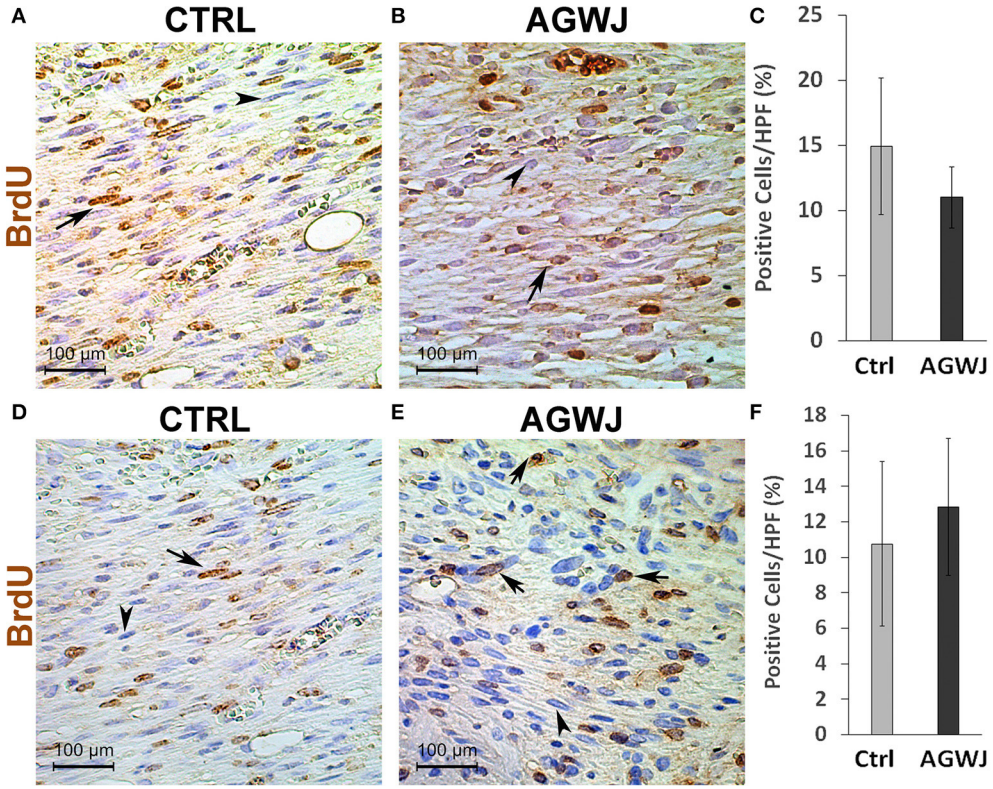

FIGURE 2 | BrdU analysis of cell proliferation in the wound bed after AGWJ treatment compared to controls. **(A)** Representative IHC image displaying BrdU-positive cells in the wound bed of a control treated wound after 5 day time point. **(B)** BrdU-positive cells in an AGWJ treated wound after 5 day time point. **(C)** Quantification of BrdU-positive cells in the wound bed after AGWJ treatment for 5 day time point compared with control treatment. The graph shows the percentage of BrdU positive cells per high power field (40×). **(D)** Representative IHC image displaying BrdU-positive cells in the wound bed of a control treated wound after 7 day time point. **(E)** BrdU-positive cells in an AGWJ treated wound after 7 day time point. **(F)** Quantification of BrdU-positive cells in the wound bed after AGWJ treatment for 7 days compared with control treatment. The graph shows the percentage of BrdU positive cells per high power field (40×). Data shown are mean ± 95% confidence interval. For the 7 day study, $N = 7$ for AGWJ treated mice and $N = 6$ for control mice. For the 5 day study, $N = 3$ for AGWJ and $N = 3$ for control treated mice. Each N represents one animal. Black arrows point to BrdU positive brown stained nuclei and arrow heads point to BrdU negative blue nuclei.

an average of 117.33 ± 22.86 cells migrated into the scratch ($n = 3$ control and $n = 3$ AGWJ, $^{**}p < 0.01$) (**Figure 3B**). Therefore, as shown in **Figure 3A**, the AGWJ treated fibroblast cells had started to close the wound after 24 h whereas the control cells had minimal migration into the scratch zone. Thus, AGWJ treatment of fibroblasts promotes their migration ability. We also observed that the AGWJ treatment altered cell morphology for fibroblasts. After 24 h the fibroblasts appeared to attain a more elongated phenotype as compared to the control media treated cells.

AGWJ Treatment Promotes Myofibroblastic Phenotype *In Vitro*

Since we detected a smaller wound size in the AGWJ treated wounds *in vivo* and our *in vitro* results demonstrated enhanced cell migration after AGWJ treatment, our findings support the notion that AGWJ augments cell migration. And that improved cell migration is the underlying mechanism for faster wound healing. Moreover, as mentioned, we observed a change in the phenotype of the cells treated with AGWJ *in vitro* and a smaller wound size *in vivo*, both of which suggest a pro myo-fibroblastic phenotype due to AGWJ treatment occurring earlier which led to faster contraction which is characteristic of enhanced wound healing. To evaluate this *in vitro*, we treated fibroblasts with AGWJ or control media and observed through immunofluorescence analysis that αSMA protein is increased dramatically in fibroblasts after AGWJ treatment (**Figure 4B**) as compared with control treated cells (**Figure 4A**). This result was corroborated by western blot analysis which detected a dramatically higher level of αSMA protein expression in AGWJ treated fibroblasts for two different human fibroblast samples (**Figure 4C**). The western blot band densitometry for αSMA was normalized to GAPDH and the quantification shows an almost 8-fold increase in αSMA protein levels after AGWJ treatment as compared with control DMEM media (**Figure 4D**). Furthermore, normal human fibroblasts display high levels of vimentin, which is reduced after AGWJ treatment for 24 h, observed in two different human fibroblast samples through western blot analysis (**Supplemental Figure 4**).

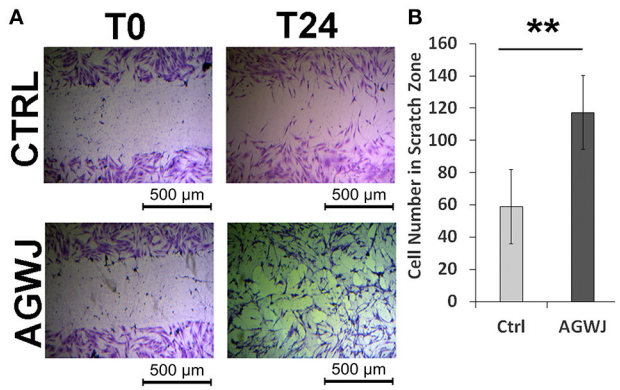

FIGURE 3 | Analysis of cell migration *in vitro* for fibroblasts. (A) The top panel shows representative images of a control treated scratch at time point 0 h compared with the control treated scratch after 24 h. The lower panel displays the fibroblast scratch assay with AGWJ treatment at time point 0 h and then the scratch zone is imaged after incubation with AGWJ for 24 h. **(B)** The graph shows the average number of fibroblast cells that have infiltrated the scratch zone after 24 h for control media treated cells compared to AGWJ treated cells. **Indicates the significance of $p < 0.01$ compared to control.

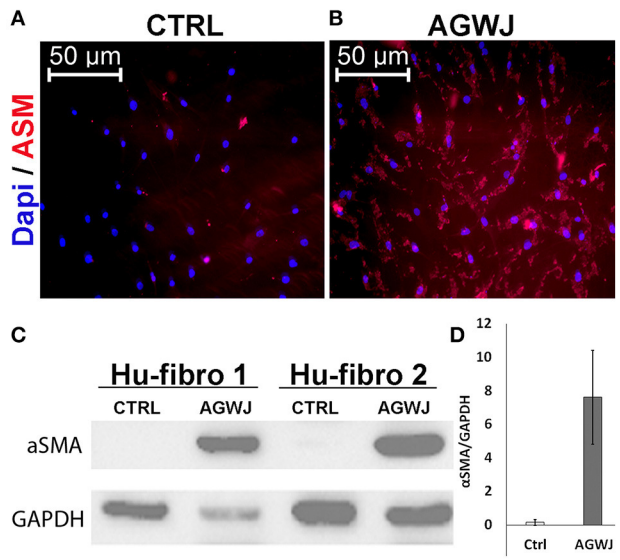

FIGURE 4 | AGWJ treatment promotes myofibroblastic phenotype *in vitro* detected through αSMA expression. (A) Immunofluorescence image of control media treated fibroblasts compared with **(B)** AGWJ treated fibroblasts after 24 h of treatment. DAPI blue fluorescence represents nucleus and rhodamine red represents αSMA. **(C)** Western blot analysis of two normal human fibroblast cells (Hu-Fibro) treated with either control DMEM media or AGWJ treatment for 24 h in order to analyze αSMA protein expression. Loading control was GAPDH protein. **(D)** Densitometry analysis of the western blot. αSMA protein expression was normalized to GAPDH.

AGWJ Augments the Differentiation of Fibroblasts to Myofibroblasts in the Wound Bed

Because we detected an elevated level of αSMA in fibroblasts *in vitro*, which is a characteristic of myofibroblasts we wanted to investigate if this result is translated *in vivo*. Immunohistochemistry analysis of αSMA in wounds excised from the day 5 and day 7 time points demonstrate that for the 5 day time point; the AGWJ treated wounds express higher levels of αSMA (**Figure 5B**) whereas the control wounds express very little to no αSMA (**Figure 5A**). Surprisingly, in contrast, for the 7 day time point, we detected that the wound beds for both the AGWJ treatment (**Figure 5D**) and the control treatment (**Figure 5C**) both expressed high levels of αSMA. Hence, it appears that AGWJ accelerates the wound healing process through earlier fibroblast differentiation into myofibroblasts as seen at day 5, and therefore shortens the proliferation phase of skin wound healing.

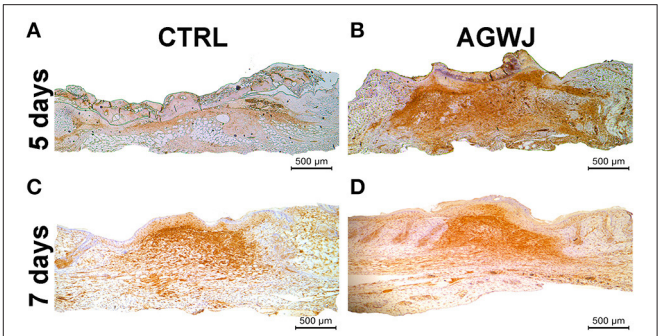

FIGURE 5 | Effect of AGWJ treatment on αSMA expression in the wound bed *in vivo*. (A) αSMA expression in the granulation tissue of control treated wounds after 5 days. **(B)** αSMA expression in the granulation tissue of AGWJ treated wounds after 5 days. **(C)** αSMA expression in the granulation tissue of control treated wounds after 7 days. **(D)** αSMA expression in the granulation tissue of AGWJ treated wounds after 7 days.

DISCUSSION

There is a substantial amount of literature which investigate the beneficial effects of cellular therapy with WJ-MSCs, alone or within a scaffold (Zebardast et al., 2010; Azari et al., 2011; Shohara et al., 2012; Arno et al., 2014; Fong et al., 2014; Ribeiro et al., 2014; Sabapathy et al., 2014). Emerging reports are showing the promising role of decellularized biological matrices for tissue repair (Boccafoschi et al., 2015). Our group has reported that WJ-MSCs conditioned-medium has positive effects on wound healing in human *in vivo* in full-thickness skin excisional wounds on a mouse model through paracrine signaling via several mechanisms: upregulation of wound healing factors' gene expression, such as TGF-ß2, HIF-1α and PAI-1 in addition to enhancing human skin fibroblasts proliferation and migration (Arno et al., 2014). It is known that the niche or microenvironment of stem cells is crucial in supporting the MSCs and that there is significant cross talk and signaling that occurs between the cells and the environment (Boccafoschi et al., 2015; Khodadi et al., 2016). Moreover, there is the secretome of stem cells which is within the Wharton's jelly. In addition to being a reservoir of MSCs, Wharton's Jelly has been reported to be a great source of pro-angiogenic and wound healing promoting factors, such as IGF-1, TGF-ß1, VEGF, PDGF, EGF, bFGF, HGF, IL-6, and IL-8 (Sobolewski et al., 2005; Liu et al., 2012; Arno et al., 2014;

Biazar, 2014; Edwards et al., 2014). These factors are also believed to stimulate the cells within Wharton's Jelly to produce large amounts of ECM components (Sobolewski et al., 2005). Because AGWJ is present in the native niche of MSCs and supports these stem cells, in addition to being a source of wound healing factors, we hypothesized that AGWJ has beneficial effects on skin wound healing. We, therefore, isolated the Wharton's jelly, and acellularized it (**Supplemental Figure 1**). In the umbilical cord, whether AGWJ promotes stem cell behavior and supports these MSCs in their niche or whether other cell types contribute to the microenvironment and consequently affects stem cell behavior is unknown.

The findings from this study established that AGWJ leads to healing at an earlier time point in a murine model demonstrated a significant reduction in wound length after AGWJ treatment as compared to control treatment after 5 days. We chose 5 days and 7 days as our time points for this study because, in a mouse model, day 5 is considered the peak of proliferation phase and day 7 is the start of the wound maturation phase in wound healing (Bielefeld et al., 2013). Despite the positive effect on wound healing of young animals that we report here, it is yet to be determined whether this effect can rescue deficient healing observed in elderly or diabetic patients. More research is warranted to address their effect on a deficient skin healing model.

We also tried to understand the mechanism of the enhanced wound healing through investigating several possible mechanisms, such as: cell viability, cell proliferation, and cell migration. We started by investigating cellularity in the wound by doing a cell count in the granulation tissue at HPF and also detecting cell proliferation through BrdU staining of the wounds. The results did not show any significant difference between AGWJ and controls. Therefore, our *in vivo* wound analysis suggests that enhanced wound healing post AGWJ treatment was not due to an increase in cell number. To further characterize this observation *in vitro*, we performed a viability assay using AGWJ and control media treatment. Cell proliferation can have an effect on cell viability and hence cellularity. Again, our data showed that AGWJ does not affect the viability of fibroblasts *in vitro*. Taken together, this set of data establishes that AGWJ's mechanism of action is not through enhancing proliferation, viability, and cellularity of cells.

We next investigated the possibility of enhanced cell migration causing faster wound closure. Cell motility and migration play critical roles during wound healing (Schneider et al., 2010; Amini-Nik et al., 2014). Indeed our *in vitro* results confirmed that AGWJ causes increased fibroblast migration. Moreover, we observed a change in the phenotype of the fibroblast cells treated with AGWJ and a smaller wound size *in vivo*, both of which suggest a pro myo-fibroblastic phenotype. IHC analysis of the wounds for αSMA showed an enhanced expression of αSMA in the granulation tissue after 5 days in comparison to control treated wounds. Surprisingly at the 7 day time point the αSMA expression in control and AGWJ treated wounds seems to be even. This suggests that AGWJ accelerates the proliferation phase of wound healing by causing a faster differentiation of fibroblasts to myofibroblasts confirmed through αSMA expression. The control wounds follow their normal course of differentiation and catch up later at 7 days post wounding. This result was supported by our *in vitro* analysis of fibroblasts post AGWJ treatment which showed an elevated expression of αSMA protein expression compared to controls.

This report shows for the first time that AGWJ enhances wound healing by accelerating the proliferation phase of skin healing mainly through enhancing cell migration and wound closure. Several diseases, including wounds in diabetic patients of elderly patients, are associated with delayed wound healing and AGWJ might be a remedy for this group of patients. Although we have found a mechanism through TGF-beta signaling pathway for the positive effect of AGWJ on skin healing, it is yet to be verified whether other factors that might contribute to this observation. Future research should focus on the further characterization of AGWJ and to find the active ingredients, particularly for the components of signaling pathways which have essential roles during skin healing, such as Wnt/β-catenin as well as TGF-β/Smad 2 signaling pathways (Amini Nik et al., 2007; Poon et al., 2009; Bielefeld et al., 2011). Since the AGWJ enhances wound healing mainly through cell migration and not cell proliferation, it might be an ideal remedy for the deficient skin healings which are associated with deficient migration. We have recently reported that elderly burn patients have reduced stem cell pool, a deficient migration of MSC and an altered activation of crucial signaling pathways for skin healing (Jeschke et al., 2015). Therefore, since our data suggests that AGWJ enhances cell migration, causes an earlier differentiation of fibroblasts to myofibroblasts and hence allows for earlier wound contraction, this treatment can have significant wound healing benefits, particularly for this group of patients.

Economy of AGWJ

The findings from this study demonstrate the discovery of AGWJ which is the very native and niche material of stem cells within umbilical cords for the purpose of skin wound healing. We collect approximately 5 ml of jelly from each umbilical cord. To this 5 ml of jelly, we added 15 ml of DMEM complete media and re-suspended the jelly so that we had a total of 20 ml solution. For our *in vivo* study on mice, we placed 50 ul of AGWJ solution mixed with 50 ul of matrigel (1:1) on each wound, covering and enhancing 0.3 cm^2 area of the wound in the animal. Collectively each umbilical cord provides AGWJ material for approximately 115 cm^2 area of the wound (**Supplemental Figure 5**). Unlike the secretome of MSCs which needs an equipped facility to isolate, isolation of AGWJ needs minimal equipment and can be performed in any facility in developing countries.

In conclusion, we demonstrate for the first time that AGWJ enhances wound healing and establish a mechanism for its role as a potential therapeutic modality for deficient skin wound healing. Because each umbilical cord provides approximately enough AGWJ to cover 115 cm^2 area of a wound, is easy to isolate and it is available globally; umbilical cord AGWJ has far reaching benefits for wound healing not just in the developed world but also in developing countries where affordable and available wound healing remedies are of critical need.

AUTHOR CONTRIBUTIONS

NB, MJ, and SA have made substantial contributions to the conception and design, data acquisition, data analysis and interpretation for this study. NB and SA were responsible for creating the animal wound model and with the help of LM these authors were responsible for the organization, analysis and interpretation of the *in-vivo* data. NB performed the cell culture and *in-vitro* experiments. LM performed data analysis blinded. EH performed the surgeries to obtain the umbilical cords for the study. SA and NB contributed to the writing of the manuscript and performing revisions. All authors gave provided approval of this version of the manuscript to be published.

ACKNOWLEDGMENTS

Ms. Jennifer He, Ms. Andrea Kaye Datu and funding agencies Toronto Hydro and Medicine by Design-Seed grant (EMHSeed Award Feb16/2016).

SUPPLEMENTARY MATERIAL

The Supplementary Material for this article can be found online at: http://journal.frontiersin.org/article/10.3389/fphys.2017.00200/full#supplementary-material

Supplemental Figure 1 | Decellularization of Wharton's Jelly. The degree of decellularization of Wharton's jelly was assessed using DAPI immunofluorescence staining nuclei. Panel one shows complete WJ before decellularization with many cells, panel two shows AGWJ without any cells.

Supplemental Figure 2 | Effect of AGWJ treatment on cellularity in the wound bed. (A) Trichome stain analysis used to quantify the cell number in the wound center. **(A)** Representative image showing cellularity in the wound bed after 5 days of control treatment. **(B)** Image showing cellularity in wound bed post AGWJ treatment after 5 day time point. **(C)** Quantification of average cell number within the wound bed comparing control treated wounds with AGWJ treated wounds after 5 days. **(D)** The representative image displaying cellularity in the wound bed after 7 days of control treatment. **(E)** Image showing cellularity in wound bed post AGWJ treatment for 7 day time point. **(F)** Quantification of average cell number within the wound bed comparing control treated wounds with AGWJ treated wounds post 7 day treatment. The graph shows the average cell number in the wound bed of control compared to AGWJ treated mice under 20× magnification. Data shown are mean ± 95% confidence interval. For the 7 day study $N = 7$ for AGWJ treated mice and $N = 6$ for control mice, each n represents one animal. For the 5 day study, $N = 3$ for AGWJ and $N = 3$ for control treated mice.

Supplemental Figure 3 | AGWJ does not affect fibroblast viability *in vitro.* Quantitative analysis of cell viability post control and AGWJ treatment for 24 h. Luminescence was read using the Synergy H4 hybrid multi-mode microplate reader.

Supplemental Figure 4 | AGWJ treatment reduces vimentin expression in fibroblasts. Western blot analysis of two normal human fibroblast cells (Hu-Fibro) treated with either control DMEM media or AGWJ treatment for 24 h. Loading control was GAPDH protein.

Supplemental Figure 5 | Schematic illustrating the isolation procedure for AGWJ and the subsequent economical use of AGWJ as a remedy for wound healing.

REFERENCES

Amini-Nik, S., Cambridge, E., Yu, W., Guo, A., Whetstone, H., Nadesan, P., et al. (2014). β-Catenin-regulated myeloid cell adhesion and migration determine wound healing. *J. Clin. Invest.* 124, 2599–2610. doi: 10.1172/JCI62059

Amini Nik, S., Ebrahim, R. P., Van Dam, K., Cassiman, J. J., and Tejpar, S. (2007). TGF-beta modulates beta-Catenin stability and signaling in mesenchymal proliferations. *Exp. Cell Res.* 313, 2887–2895. doi: 10.1016/j.yexcr.2007.05.024

Amini-Nik, S., Glancy, D., Boimer, C., Whetstone, H., Keller, C., Alman, B., et al. (2011). Pax7 expressing cells contribute to dermal wound repair, regulating scar size through a beta-catenin mediated process. *Stem Cells* 29, 1371–1379. doi: 10.1002/stem.688

Arno, A. I., Amini-Nik, S., Blit, P. H., Al-Shehab, M., Belo, C., Herer, E., et al. (2014). Effect of human Wharton's jelly mesenchymal stem cell paracrine signaling on keloid fibroblasts. *Stem Cells Transl. Med.* 3, 299–307. doi: 10.5966/sctm.2013-0120

Atiyeh, B. S., Ioannovich, J., Al-Amm, C. A., and El-Musa, K. A. (2002). Management of acute and chronic open wounds: the importance of moist environment in optimal wound healing. *Curr. Pharm. Biotechnol.* 3, 179–195. doi: 10.2174/1389201023378283

Azari, O., Babaei, H., Derakhshanfar, A., Nematollahi-Mahani, S. N., Poursahebi, R., and Moshrefi, M. (2011). Effects of transplanted mesenchymal stem cells isolated from Wharton's jelly of caprine umbilical cord on cutaneous wound healing; histopathological evaluation. *Vet. Res. Commun.* 35, 211–222. doi: 10.1007/s11259-011-9464-z

Biazar, E. (2014). Use of umbilical cord and cord blood-derived stem cells for tissue repair and regeneration. *Expert Opin. Biol. Ther.* 14, 301–310. doi: 10.1517/14712598.2014.867943

Bielefeld, K. A., Amini-Nik, S., and Alman, B. A. (2013). Cutaneous wound healing: recruiting developmental pathways for regeneration. *Cell. Mol. Life Sci.* 70, 2059–2081. doi: 10.1007/s00018-012-1152-9

Bielefeld, K. A., Amini-Nik, S., Whetstone, H., Poon, R., Youn, A., Wang, J., et al. (2011). Fibronectin and beta-catenin act in a regulatory loop in dermal fibroblasts to modulate cutaneous healing. *J. Biol. Chem.* 286, 27687–27697. doi: 10.1074/jbc.M111.261677

Boccafoschi, F., Botta, M., Fusaro, L., Copes, F., Ramella, M., and Cannas, M. (2015). Decellularized biological matrices: an interesting approach for cardiovascular tissue repair and regeneration. *J. Tissue Eng. Regen. Med.* doi: 10.1002/term.2103. [Epub ahead of print].

Branski, L. K., Gauglitz, G. G., Herndon, D. N., and Jeschke, M. G. (2009). A review of gene and stem cell therapy in cutaneous wound healing. *Burns* 35, 171–180. doi: 10.1016/j.burns.2008.03.009

Du, T., Zou, X., Cheng, J., Wu, S., Zhong, L., Ju, G., et al. (2013). Human Wharton's jelly-derived mesenchymal stromal cells reduce renal fibrosis through induction of native and foreign hepatocyte growth factor sythesis in injured tubular epithelial cells. *Stem Cell Res. Ther* 4:59. doi: 10.1186/scrt215

Edmondson, S. R., Thumiger, S. P., Werther, G. A., and Wraight, C. J. (2003). Epidermal homeostasis: the role of the growth hormone and insulin-like growth factor systems. *Endocr. Rev.* 24, 737–764. doi: 10.1210/er.2002-0021

Edwards, S. S., Zavala, G., Prieto, C. P., Elliott, M., Martínez, S., Egaña, J. T., et al. (2014). Functional analysis reveals angiogenic potential of human mesenchymal stem cells from Wharton's jelly in dermal regeneration. *Angiogenesis* 17, 851–866. doi: 10.1007/s10456-014-9432-7

Fong, C. Y., Tam, K., Cheyyatraivendran, S., Gan, S. U., Gauthaman, K., Armugam, A., et al. (2014). Human Wharton's jelly stem cells and its conditioned medium enhance healing of excisional and diabetic wounds. *J. Cell. Biochem.* 115, 290–302. doi: 10.1002/jcb.24661

Gosain, A., and DiPietro, L. A. (2004). Aging and wound healing. *World J. Surg.* 28, 321–326. doi: 10.1007/s00268-003-7397-6

Jeschke, M. G., Patsouris, D., Stanojcic, M., Abdullahi, A., Rehou, S., Pinto, R., et al. (2015). Pathophysiologic response to burns in the elderly. *EBioMedicine* 2, 1536–1548. doi: 10.1016/j.ebiom.2015.07.040

Jeschke, M. G., Pinto, R., Costford, S. R., and Amini-Nik, S. (2016). Threshold age and burn size associated with poor outcomes in the elderly after burn injury. *Burns* 42, 276–281. doi: 10.1016/j.burns.2015.12.008

Khodadi, E., Shahrabi, S., Shahjahani, M., Azandeh, S., and Saki, N. (2016). Role of stem cell factor in the placental niche. *Cell Tissue Res.* 366, 523–531. doi: 10.1007/s00441-016-2429-3

Liu, S., Yuan, M., Hou, K., Zhang, L., Zheng, X., Zhao, B., et al. (2012). Immune characterization of mesenchymal stem cells in human umbilical cord Wharton's jelly and derived cartilage cells. *Cell. Immunol.* 278, 35–44. doi: 10.1016/j.cellimm.2012.06.010

Marfia, G., Navone, S. E., Di Vito, C., Ughi, N., Tabano, S., Miozzo, M., et al. (2015). Mesenchymal stem cells: potential for therapy and treatment of chronic non-healing skin wounds. *Organogenesis* 11, 183–206. doi: 10.1080/15476278.2015.1126018

Markeson, D., Pleat, J. M., Sharpe, J. R., Harris, A. L., Seifalian, A. M., and Watt, S. M. (2015). Scarring, stem cells, scaffolds and skin repair. *J. Tissue Eng. Regen. Med.* 9, 649–668. doi: 10.1002/term.1841

McElreavey, K. D., Irvine, A. I., Ennis, K. T., and McLean, W. H. (1991). Isolation, culture and characterisation of fibroblast-like cells derived from the Wharton's jelly portion of human umbilical cord. *Biochem. Soc. Transact.* 19:29s. doi: 10.1042/bst019029s

Moodley, Y., Atienza, D., Manuelpillai, U., Samuel, C. S., Tchongue, J., Ilancheran, S., et al. (2009). Human umbilical cord mesenchymal stem cells reduce fibrosis of bleomycin-induced lung injury. *Am. J. Pathol.* 175, 303–313. doi: 10.2353/ajpath.2009.080629

Nicholas, M. N., Jeschke, M. G., and Amini-Nik, S. (2016a). Cellularized bilayer pullulan-gelatin hydrogel for skin regeneration. *Tissue Eng. Part A* 22, 754–764. doi: 10.1089/ten.tea.2015.0536

Nicholas, M. N., Jeschke, M. G., and Amini-Nik, S. (2016b). Methodologies in creating skin substitutes. *Cell. Mol. Life Sci.* 73, 3453–3472. doi: 10.1007/s00018-016-2252-8

Nunan, R., Harding, K., G., and Martin, P. (2014). Clinical challenges of chronic wounds: searching for an optimal animal model to recapitulate their complexity. *Dis. Models Mechan.* 7, 1205–1213. doi: 10.1242/dmm.016782

Pirjali, T., Azarpira, N., Ayatollahi, M., Aghdaie, M. H., Geramizadeh, B., and Talai, T. (2013). Isolation and characterization of human mesenchymal stem cells derived from human umbilical cord wharton's jelly and amniotic membrane. *Int. J. Organ Transplant. Med.* 4, 111–116.

Poon, R., Nik, S. A., Ahn, J., Slade, L., and Alman, B. A. (2009). Beta-catenin and transforming growth factor beta have distinct roles regulating fibroblast cell motility and the induction of collagen lattice contraction. *BMC Cell Biol.* 10:38. doi: 10.1186/1471-2121-10-38

Ribeiro, J., Pereira, T., Amorim, I., Caseiro, A. R., Lopes, M. A., Lima, J., et al. (2014). Cell therapy with human MSCs isolated from the umbilical cord Wharton jelly associated to a PVA membrane in the treatment of chronic skin wounds. *Int. J. Med. Sci.* 11, 979–987. doi: 10.7150/ijms.9139

Sabapathy, V., Sundaram, B., V. M. S., Mankuzhy, P., and Kumar, S. (2014). Human Wharton's Jelly Mesenchymal Stem Cells plasticity augments scar-free skin wound healing with hair growth. *PLoS ONE* 9:*E*93726. doi: 10.1371/journal.pone.0093726

Schneider, L., Cammer, M., Lehman, J., Nielsen, S. K., Guerra, C. F., Veland, I. R., et al. (2010). Directional cell migration and chemotaxis in wound healing response to PDGF-AA are coordinated by the primary cilium in fibroblasts. *Cellular Physiol. Biochem.* 25, 279–292. doi: 10.1159/000276562

Shalitin, N., Schlesinger, H., Levy, M. J., Kessler, E., and Kessler-Icekson, G. (2003). Expression of procollagen C-proteinase enhancer in cultured rat heart fibroblasts: evidence for co-regulation with type I collagen. *J. Cell. Biochem.* 90, 397–407. doi: 10.1002/jcb.10646

Shohara, R., Yamamoto, A., Takikawa, S., Iwase, A., Hibi, H., Kikkawa, F., et al. (2012). Mesenchymal stromal cells of human umbilical cord Wharton's jelly accelerate wound healing by paracrine mechanisms. *Cytotherapy* 14, 1171–1181. doi: 10.3109/14653249.2012.706705

Singer, A. J., and Clark, R. A. (1999). Cutaneous wound healing. *N. Eng. J. Med.* 341, 738–746. doi: 10.1056/NEJM199909023411006

Sobolewski, K., Malkowski, A., Bankowski, E., and Jaworski, S. (2005). Wharton's jelly as a reservoir of peptide growth factors. *Placenta* 26, 747–752. doi: 10.1016/j.placenta.2004.10.008

Valacchi, G., Zanardi, I., Sticozzi, C., Bocci, V., and Travagli, V. (2012). Emerging topics in cutaneous wound repair. *Ann. N.Y. Acad. Sci.* 1259, 136–144. doi: 10.1111/j.1749-6632.2012.06636.x

Whitney, J. D. (2005). Overview: acute and chronic wounds. *Nurs. Clin. North Am.* 40, 191–205. doi: 10.1016/j.cnur.2004.09.002

Yu, C., Wang, F., Jin, C., Huang, X., Miller, D. L., Basilico, C., et al. (2003). Role of fibroblast growth factor type 1 and 2 in carbon tetrachloride-induced hepatic injury and fibrogenesis. *Am. J. Pathol.* 163, 1653–1662. doi: 10.1016/S0002-9440(10)63522-5

Zebardast, N., Lickorish, D., and Davies, J. E. (2010). Human umbilical cord perivascular cells (HUCPVC): a mesenchymal cell source for dermal wound healing. *Organogenesis* 6, 197–203. doi: 10.4161/org.6.4.12393

Conflict of Interest Statement: The authors declare that the research was conducted in the absence of any commercial or financial relationships that could be construed as a potential conflict of interest.

frontiers in Physiology

ORIGINAL RESEARCH
published: 06 December 2017
doi: 10.3389/fphys.2017.01004

P311 Deficiency Leads to Attenuated Angiogenesis in Cutaneous Wound Healing

Song Wang[1], Xiaorong Zhang[1], Wei Qian[1], Daijun Zhou[1], Xunzhou Yu[1], Rixing Zhan[1], Ying Wang[1], Jun Wu[2], Weifeng He[1] and Gaoxing Luo[1]**

[1] State Key Laboratory of Trauma, Burn and Combined Injury, Institute of Burn Research, Southwest Hospital, Third Military Medical University, Chongqing, China, [2] Department of Burns, The First Affiliated Hospital of Sun Yat-sen University, Guangzhou, China

P311 was identified to markedly promote cutaneous wound healing by our group. Angiogenesis plays a key role in wound healing. In this study, we sought to define the role of P311 in skin wound angiogenesis. It was noted that P311 was expressed in endothelial cells in the dermis of murine and human skin wounds. The expression of P311 was confirmed in cultured murine dermal microvascular endothelial cells (mDMECs). Moreover, it was found that knockout of P311 could attenuate the formation of tubes and motility of mDMECs significantly *in vitro*. In the subcutaneous Matrigel implant model, the angiogenesis was reduced significantly in P311 knockout mice. In addition, wound healing was delayed in P311 knockout mice compared with that in the wild type. Granulation tissue formation during the defective wound healing showed thinner and blood vessel numbers in wound areas in P311 knockout mice were decreased significantly. A reduction in VEGF and TGFβ1 was also found in P311 KO mice wounds, which implied that P311 may modulate the exprssion of VEGF and TGFβ1 in wound healing. Together, our findings suggest that P311 plays an important role in angiogenesis in wound healing.

Keywords: wound healing, angiogenesis, P311, dermal microvascular endothelial cells, matrigel plug assay

OPEN ACCESS

Edited by:
Marianna Bei,
Harvard Medical School, Harvard University, United States

Reviewed by:
Riikka Kivelä,
University of Helsinki, Finland
Enzo Spisni,
Università di Bologna, Italy

****Correspondence:***
Weifeng He
whe761211@aliyun.com
Gaoxing Luo
logxw@yahoo.com

Specialty section:
This article was submitted to Clinical and Translational Physiology, a section of the journal Frontiers in Physiology

Received: *18 September 2017*
Accepted: *21 November 2017*
Published: *06 December 2017*

Citation:
Wang S, Zhang X, Qian W, Zhou D, Yu X, Zhan R, Wang Y, Wu J, He W and Luo G (2017) P311 Deficiency Leads to Attenuated Angiogenesis in Cutaneous Wound Healing. Front. Physiol. 8:1004. doi: 10.3389/fphys.2017.01004

INTRODUCTION

P311 (also known as PTZ17, Neuronal protein 3.1) is a highly conserved 8-kDa intracellular protein containing 68 amino acids (Yao et al., 2017). Following firstly identified to expressed in the embryonic brain in mice by Studler (Studler et al., 1993), P311 was found to express in almost all kinds of cells, like motoneurons (Fujitani et al., 2004), kidney tubular epithelial cells (Yao et al., 2015), glioblastomas (McDonough et al., 2005), epidermal stem cells (Li et al., 2016), fibroblast (Tan et al., 2010; Cheng et al., 2017), smooth muscle cells (Badri et al., 2013), which implied wide biological functions of P311. Actually, P311 has been shown to promote the nerve (Fujitani et al., 2004) and lung regeneration (Zhao et al., 2006), glioma invasion (McDonough et al., 2005), and to induce myofibroblast differentiation (Pan et al., 2002; Tan et al., 2010; Li et al., 2016), cell migration (McDonough et al., 2005; Yao et al., 2017). Moreover, a decreased vascular smooth muscle cell contractility, hypotonic blood vessels, and vascular hypotension was found in P311 knockout mice compared with the wild type (Badri et al., 2013), and even a changed behavioral responses in learning and memory (Taylor et al., 2008).However, the molecular mechanisms of P311 biological

function have remained unknown. Once the PEST domain (rich in Pro, Glu, Ser, and Thr) in the N-terminus of P311 was thought to be the functional motif that might be the mechanism to indicate function, as the domain also found in short-lived proteins such as transcription factors, cytokines, and signal molecules (Sommer and Wolf, 2014; Varshavsky, 2014). More recently, we found that P311 could increased the activity of Rho A and Rac1 (Yao et al., 2017), which are critical signal transducers for inducing the formation of lamellipodia, filopodia, invadopodia, and blebs during cell migration (Sadok and Marshall, 2014). In addition, P311 was identified as a inducer of EpMyT $(Epidermal stem cell transdifferentiate into myofibroblasts) through TGFβ1/Smad signaling (Li et al., 2016).

Angiogenesis, the process by which new blood vessels are established from preexisting ones (Carmeliet, 2005), is critical to wound healing (Johnson and Wilgus, 2014). Microvascular endothelial cells are the principal parenchymal cells participating in wound angiogenesis (Tonnesen et al., 2000) that involves a phenotypic alteration of endothelial cells, directed migration, and various mitogenic stimuli (Li et al., 2003). Our previous studies demonstrated that P311 was a crucial factor in wound healing (Li et al., 2016; Yao et al., 2017). However, the possible role of P311 in cutaneous wounds angiogenesis was still unknown.

Here we stated that in skin wound healing P311 deficiency resulted in an attenuated angiogenesis. Immunofluorescence results manifested that dermal microvascular endothelial cells expressed protein P311 and highly expressed it under the injury condition, indicating a potential role for P311 in angiogenesis. We then found that a deficiency of P311 decreased the function of endothelial cells (ECs) *in vitro* and angiogenesis in subcutaneous Matrigel plugs *in vivo*. In addition, in full-thickness excisional skin wounds, we observed that P311 knockout leaded a weakened angiogenic response and tissue repair.

MATERIALS AND METHODS

Human Skin Wound Tissues

Human skin wound specimens were obtained from 4 patients whose limbs or trunks suffered injury from flame or boiling water with the patient's consent. Ethics approval was granted by the Medical and Ethical Committees of the Southwest Hospital, the Third Military Medical University.

Mice

The P311 knockout (KO) mice were created, characterized, and genotyped as described previously (Taylor et al., 2008) and kindly gifted by Prof. Gregory A Taylor. All the mice were maintained in the Animal Institutes of Daping Hospital, the Third Military Medical University, with the animal license SCXK(J)2007-017. All protocols involving animals were considered and approved by the Southwestern Hospital Institutional Review Board.

Culture and Characterization of mDMECs

Murine dermal microvascular endothelial cells (mDMECs) were isolated from 3-day-old mouse skin and purified them using magnetic sorting method as reported before (Talavera-Adame et al., 2011) with some modifications. Briefly, the whole skin sheets were washed twice with sterile PBS, cut into 5 × 5 mm pieces, washed again with PBS and digested with 0.5 g/l of Dispase II (04942078001; Roche) at 4°C overnight. Next, the epidermis were kept separate from dermis carefully. The dermal sheets were incubated in 10 ml Medium 199 (M0393, Sigma) containing 40 mg collagenase I (LS004196, Worthington), 0.01% DNase I, and 2% FBS for 45 min at 37°C to release cells. The isolated cells were subjected to purification by magnetic activated cell sorting (MACS) at Passage0 and Passage 2 with CD31 MicroBeads (130-097-418, Miltenyl Biotec). Magnetic sorting was performed by MACS kit according to manufacturer's instructions. The complete medium containing Medium 131, Kit (M131500, Gibco), Microvascular Growth Supplement (MVGS) (S00525, Gibco), 10% fetal bovine serum (FBS) (10099141, Gibco) and 100 U/mL of penicillin and streptomycin (15140122, Gibco) was used to culture the cells. The mDMECs were characterized by CD31 and CD34 as described previously (Cha et al., 2005). FITC-conjugated specific CD31 (11-0311-8, Bioscience) and PE-conjugated specific CD34 (119307, Biolegend) were used to identify the cells with Attune Acoustic Focusing Cytometer (Applied Biosystems, Life Technologies, CA, USA).

Quantitative Real-Time PCR

Total RNA was extracted from cells with the RNeasy Mini Kit (QIAGEN, 74104). According to the manufacturer's instructions, we synthesized the cDNA with a cDNA Synthesis Kit (TOYOBO, FSK-100). SYBR Green Master Mix (Toyobo, QPK-201) was used to perform the Real-time PCR on 7500 Real Time PCR System (Applied Biosystems Instruments) with the following primer: P311, 5′-GAGGCTTCCTAAGGGAAGACTT-3′ and 5′-AAGTGGAGGTAAC TGATTCTTGG-3′; GAPDH, 5′-CGTGCCGCCTGGAGAAAC-3′ and 5′-AGTGGGAGTTGCTGTTGAAGTC-3′.

Tube Formation Assay *in Vitro*

As described previously (DeCicco-Skinner et al., 2014), 2×10^4 mDMECs were seeded into each well of 96-well plate, which was coated with Matrigel. Eight hours later, the tube formation was photographed. The number of nobes and length of tubes was measured by the ImageJ 1.48V software (NIH, USA). Each group has six replicates in one experiment. The experiment was repeated for three times.

Scratch Wound Migration Assay

As described previously (Yao et al., 2017), the 2×10^4 mDMECs were seeded into each well of 24-well plates with complete medium and cultured to reach confluence. The scratching wounds were created in the monolayer (0 h) with the pipette tips and then monitored for 24 h using a Zeiss video microscope. Measurements were performed using ImageJ 1.48V software (NIH, USA). Each group has six replicates in one experiment. The experiment was repeated for three times.

Proliferation Assays

Proliferation assays were performed using CCK8 reagent (CK04, Dojindo). 3×10^3 mDMECs were seeded into each well of 96-well plate with complete medium. The absorbance was measured

at 450 nm on 1, 3, 5, 7 d after culturing the cells. Each group has six replicates in one experiment. The experiment was repeated for three times.

Cell Cycle Analysis

According to the manufacturer of Cell cycle kit (GC001, G.fan), the cells were fixed, washed, stained for propidium iodide (PI) solution containing 200 mg/ml RNase A and 0.1% Triton-X-100. We used Attune Acoustic Focusing Cytometer (Applied Biosystems, Life Technologies, CA, USA) to analyze the prepared cells, and then the data were analyzed using FlowJo software (Tree Star Incorporation, USA). Each group has five replicates in one experiment. The experiment was repeated for three times.

Matrigel Plug Assay

Matrigel plug assay was performed as described before (Herkenne et al., 2015). Briefly, 500 µl Matrigel (BD Biosciences) supplemented with VEGF (500 ng/ml), and heparin (0.0025 U/ml) was injected subcutaneously into the right or left flanks of the mice. Seven days later, the matrigel were harvested, fixed with 4% paraformaldehyde, embedded in parafin and sectioned. The sections were stained with H&E and examined under a light microscope (LEICA, Germany, CTR6000). The number of endothelial cell nuclei was counted in 5–10 no-overlapping visual fields.

Wound-Healing Assays

The male and age-matched (12-week-old) mice were selected from the P311 WT and KO mice. The full-thickness excisional skin wound model was created as described previously (Xu et al., 2015). Briefly before the surgery, the hair of the dorsal surface of mice was shaved and cleaned. During anesthetized with 1% pentobarbital via intraperitoneal injection (0.01 mg/g of body weight), two full-thickness excisional skin wounds were made on the dorsal surface with a 4-mm round skin biopsy punch. On day 0, day 3, day 5, day 7, the wounds were photographed using a digital camera. The wounds were measured by the ImageJ 1.48V software (NIH, USA). The amount of wound (wound area%) was calculated using the following formula:

$$Wound\ area\ (\%) = SW_n/SW_0 \times 100\%$$

SW_0 stood for the size of the initial wound area and SW_n represented for the size of wound area on the nth day postsurgery.

Immunofluorescence and Immunohistochemistry Staining

The procedure of Immunofluorescence (IF) and Immunohistochemistry (IHC) staining were performed as described previously (Li et al., 2016). Briefly, for the cultured mDMECs, the cells were washed with PBS three times and fixed in 4% paraformaldehyde (PFA) for 20 min at room temperature. Then after another three times in PBS and blocking in 10% donkey serum, the cells were incubated with the primary antibody at 4°C overnight. For the section, the formalin-fixed and paraffin-embedded samples were sectioned and mounted on polylysine-coated slides. Followed by deparaffinized and rehydrated, the sections were incubated in boiling in 10 mM citrate buffers (pH 6.0) for 15 min to unmask the antigen. Then after blocking, the sections were incubated with the primary antibody as indicated above. For the IF, the secondary antibody conjugated with Alexa Fluor 488 or CY3 was used to visualize the signals. Avidin peroxidase reagent (SP-9001, Zhongshan Biology Company) coordinating with 3,30-diaminobenzidine tetrahydrochloride (DAB) chromogenic agent (ZLI-9017, Zhongshan Biology Company) was used to visualize the signals in IHC. The primary antibodies were listed: CD31 (1:100, Abcam, ab28364,); vWF (1:200, Abcam, ab11713); P311(1:100, Novus, NBP1-84315); TGF-β1(1:200, Novus, NB100-91995) and VEGF (1:100, Abcam, AB46154). The sections were reviewed by a light microscope (LEICA, Germany, CTR6000).

Hematoxylin-Eosin (H&E) Staining and Analysis

The mice were sacrificed on 3rd and 5th day after wounding and then the samples were fixed with 4% paraformaldehyde, embedded in paraffin, sectioned and mounted on slides. For quantification, sections were stained with HE and photographed. Measurements were performed using ImageJ 1.48V software (NIH, USA).

Western Blots

The procedure was performed as described previously (Cheng et al., 2017). Briefly, after grounding in liquid nitrogen, homogenizing with the whole Cell Lysis Kit (Keygen, KGP2100) and centrifuging at 12,000 g for 15 min, The supernatants were collected from the skin wounds. The protein concentrations were determined by BCA Assay (Pierce, 23225). Forty milligrams of proteins for each sample were separated on 10% SDS–PAGE gel, and then transferred electrophoretically to polyvinylidene difluoride (PVDF) (Millipore) membranes. After blocked with 3% bovine serum albumin (BSA), incubated with primary antibody at 4°C overnight and incubated with horseradish peroxidase-conjugated secondary antibodies at room temperature for 1 h, the Molecular Imager ChemiDoc TMXRS+ Imaging System (BioRad) and an enhanced chemiluminescence (ECL) detection kit (Pierce, 35055) were cooperated to detect the signal. The primary antibodies were as follows: CD31 (1:500, Abcam, ab28364,); VEGF (1:1000, Abcam, AB46154); TGF-β1(1:500, Novus, NB100-91995).

Measurement of VEGF and TGF-β1 Concentrations in the Wounds by ELISA

After homogenizing, the acidified lysates from normal skin, healing wounds were centrifuged at 12,000 g for 15 min at 4°C. The supernatants were used to measure the VEGF and TGF-β1 concentrations by ELISA. According to the manufacturer's instructions, the assays for VEGF and TGF-β1 were performed with the ELISA (enzyme-linked immunosorbent assay) kits (Abcam, ab100752) and (R&D Systems, DY1679-05), respectively.

Statistical Analysis

The data were presented as mean ± *SD* (standard deviation) and SPSS 18.0 software was used to analyse the data with unpaired, two-tailed Student's *T*-test. $P < 0.05$ was considered statistically significant.

RESULTS

Localization of P311 in Dermis

Previous study has reported that P311 expression was up-regulated in skin wounds and scars (Cheng et al., 2017), while little P311 protein was detected in normal skin (Cheng et al., 2017; Yao et al., 2017). To localize P311 in skin, the samples from the human skin wounds were selected and immunohistochemistry staining of vertical sections of the samples was performed. Expression of P311 was found in epidermal stem cells in epidermis and fibroblast was also found to express P311 in dermis (**Figure 1A**), which was consistent with our previous studies (Li et al., 2016; Cheng et al., 2017; Yao et al., 2017). Intriguingly, we found some $P311^+$ cells in the blood tube-like structures in human skin wounds (**Figure 1A**), which implied that the vascular endothelial cells might express P311. To further confirm, immunofluorescence staining of sections of skin wounds from P311wild type (WT) mice was performed. The vWF^+ ECs were found to express P311 in the granulation tissue (**Figure 1B**), which meant the vascular endothelial cells expressed P311.

Expression of P311 in mDMECs

To clarify the expression of P311 in vascular endothelial cells, immunofluorescence staining was performed to detect the expression of P311 in murine dermal microvascular endothelial cells (mDMECs), the vWF^+ cells. mDMECs were isolated from the skin of 3-day-old P311 WT mice by magnetic separation with CD31 MicroBeads. As shown in Supplementary Figure 1A, characteristic cobble-stone morphology of confluent endothelial cells (ECs) was observed. Approximately 89.2% of cultured cells were $CD31^+$ cells and 90.7% of cultured cells were $CD34^+$ cells, which are widely characterized as endothelial cells (Supplementary Figure 1B). Immunofluorescence result showed that almost all the cultured cells expressed vWF and P311 (**Figure 1D**); after a 48-h stimulation of IL1β (a common injury signal), the vWF^+ cells highly expressed P311 (**Figure 1E**). Real-time quantitative PCR (qPCR) studies demonstrated that P311 mRNA expression was increased after a 48-h stimulation of IL1β (Supplementary Figure 2).

Taken together, these results showed that dermal microvascular endothelial cells expressed protein P311 and highly expressed it under the injury condition.

P311 Deficiency Impaires Endothelial Cell Migration and Tube Formation *in Vitro*

The dermal microvascular endothelium plays a central role in angiogenesis during skin wound healing. So we isolated mDMECs to assess the potential influence of P311 on ECs function *in vitro*. No difference was observed in the morphology and purity of the mDMECs isolated from P311 WT and P311 KO mice (Supplementary Figure 1A). The P311KO mDMECs showed an impaired ability of tube formation (**Figures 2A,B**). In matrigel assays, which allow determination of the ECs potential to give rise to blood vessel-like tubular structures *in vitro*, thus mimicking angiogenesis, 8 h after seeding P311KO mDMECs on Matrigel, the number of nodes was significantly less ($P < 0.01$) and total length of tubes was significantly shorter ($P < 0.01$) compared with the P311 WT mDMECs.

ECs migration is indispensable for neovessel formation. We examined the effect of P311 on ECs migratory capacity. As shown in **Figures 2C,D** and Supplementary S1, P311 deficiency impaired mDMECs migration *in vitro*. In wound scratch assays, time-lapse microscopy was used to measure the migration rate of mDMECs into a denuded area over a 24-h period. The entire denuded area was almost filled by P31 WT mDMECs within 24 h, whereas P311 KO mDMECs had covered the area only partially.

Finally, we tested the effect of P311 on ECs proliferation, which is intrinsic to the angiogenesis process. Flow cytometry was utilized to analyze the impact of P311 on mDMECs cycle progression. In almost the same way, both kinds of mDMECs entered the cell cycle and progressed through S-phase and G2-M (**Figures 2F,G**). Meanwhile, CCK8 assay was performed after the cells were cultured for 1, 3, 5, 7 d, and no significant difference was observed at any time point between the P311 WT and P311 KO mDMECs.

Together, P311 deficiency mainly impaired the abilities of mDMECs tube formation and migration *in vitro*.

Role of P311 for Angiogenesis *in Vivo*

To further determine whether P311 knockout also affects angiogenesis *in vivo*, we performed matrigel plug assays in P311 WT and P311 KO mice. As shown in **Figure 3**, the number of endothelial cell, which invaded into the plugs of P311 KO mice, was significantly lower compared with that of P311WT mice. Thus, the above data indicate that P311 shows a pro-angiogenic effects *in vitro* and *in vivo*.

Delayed Wound Healing in P311 KO Mice

Angiogenesis, the process by which new blood vessels are formed from preexisting ones, plays an essential role in tissue regeneration. Based on observations above, we hypothesized that P311 might impact tissue regeneration processes through modifying the angiogenesis and we studied the process of full-thickness skin wounds in P311 WT and P311 KO mice to test this hypothesis.

Macroscopic Analysis

Figure 4 showed the macroscopic analysis of the wound closure. We found that on the 3rd day after wounding to the wound closure, skin wounds in P311 KO mice maintained a macroscopic greater wound opening than that in P311 WT mice. Quantification of the digitized images of the wound areas revealed that on 7th day post-wound, only ∼16.58% of the wound area was left in P311 WT mice, but almost 38.82% wound area was still open in P311 KO mice ($P311^{+/+}$, 27.16% vs. $P311^{-/-}$, 49.48%, $P < 0.05$, on 5th day; $P311^{+/+}$, 52.49% vs. $P311^{-/-}$,

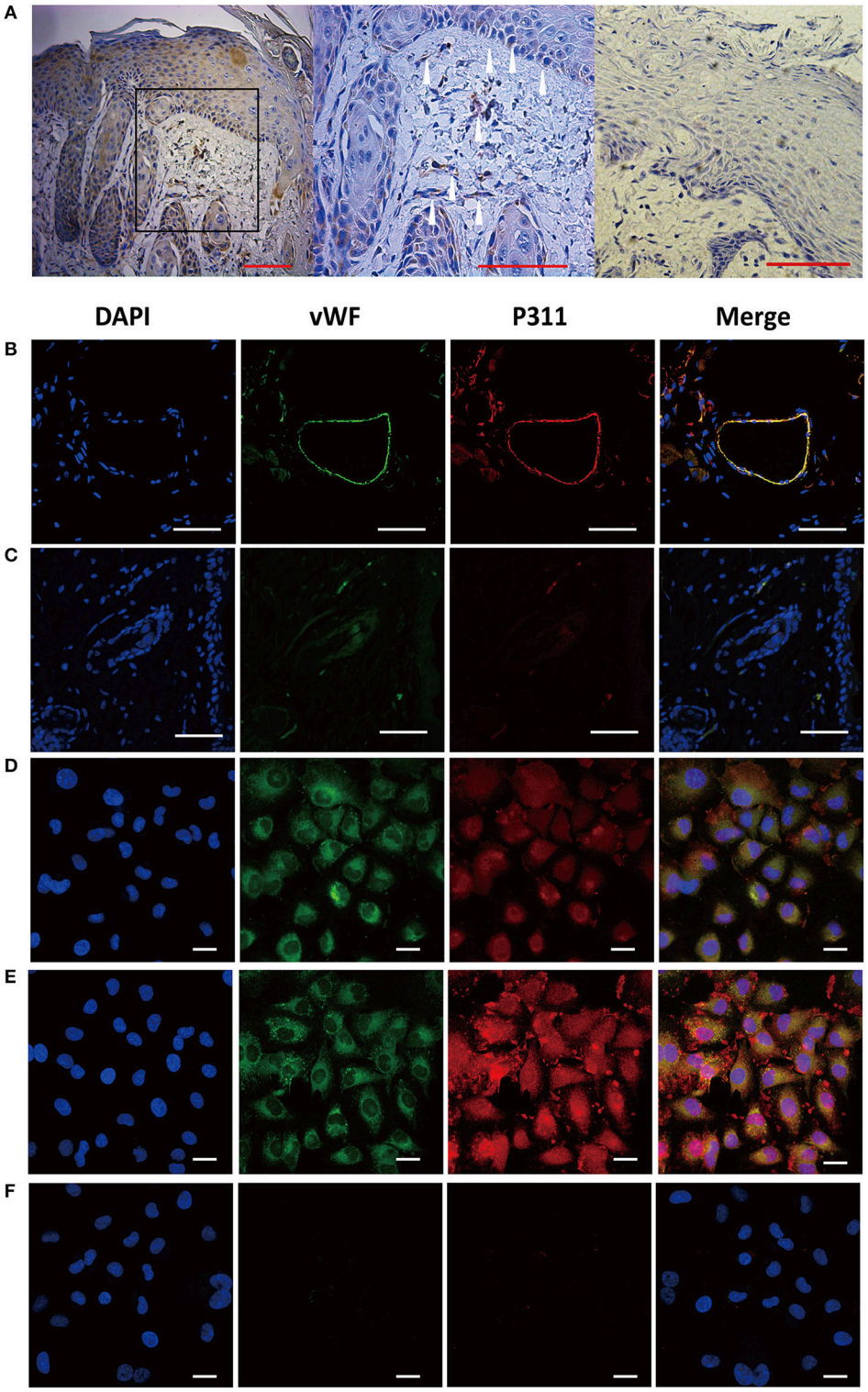

FIGURE 1 | Expression of P311 in dermis and dermal microvascular cells. **(A)** Representative IHC stains for P311 in dermis of human skin wounds. Positivity is represented by brown color. The white arrowheads, P311^{+} cells. Negative control without primary antibody was shown in the right panel. Scar bar = 100 μm. **(B)** Localization of P311 in relationship to ECs (vWF+) in mouse dermis. Scar bar = 100 μm. **(C)** Negative control without primary antibody was shown compared with **(B)**. Immunoflorescence for vWF and P311 was performed in mouse dermal microvascular cells **(D)** and the cells stimulating by IL1β (a common injury signals) **(E)** for 48 h. **(F)** Negative control without primary antibody was shown compared with **(D,E)**. Nuclei were stained by DAPI in blue, vWF was labeled by AF488 in green, and P311 was labeled by AF594 in red. Scar bar = 25 μm.

65.51%, $P < 0.05$, on 3th day). Meanwhile, P311 deficiency prolonged wound closure time (**Figure 4C**). The average wound closure time in P311 WT mice and P311 KO were 6.2 and 7.8 days, respectively.

Microscopic Analysis

On the HE staining sections, Measurement of the granulation tissue thickness indicated that P311 deficiency reduced granulation tissue remodeling, as the average thickness was thinner in P311 KO mice than that in P311 WT mice ($P311^{+/+}$, 300 μm vs. $P311^{-/-}$, 229.5 μm, $P < 0.05$, on 5th day; $P311^{+/+}$, 208.167 μm vs. $P311^{-/-}$, 126.67 μm, $P < 0.05$, on 3rd day; **Figures 5A,D,E**). Comparing the average number of neocapillaries in the wound, significant difference occurred between the two groups ($P311^{+/+}$, 20 vs. $P311^{-/-}$, 13, $P < 0.05$, on 5th day; $P311^{+/+}$, 14.67 vs. $P311^{-/-}$, 7.67, $P < 0.05$,

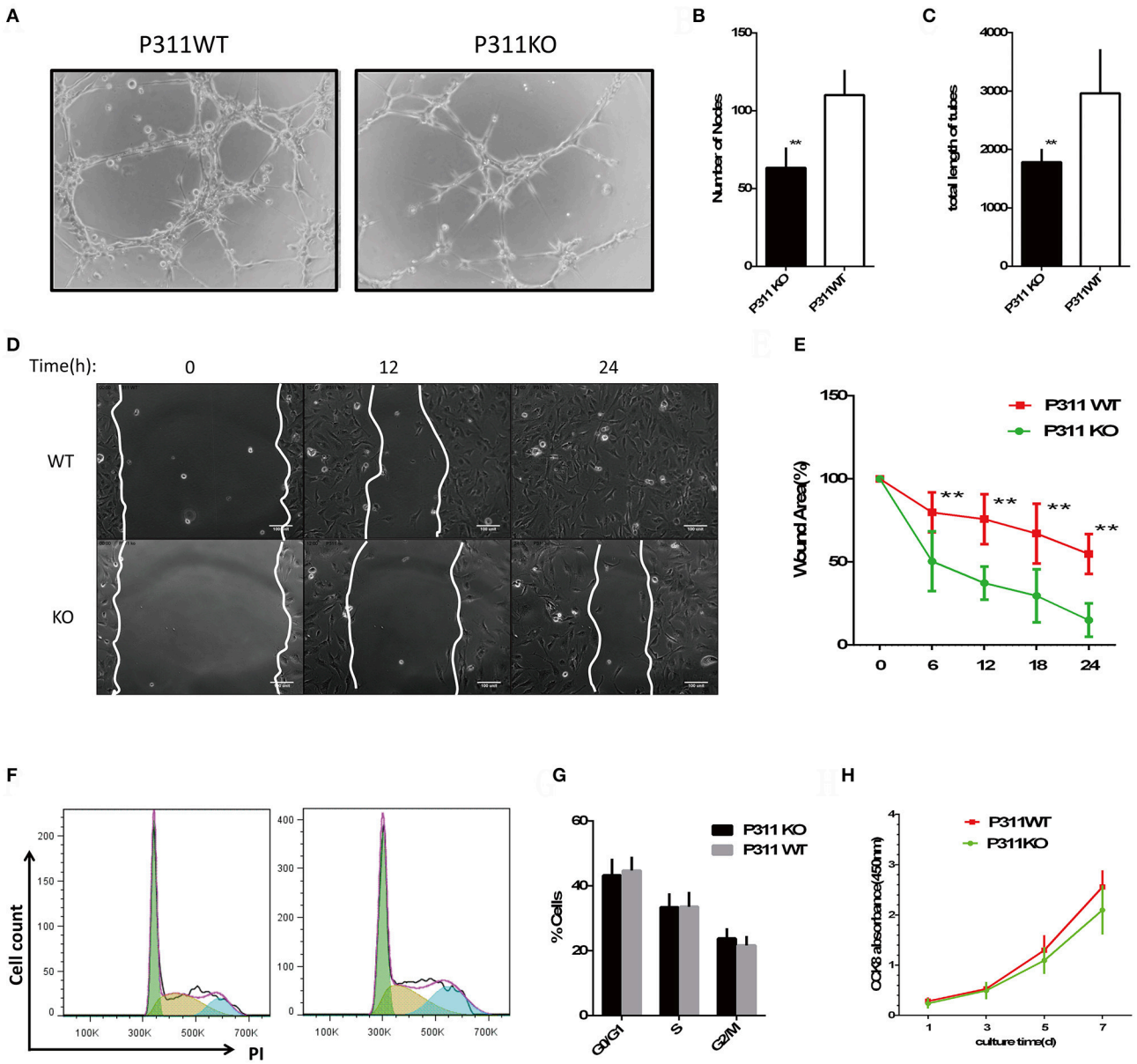

FIGURE 2 | Effect of P311 deficiency on endothelial cell function *in vitro*. **(A)** Representative images of tube formation in Matrigel. Scar bar=100 μm. **(B,C)** Quantitation of tube formation ($n = 6$ per group). **(B)** Number of nobes. **(C)** Total length of tubes. **(D)** Representative images of recovery of scratched areas by cell migration at 12 and 24 h ($n = 6$ per group). The white line stands for the leading edge of migration cells. Scale bars=100 μm. **(E)** Quantitation of the wound area ($n = 6$ per group). **(F)** Representative flow cytometry cell cycle of PI. **(G)** Quantitation data of flow cytometry cell cycle ($n = 5$ per group). **(H)** CCK8 assay was performed to assess the effect of P311 on the proliferation ($n = 6$ per group). Data were expressed as means ± *SD*. $^{**}P < 0.01$, P311 WT vs. KO. All experiments were repeated for three times with reproducible results.

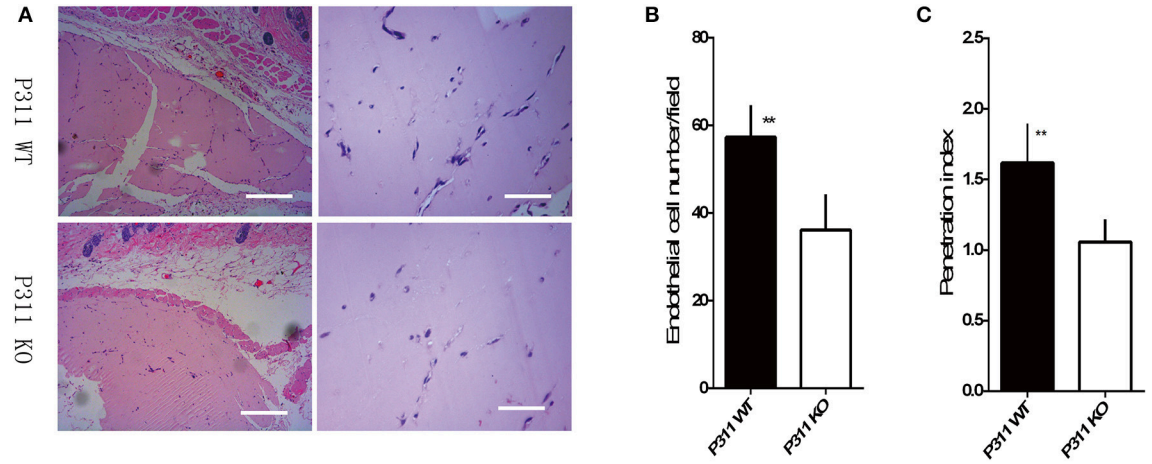

FIGURE 3 | Effect of P311 on angiogenesis in subcutaneous Matrigel plugs. **(A)** Representative cross-sections of H&E-stained of the Matrigel plugs, harvested on the 7th day after implantation into P311 WT and P311 KO mice. Scale bars = 200, 50 μm. **(B,C)** Quantitation of neoangiogenesis. **(B)** Number of endothelial cell nuclei in the matrigel implants ($n = 4$ per group). **(C)** Penetration Index (Penetration of new vessels into the implants, penetration index= area of vessels/overall Matrigel area) ($n = 4$ per group). Data were expressed as means ± *SD*. $^{**}P < 0.01$, P311 WT vs. KO. The experiment was repeated for three times with reproducible results.

on 3rd day). We also found that P311 knockout delayed the wound re-epithelialization significantly, in consistent with a previous study that identified P311 as a promoter of epidermal stem cell migration (Yao et al., 2017). The average length of the neo-epithelium was significantly shorter ($P311^{+/+}$, 472.17 μm vs. $P311^{-/-}$, 328.17 μm, $P < 0.05$, on 5th day; $P311^{+/+}$, 235.00 μm vs. $P311^{-/-}$, 143.00 μm, $P < 0.05$, on 3th day) and the average gap of the two neoepidermal leading edges was significantly larger ($P311^{+/+}$, 706 μm vs. $P311^{-/-}$, 864 μm, $P < 0.05$, on 5th day; $P311^{+/+}$, 963.67 μm vs. $P311^{-/-}$, 1208.67 μm, $P < 0.05$, on 3th day) in $P311^{-/-}$ mice (**Figures 5A–C**).

On immunohistochemical staining sections, CD31 staining was performed to visible the microvessels in the granulation tissues. Consistent with the observation on HE staining, we observed a significantly less efficient growth of new vessels into the wounds in P311 KO wound mice, compared with P311 WT wound mice, while no difference was noted between the P311 WT normal skin and P311 KO normal skin (**Figure 6A**). A significant increase in VEGF and TGFβ1 was observed after injury (normal vs. wound), and a reduction in VEGF and TGFβ1 immunoreactivity consistent with the decrease in neoangiogenesis was also observed in P311 KO mice, compared with P311 WT wound mice in the same tissues (**Figure 6A**). The decreased expression of CD31, VEGF, and TGFβ1 in the samples was further confirmed by Western blotting analysis (**Figure 6B**). The CD31, VEGF, and TGFβ1 protein levels in P311 WT wounds (D5) increased significantly, compared with P311 KO wounds ($P < 0.05$) and P311 normal skin. The concentration of VEGF and TGFβ1 in supernatants of P311 KO wound mice as detected by ELISA was significantly lower than in that of P311 WT wound mice (**Figures 6C,D**). Thus, P311 deficiency leads to attenuated angiogenesis in cutaneous wound healing.

DISCUSSION

Angiogenesis, which is highly regulated by diverse factors in a consecutive, concerted, or synergistic manner (Li et al., 2003), plays a fundamental role in wound healing, tumor growth, invasion, and metastasis (Carmeliet, 2005). More recently, we found that P311 could promote cutaneous wound healing through increasing the activity of RhoA and Rac1 (Yao et al., 2017) and inducing EpMyT (Epidermal stem cell transdifferentiate into myofibroblasts; Li et al., 2016). Hence, we carried out experiments to determine whether P311 may have a function in angiogenesis in wound healing.

Here, for the first time, we demonstrated that P311 could promote angiogenesis in wound healing by changed the endothelial response. This function was supported by the following findings of our present study: (1) P311 was colocalized with vWF^{+} ECs in murine dermis and dermal microvascular endothelial cells (mDMECs) expressed protein P311 and highly expressed it under the injury condition. (2) P311 deficiency mDMECs showed decreased abilities in tube formation and migration *in vitro*. (3) *In vivo*, compared with the P311 WT mice, a significantly less number of ECs was detected in subcutaneous Matrigel implant in P311 KO mice. (4) P311 KO mice showed impaired granulation tissue formation and less $CD31^{+}$ ECs in the granulation tissues in wound healing.

Microvascular endothelial cells are the principal parenchymal cells involved in wound angiogenesis (Li et al., 2003). However, no experiments were performed to define whether the microvascular endothelial cells express P311. Using immunofluorescence, we determined that P311 colocalized with vWF^{+} ECs in murine dermis. Further the expression of vWF and P311 in isolated murine dermal microvascular endothelial cells (mDMECs) at steady state and injury condition was detected. These results demonstrated that mDMECs expressed protein

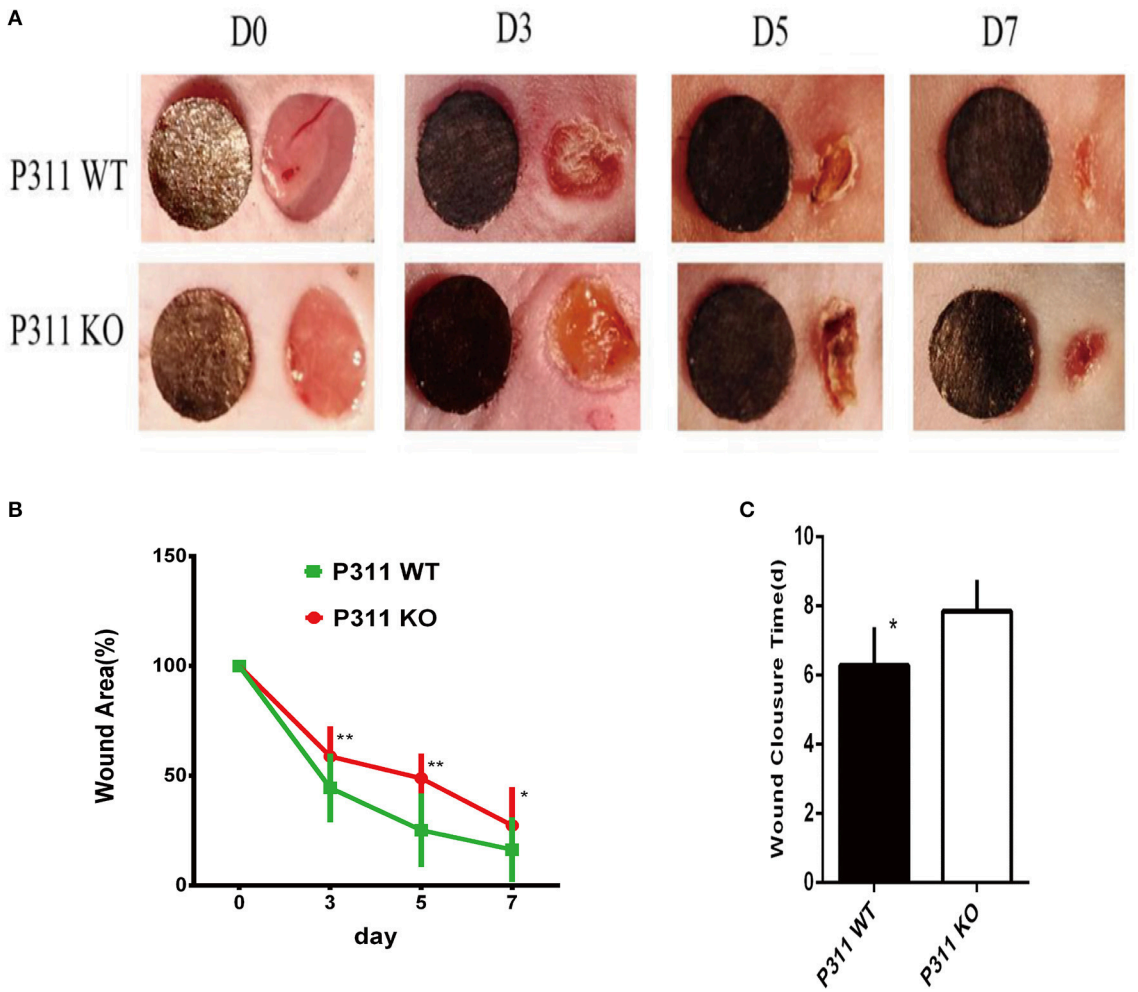

FIGURE 4 | Delayed wound healing in P311-null mice. **(A)** The macroscopic appearance of the wounds post-surgery at different time-points. **(B)** The amounts of wound healing at different time ($n = 6$ per group). **(C)** Wound closure times ($n = 6$ per group). Data were expressed as means ± *SD*. $^{*}P < 0.05$, $^{**}P < 0.01$, P311 WT vs. KO. The experiment was repeated for three times with reproducible results.

P311 and highly expressed it under the injury condition *in vivo* and *in vitro*. Previous studies have showed that P311 expression was little in cells from normal tissue and was obviously increased in cells from injured tissue, implying that P311 might be an injury-dependent protein (Cheng et al., 2017; Yao et al., 2017). Then we examined the influence of P311 deficiency on ECs function *in vitro* using the isolated mDMECs. In consistent with results reported before (Shi et al., 2006; Yao et al., 2017), P311 deficiency mDMECs showed a decreased migration ability. Meantime, the formation of tubes in P311 deficiency mDMECs was also reduced. However, the cell proliferation was almost the same in both mDMECs. In the subcutaneous Matrigel implant, a significant decrease of neoangiogenesis was observed in P311 KO mice. Therefore, it is likely that P311 reduced neoangiogenesis by altering endothelial cell response.

To investigate the effect of the P311 on angiogenesis in wound healing, full-thickness excisional skin wound model was created with P311 KO and P311 WT mice. In a macroscopic analysis, wound healing was significantly delayed in P311 KO mice. Moreover, the average wound closure time was even longer in P311 KO mice. Wounds from P311 KO mice displayed a thinner granulation tissue and $CD31^{+}$EC numbers were reduced in granulation tissue in P311 KO mice, which was further confirmed by western blot. The results indicate that P311 may promote wound healing by enhancing angiogenesis in granulation tissue. Together, P311 regulates angiogenesis in granulation tissue by directly altering endothelial cell response.

In addition, a reduction in VEGF and TGFβ1 was also found in P311 KO mice wounds. The two are both the most critical angiogenic factors that modify the vasculogenesis and angiogenesis (Pardali and Ten, 2009; Pardali et al., 2010; Shibuya, 2013). Vascular endothelial growth factor (VEGF) regulates angiogenesis by binding to the tyrosine kinase receptor VEGFR2, inducing the dimerization, phosphorylation of the receptor and the downstream signaling pathways (Adams and Alitalo, 2007; Koch and Claesson-Welsh, 2012). As endothelial cells

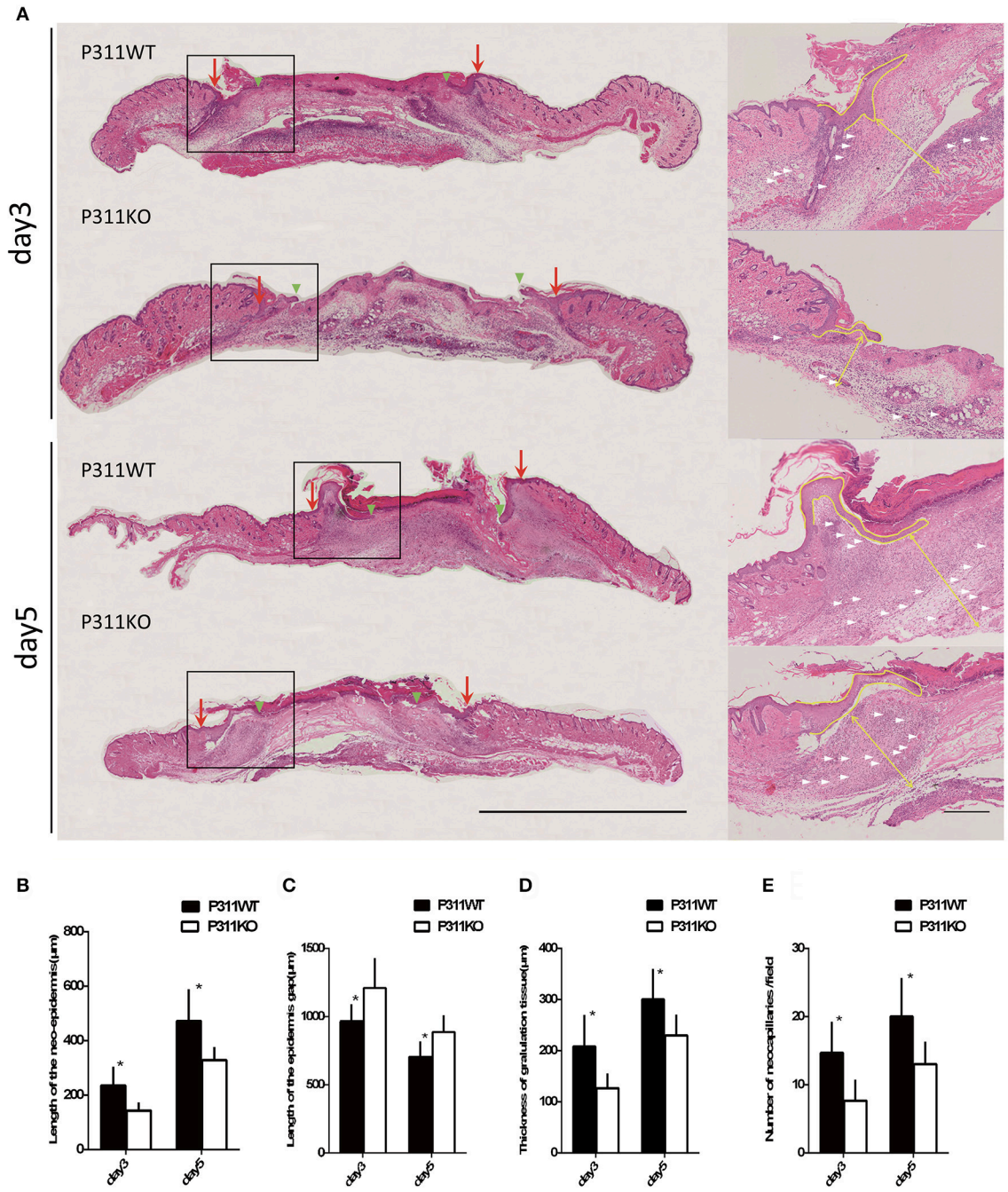

FIGURE 5 | Effect of P311 expression on wound re-epithelialization and granulation tissue. **(A)** H&E-stained sections of excisional skin wound samples from P311 WT and P311 KO mice on 3rd day and 5th day after wounding. Scale bars = 1,000, 200 μm. s, scab; g, granulation tissue; d, dermis; ne, neo-epithelium; pc, panniculus carnosus. Red arrows indicate wound edges; green arrowheads, tips of epithelial tongues; white arrows, microvessels. **(B)** Quantitation of the neo-epidermal length ($n = 6$ per group). **(C)** Quantitation of the wound width ($n = 6$ per group). **(D)** Quantitation of the thickness of granulation tissue ($n = 6$ per group). **(E)** Quantitation of the neocapillaries ($n = 6$ per group). Data were expressed as means ± *SD*. *$P < 0.05$, P311 WT vs. KO. The experiment was repeated for three times with reproducible results.

are able to produce VEGF and express P311, we speculated that P311 might induce the stimulating effects of VEGF, thus leading to altered endothelial cell response, and then modifying angiogenesis. P311-VEGF/VEGFR2-ECs response may be the mechanism under the angiogenesis. Further study is necessary to confirm the hypothesis.

TGF-β signaling pathways also have been strongly proved to be crucial in vasculogenesis and angiogenesis by a series of

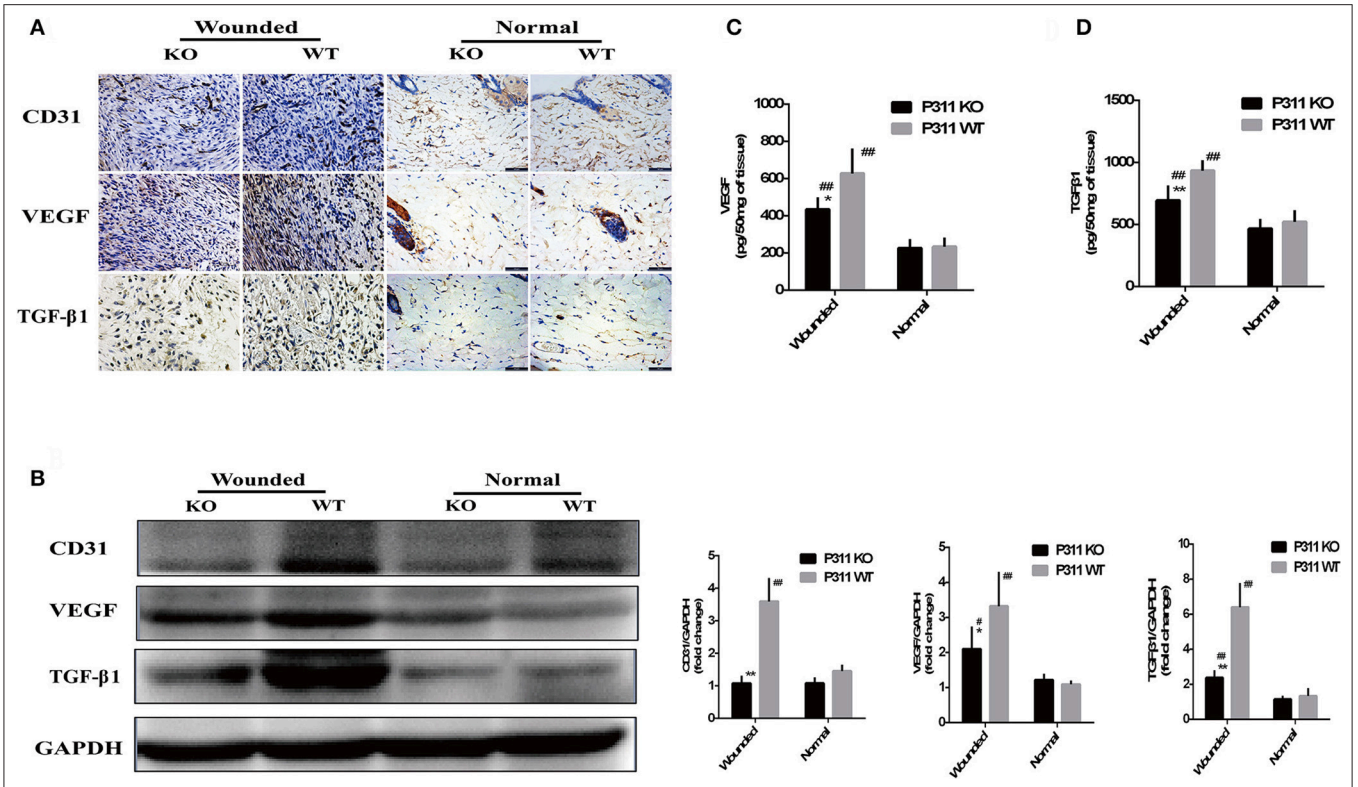

FIGURE 6 | Effect of P311 expression on wound angiogenesis. **(A)** IHC staining of granulation tissues (day 5) for CD31, VEGF, and TGFβ1. **(B)** Western blot showed the expression of CD31, VEGF, and TGFβ1 in each group. Quantitation of the protein levels of CD31, VEGF, and TGFβ1 in each group (day 5). Levels of VEGF **(C)** and TGFβ1 **(D)** releasing during skin wound (day 5) were measured by sandwich ELISA. Data were expressed as means ± *SD*. $n = 5$ per group. $^{*}P < 0.05$, $^{**}P < 0.01$, P311 WT vs. KO. $^{\#}P < 0.05$, $^{\#\#}P < 0.01$, wounded vs. normal. The experiment was repeated for three times with reproducible results.

genetic manipulations of the pathway components. Recently, P311 was identified as a regulator of TGF-βs and a RNA-binding protein to stimulate TGF-βs translation *in vitro* and *in vivo* by Lucia Schuger group and our group (Li et al., 2016; Cheng et al., 2017). So we speculated that in wound healing P311 might modulate angiogenesis by affecting the secretion of TGFβ. Moreover, TGF-β was found to increase the secretion of VEGF (Trompezinski et al., 2000). So P311 also might modulate angiogenesis through P311-TGFβ-VEGF/VEGFR2 signaling pathway. More studies are needed to further confirm the exact mechanism in P311 modulating the angiogenesis in wound healing.

In summary, for the first time, we demonstrated that P311 could promote angiogenesis in wound healing by changed the endothelial response.

ETHICS STATEMENT

In the study, all human experiments were carried out in accordance with the recommendations of the Medical and Ethical Committees of the Southwest Hospital, the Third Military Medical University with written informed consent from all subjects. All subjects gave written informed consent in accordance with the Declaration of Helsinki. The protocol was approved by the Medical and Ethical Committees of the Southwest Hospital, the Third Military Medical University. All animal experimental protocols were approved by the Animal Experimental Ethics Committees of the Third Military Medical University and were also performed in accordance with the guidelines of the Third Military Medical University.

AUTHOR CONTRIBUTIONS

SW, WH, JW, and GL have made substantial contributions to the conception or design of the work. The majority of the experiments were conducted by SW and XZ. WQ, DZ, XY and GL contributed to collection, analysis, interpretation of the data for the study. SW wrote the first draft of the manuscript. Then RZ, YW, JW, WH and GL revised and edited the manuscript critically for important intellectual content. GL was responsible for obtaining funds. All authors read and approved the manuscript.

FUNDING

This work was supported by grants from China's NSFC grants program (81630055) and (81471870).

ACKNOWLEDGMENTS

We wish to thank Prof. Gregory A. Taylor from Duke University Medical Center for kindly providing the P311 KO mice.

SUPPLEMENTARY MATERIAL

The Supplementary Material for this article can be found online at: https://www.frontiersin.org/articles/10.3389/fphys.2017.01004/full#supplementary-material

REFERENCES

Adams, R. H., and Alitalo, K. (2007). Molecular regulation of angiogenesis and lymphangiogenesis. *Nat. Rev. Mol. Cell Biol.* 8, 464–478. doi: 10.1038/nrm2183

Badri, K. R., Yue, M., Carretero, O. A., Aramgam, S. L., Cao, J., Sharkady, S., et al. (2013). Blood pressure homeostasis is maintained by a P311-TGF-beta axis. *J. Clin. Invest*. 123, 4502–4512. doi: 10.1172/JCI69884

Carmeliet, P. (2005). Angiogenesis in life, disease and medicine. *Nature* 438, 932–936. doi: 10.1038/nature04478

Cha, S. T., Talavera, D., Demir, E., Nath, A. K., and Sierra-Honigmann, M. R. (2005). A method of isolation and culture of microvascular endothelial cells from mouse skin. *Microvasc. Res.* 70, 198–204. doi: 10.1016/j.mvr.2005.08.002

Cheng, T., Yue, M., Aslam, M. N., Wang, X., Shekhawat, G., Varani, J., et al. (2017). Neuronal Protein 3.1 deficiency leads to reduced cutaneous scar collagen deposition and tensile strength due to impaired transforming growth factor-beta1 to -beta3 translation. *Am. J. Pathol.* 187, 292–303. doi: 10.1016/j.ajpath.2016.10.004

DeCicco-Skinner, K. L., Henry, G. H., Cataisson, C., Tabib, T., Gwilliam, J. C., Watson, N. J., et al. (2014). Endothelial cell tube formation assay for the *in vitro* study of angiogenesis. *J. Vis. Exp.* 91:e51312. doi: 10.3791/51312

Fujitani, M., Yamagishi, S., Che, Y. H., Hata, K., Kubo, T., Ino, H., et al. (2004). P311 accelerates nerve regeneration of the axotomized facial nerve. *J. Neurochem*. 91, 737–744. doi: 10.1111/j.1471-4159.2004.02738.x

Herkenne, S., Paques, C., Nivelles, O., Lion, M., Bajou, K., Pollenus, T., et al. (2015). The interaction of uPAR with VEGFR2 promotes VEGF-induced angiogenesis. *Sci. Signal.* 8:ra117. doi: 10.1126/scisignal.aaa2403

Johnson, K. E., and Wilgus, T. A. (2014). Vascular endothelial growth factor and angiogenesis in the regulation of cutaneous wound repair. *Adv. Wound Care* 3, 647–661. doi: 10.1089/wound.2013.0517

Koch, S., and Claesson-Welsh, L. (2012). Signal transduction by vascular endothelial growth factor receptors. *Cold Spring Harb. Perspect. Med.* 2:a006502. doi: 10.1101/cshperspect.a006502

Li, H., Yao, Z., He, W., Gao, H., Bai, Y., Yang, S., et al. (2016). P311 induces the transdifferentiation of epidermal stem cells to myofibroblast-like cells by stimulating transforming growth factor beta1 expression. *Stem Cell Res. Ther.* 7:175. doi: 10.1186/s13287-016-0421-1

Li, J., Zhang, Y. P., and Kirsner, R. S. (2003). Angiogenesis in wound repair: angiogenic growth factors and the extracellular matrix. *Microsc. Res. Technol.* 60, 107–114. doi: 10.1002/jemt.10249

McDonough, W. S., Tran, N. L., and Berens, M. E. (2005). Regulation of glioma cell migration by serine-phosphorylated P311. *Neoplasia* 7, 862–872. doi: 10.1593/neo.05190

Pan, D., Zhe, X., Jakkaraju, S., Taylor, G. A., and Schuger, L. (2002). P311 induces a TGF-beta1-independent, nonfibrogenic myofibroblast phenotype. *J. Clin. Invest*. 110, 1349–1358. doi: 10.1172/JCI0215614

Pardali, E., and Ten, D. P., (2009). Transforming growth factor-beta signaling and tumor angiogenesis. *Front. Biosci.* 14, 4848–4861. doi: 10.2741/3573

Pardali, E., Goumans, M. J., and Ten, D. P., (2010). Signaling by members of the TGF-beta family in vascular morphogenesis and disease. *Trends Cell Biol*. 20, 556–567. doi: 10.1016/j.tcb.2010.06.006

Sadok, A., and Marshall, C. J. (2014). Rho GTPases: masters of cell migration. *Small GTPases* 5:e29710. doi: 10.4161/sgtp.29710

Shi, J., Badri, K. R., Choudhury, R., and Schuger, L. (2006). P311-induced myofibroblasts exhibit ameboid-like migration through RalA activation. *Exp. Cell Res.* 312, 3432–3442. doi: 10.1016/j.yexcr.2006.07.016

Shibuya, M. (2013). Vascular endothelial growth factor and its receptor system: physiological functions in angiogenesis and pathological roles in various diseases. *J. Biochem*. 153, 13–19. doi: 10.1093/jb/mvs136

Sommer, T., and Wolf, D. H. (2014). The ubiquitin-proteasome-system. *Biochim. Biophys. Acta* 1843:1. doi: 10.1016/j.bbamcr.2013.09.009

Studler, J. M., Glowinski, J., and Lévi-Strauss, M. (1993). An abundant mRNA of the embryonic brain persists at a high level in cerebellum, hippocampus and olfactory bulb during adulthood. *Eur. J. Neurosci*. 5, 614–623. doi: 10.1111/j.1460-9568.1993.tb00527.x

Talavera-Adame, D., Ng, T. T., Gupta, A., Kurtovic, S., Wu, G. D., and Dafoe, D. C. (2011). Characterization of microvascular endothelial cells isolated from the dermis of adult mouse tails. *Microvasc. Res.* 82, 97–104. doi: 10.1016/j.mvr.2011.04.009

Tan, J., Peng, X., Luo, G., Ma, B., Cao, C., He, W., et al. (2010). Investigating the role of P311 in the hypertrophic scar. *PLoS ONE* 5:e9995. doi: 10.1371/journal.pone.0009995

Taylor, G. A., Rodriguiz, R. M., Greene, R. I., Daniell, X., Henry, S. C., Crooks, K. R., et al. (2008). Behavioral characterization of P311 knockout mice. *Genes Brain Behav*. 7, 786–795. doi: 10.1111/j.1601-183X.2008.00420.x

Tonnesen, M. G., Feng, X., and Clark, R. A. (2000). Angiogenesis in wound healing. *J. Invest. Dermatol. Symp. Proc.* 5, 40–46. doi: 10.1046/j.1087-0024.2000.00014.x

Trompezinski, S., Pernet, I., Mayoux, C., Schmitt, D., and Viac, J. (2000). Transforming growth factor-beta1 and ultraviolet A1 radiation increase production of vascular endothelial growth factor but not endothelin-1 in human dermal fibroblasts. *Br. J. Dermatol.* 143, 539–545. doi: 10.1111/j.1365-2133.2000.03707.x

Varshavsky, A. (2014). Discovery of the biology of the ubiquitin system. *JAMA* 311, 1969–1970. doi: 10.1001/jama.2014.5549

Xu, R., Luo, G., Xia, H., He, W., Zhao, J., Liu, B., et al. (2015). Novel bilayer wound dressing composed of silicone rubber with particular micropores enhanced wound re-epithelialization and contraction. *Biomaterials* 40, 1–11. doi: 10.1016/j.biomaterials.2014.10.077

Yao, Z., Li, H., He, W., Yang, S., Zhang, X., Zhan, R., et al. (2017). P311 accelerates skin wound reepithelialization by promoting epidermal stem cell migration through RhoA and Rac1 activation. *Stem Cells Dev*. 26, 451–460. doi: 10.1089/scd.2016.0249

Yao, Z., Yang, S., He, W., Li, L., Xu, R., Zhang, X., et al. (2015). P311 promotes renal fibrosis via TGFbeta1/Smad signaling. *Sci. Rep.* 5:17032. doi: 10.1038/srep17032

Zhao, L., Leung, J. K., Yamamoto, H., Goswami, S., Kheradmand, F., and Vu, T. H. (2006). Identification of P311 as a potential gene regulating alveolar generation. *Am. J. Respir. Cell Mol. Biol.* 35, 48–54. doi: 10.1165/rcmb.2005-0475OC

Conflict of Interest Statement: The authors declare that the research was conducted in the absence of any commercial or financial relationships that could be construed as a potential conflict of interest.

frontiers in Physiology

ORIGINAL RESEARCH
published: 01 December 2017
doi: 10.3389/fphys.2017.00967

Prediction of Scar Size in Rats Six Months after Burns Based on Early Post-injury Polarization-Sensitive Optical Frequency Domain Imaging

*Eli Kravez[1], Martin Villiger[2], Brett Bouma[2,3], Martin Yarmush[4,5], Zohar Yakhini[1] and Alexander Golberg[4,6]**

[1] School of Computer Science, Interdisciplinary Center Herzliya, Herzliya, Israel, [2] Wellman Center for Photomedicine, Massachusetts General Hospital, Harvard Medical School, Boston, MA, United States, [3] Institute of Medical Engineering and Science, Massachusetts Institute of Technology, Cambridge, MA, United States, [4] Department of Surgery, Center for Engineering in Medicine, Massachusetts General Hospital, Shriners Burns Hospital for Children, Harvard Medical School, Boston, MA, United States, [5] Department of Biomedical Engineering, Rutgers University, Piscataway, NJ, United States, [6] Porter School of Environmental Studies, Tel Aviv University, Tel Aviv, Israel

OPEN ACCESS

Edited by:
Marianna Bei,
Harvard Medical School, Harvard University, United States

Reviewed by:
Leila Cuttle,
Queensland University of Technology, Australia
Dale Wesley Edgar,
University of Notre Dame Australia, Australia

***Correspondence:**
Alexander Golberg
agolberg@tauex.tau.ac.il

Specialty section:
This article was submitted to Clinical and Translational Physiology, a section of the journal Frontiers in Physiology

Received: 01 August 2017
Accepted: 14 November 2017
Published: 01 December 2017

Citation:
Kravez E, Villiger M, Bouma B, Yarmush M, Yakhini Z and Golberg A (2017) Prediction of Scar Size in Rats Six Months after Burns Based on Early Post-injury Polarization-Sensitive Optical Frequency Domain Imaging. Front. Physiol. 8:967. doi: 10.3389/fphys.2017.00967

Hypertrophic scars remain a major clinical problem in the rehabilitation of burn survivors and lead to physical, aesthetic, functional, psychological, and social stresses. Prediction of healing outcome and scar formation is critical for deciding on the best treatment plan. Both subjective and objective scales have been devised to assess scar severity. Whereas scales of the first type preclude cross-comparison between observers, those of the second type are based on imaging modalities that either lack the ability to image individual layers of the scar or only provide very limited fields of view. To overcome these deficiencies, this work aimed at developing a predictive model of scar formation based on polarization sensitive optical frequency domain imaging (PS-OFDI), which offers comprehensive subsurface imaging. We report on a linear regression model that predicts the size of a scar 6 months after third-degree burn injuries in rats based on early post-injury PS-OFDI and measurements of scar area. When predicting the scar area at month 6 based on the homogeneity and the degree of polarization (DOP), which are signatures derived from the PS-OFDI signal, together with the scar area measured at months 2 and 3, we achieved predictions with a Pearson coefficient of 0.57 ($p < 10^{-4}$) and a Spearman coefficient of 0.66 ($p < 10^{-5}$), which were significant in comparison to prediction models trained on randomly shuffled data. As the model in this study was developed on the rat burn model, the methodology can be used in larger studies that are more relevant to humans; however, the actual model inferred herein is not translatable. Nevertheless, our analysis and modeling methodology can be extended to perform larger wound healing studies in different contexts. This study opens new possibilities for quantitative and objective assessment of scar severity that could help to determine the optimal course of therapy.

Keywords: scars size prediction, burn injury, wound healing diagnosis, optical coherence tomography, skin imaging

INTRODUCTION

Burns is a global public health problem, accounting for an estimated 265,000 deaths annually (WHO, 2016). A review of literature published since 1965 reported a 32–72% prevalence rate of hypertrophic scarring in patients suffering from burn injuries (Lawrence et al., 2012). Although tremendous progress has been achieved in the last decades in saving lives after burn injuries, hypertrophic scars remain a major clinical problem in the rehabilitation of burn survivors, leading to physical, aesthetic, functional, psychological, and social stresses (Lawrence and Fauerbach, 2003; Aarabi et al., 2007; Baillie et al., 2014). Moreover, molecular mechanisms behind scar formation are not completely understood and it remains challenging to provide early prediction of the long term scar outcome (Tziotzios et al., 2012; Koppenol et al., 2017).

Prediction of scarring outcome at the early time points after injury is important for the decisions about burn wound management and treatment planning and assessment (Sheridan, 2012; Koppenol et al., 2017). Therefore, a range of subjective and objective scales has been devised to assist the caregiver in the decision making (Heimbach et al., 1984). The subjective scales, such as The Vancouver Scar Scale (VSS), Manchester Scar Scale (MSS), Patient and Observer Scar Assessment Scale (POSAS), Visual Analog Scale (VAS), and Stony Brook Scar Evaluation Scale (SBSES), consider factors such as scar height or thickness, pliability, surface area, texture, pigmentation, and vascularity (Nedelec et al., 2000; Fearmonti et al., 2010). However, they are dependent on the observer and are difficult to compare. In search of more objective diagnostic burn criteria, a wide spectrum of methods has been explored: biopsy and histology (Sheridan, 2012), fluorescent imaging (Sheridan et al., 2015), near-infrared light spectroscopy (Cross et al., 2007), confocal, and multiphoton microscopy (Chen et al., 2011), laser Doppler techniques (Jaskille et al., 2010), and non-contact high-frequency ultrasonography (Lin et al., 2011), as well as thermography (Liddington and Shakespeare, 1996). To date, these strategies fall into one of two categories: (1) they lack the ability to image individual layers of the wound and provide an accumulated bulk signal, making the diagnosis of burn depth unreliable, and (2) although providing high spatial resolution and depth-sectioning, the limited field of view and long acquisition times make them impractical in a clinical setting. In contrast, Optical Frequency Domain Imaging (OFDI) and related implementations of optical coherence tomography (OCT) provide depth-resolved images of the tissue architecture and functional vasculature with an interesting trade off of the field of view, spatial resolution, and imaging speed, that can help to overcome the barriers encountered by alternative modalities (Park et al., 2001; Kim et al., 2012; Villiger et al., 2013a,b).

OFDI is an optical imaging modality that captures micrometer-resolution, three-dimensional images of the subsurface microstructure of biological tissues. Polarization Sensitive (PS) OFDI further improves structural imaging by providing insight into the polarization properties of the tissue by measuring the polarization state of the light backscattered by the tissue. The polarization state of light is altered by propagating through a medium that exhibits birefringence. Quantifying the rate of this change with depth provides a measure of tissue birefringence. The majority of the extracellular matrix of skin consists of collagen, which is a prominent source of birefringence. In skin undergoing thermal injury, the collagen proteins denature, in the process of which they lose their birefringence. Hence, burns are characterized by a lower birefringence, a feature which previously has been used to assess burn depth (Park et al., 2001; Kim et al., 2012). In addition to birefringence, PS-OFDI can also assess depolarization, which corresponds to a randomization of the measured polarization states. This randomization is expressed by the Degree of Polarization (DOP), ranging from 0 for completely randomized polarization states to 1 for perfectly aligned polarization states. Collagen fibers that are uniformly arranged result in deterministic polarization states that vary along depth due to tissue birefringence (Lo et al., 2016) but are locally uniform and result in high DOP. In contrast, collagen fibers that are disorganized on a size scale smaller than the focal volume of the probing beam result in a randomization of the measured polarization states and a reduced DOP (Lo et al., 2016).

We previously have developed reconstruction strategies that mitigate artifacts resulting from polarization sensitive measurements through fiber-based imaging systems and provide maps of tissue birefringence and DOP in animal models (Villiger et al., 2013a,b). We have also shown that PS-OFDI provides valuable insights into the structural remodeling taking place during scar formation in a mechanical tension induced HTS model in rats (Lo et al., 2016). Compared to normal skin with heterogeneous birefringence and low DOP, HTS was characterized by an initially low birefringence, which increased as collagen fibers remodeled, and a persistently high DOP (Lo et al., 2016). In additional work, we showed that PS-OFDI signature could differentiate between third-degree burn scars treated with different therapy plans of partially irreversible electroporation (Golberg et al., 2016).

The goal of the present work was to develop a linear regression model that predicts the size of the scar 6 months after a third-degree burn in rats based on PS-OFDI imaging at early time points. Linear regression models are the simplest prediction models for quantitative inference [see ref (Rice, 2010) as well as (Stanton, 2001) for a historical perspective]. Such models are used in diverse contexts including biology and medical science (Motulsky and Christopoulos, 2002) as well as economics and social science (Greene, 2011). Accurately predicting the healing outcome of burn injuries based on non-invasive imaging at early time points would be a crucial diagnostic capability that could open new options for management and care of burn patients.

MATERIALS AND METHODS

Animals

Female Sprague-Dawley rats (∼250 g, $N = 18$, 6-week-old) were purchased in Charles River Laboratories (Wilmington, MA). The animals were housed in cages with access to food and water *ad libitum* and were maintained on a 12-h light/dark cycle in a temperature-controlled room. All animal procedures were

approved by the Institutional Animal Care and Use Committee (IACUC) of the Massachusetts General Hospital. All procedures were in accordance with the guidelines of the National Research Council. The animals were treated humanely.

Scar Models

For statistical prediction of the resulting scar size, a dataset with a range of different scar sizes is needed. We used the data from our previous work where we showed the ability of partially irreversible electroporation (pIRE) to reduce the size of scars in rats, 6 months after injury (Golberg et al., 2016). Third degree burns were treated at various time points after injury with different pulsed electric field parameters, resulting in a range of scar sizes 6 months after the initial injury, as reported in Golberg et al. (2016). In brief, animals were anesthetized with isoflurane and their fur was clipped along the dorsal surfaces. Burns were incurred by pressing the end of a pre-heated ($\geq$95°C) brass block against the rat's dorsum for 10 s, resulting in a non-lethal, full-thickness, third-degree burn, measuring $\sim$1 cm^2, which is 0.25% of the total body surface area (TBSA; Golberg et al., 2016). Four burn injuries were performed on each animal at sites separated by 2 cm along the head to tail axis, accounting for 1% TBSA of total burn area. The depth of the burn was evaluated histologicaly in 9 animals at time 0, 12 h and 1 week after the injury ($n = 3$ animals per time point; Golberg et al., 2016). One burn served as control and three burns with treated with pIRE using contact electrodes with a surface area of 1 cm^2, separated by a 2 mm gap (Golberg et al., 2016). Square pulses of 70 μs duration at a 3 Hz repetition rate were delivered using a BTX 830 pulse generator (Harvard Apparatus Inc., Holliston, MA; Golberg et al., 2016). Voltage, number of pulses, and treatment frequency very varied between different groups of animals and are described in Table S1 (Golberg et al., 2016). In total we analyzed 3 replicate wounds per treatment condition for each of the 9 different treatment conditions.

Polarization-Sensitive Optical Frequency Domain Imaging

PS-OCT was performed as reported in detail previously (Villiger et al., 2013a; Lo et al., 2016), at 1, 2, 3, 5, and 6 months after the burn injury. The system operated with a wavelength-swept laser source at an A-line rate of 54 kHz and a center wavelength of 1,320 nm, achieving an axial resolution of 9.4 μm in tissue. We scanned rectangular surface areas of 10 × 5 mm, consisting of 2,048 A-lines/image × 256 images, with a focused beam featuring a lateral resolution of 15 μm. The lesions were covered with a thin layer of ultrasound-gel as an immersion liquid and apposed against a glass slide to center the superficial layers in focus. Two to three volumes were acquired for each lesion and time point, and the volume that aligned most accurately with the lesion was selected for further analysis. For PS-OCT, the polarization state of the light directed to the sample was alternated between linear and circular polarization between adjacent A-lines, and the signal was detected with a polarization diverse receiver.

The data were reconstructed with spectral binning (Villiger et al., 2013a), using 1/5th of the spectral bandwidth, a lateral Gaussian filter with a full width at half maximum (FWHM) equal to 12 adjacent A-lines, and an axial offset of 48 μm to derive depth-resolved tissue birefringence. Tissue birefringence was expressed in deg/μm, corresponding to the amount of retardation per sample path. The DOP was evaluated independently for each spectral bin and input polarization state over the same lateral Gaussian kernel, and then averaged:

$$DOP = \frac{1}{2N} \sum_{p=1}^{2} \sum_{n=1}^{N} \frac{\sqrt{Q_{p,n}^2 + U_{p,n}^2 + V_{p,n}^2}}{I_{p,n}} \quad (1)$$

where Q, U, V, and I are the spatially averaged components of the Stokes vector, n denotes the spectral bin and p the input polarization state. DOP expresses the randomness of the measured polarization states and scales from 0 (completely random) to unity (uniform). Close to the surface, the polarization states are usually well maintained, resulting in a DOP close to unity. As the light propagates deeper and depending on the depolarizing properties of the tissue, the light gets increasingly depolarized, resulting in lower DOP values. The structural intensity tomograms are displayed in logarithmic scale as gray scale images. Birefringence was mapped from 0 to 1.2 deg/μm with an isoluminant color map (Geissbuehler and Lasser, 2013) and overlayed with the gray-scale intensity image. DOP is scaled from 0.5 to 1 and is rendered in the same color map.

For quantitative analysis of the polarization properties, we defined a cylindrical region of interest with a diameter of 1 mm centered on the lesion at each time point and extending from the epidermis to the subcutaneous fat. We found that both mature scars and normal skin resulted in high mean birefringence values.

In scars, the birefringence is very uniform and accompanied by a high DOP. In contrast, the mesh-like arrangement of collagen fibrils in the normal skin results in a spot-like, heterogeneous appearance of birefringence in normal skin, paired with low DOP. Hence, we used a measure of homogeneity of the birefringence to best capture the scar status. Homogeneity was evaluated with the "graycomatrix" function, available in the image processing toolbox in Matlab (MathWorks, Natick, MA, USA). It was computed with an offset of 5 pixels in the axial direction, and dividing the birefringence into 12 levels ranging from 0 to 1 deg/μm over the entire cylindrical region of interest. Homogeneity results in a value from 0 (not homogeneous) to 1 (very homogeneous). As a second polarization metric, we computed the average slope of the DOP (DOPSlope). The DOP values were averaged at each depth across the tissue cylinder and then fit with a straight line to express its downward slope per millimeter.

Quantification of Scar Area

Scar surface areas were quantified from digital images, captured at each time point, with ImageJ software (Schneider et al., 2012). All scar edges were traced manually and the area was quantified using a calibrated internal length standard for each image.

Linear Regression Model to Predict Scar Area

The data set consists of 36 data points (wounds): 9 animals with 4 lesions each (1 untreated burn and 3 burns treated with pIRE). For each wound three features were measured each month (Scar_Area, Homogeneity, and DOPSlope).

We performed linear regression using two types of data vectors as features for predicting the scar size at 6 months after the burn injury:

a) 3-dimensional data vectors, including Scar_Area, Homogeneity, and DOPSlope for only a single month from months 1 to 3.
b) 6-dimensional data vectors, including the same features, taken from a pair of months from months 1 to 3.
c) 9-dimensional data vectors, including the same features, taken from months 1, 2, and 3.

We first transformed all feature values into z-score explanatory variables:

$$z = \frac{(x - \mu)}{\sigma} \tag{2}$$

Where μ and σ are the mean and standard deviation for the feature, across the 36 samples, and x is the measured feature value.

We used leave-one-out cross-validation (LOOCV) as follows—we built a linear regression based on 35 samples and predicted the target value (scar size at month 6) for the hidden data point. This process was repeated 36 times (each sample left out once). The LOOCV process results in 36 predictions for the scar area at month 6.

We then calculated the Pearson and Spearman correlations (Rice, 2010) between the vector of predicted values and the vector of actual measured scar sizes. The Root Mean Square Error (RMSE) of the prediction model was also determined as follows:

$$RMSE = \sqrt{\frac{1}{n}\sum_{1}^{i}(x_i - \hat{x}_i)^2} \tag{3}$$

where x_i is the measured value for the scar size, $\hat{x}_i$ is the value predicted by a given model, and n is the number of samples.

We chose to use several approaches to measure the prediction quality as they represent different aspects that may be of interest. Pearson correlation provides an estimate of how the predicted values are linearly associated with the measured ones. Spearman correlation provides an estimate of how monotonic the predicted values are compared to the measured ones. That is—how predictive the early post-injury measurements are in being able to answer questions like—will Scar A be larger than Scar B at month 6? RMSE provides an intuitive quantitative estimate of the absolute error.

Amongst these approaches to evaluating performance Spearman correlation is the most robust one, insensitive to the variation that can be calibrated in practice and to the statistical model selection.

Random Control

As a random control, we shuffled the measured values at month 6 and performed the same LOOCV analysis for the shuffled data. This way we disconnect the relationship between the measurements at month 1–3 and the corresponding 6th¯month scar size. This yields datasets that are identical to the original ones but with shuffled 6th-month scar size. The shuffling and LOOCV analysis were repeated 1,000 times. For each such shuffled instance, we compute the Pearson and Spearman of the predicted Scar_Area at 6th month to the input (shuffled) Scar_Area at 6th month. Thereby we obtain an empirical p-value for the observed performance of predicting the actual real data and can rule out overfitting. We performed this analysis for all model types described above.

RESULTS

Our hypothesis is that PS-OFDI signatures measured at the early time points after the burn injury allow predicting the final wound healing outcome. To test this hypothesis, we simplified this complex process and defined the scar size (area in mm^2) at 6 months after the injury as the healing outcome and modeled it in response to the PS-OFDI signatures and the scar size at early time points. We used the homogeneity of the birefringence (Hom) and the slope of the DOP (DOPSlope) as signatures derived from the PS-OFDI measurements. These parameters were evaluated in a cylindrical region of interest in the center of each lesion (2–3 volumes per lesion), extending from the epidermis to the subcutaneous fat. Together with the scar size, as measured from digital photographs, this leads to the following model:

$$\begin{aligned} Scar\_Area_{(6m)} = \beta_0 + \sum_{i=1}^{K} \alpha_i Scar\_Area_i + \gamma_i Hom_i \\ + \delta_i DOPSlope_i, \end{aligned} \tag{4}$$

where Scar_Area is the surface area of the burn scar (mm^2), Hom, and DOP_Slope are the OFDI derived homogeneity and DOP slope (Golberg et al., 2016), i indicates the time point in months after the burn injury, K is the set of employed time points (1, 2, or 3 months after the injury with all combinations), β_0 is the intercept, and α, γ, and δ are scalar coefficients obtained by linear regression.

For the construction of the multivariable regression model, we used data, generated in our previous study, where we treated third-degree burns in rats with various pIRE therapy parameters to investigate their impact on the resulting scar size (Golberg et al., 2016). These experiments generated a data set of 36 individual scars of various sizes on 9 animals (one untreated scar per animal and three pIRE treated scars with three biological repeats), measured longitudinally up to 6 months after the burn injury (**Figure 1A**). A total of 216 measurements for Scar_Area, Hom, and DOPSlope as shown in **Table 1** and **Figures 1B–D, 2** were used. We used Scar_Area, Hom, and DOPSlope from

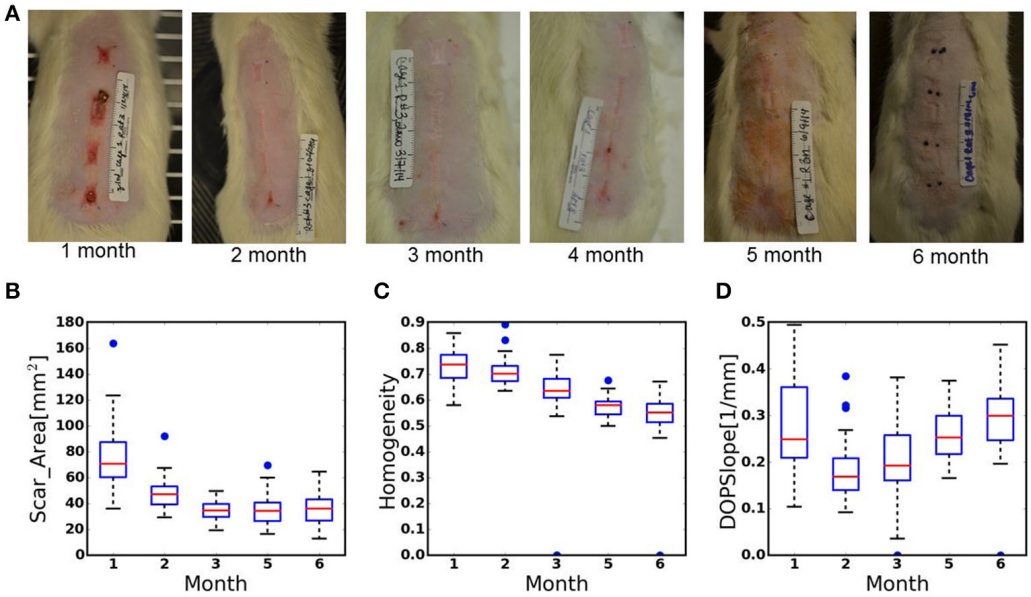

FIGURE 1 | (A) Digital images of scar remodeling over time up to 6 months after third-degree burn injury. **(B–D)** Box-plots of the data recorded from the scars during 6 months of healing. **(B)**. Scar_Area, **(C)**. Homogeneity of birefringence, **(D)**. The slope of the DOP. Plot annotations were defined as follows. Boxes: the main body of the boxplot showing the quartiles and the median's confidence intervals if enabled. Medians: horizontal lines at the median of each box. Whiskers: the vertical lines extending to the most extreme, non-outlier data points. Caps: the horizontal lines at the ends of the whiskers ($n = 36$ wounds, 9 animals).

TABLE 1 | Measured parameters of third-degree burn scars in rats with/without pIRE treatment.

	Scar_Area (mm^2)					Hom					DOPSlope (1/mm)				
Month	**1**	**2**	**3**	**5**	**6**	**1**	**2**	**3**	**5**	**6**	**1**	**2**	**3**	**5**	**6**
Mean	76.13	48.07	33.77	34.72	36.09	0.734	0.7	0.593	0.573	0.539	0.281	0.185	0.195	0.256	0.295
Std	25.22	12.36	7.65	11.01	12.79	0.071	0.055	0.189	0.04	0.1	0.1	0.067	0.09	0.054	0.087
Min	36.068	29.448	19.3	16.519	12.737	0.58	0.635	0.0	0.5	0.0	0.104	0.092	0.0	0.166	0.0
25%	60.2	39.13	29.74	26.61	26.847	0.685	0.672	0.6	0.544	0.514	0.209	0.14	0.16	0.217	0.246
50%	70.69	46.97	34.51	34.29	35.91	0.736	0.701	0.634	0.579	0.552	0.249	0.168	0.192	0.253	0.299
75%	87.46	53.26	39.68	40.6	43.32	0.774	0.731	0.681	0.594	0.585	0.361	0.2	0.257	0.299	0.335
Max	163.736	92.247	49.528	69.56	64.71	0.858	0.892	0.775	0.676	0.671	0.495	0.385	0.382	0.375	0.452

Dataset is based on individual 36 scars, measured over a period of 6 months after initial burn injury, as reported in Golberg et al. (2016). Shown data is an average of 9 animals (4 wounds per animal). OFDI data for each wound includes an average from 2 to 3 acquired volumes.

various combinations of measurements at months 1–3 to predict the scar size in the 6th month.

First, we attempted to predict the Scar_Area at month 6 based on the Scar_Area, Hom, and DOPSlope measured only at the single time point of month 1, 2, or 3 after the injury (pIRE therapy was ongoing during this period; Golberg et al., 2016). The predictions based on the measurements 1 month after the burn injury were not significantly correlated to the actual measured scar size (Pearson coefficient -0.05, $p < 0.39$ and Spearman coefficient 0.01, $p < 0.48$, **Figure 3A**). The predictions based on the measurements performed 2 months after the burn injury were more significantly correlated (Pearson coefficient 0.36, $p < 0.015$ and Spearman coefficient 0.47, $p < 0.002$, **Figure 3B**). The predictions based on the measurements taken 3 months after the burn injury were also significant (Pearson coefficient 0.41, $p < 0.006$ and Spearman coefficient 0.41, $p < 0.006$, **Figure 3C**).

Next, we extended the model to predict the Scar_Area at month 6 based on the Scar_Area, Hom, and DOPSlope measured at 2 or 3-time points 1, 2, and 3 months after the burn injury. Predictions of the scar areas at month 6 were the most accurate when based on the combined measurements of months 2 and 3 (Pearson coefficient 0.57, $p < 10^{-4}$ and Spearman coefficient 0.66, $p < 10^{-5}$, **Figure 4B**). The prediction based on measurements at all 3-time points, months 1, 2 and 3 followed closely in performance (Pearson coefficient 0.51, $p < 7{\cdot}10^{-4}$ and Spearman coefficient 0.59, $p < 8{\cdot}10^{-5}$, **Figure 4D**). Models of the scar area based on the combined measurements of months 1 and 2 (**Figure 4A**) or 1 and 3 (**Figure 4C**) were less significant and resulted in a Pearson coefficient of 0.36,

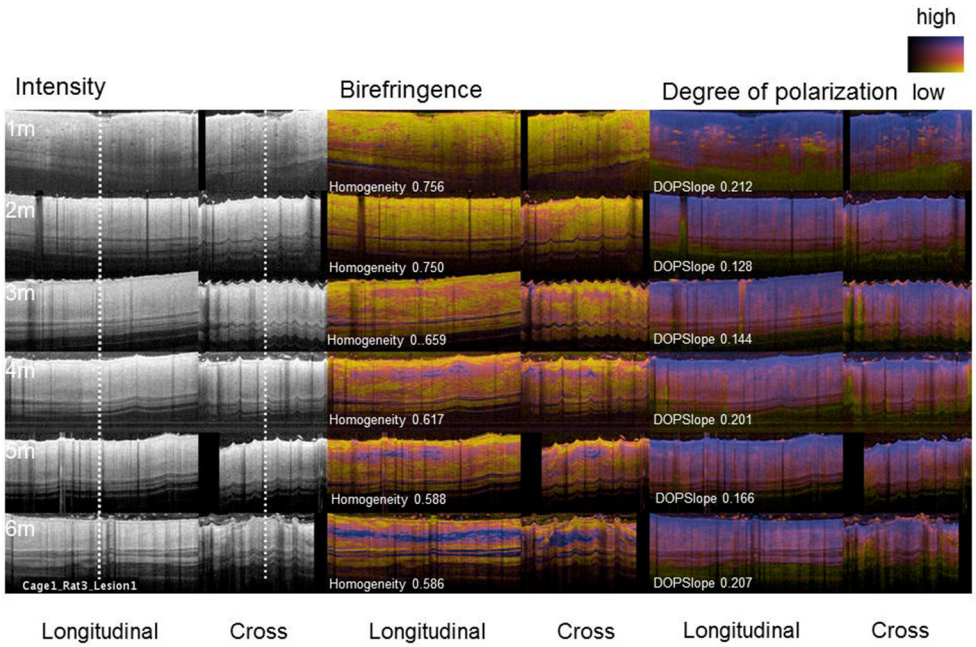

FIGURE 2 | PS-OFDI images of a developing scar following third degree burn injury in the dorsal skin of a rat. Longitudinal and cross-sectional views of the healing burn wounds at several time points in the same animal ($n = 36$ wounds, 9 animals, 2–3 volumes acquired from each wound).

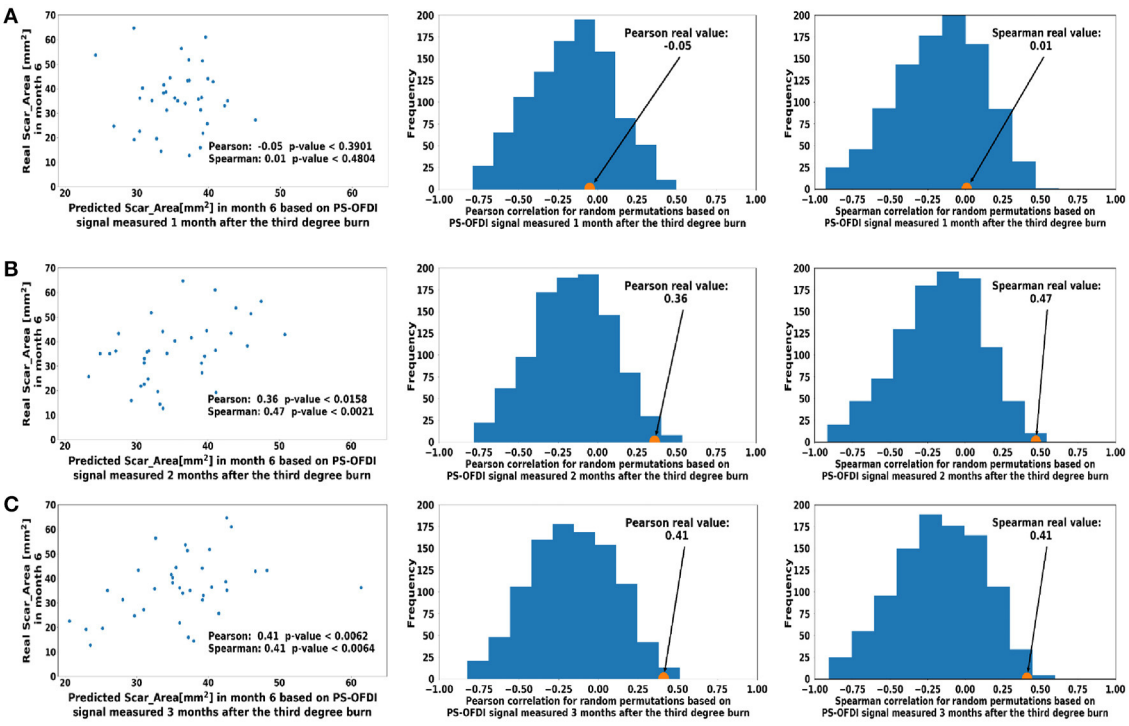

FIGURE 3 | Predicted scar area at month 6 based on measurements taken at a single time point **(A)**. Month 1 **(B)**. Month 2 **(C)**. Month 3 after third-degree burn injury. The control histograms of the correlation coefficients corresponding to randomly shuffled measurements appear on the right-hand side of each panel.

$p < 0.016$ and Spearman coefficient of 0.41, $p < 0.006$ for months 1 and 2, and a Pearson coefficient of 0.35, $p < 0.018$ and Spearman coefficient of 0.37, $p < 0.013$ for months 1 and 3, respectively. The summary of the model comparison appears in **Table 2**. The model coefficients are **Figure 4** reported in Tables S2–S8.

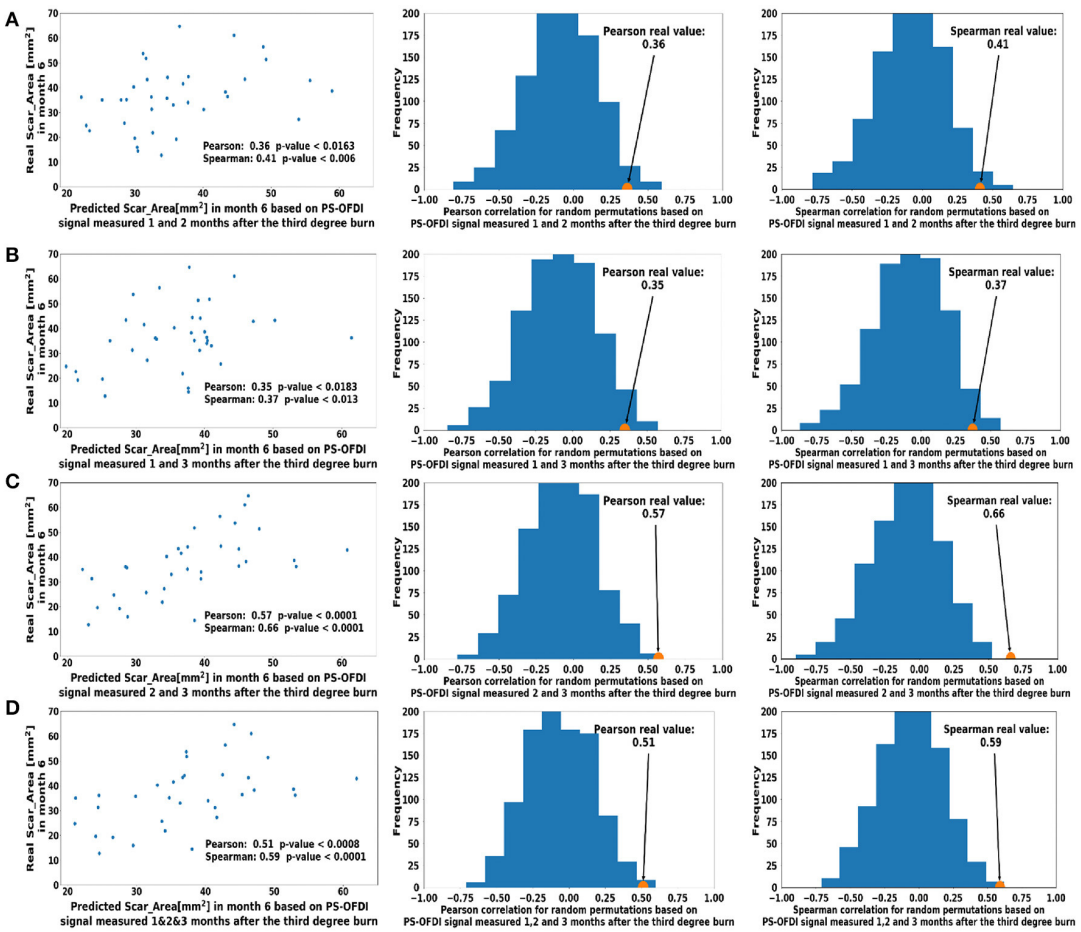

FIGURE 4 | Predicted scar area at month 6 based on multiple measurements taken at **(A)**. Month 1 and Month 2 **(B)**. Month 2 and Month 3 **(C)**. Month 1 and 3 **(D)**. Month 1, 2, and 3 after the third-degree burn injury. The control histograms of the correlation coefficients corresponding to randomly shuffled measurements appear on the right-hand side of each panel.

TABLE 2 | Summary of the linear regression model for predicting the scar area 6 months after third-degree burn injury based on early time point measurements with PS-OFDI.

PS-OFDI measurements time points	Pearson coefficient (*p*-value)	Spearman coefficient (*p*-value)	RMSE
Month 1	−0.04 (0.39)	0.008(0.48)	13.63
Month 2	0.358(0.015)	0.465(0.002)	12.36
Month 3	0.412(0.006)	0.41(0.006)	11.7
Month 1&2	0.356(0.016)	0.413(0.006)	12.6
Month 1&3	0.349(0.018)	0.37(0.012)	12.4
Month 2&3	0.569(0.0001)	0.658(<0.0001)	10.81
Month 1&2&3	0.508(0.0007)	0.587(<0.0001)	11.61

DISCUSSION

Our long-term goal is to develop a metric based on PS-OFDI signatures to assess scar severity and predict the healing potential of burn wounds. Working toward this goal, in the current study, we tracked the remodeling of healing burns in rats, subject to different pIRE treatment plans with PS-OFDI. Burn injuries in rats have obvious limitations in modeling the healing of burn wounds in humans (Ramos et al., 2008); yet such animal studies (Mitsunaga et al., 2012) enable the development and investigation of PS-OFDI signatures *in vivo* during wound healing and are an essential step toward diagnostic applications in human patients (Lo et al., 2016).

In this study, we showed that the scar size 6 months after third-degree burn injury in rats can be accurately estimated from non-invasive measurements with PS-OFDI performed in the first 3 months after the injury. The best results (Pearson coefficient 0.57, $p < 10^{-4}$ and Spearman coefficient 0.66, $p < 10^{-5}$, **Figure 4C**) was achieved when predicting the scar area at month 6 from the scar area, the birefringence homogeneity and the slope of the DOP measured 2 and 3 months after the injury.

The results of this study point to the potential of developing an approach for predicting clinically important scar properties early in the treatment process. The relevance and scope of the current results are, however, limited. Our results are clearly valid in the context of scars in rats and under the protocols used herein.

It is likely that models can be developed for human scars, of many possible types, but the parameters presented are clearly not directly transferable. Even in the context of rats models, a major limitation of this current study is the limited number of tested samples. While the sample size is sufficient to support a strong confidence level that the prediction quality is not spurious larger data sets, with hundreds of independent scars, are required to construct and test more precise prediction models. Such larger samples will allow for more rigorous statistical testing, replacing the LOOCV approach used here. The sample size limitation also dictated a composition of our analyzed cohort that is composed of untreated samples as well as from several different treatments. A more uniform design can lead to even more accurate results but could not be used here as the sample set would become too small.

The predicted quantity at month 6 clearly depends on the rat's month 3 to month 6 history which is not captured by the month 1 to month 3 measurements. Prediction accuracy is also affected by the measurement accuracy. Scar size was manually measured and therefore, the measurement depends on the evaluator. Automated assessment of the scar size, for example using OCT, would be favorable and remove bias, however this method was not performed in the present study as the method will limit the observed field of view. In addition, genetic variation between the rats in this study could have affected scarring potential but are not yet captured in our model. Larger studies will not be able to resolve prediction errors due to these factors. They can allow more complex models, however, and the inclusion of more factors, such as quantitative histological features information (Quinn et al., 2014). Since different signals would likely be detected in human wounds in comparison to wounds in rats, as indicated above, larger future studies should also address differences and how model parameters can translate to human scars. Our analysis and modeling methodology can be extended to perform larger studies in different contexts.

AUTHOR CONTRIBUTIONS

EK and ZY developed the prediction model and drafted the manuscript, MV and BB conducted the PS-OFDI analysis, EK, ZY, MV, MY, AG drafted the manuscript, AG conceived the study and performed data analysis. All authors read and edited the manuscript.

ACKNOWLEDGMENTS

AG and MY acknowledge United States- Israel Binational Science Foundation (BSF) for the support of this work grant #2015286. Research in this publication was also supported in part by the Department of Defense, Air Force Office of Scientific Research under agreement number FA9550-13-1-0068, and the National Institute of Biomedical Imaging and Bioengineering of the National Institutes of Health, award P41 EB015903.

SUPPLEMENTARY MATERIAL

The Supplementary Material for this article can be found online at: https://www.frontiersin.org/articles/10.3389/fphys.2017.00967/full#supplementary-material

REFERENCES

Aarabi, S., Longaker, M. T., and Gurtner, G. C. (2007). Hypertrophic scar formation following burns and trauma: new approaches to treatment. *PLoS Med*. 4:e234. doi: 10.1371/journal.pmed.0040234

Baillie, S. E., Sellwood, W., and Wisely, J. A. (2014). Post-traumatic growth in adults following a burn. *Burns* 40, 1089–1096. doi: 10.1016/j.burns.2014.04.007

Chen, A. C., McNeilly, C., Liu, A. P., Flaim, C. J., Cuttle, L., Kendall, M., et al. (2011). Second harmonic generation and multiphoton microscopic detection of collagen without the need for species specific antibodies. *Burns* 37, 1001–1009. doi: 10.1016/j.burns.2011.03.013

Cross, K. M., Leonardi, L., Payette, J. R., Gomez, M., Levasseur, M. A., Schattka, B. J., et al. (2007). Clinical utilization of near-infrared spectroscopy devices for burn depth assessment. *Wound Repair Regen*. 15, 332–340. doi: 10.1111/j.1524-475X.2007.00235.x

Fearmonti, R., Bond, J., Erdmann, D., and Levinson, H. (2010). A review of scar scales and scar measuring devices. *Eplasty* 10:e43.

Geissbuehler, M., and Lasser, T. (2013). How to display data by color schemes compatible with red-green color perception deficiencies. *Opt. Express* 21, 9862–9874. doi: 10.1364/OE.21.009862

Golberg, A., Villiger, M., Khan, S., Quinn, K. P., Lo, W. C., Bouma, B. E., et al. (2016). Preventing scars after injury with partial irreversible electroporation. *J. Invest. Dermatol.* 136, 2297–2304. doi: 10.1016/j.jid.2016.06.620

Greene, W. (2011). *Econometric Analysis*, *7th Edn*. New York, NY: Pearson.

Heimbach, D. M., Afromowitz, M. A., Engrav, L. H., Marvin, J. A., and Perry, B. (1984). Burn depth estimation–man or machine. *J. Trauma* 24, 373–378.

Jaskille, A. D., Ramella-Roman, J. C., Shupp, J. W., Jordan, M. H., and Jeng, J. C. (2010). Critical review of burn depth assessment techniques: part II. review of laser doppler technology. *J. Burn Care. Res.* 31, 151–157. doi: 10.1097/BCR.0b013e3181c7ed60

Kim, K. H., Pierce, M. C., Maguluri, G., Park, B. H., Yoon, S. J., Lydon, M., et al. (2012). *In vivo* imaging of human burn injuries with polarization-sensitive optical coherence tomography. *J. Biomed. Opt*. 17:66012. doi: 10.1117/1.JBO.17.6.066012

Koppenol, D. C., Vermolen, F. J., Niessen, F. B., van Zuijlen, P. P. M., and Vuik, K. (2017). A mathematical model for the simulation of the formation and the subsequent regression of hypertrophic scar tissue after dermal wounding. *Biomech. Model Mechanobiol.* 16, 15–32. doi: 10.1007/s10237-016-0799-9

Lawrence, J. W., and Fauerbach, J. A. (2003). Personality, coping, chronic stress, social support and PTSD symptoms among adult burn survivors: a path analysis. *J. Burn Care Rehabil.* 24, 63–72. doi: 10.1097/01.BCR.0000045663.57246.ED

Lawrence, J. W., Mason, S. T., Schomer, K., and Klein, M. B. (2012). Epidemiology and impact of scarring after burn injury. *J. Burn Care Res.* 33, 136–146. doi: 10.1097/BCR.0b013e3182374452

Liddington, M. I., and Shakespeare, P. G. (1996). Timing of the thermographic assessment of burns. *Burns* 22, 26–28.

Lin, Y.-H., Huang, C.-C., and Wang S-. (2011). Quantitative assessments of burn degree by high-frequency ultrasonic backscattering and statistical model. *Phys. Med. Biol.* 56, 757–773. doi: 10.1088/0031-9155/56/3/014

Lo, W. C., Villiger, M., Golberg, A., Broelsch, G. F., Khan, S., Lian, C. G., et al. (2016). Longitudinal, 3D imaging of collagen remodeling in murine hypertrophic scars *in vivo* using polarization-sensitive optical frequency domain imaging. *J. Invest. Dermatol.* 136, 84–92. doi: 10.1038/JID.2015.399

Mitsunaga, J. K. Jr., Gragnani, A., Ramos, M. L., and Ferreira, L. M. (2012). Rat an experimental model for burns: a systematic review. *Acta Cir. Bras*. 27, 417–423.

Motulsky, H., and Christopoulos, A. (2002).*Fitting Models to Biological Data Using Linear and Nonlinear Regression. A Practical Guide to Curve Fitting*. San Diego, CA: GraphPad Software Inc.

Nedelec, B., Shankiowsky, H. A., and Tredget, E. E. (2000). Rating the resolving hypertrophic scar: comparison of the vancouver scar scale and scar volume. *J. Burn Care Rehabil.* 21, 205–212. doi: 10.1097/00004630-200021030-00005

Park, B. H., Saxer, C., Srinivas, S. M., Nelson, J. S., and de Boer, J. F. (2001). *In vivo* burn depth determination by high-speed fiber-based polarization sensitive optical coherence tomography. *J. Biomed. Opt*. 6, 474–479. doi: 10.1117/1.1413208

Quinn, K. P., Golberg, A., Broelsch, G. F., Khan, S., Villiger, M., Bouma, B. et al. (2014). An automated image processing method to quantify collagen fiber organization within cutaneous scar tissue. *Exp. Dermatol*. 24, 78–80. doi: 10.1111/exd.12553

Ramos, M. L., Gragnani, A., and Ferreira, L. M. (2008). Is there an ideal animal model to study hypertrophic scarring? *J. Burn Care Res*. 29, 363–368. doi: 10.1097/BCR.0b013e3181667557

Rice, J. (2010). *Mathematical Statistics and Data Analysis*, *3rd Edn.* Belmont, CA: Cengage Learning.

Schneider, C. A., Rasband, W. S., and Eliceiri, K. W. (2012). NIH image to imagej: 25 years of image analysis. *Nat. Methods* 9, 671–675. doi: 10.1038/nmeth.2089

Sheridan, R. L. (2012). *Burns. A Practical Approach to Immediate Treatment and Long-Term Care.* London: Manson Publishing.

Sheridan, R. L., Schomaker, K. T., Lucchina, L. C., Hurley, J., Yin, L. M., Tompkins, R. G., et al. (2015). Burn depth estimation by use of indocyanine green fluorescence: initial human trial. *J. Burn Care Rehabil*. 16, 602–604.

Stanton, J. M. (2001). Galton, Pearson, and the peas: a brief history of linear regression for statistics instructors. *J. Stat. Educ*. 9, 1–13.

Tziotzios, C., Profyris, C., and Sterling, J. (2012). Cutaneous scarring: pathophysiology, molecular mechanisms, and scar reduction therapeutics. *J. Am. Acad. Dermatol*. 66, 13–24. quiz 25–26. doi: 10.1016/j.jaad.2011.08.035

Villiger, M., Zhang, E. Z., Nadkarni, S. K., Oh, W. Y., Vakoc, B. J., and Bouma, B. E. (2013a). Spectral binning for mitigation of polarization mode dispersion artifacts in catheter-based optical frequency domain imaging. *Opt. Express* 21, 16353–16369. doi: 10.1364/OE.21.016353

Villiger, M., Zhang, E. Z., Nadkarni, S., Oh, W.-Y., Bouma, B. E., and Vakoc, B. J. (2013b). Artifacts in polarization-sensitive optical coherence tomography caused by polarization mode dispersion. *Opt Lett*. 38, 923–925. doi: 10.1364/OL.38.000923

WHO. (2016). *Burns. Fact Sheet*. Available online at: http://www.who.int/mediacentre/factsheets/fs365/en/

Conflict of Interest Statement: The authors declare that the research was conducted in the absence of any commercial or financial relationships that could be construed as a potential conflict of interest.

frontiers in Physiology

ORIGINAL RESEARCH
published: 07 November 2017
doi: 10.3389/fphys.2017.00885

The Superficial Dermis May Initiate Keloid Formation: Histological Analysis of the Keloid Dermis at Different Depths

Hu Jiao[1], *Tiran Zhang*[2], *Jincai Fan*[2] *and Ran Xiao*[1]*

[1] The Research Center of Plastic Surgery Hospital, Chinese Academy of Medical Sciences & Peking Union Medical College, Beijing, China, [2] Scar Plastic Department of Plastic Surgery Hospital, Chinese Academy of Medical Sciences & Peking Union Medical College, Beijing, China

Several studies have reported on certain aspects of the characteristics of different sites within a keloid lesion, but detailed studies on the keloid dermis at different depths within a keloid lesion are scarce. The aim of this study was to investigate the histology of the keloid dermis at different depths. This study included 19 keloid tissue samples that were collected from 19 patients and 19 normal skin samples, which were harvested from subjects without keloids or hypertrophic scar. Samples were studied by light microscopy using routine hematoxylin and eosin histochemical staining, and immunohistochemistry to detect CD20-positive B-lymphocytes and CD3-positive T-lymphocytes. Sirius Red histochemical staining was used to determine the type of collagen in keloid tissue and normal skin samples. The migratory properties of fibroblasts within the keloid dermis at different depths was compared, using an *in vitro* migration assay. The findings of this study showed that although the papillary and reticular dermis could be clearly distinguished in normal skin, three tissue layers were identified in the keloid dermis. The superficial dermis of keloid was characterized by active fibroblasts and lymphocytes; the middle dermis contained dense extracellular matrix (ECM) with large numbers fibroblasts, and the deep dermis was poorly cellular and characterized by hyalinized collagen bundles. In the keloid samples, from the superficial to the deep dermis, type I collagen increased and type III collagen decreased, and fibroblasts from the superficial dermis of the keloid were found to migrate more rapidly. In conclusion, the findings of this study showed that different depths within the keloid dermis displayed different biological features. The superficial dermis may initiate keloid formation, in which layer intralesional injection of pharmaceuticals and other treatments should be performed for keloid.

Keywords: keloid, histology, fibroblast, lymphocyte, collagen

OPEN ACCESS

Edited by:
Marianna Bei,
Harvard Medical School,
United States

Reviewed by:
Jean Kanitakis,
Hospices Civils de Lyon, France
Evangeli S Lampri,
University of Ioannina, Greece

***Correspondence:**
Ran Xiao
xiaoran@psh.pumc.edu.cn

Specialty section:
This article was submitted to Clinical and Translational Physiology, a section of the journal Frontiers in Physiology

Received: *20 March 2017*
Accepted: *19 October 2017*
Published: *07 November 2017*

Citation:
Jiao H, Zhang T, Fan J and Xiao R (2017) The Superficial Dermis May Initiate Keloid Formation: Histological Analysis of the Keloid Dermis at Different Depths. Front. Physiol. 8:885. doi: 10.3389/fphys.2017.00885

INTRODUCTION

Keloid is a fibrotic skin condition that typically results from abnormal wound healing. Keloid is characterized by the deposition of an excess of extracellular matrix (ECM). Unlike normal or hypertrophic scars, keloids do not regress with time, but persist indefinitely and extend beyond the original wound margin to invade the surrounding normal skin tissue (Trace et al., 2016). Keloids

are not only aesthetically displeasing, but they can also be both painful and functionally disabling, causing physical and psychological distress for patients (Bayat et al., 2003; Brown et al., 2008). There are several treatment approaches for keloid that have been described, including silicone dressings, pressure dressings, onion extract, corticosteroids, 5-fluorouracil, bleomycin, cryosurgery, laser therapy, and radiotherapy (Kelly, 2009; Tziotzios et al., 2012). Intralesional injection of corticosteroids alone or in combination with other therapeutic agents is the first-line treatment for keloid (Yedomon et al., 2012), but several studies have reported variable treatment efficacy (50–100%) and keloid recurrence (9–50%) (Tziotzios et al., 2012). These varied results may result from different injection protocols, including injections into the superficial or deep dermis or the center or the margin of the lesion, but this remains unclear.

Although numerous studies on keloids have been performed since the initial description by Alibert in 1806, there have been many contradictory reports in the literature. Findings from the examination of biopsies from different sites of keloid lesions may have come to different conclusions. For example, several studies have reported a variety of different biological features in the center or margin of the keloid lesion. It has been reported that fibroblasts from the keloid margin exhibit an increased proliferation rate and produce more type I and type III collagen compared with fibroblasts from intralesional sites (Syed et al., 2011). Cell morphology and fatty acid content were also different between the peripheral and central sites of the keloid (Louw et al., 1997). Protein profiling analysis has shown that mitochondrial-associated proteins were upregulated in the margin of the keloid when compared with in the center (Javad and Day, 2012). Also, the depth of the dermis included in the keloid specimen may also contribute to the conflicting findings from keloid studies. The specific immunophenotyping of the papillary dermis and the reticular dermis has been found in keloids (Bagabir et al., 2012). Unique gene expression patterns were reported in the deeper part and the superficial part of the keloid center (Seifert et al., 2008). However, in previous studies, the histological characteristics at different depths within the keloid dermis have not been specially studied.

In the current study, we investigated the histology and biology of keloid lesion at different depths, focusing on the cellular composition and collagen composition and the biological behavior of the fibroblasts at the different levels within the keloid dermis. To define the histopathology of the different keloid dermis depths would be helpful to obtain insight into the pathogenesis and the efficient treatment layer of keloids.

MATERIALS AND METHODS

Patients and Samples

Nineteen keloid skin specimens were surgically excised from patients, seven men and 12 women (mean age 29.4 years; range 19–59 years). Patients fulfilled the currently accepted criteria for keloid, defined as the presence of typical skin lesions confirmed by two plastic surgeons. None of the patients included in the study had treatment within the previous 6 months. All keloid lesions caused pain or itching or displayed redness. The duration of the skin keloids ranged from 1.5 to 5 years. Keloids were located on the anterior chest wall (six), shoulder (two), chin (one), ear (seven), arm (one) or abdomen (two), and resulted from surgery (two), acne (two), vaccination (two), trauma (two), piercing (six), or were spontaneous (five).

Nineteen normal skin specimens were obtained from age-matched and sex-matched healthy control subjects who underwent surgical procedures for cosmetic or other reasons, of which eight biopsies were from periauricular skin, five were from the anterior chest wall, four were from the abdomen, one was from the shoulder and one was from the arm. Healthy control subjects had neither keloids nor hypertrophic scars. All patients and healthy control subjects were Asian.

This study was carried out in accordance with the recommendations of the Plastic Surgery Hospital Research Guidelines. All subjects gave written informed consent in accordance with the Declaration of Helsinki. The study protocol was approved by the Ethical Committee of the Plastic Surgery Hospital, Chinese Academy of Medical Sciences and Peking Union Medical College.

Hematoxylin and Eosin (H&E) Histochemical Staining

Excised keloids were fixed in 10% formalin for 24 h and dehydrated by standard histological procedures (Santucci et al., 2001). Excision samples were sectioned through the center of the lesion, embedded in paraffin wax, cut on a microtome (5 μm sections) to obtain sections perpendicular to the skin surface, and thin sections were mounted on glass slides. The slides were deparaffinized and hydrated using normal procedures and stained with hematoxylin and eosin (H&E). The slides were viewed using standard light microscopy.

Immunohistochemistry

Immunohistochemical staining was conducted as previously described (Bagabir et al., 2012). Briefly, antigen was retrieved by pressure cooking for 3 min in citrate buffer (pH = 6.0). Endogenous peroxidase was blocked in 0.3% hydrogen peroxide in methanol for 30 min, and nonspecific antibody binding was blocked with 1% bovine serum albumen (BSA). Mouse monoclonal antibodies directed against CD3 and CD20 (Zhongshan, Beijing, China) were used as primary antibodies and incubated overnight at 4°C. Horseradish peroxidase-conjugated rabbit anti-mouse IgG was incubated for 45 min at room temperature as the secondary antibody and was purchased from Abcam (Hong Kong, China). Staining was achieved using a diaminobenzidine (DAB) staining kit (Zhongshan, Beijing, China) at room temperature for 5 min. Sections were counterstained with hematoxylin.

Sirius Red Staining for Collagen

For Sirius Red staining, the slides were deparaffinized and hydrated as in the case of H&E staining. Then the sections were immersed in Sirius Red solution (0.1% Sirius Red in saturated picric acid, pH 2.0) for 1 h, rinsed briefly in 0.01 M HCl solution and then in water for 1 min, counterstained with hematoxylin

for 1 min, differentiated in acid alcohol solution, rehydrated and mounted. Slides were visualized under polarized light microscopy, and photomicrographs were taken with identical exposure settings for all sections, as previous described (Meruane et al., 2012; Wang et al., 2017).

Fibroblasts Migration

To investigate the migration of fibroblasts from keloid dermis at different depths, tissue culture was carried out. The keloid dermis was cut into a strip that contained the superficial dermis (SD), mid-dermis (MD), and deep dermis (DD). The strip of skin tissue containing the keloid dermis was placed horizontally onto the bottom of a tissue culture dish and covered with a sterilized glass coverslip. Tissues were maintained in Dulbecco's modified Eagle's medium (DMEM), supplemented with 10% fetal bovine serum (FBS) and incubated in a carbon dioxide incubator at 37°C. After 7 days, fibroblast migration was observed under microscopy and the migration distance (the perpendicular distance between the farthest fibroblast and the border of dermis strip) was measured.

Statistical Analysis

Statistical analysis was performed using SPSS version 16.0 (SPSS, Chicago, USA). Data were presented as the mean ± SD (standard deviation). Data were analyzed using Fisher's Least Significant Difference test to compare data between individual experimental groups. The level of statistical significance was $P < 0.05$.

RESULTS

Histology of Normal Skin

The histology of keloid skin tissues and normal skin were viewed by light microscopy following routine hematoxylin and eosin (H&E) histochemical staining. In the normal skin, two layers of the superficial papillary dermis and the deeper, thicker reticular dermis were clearly distinguished (data not shown). In the dermis of the normal skin, the ECM was less compact, with fine, loosely and irregularly arranged collagen bundles and few cells. Although the thickness of the dermis from different skin biopsies was different, they showed similar histology.

Histology of the Keloid Dermis at Different Depths

The dermis in the keloid skin showed distinct histological features at different depths, with three tissue layers identified. The superficial dermis (SD), directly beneath the epidermis, was the thinnest tissue layer (643 ± 380 μm) and was morphologically similar to the granulation tissue observed in normal wound healing. In this layer, we found a heavy infiltrate of cells, including spindle-shaped fibroblasts and lymphocytes. The collagen bundles in the superficial dermis of the keloid were fine and organized parallel to each other (**Figure 1**).

The mid-dermis (MD) of the keloid was the thickest layer accounting for more than half of the thickness of the lesion, with compact collagen fibers and the most prominent fibroblast infiltration (**Figure 1**). Different histological characteristics were also evident from the superficial to deep regions in this layer. For example, in the superficial zone, the nuclei of the spindle-shaped cells were large and oval with prominent nucleoli, suggesting these cells were activated fibroblasts. However, the cell nuclei in the deep zone were small and exhibited pyknosis, suggesting that these cells were static fibrocytes. Collagen fibers were thick and hyalinized fibers were found in the MD.

The third layer in the keloid dermis was the deep dermis (DD), which featured prominent degeneration and necrosis of dermal cells (**Figure 1**). Atrophic and degenerate cells, the basophilic nuclear remnants of which scattered in the ECM, were observed here. Collagen bundles were abnormally thick as well as randomly and loosely organized, and more hyalinized collagen fibers were found in this layer.

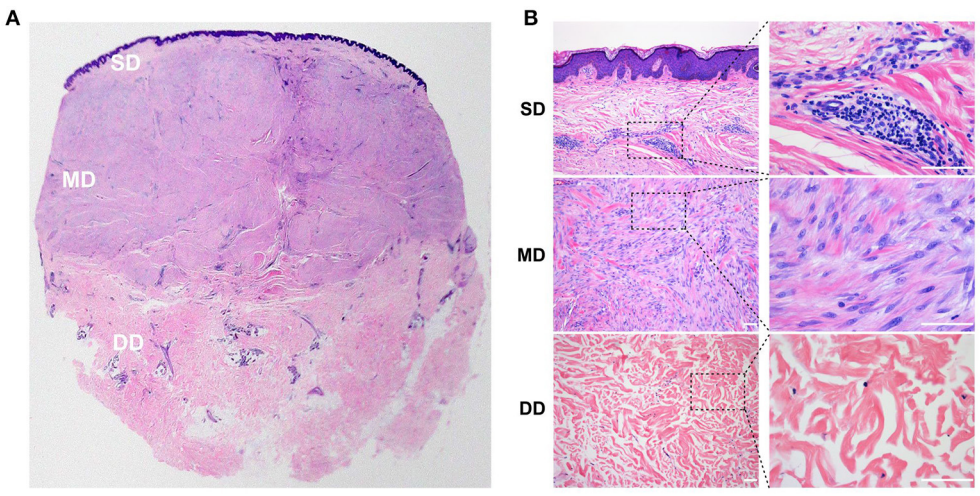

FIGURE 1 | Histology of the keloid dermis at different depths. **(A,B)** In the SD, a heavy infiltrate of fibroblasts and lymphocytes was found, and collagen bundles were fine and organized parallel to each other. **(A,B)** In the MD, compact collagen bundles and abundant fibroblasts were found. **(A,B)** Atrophic and degenerate cells, as well as hyalinized collagen fibers were found in the DD. SD, superficial dermis; MD, middle dermis; DD, deep dermis. Scale bar = 100 μm.

Though keloid lesions were harvested from different parts of the body, there were no obvious differences in their histology. In our study, keloid duration was also not related to the histology, which may have resulted from small sample size and short duration of disease.

Lymphocyte Infiltration in the Keloid Dermis at Different Depths

To confirm whether those small round cells with large nucleus infiltrated in the SD of the keloid the markers of T-lymphocytes and B-lymphocytes, CD3 and CD20 were examined by immunohistochemistry staining (**Figure 2**). Results showed the small round cells were positive for CD3 or CD20. $CD3^+$ T-lymphocytes were mainly located in close association with vessels, whereas $CD20^+$ B-lymphocytes formed large and compact aggregates in the SD of the keloid. However, few of CD3- positive T-lymphocytes or CD20-positive B-lymphocytes were found in the MD or DD of the keloid, or in the dermis of normal skin.

Histology of the Keloid Dermis at Different Sites

We also observed the surrounding normal skin tissue, the margin and the center of the keloid tissue. The interface between the keloid tissue and the surrounding normal skin tissue was identifiable microscopically. The ECM was loose and skin appendages were present in normal skin; the ECM was dense and the skin appendages were absent in keloids (**Figure 3A**). In addition, the macroscopically normal skin surrounding the keloid lesion exhibited a prominent infiltration of lymphocytes (**Figure 3C**). Also, the infiltration of lymphocytes in the margin

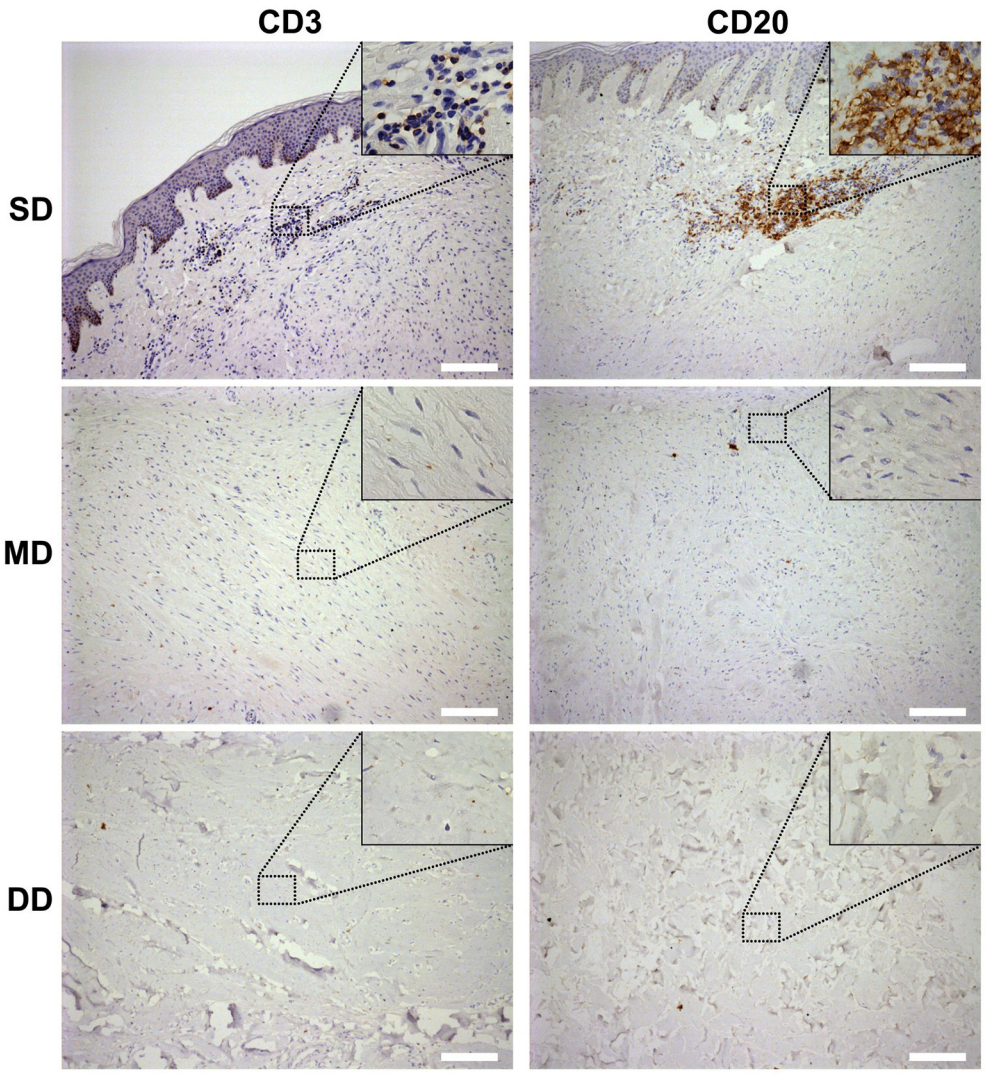

FIGURE 2 | Lymphocyte infiltration in the keloid dermis at different depths. $CD3^+$ T-lymphocytes and $CD20^+$ B-lymphocytes in keloid was detected by immunohistochemistry staining. SD, the superficial dermis of keloids; MD, the middle dermis of keloids; DD, the deep dermis of keloids. Scale bar = 200 μm.

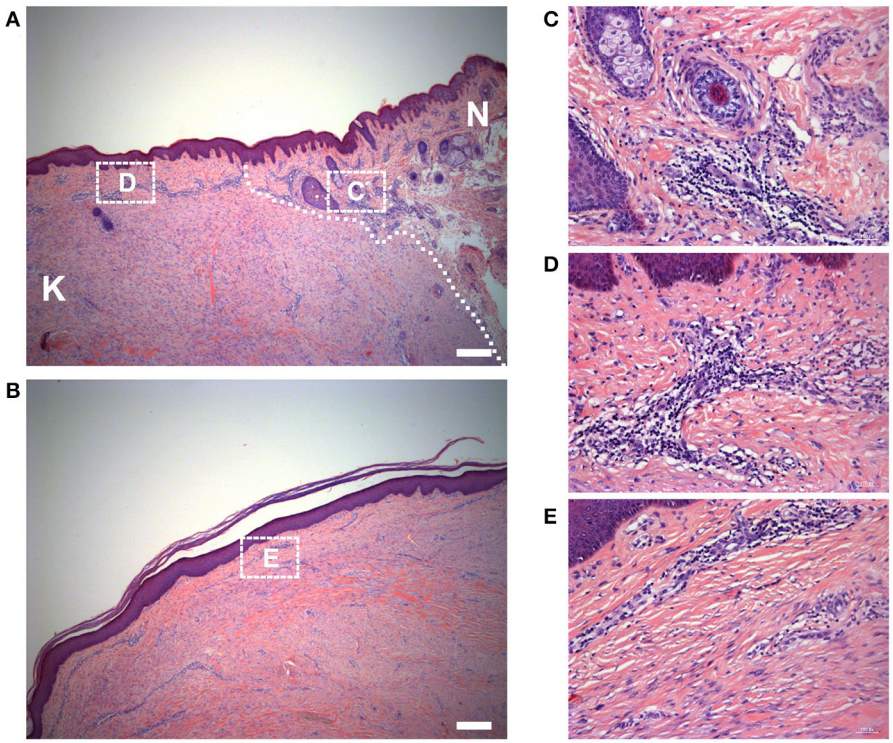

FIGURE 3 | Histology of the keloid dermis at different sites. **(A)** The boundary and **(B)** the center of keloid lesion were observed. The interface of lesion and normal skin was identifiable microscopically (white dotted line indicated) and **(C)** the macroscopically normal-appearing skin surrounding the keloid lesion exhibited a prominent infiltration of lymphocytes. **(B,E)** In the center of the keloid lesion, the infiltration of lymphocytes was less than it in the margin of the lesion **(D)**. K, keloid; N, the macroscopically normal-appearing skin surrounding the keloid lesion. Scale bar = 200 μm.

of the keloid lesion (**Figure 3D**) was greater than in the center of the lesion (**Figures 3B,E**).

Collagen Composition in Keloid Lesions and Normal Skin

To determine the type of collagen in keloid lesions and normal skin, Sirius Red staining was performed. In the dermis of the normal skin, type I collagen fibers (yellow) were the main component of ECM, while type III (green) comprised only a small portion. Also, the composition of collagen fibers did not display differences at different depths in normal skin. Consistent with the results of the H&E staining, type I and III collagen fibers were fine, as well as loosely and irregularly arranged in the normal dermis (**Figure 4**).

Compared with the normal skin, collagen fibers were thicker in the dermis of the keloid and the composition was different at different depths (**Figure 4**). In the SD of the keloid, the amount of type III collagen fibers was significantly greater than type I collagen fibers. Type III collagen fibers progressively decreased in the MD of the keloid, whereas type I collagen increased. Type I collagen fibers comprised the majority of the ECM in the DD of the keloid. Also, parallel arrangement of type I and III collagen fibers was found in the SD and MD of keloid, but in the DD of keloid, collagen fibers were irregularly arranged.

Fibroblasts Migration in Keloid Dermis at Different Depths

The migration of fibroblasts from keloid dermis at different depths was investigated using tissue culture (**Figure 5**). Seven days after incubation, fibroblasts had migrated from the SD of keloid tissue. There were a few fibroblasts observed migrating from the MD of the keloid. However, there were no fibroblasts migrating from the DD of the keloid. The migration distance was measured and results showed fibroblasts from SD migrated fastest.

DISCUSSION

In the present study, different histological features were identified at different depths in the keloid dermis, which may explain the conflicting findings from different studies. Taking collagen fibers as an example, some studies have reported that collagen fibers are haphazardly oriented in keloid lesions (Santucci et al., 2001), but others have reported collagen fibers to be organized in a more parallel manner (Verhaegen et al., 2009). Moreover, some studies have reported the type I/III collagen ratio is increased in keloids (Weber et al., 1978; Hayakawa et al., 1979), while other studies have suggested that the ratio is decreased (Friedman et al., 1993). As this study has demonstrated a different orientation and type

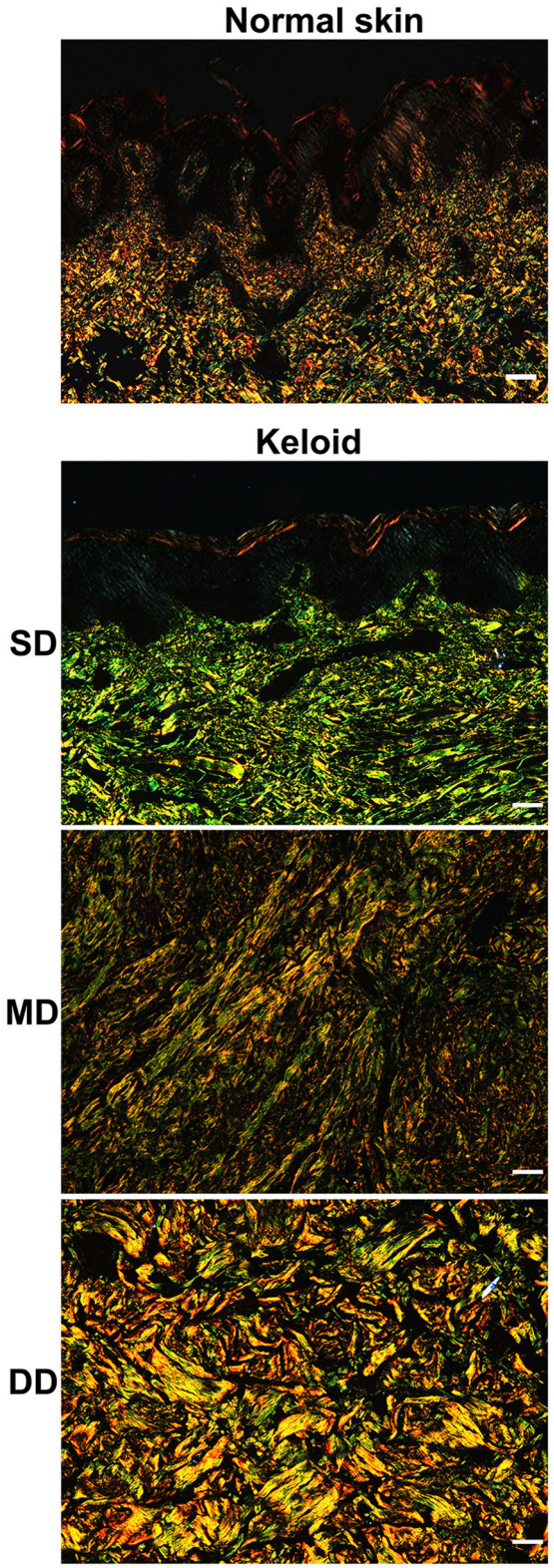

FIGURE 4 | Collagen composition in keloid lesions and normal skin**.** The type of collagen composition was determined by sirius red staining. Scale bar = 100 μm. SD, superficial dermis; MD, middle dermis; DD, deep dermis.

of collagen in different depths of the keloid dermis, contradictory conclusions may be due to the different depths of the biopsies of the keloids that were performed.

A number of studies have indicated an important role for lymphocytes in the development of fibrosis. In a study we previously reported, we showed that B-lymphocytes and T-lymphocytes were present in keloid dermis (Jiao et al., 2015). In the present study, the infiltration of T-lymphocytes was found to be perivascular in the SD of the keloid. It has been reported that perivascular T-lymphocyte infiltration, consisting mainly of activated T-lymphocytes, is found in the skin of patients with systemic sclerosis (Kalogerou et al., 2005), which is also a fibrotic skin disease. T-lymphocytes are believed to promote fibrosis by secreting cytokines such as IL-4, IL-5, IL-6, IL-10, and IL-13 to stimulate the synthesis of collagen by human fibroblasts (Wynn, 2004). B-lymphocytes could directly or indirectly induce tissue fibrosis by local effects, such as antigen presentation, cytokine release, T cell differentiation, dendritic cell modulation, and/or cell-cell contact, or by long-range effects via antibodies (Lipsky, 2001; Marra et al., 2009). For example, B-lymphocytes produce cytokines IL-4, IL-6, IL-13 and TGF-β1 directly promoting a fibrosis response (Mosmann, 2000; Hasegawa et al., 2005). Additionally, the cell-cell interaction has been observed between the fibroblasts and lymphocytes in keloid (Shaker et al., 2011), indicating lymphocytes may promote fibroblasts to synthesize collagen through direct gap junctions.

The predominant collagen types in the human dermis are types I and III, which account for >95% of the bulk of all of the collagen, with approximately 85% being type I collagen (Uitto et al., 1985). At the beginning of wound healing, fibroblasts synthesize type III collagen, which happens as early as 2 or 3 days following wounding. As wound healing progresses, the synthesis of type III collagen is decreased gradually, accompanied by a type I collagen increase at 6 or 7 days following wounding (Diegelmann et al., 1975; Hayakawa et al., 1979). In the current study, type III collagen accounted for the majority of ECM in the superficial tissue layer of the keloid, and the infiltration of lymphocytes and activated fibroblasts were also found in this layer. From the superficial to deep layers of the keloid dermis, the number of fibroblasts decreased and the fibroblasts were transformed from an active state to a static state, and the type I /III collagen ratio and the amount of hyalinized collagen increased.

One of the key features of keloids is the progressive invasion into the adjacent normal skin, exceeding the original wound margin. Migration is a cellular behavior commonly observed during wound healing and metastasis, where fibroblasts or cancer cells undergo dynamic responses featured by rapid focal adhesion turnovers, actin polymerizations and traction force generations (Footer et al., 2007; Harn et al., 2015). Research has indicated that fibroblasts from keloid dermis show a higher migration pattern in comparison with fibroblasts from normal skin or hypertrophic scar (Lim et al., 2006; Song et al., 2012; Yun et al., 2015). In the present study, we also showed that fibroblasts from the superficial dermis of keloid migrate more rapidly when compared with fibroblasts from the middle or deep dermis.

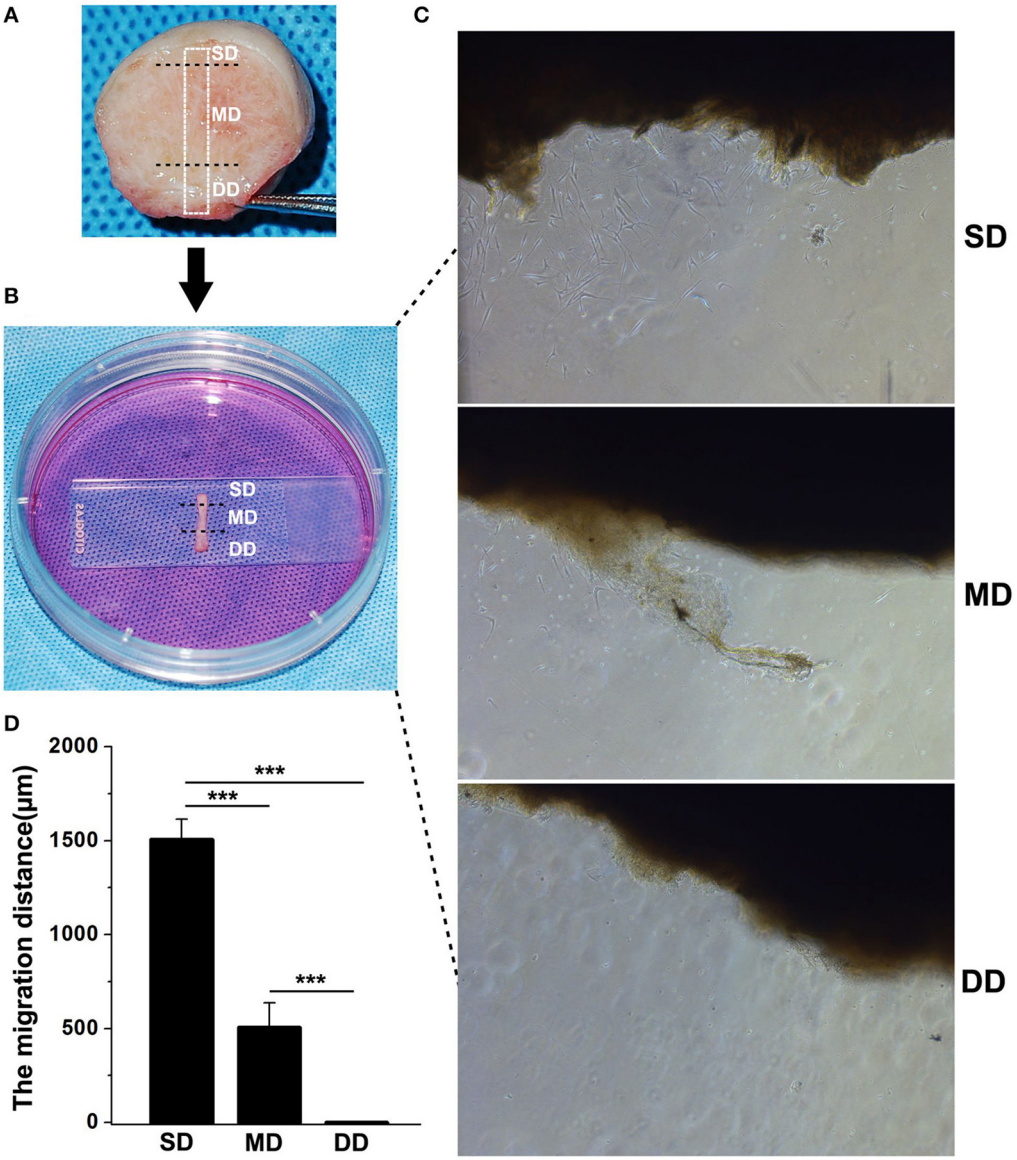

FIGURE 5 | Fibroblasts migration in keloid dermis at different depths. **(A)** Tissue strip containing full-thickness keloid dermis was cut out. **(B)** Tissue strip was fixed by glass and cultured in medium. **(C)** Fibroblast migrating was observed after 7 days and **(D)** The migration distance was measured. SD, superficial dermis; MD, middle dermis; DD, deep dermis. ***Behavior, $p < 0.001$.

Our results suggest the SD may initiate keloid formation. In the SD, lymphocytes may produce certain cytokines in a paracrine manner and increase the proliferation of fibroblasts and the synthesis of collagen. With the deposition of ECM, fibroblasts are buried in the ECM, which reduces the effects of lymphocytes, and these fibroblasts produce more type I instead of type III collagen. In the deep layer of the keloid dermis, the disappearance of fibroblasts may be due to apoptosis or some other mechanism, decrease in ECM synthesis results in degeneration of collagen fibers, which may explain why few cells and hyalinized collagen fibers were found in the DD of keloid lesions.

Because the SD is important for keloid formation and the infiltration of lymphocytes is increased in the margin of keloids, we would suggest that intralesional injection and other treatments should be performed in the superficial layer of the keloid dermis, especially in the margin of keloids. Because the superficial layer is easily accessed, the development of some medicine for external use feasible. Also, this study has shown that pathological changes were found in the surrounding normal skin, where treatment should also be performed. Our study provides a better understanding of the histological features of the keloid dermis to help guide such local therapeutic strategies.

AUTHOR CONTRIBUTIONS

HJ conceived and performed the experiments, collected and analyzed the data, and drafted the manuscript. TZ assisted with the collection of data. JF helped in harvesting the keloids and normal skin specimens. RX conceived and designed the project, oversaw the collection of results and data interpretation, wrote the manuscript and had primary responsibility for final content. All authors read and approved the final manuscript.

FUNDING

This work was funded by CAMS Initiative for Innovative Medicine (CAMS-I2M) (2016-I2M-1-017).

REFERENCES

Bagabir, R., Byers, R. J., Chaudhry, I. H., Müller, W., Paus, R., and Bayat, A. (2012). Site-specific immunophenotyping of keloid disease demonstrates immune upregulation and the presence of lymphoid aggregates. *Br. J. Dermatol.* 167, 1053–1066. doi: 10.1111/j.1365-2133.2012.11190.x

Bayat, A., Mcgrouther, D. A., and Ferguson, M. W. (2003). Skin scarring. *BMJ* 326:88. doi: 10.1136/bmj.326.7380.88

Brown, B. C., Mckenna, S. P., Siddhi, K., Mcgrouther, D. A., and Bayat, A. (2008). The hidden cost of skin scars: quality of life after skin scarring. *J. Plast Reconstr. Aesthet. Surg.* 61, 1049–1058. doi: 10.1016/j.bjps.2008.03.020

Diegelmann, R. F., Rothkopf, L. C., and Cohen, I. K. (1975). Measurement of collagen biosynthesis during wound healing. *J. Surg. Res.* 19, 239–243. doi: 10.1016/0022-4804(75)90087-6

Footer, M. J., Kerssemakers, J. W., Theriot, J. A., and Dogterom, M. (2007). Direct measurement of force generation by actin filament polymerization using an optical trap. *Proc. Natl. Acad. Sci. U.S.A.* 104, 2181–2186. doi: 10.1073/pnas.0607052104

Friedman, D. W., Boyd, C. D., Mackenzie, J. W., Norton, P., Olson, R. M., and Deak, S. B. (1993). Regulation of collagen gene expression in keloids and hypertrophic scars. *J. Surg. Res.* 55, 214–222. doi: 10.1006/jsre.1993.1132

Harn, H. I., Wang, Y. K., Hsu, C. K., Ho, Y. T., Huang, Y. W., Chiu, W. T., et al. (2015). Mechanical coupling of cytoskeletal elasticity and force generation is crucial for understanding the migrating nature of keloid fibroblasts. *Exp. Dermatol.* 24, 579–584. doi: 10.1111/exd.12731

Hasegawa, M., Fujimoto, M., Takehara, K., and Sato, S. (2005). Pathogenesis of systemic sclerosis: altered B cell function is the key linking systemic autoimmunity and tissue fibrosis. *J. Dermatol. Sci.* 39, 1–7. doi: 10.1016/j.jdermsci.2005.03.013

Hayakawa, T., Hashimoto, Y., Myokei, Y., Aoyama, H., and Izawa, Y. (1979). Changes in type of collagen during the development of human post-burn hypertrophic scars. *Clin. Chim. Acta* 93, 119–125. doi: 10.1016/0009-8981(79)90252-3

Javad, F., and Day, P. J. (2012). Protein profiling of keloidal scar tissue. *Arch. Dermatol. Res.* 304, 533–540. doi: 10.1007/s00403-012-1224-6

Jiao, H., Fan, J., Cai, J., Pan, B., Yan, L., Dong, P., et al. (2015). Analysis of Characteristics similar to autoimmune disease in keloid patients. *Aesthetic Plast Surg.* 39, 818–825. doi: 10.1007/s00266-015-0542-4

Kalogerou, A., Gelou, E., Mountantonakis, S., Settas, L., Zafiriou, E., and Sakkas, L. (2005). Early T cell activation in the skin from patients with systemic sclerosis. *Ann. Rheum. Dis.* 64, 1233–1235. doi: 10.1136/ard.2004.027094

Kelly, A. P. (2009). Update on the management of keloids. *Semin Cutan Med. Surg.* 28, 71–76. doi: 10.1016/j.sder.2009.04.002

Lim, C. P., Phan, T. T., Lim, I. J., and Cao, X. (2006). Stat3 contributes to keloid pathogenesis via promoting collagen production, cell proliferation and migration. *Oncogene* 25, 5416–5425. doi: 10.1038/sj.onc.1209531

Lipsky, P. E. (2001). Systemic lupus erythematosus: an autoimmune disease of B cell hyperactivity. *Nat. Immunol.* 2, 764–766. doi: 10.1038/ni0901-764

Louw, L., Van Der Westhuizen, J. P., Duyvene De Wit, L., and Edwards, G. (1997). Keloids: peripheral and central differences in cell morphology and fatty acid compositions of lipids. *Adv. Exp. Med. Biol.* 407, 515–520. doi: 10.1007/978-1-4899-1813-0_77

Marra, F., Aleffi, S., Galastri, S., and Provenzano, A. (2009). Mononuclear cells in liver fibrosis. *Semin. Immunopathol.* 31, 345–358. doi: 10.1007/s00281-009-0169-0

Meruane, M. A., Rojas, M., and Marcelain, K. (2012). The use of adipose tissue-derived stem cells within a dermal substitute improves skin regeneration by increasing neoangiogenesis and collagen synthesis. *Plast Reconstr. Surg.* 130, 53–63. doi: 10.1097/PRS.0b013e3182547e04

Mosmann, T. (2000). Complexity or coherence? Cytokine secretion by B cells. *Nat. Immunol.* 1, 465–466. doi: 10.1038/82707

Santucci, M., Borgognoni, L., Reali, U. M., and Gabbiani, G. (2001). Keloids and hypertrophic scars of Caucasians show distinctive morphologic and immunophenotypic profiles. *Virchows Arch.* 438, 457–463. doi: 10.1007/s004280000335

Seifert, O., Bayat, A., Geffers, R., Dienus, K., Buer, J., Löfgren, S., et al. (2008). Identification of unique gene expression patterns within different lesional sites of keloids. *Wound Repair Regen.* 16, 254–265. doi: 10.1111/j.1524-475X.2007.00343.x

Shaker, S. A., Ayuob, N. N., and Hajrah, N. H. (2011). Cell talk: a phenomenon observed in the keloid scar by immunohistochemical study. *Appl. Immunohistochem. Mol. Morphol.* 19, 153–159. doi: 10.1097/PAI.0b013e3181efa2ef

Song, J., Xu, H., Lu, Q., Xu, Z., Bian, D., Xia, Y., et al. (2012). Madecassoside suppresses migration of fibroblasts from keloids: involvement of p38 kinase and PI3K signaling pathways. *Burns* 38, 677–684. doi: 10.1016/j.burns.2011.12.017

Syed, F., Ahmadi, E., Iqbal, S. A., Singh, S., Mcgrouther, D. A., and Bayat, A. (2011). Fibroblasts from the growing margin of keloid scars produce higher levels of collagen I and III compared with intralesional and extralesional sites: clinical implications for lesional site-directed therapy. *Br. J. Dermatol.* 164, 83–96. doi: 10.1111/j.1365-2133.2010.10048.x

Trace, A. P., Enos, C. W., Mantel, A., and Harvey, V. M. (2016). Keloids and hypertrophic scars: a spectrum of clinical challenges. *Am. J. Clin. Dermatol.* 17, 201–223. doi: 10.1007/s40257-016-0175-7

Tziotzios, C., Profyris, C., and Sterling, J. (2012). Cutaneous scarring: Pathophysiology, molecular mechanisms, and scar reduction therapeutics Part, I. I. Strategies to reduce scar formation after dermatologic procedures. *J. Am. Acad. Dermatol.* 66, 13–24. doi: 10.1016/j.jaad.2011.08.035

Uitto, J., Perejda, A. J., Abergel, R. P., Chu, M. L., and Ramirez, F. (1985). Altered steady-state ratio of type I/III procollagen mRNAs correlates with selectively increased type I procollagen biosynthesis in cultured keloid fibroblasts. *Proc. Natl. Acad. Sci. U.S.A.* 82, 5935–5939. doi: 10.1073/pnas.82.17.5935

Verhaegen, P. D., Van Zuijlen, P. P., Pennings, N. M., Van Marle, J., Niessen, F. B., Van Der Horst, C. M., et al. (2009). Differences in collagen architecture between keloid, hypertrophic scar, normotrophic scar, and normal skin: an objective histopathological analysis. *Wound Repair Regen.* 17, 649–656. doi: 10.1111/j.1524-475X.2009.00533.x

Wang, Y., Yao, B., Li, H., Zhang, Y., Gao, H., Gao, Y., et al. (2017). Assessment of tumor stiffness with shear wave elastography in a human prostate cancer xenograft implantation model. *J. Ultrasound Med.* 36, 955–963. doi: 10.7863/ultra.16.03066

Weber, L., Meigel, W. N., and Spier, W. (1978). Collagen polymorphism in pathologic human scars. *Arch. Dermatol. Res.* 261, 63–71. doi: 10.1007/BF00455376

Wynn, T. A. (2004). Fibrotic disease and the T(H)1/T(H)2 paradigm. *Nat. Rev. Immunol.* 4, 583–594. doi: 10.1038/nri1412

Yedomon, G. H., Adegbidi, H., Atadokpede, F., Akpadjan, F., Mouto, E. J., and Do Ango-Padonou, F. (2012). [Keloids on dark skin: a consecutive series of 456 cases]. *Med. Sante Trop.* 22, 287–291. doi: 10.1684/mst.2012.0052.

Yun, I. S., Lee, M. H., Rah, D. K., Lew, D. H., Park, J. C., and Lee, W. J. (2015). Heat Shock Protein 90 Inhibitor (17-AAG) Induces apoptosis and decreases cell migration/motility of keloid fibroblasts. *Plast Reconstr. Surg.* 136, 44e−53e. doi: 10.1097/PRS.0000000000001362

Conflict of Interest Statement: The authors declare that the research was conducted in the absence of any commercial or financial relationships that could be construed as a potential conflict of interest.

frontiers in Physiology

ORIGINAL RESEARCH
published: 11 January 2017
doi: 10.3389/fphys.2016.00683

Development of Chitosan/Poly(Vinyl Alcohol) Electrospun Nanofibers for Infection Related Wound Healing

Mian Wang[1], *Amit K. Roy*[1]* *and Thomas J. Webster*[1, 2, 3]*

[1] *Department of Chemical Engineering, Northeastern University, Boston, MA, USA,* [2] *Wenzhou Institute of Biomaterials and Engineering, Wenzhou Medical University, Wenzhou, China,* [3] *Center of Excellence for Advanced Materials Research, King Abdulaziz University, Jeddah, Saudi Arabia*

Chitosan is a cheap resource, which is widely used in biomedical applications due to its biocompatible and antibacterial properties. In this study, composite nanofibrous membranes of chitosan (CS) and poly(vinyl alcohol) (PVA) loaded with antibiotics at different ratios were successfully fabricated by electrospinning. The composite nanofibers were subjected to further analysis by scanning electron microscopy (SEM). SEM images revealed that the volumetric ratio of CS/PVA at 50/50 achieved an optimal nanofibrous structure (i.e., that most similar to natural tissues) compared with other volumetric ratios, which indicated that this CS/PVA electrospun scaffold has great potential to be used for infection related wound dressing for skin tissue regeneration.

Keywords: nanostructures, wound healing, chitosan, fibers, polyvivl alcohol

OPEN ACCESS

Edited by:
Marianna Bei,
Harvard Medical School, USA

Reviewed by:
Sunita Nair,
Capita India Pvt. Ltd., India
Ajeet Kumar,
Clarkson University, USA

***Correspondence:**
Amit K. Roy
akroy99@yahoo.com
Thomas J. Webster
th.webster@neu.edu

Specialty section:
This article was submitted to Clinical and Translational Physiology, a section of the journal Frontiers in Physiology

Received: *25 June 2016*
Accepted: *22 December 2016*
Published: *11 January 2017*

Citation:
Wang M, Roy AK and Webster TJ (2017) Development of Chitosan/Poly(Vinyl Alcohol) Electrospun Nanofibers for Infection Related Wound Healing. Front. Physiol. 7:683. doi: 10.3389/fphys.2016.00683

INTRODUCTION

Chronic dermal wounds, such as infected diabetic foot ulcers, represent a major health problem that affects millions of people worldwide and induces billions of dollars in social and economic costs; the poor treatment outcomes result in high healthcare costs. Such data explain the large research efforts now focused on developing new therapeutic approaches to improve wound healing (Dwivedi et al., 2016). The entire process of normal infection related wound healing requires the formulation of scaffolds with high regeneration properties. Recently electrospinning technology was used as a very popular method to fabricate tissue-engineering scaffolds (Field and Kerstein, 1994; Tchemtchoua et al., 2011). The nanofibrous membrane prepared by electrospinning has its advantages such as high porosity and nanoscale morphology. The electropinning membrane is also important for cell attachment, proliferation, and anti-infection in quick and scarless wound healing. In addition, the wet scaffold plays a very important role in wound healing since water swells in the scaffold and is of great help to reduce necrotic tissue. This is one of the reasons why chitosan is chosen for infection related wound healing because of the rich number of hydrogen bonds between chitosan chains (Homayoni et al., 2009). Previous research revealed that the swelling ratio of chitosan nanofibers is 70% more than chitosan particles (Cooper et al., 2013). Therefore, the objective of this project was to use an electrospinning method to fabricate porous nanofibers loaded with growth factors inside of nanofibers for infection related wound healing improvement.

MATERIALS AND METHODS

Chitosan solution and poly (vinyl alcohol) (PVA) solution were prepared as described before (Zhou et al., 2013). 3% (w/v) chitosan(Sigma, US) and 8% (w/v) poly (vinyl alcohol) (PVA) (Sigma,

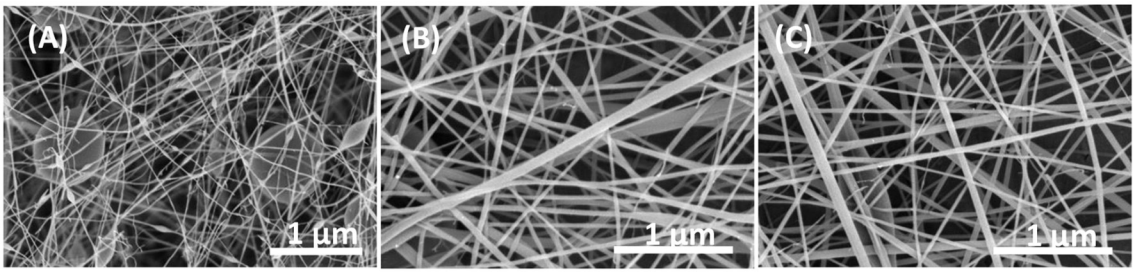

FIGURE 1 | SEM images of (A) ratio of 80/20 of CS/PVA, **(B)** ratio of 50/50 of CS/PVA, and **(C)** ratio of 20/80 of CS/PVA.

US) solutions were optimized and mixed together at different ratios of 80/20, 50/50, and 20/80 (CS/PVA) and were distributed using a sonication method. Ampicillin, one of the most widely used antibiotics, was dissolved in PVA solution with 1% (w/w). The well-distributed CS/PVA solution was then pumped into a plastic syringe separately and electrospinning performed at room temperature. Electrospinning was performed with 17 kV of electric potential applied to a metallic needle using a DC power supply, and the distance between the needle and collector was fixed at 12 cm. The nanofibrous matrix was collected on the surface of aluminum foil and dried at room temperature in vacuum environment overnight. Then, the crosslinking process was carried out in an aqueous glutaraldehyde solution (50%, v/v) (Zhou et al., 2013). The membrane was crosslinked in glutaraldehyde vapor at room temperature for 4 days. After crosslinking, the samples were washed with distilled water and dried in an oven for 24 h. The morphology and diameter of the electrospun samples were observed by scanning electron microscopy (SEM). Mechanical test and antibacterial study will be further investigated in the following studies. All experiments were run in triplicate and repeated three times for each group.

RESULTS AND DISCUSSION

Chitosan and PVA had been widely investigated for a very long time due to their biocompatible and antibacterial properties. SEM images of nanofibers resulting from different ratio of CS/PVA are shown in **Figure 1**. It could be found that when the ratio of CS to PVA was equal to 50/50, smooth, and homogeneous fibers were obtained. When the content of chitosan increased, larger fiber diameters were found, which was due to the relatively higher molecule weight of chitosan resulting in a solution hard to electrospun. Besides, numerous beads could be observed based on SEM images (**Figure 1A**), which also indicated that chitosan with higher molecular weights was hard to electrospun. However, as the ratio of PVA in the mixture increased, the fiber morphology was uneven and very weak as shown in **Figure 1C**. It might be thought that when a single jet split into multiple filaments because of radical charge repulsion, the polymer solution with high concentrations of PVA could not stand this radical charge repulsion, which resulted in freaking and smaller diameter nanofibers. SEM results indicated that for the CS and PVA at a ratio of 50/50, the nanofibers had optimal nanofibrous structures (i.e., closer to that of natural tissues), making them potential for further study. In addition, both chitosan and antibiotics loaded by PVA has very good effect on antibacterial study based on a previous study (Uygun et al., 2011). All those properties make these CS/PVA/Antibiotics electrospun matrices good wound dressing candidates for infection related wound healing studies.

CONCLUSIONS

In this study, CS/PVA nanofibers were successfully prepared by electrospinning different ratios of CS/PVA solutions. SEM images showed that nanofibers had larger and more nanobeads formed with increasing concentrations of CS, while narrower and breaking nanofibers could be observed if the mixed solution was more than 75% PVA. The results from SEM images showed that the ratio of CS and PVA at 50/50 achieved a nanofibrous structure the most similar to natural tissues. These novel electrospun scaffolds have the potential to be used for infection related wound dressing for skin tissue regeneration.

AUTHOR CONTRIBUTIONS

MW Performed experiments. AR, Designed and written the paper. TW, Designed and edited.

ACKNOWLEDGMENTS

The authors would like to acknowledge Northeastern University for funding and Dr. William H. Fowle of Northeastern University for help with SEM images.

REFERENCES

Cooper, A., Oldinski, R., Ma, H., Bryers, J. D., and Zhang, M. (2013). Chitosan-based nanofibrous membranes for antibacterial filter applications. *Carbohydr. Polym.* 92, 254–259. doi: 10.1016/j.carbpol.2012.08.114

Dwivedi, C., Pandey, H., Pandey, A. C., Ramteke, P. W. (2016). Nanofibre based smart pharmaceutical scaffolds for wound repair and regenerations. *Curr. Pharm. Des.* 22, 1460–1471. doi: 10.2174/1381612822666151215103553

Field, F. K., and Kerstein, M. D. (1994). Overview of wound healing in a moist environment. *Am. J. Surg.* 167, 2S–6S.

Homayoni, H., Ravandi, S. A. H., and Valizadeh, M. (2009). Electrospinning of chitosan nanofibers: processing optimization. *Carbohydr. Polym.* 77, 656–661. doi: 10.1016/j.carbpol.2009.02.008

Tchemtchoua, V. T., Atanasova, G., Aqil, A., Filée, P., Garbacki, N., Vanhooteghem, O., et al. (2011). Development of a Chitosan Nanofibrillar Scaffold for skin repair and regeneration. *Biomacromolecules* 12, 3194–3204. doi: 10.1021/bm200680q

Uygun, A., Kiristi, M., Oksuz, L., Manolache, S., and Ulusoy, S. (2011). RF hydrazine plasma modification of chitosan for antibacterial activity and nanofiber applications. *Carbohydr. Res.* 346, 259–265. doi: 10.1016/j.carres.2010.11.020

Zhou, Y., Yang, H., Liu, X., Mao, J., Gu, S., and Xu, W. (2013). Electrospinning of carboxyethyl chitosan/poly(vinyl alcohol)/silk fibroin nanoparticles for wound dressings. *Int. J. Biol. Macromol.* 53, 88–92. doi: 10.1016/j.ijbiomac.2012.11.013

Conflict of Interest Statement: The authors declare that the research was conducted in the absence of any commercial or financial relationships that could be construed as a potential conflict of interest.

frontiers in Physiology

ORIGINAL RESEARCH
published: 14 July 2016
doi: 10.3389/fphys.2016.00297

Addition of Selenium Nanoparticles to Electrospun Silk Scaffold Improves the Mammalian Cell Activity While Reducing Bacterial Growth

Stanley Chung[1]*, *Batur Ercan*[1], *Amit K. Roy*[1,2] and *Thomas J. Webster*[1,2,3,4]*

[1] Department of Chemical Engineering, Northeastern University, Boston, MA, USA, [2] Wenzhou Institute of Biomaterials and Engineering, Wenzhou Medical University, Wenzhou, China, [3] Center of Excellence for Advanced Materials Research, King Abdulaziz University, Jeddah, Saudi Arabia, [4] Department of Bioengineering, Northeastern University, Boston, MA, USA

Silk possesses many beneficial wound healing properties, and electrospun scaffolds are especially applicable for skin applications, due to their smaller interstices and higher surface areas. However, purified silk promotes microbial growth. Selenium nanoparticles have shown excellent antibacterial properties and are a novel antimicrobial chemistry. Here, electrospun silk scaffolds were doped with selenium nanoparticles to impart antibacterial properties to the silk scaffolds. Results showed significantly improved bacterial inhibition and mild improvement in human dermal fibroblast metabolic activity. These results suggest that the addition of selenium nanoparticles to electrospun silk is a promising approach to improve wound healing with reduced infection, without relying on antibiotics.

Keywords: silk, electrospinning, antibacterial nanoparticles

OPEN ACCESS

Edited by:
Marianna Bei,
Harvard Medical School, USA

Reviewed by:
Henrique De Amorim Almeida,
Polytechnic Institute of Leiria, Portugal
Miguel Angel Mateos Timoneda,
Institute for Bioengineering of Catalonia, Spain

***Correspondence:**
Stanley Chung
chung.st@husky.neu.edu
Thomas J. Webster
th.webster@neu.edu

Specialty section:
This article was submitted to Clinical and Translational Physiology, a section of the journal Frontiers in Physiology

Received: *26 April 2016*
Accepted: *28 June 2016*
Published: *14 July 2016*

Citation:
Chung S, Ercan B, Roy AK and Webster TJ (2016) Addition of Selenium Nanoparticles to Electrospun Silk Scaffold Improves the Mammalian Cell Activity While Reducing Bacterial Growth. Front. Physiol. 7:297. doi: 10.3389/fphys.2016.00297

INTRODUCTION

Researchers in the tissue engineering field work toward repairing and/or regenerating damaged tissues and organs through a combination of biomaterial scaffolds, cell signaling moieties, and cell (Langer and Vacanti, 1993). The ideal tissue engineering scaffold closely mimics the physical and chemical makeup of the organ to be replaced and should serve as an artificial extracellular matrix to support cell growth and differentiation. Electrospun scaffolds closely mimic the physical composition of native extracellular matrix (ECM) morphology.

Electrospinning works by applying a high voltage field to a solution of polymer dissolved in a conductive solvent (Sill and von Recum, 2008). The voltage induces electrostatic repulsion within the polymer solution and forms a cone like structure, the Taylor cone, held together by the force balance of the electrostatic repulsion and surface tension. Eventually, the electrostatic repulsion overcomes the surface tension forces holding the polymer solution together. Once this critical limit has been reached, a polymer jet is formed out of the edge of the Taylor cone toward a positively charged collector, and the solvent is evaporated in the flight path from the cone to the collector, leaving a polymer matrix with fibers relevant to physiological regime. The physical parameters of the scaffold may be adjusted based on polymer composition, solvent mixture, voltage, and many other parameters used to create the matrix. Researchers also have a high degree of control over the fiber orientation of electrospun scaffolds by adjusting the type of collector. Because of these processing advantages, electrospinning has been researched for a variety of tissue engineering applications

such as cardio (Hajiali et al., 2011; Liu et al., 2011; Du et al., 2012), bone (Shin et al., 2010; Cai et al., 2012; Frohbergh et al., 2012; Liu et al., 2014), neural (Wang et al., 2011; Guan et al., 2013; Kador et al., 2013; Prabhakaran et al., 2013; Baiguera et al., 2014; Irani et al., 2014), skin (Dhandayuthapani et al., 2010; Jin et al., 2011; Kuppan et al., 2011; Rnjak-Kovacina et al., 2011), tendon/ligament (Howell et al., 2004; Sahoo et al., 2010a,b; James et al., 2011; Cardwell et al., 2012), and stem cell expansion/differentiation (Shin et al., 2010; Sahoo et al., 2010a; James et al., 2011; Jin et al., 2011; Wang et al., 2011; Cardwell et al., 2012; Irani et al., 2014).

Electrospun scaffolds promote many beneficial cellular responses for tissue engineering and are generally better for cell proliferation and differentiation than 2D substrates. In particular, silk electrospun scaffolds demonstrate good responses as tissue engineering scaffold for wound healing (Wharram et al., 2010; Gil et al., 2013; Lee et al., 2014). Silk promotes collagen synthesis, re-epithelialization, wound healing, atopic dermatitis alleviation, and scar reduction (Ricci et al., 2004; Fini et al., 2005; Roh et al., 2006; Okabayashi et al., 2009). However, pure silk shows negligible or even negative antibacterial properties (Kaur et al., 2014). Previously, groups have loaded electrospun silk scaffold with silver nanoparticles to impart anti-bacterial properties (Kang et al., 2007). However, silver is a commonly used antibiotic that has become resistant in certain strains of bacteria (Silver, 2003).

Selenium nanoparticles are a novel antibiotic chemistry to which there is no known bacterial resistance (Tran and Webster, 2011, 2013; Wang and Webster, 2012, 2013; Shakibaie et al., 2015). Selenium is a common trace element in the body and is important to healthy nutrition, especially in the formation of selenoproteins (Andrews et al., 2011; Santhosh Kumar and Priyadarsini, 2014). Selenium has been suggested to have anticancer effects as well (Clark et al., 1996). Here, we doped selenium nanoparticles to electrospun silk scaffold to impart antibacterial properties to silk (Rockwood et al., 2011). Human dermal fibroblasts were used to determine the *in vitro* changes in metabolic activity while *Staphylococcus aureus* were used to determine the effects of the bacterial inhibition.

MATERIALS AND METHODS

Materials

Bombyx mori silk cocoons were obtained from Mulberry Farms (Fallbrook, CA). Formic acid was purchased from Sigma-Aldrich (Saint Louis, MO). Selenium nanoparticles were synthesized as described below.

Extraction of Silk Fibroin from *Bombyx Mori* Silk Cocoons

Silk fibroin was prepared from *Bombyx mori* cocoons according to previously established protocols with minor modifications (Rockwood et al., 2011). *B. mori* silk cocoons were cut into small pieces and boiled in 0.02 M Na_2CO_3 (Sigma-Aldrich) for 30 min to remove the glue-like sericin coating layer from the structural fibroin protein which was then rinsed 3x with distilled water (diH_2O). The obtained silk fibroin fibers were dried overnight, dissolved in a LiBr (Sigma-Aldrich) solution (9.3 M) at 60°C for 4 h, and dialyzed through a cellulose membrane (ThermoFisher, Waltham, MA, 3500, MWCO) across distilled water for 4 days. The obtained silk solutions were centrifuged thrice at 4200 g and lyophilized for 4 days before resuspending in formic acid for a final concentration of 8% silk/formic acid.

Electrospinning of Silk/Formic Acid Solution

Eight percentage of silk solution was then electrospun at 18,000 volts, room temperature, 0% relative humidity, and 60 cm to collector. These conditions were optimized to produce fibers with dimensions that resemble those from the native extracellular matrix. Afterwards, 70% methanol (Sigma-Aldrich) was used to treat the electrospun silk to prevent hydrolysis of the membrane. Treated silk membranes were dried overnight in the fume hood.

Selenium Nanoparticle Synthesis

0.1 M sodium selenite [Alfa Aesar, Ward Hill, MA, $Na_2SeO_3(H_2O)_5$] and 0.1 M glutathione, GSH (Alfa Aesar), ($C_{10}H_{17}N_3O_6S$) were added onto the treated membranes before 0.2 M sodium hydroxide (NaOH) was added to precipate the sodium nanoparticles. Finally, double distilled deionized water was added thrice to quench the reaction and wash the membranes.

Specimen Characterization

Imaging of the specimens was conducted with a Hitachi S4800 Tokyo, Japan Scanning Electron Microscope (SEM, Hitachi S4800 SEM, Tokyo, Japan). A 4.5 nm layer of platinum was sputter coated (Cressington 208; Cressington Scientific Instruments, Watford, UK) onto the membranes to provide a conductive surface. SEM analysis was conducted with a 3 kV accelerating voltage. Characterization was completed using both secondary electrons and backscatter electrons, which impart a stronger signal to heavier elements, such as selenium.

Cellular Assays

Mammalian Cell Activity Culture and Characterization

Passages 3–12 human dermal fibroblast (HDF, Lonza, Basel, Switzerland) were cultured in Dulbecco's Modified Eagle Medium (DMEM, Sigma Aldrich) supplemented with 10% fetal bovine serum (Hyclone, Logan, UT) and 1% penicillin/streptomycin (P/S, Sigma Aldrich) in a 37°C, humidified, 5% CO_2/95% air environment.

MTS assay (Promega, Fitchburg, WI) was used to determine the metabolic cell activity of the HDFs. Before cell seeding, the electrospun silk scaffolds were washed with 70% ethanol (Sigma-Aldrich) before rinsing with double distilled deionized water. HDFs were cultured to ∼90% confluence, rinsed with Dulbecco's phosphate-buffered saline without calcium chloride and magnesium chloride (dPBS, Sigma Aldrich), and detached from the tissue culture plate by using 0.25% trypsin-EDTA (Sigma-Aldrich). Detached cells were then centrifuged at 2000 r.p.m. and resuspended at a density of 50,000 cells/ml before seeding onto the silk scaffolds in a 96 well-plate at 100 μl in each well (5000 cells/well). The HDFs incubated for 1, 2, and 4 days. Afterwards, the medium was removed from the sample and

100 μl solution of 1:5 MTS dye with DMEM medium (v/v) were added to each well. Samples were placed back into the incubator for 2.5 h. to allow the MTS to react with the metabolic products of the adherent cells before reading in a SpectraMax M3 microplate reader (Molecular Devices, Sunnyvale, CA) at an absorbance wavelength of 490 nm. The absorbance values of wells containing only DMEM medium without cells were subtracted from the absorbance values of the wells containing cells. The metabolic activity of each well was compared with the metabolic activity of known numbers of cells by a standard curve constructed at the beginning of each trial.

Bacterial Cell Activity Measurement

Staphylococcus aureus (ATCC-12600) were inoculated in 3% tryptic soy broth (TSB, Sigma-Aldrich) overnight. After 24 h., the *Staphylococcus aureus* were diluted with TSB until absorbance value reached 0.52 at wavelength of 562 nm. This corresponded with a cell density of 10^9 colony forming units (CFU)/ml. Afterwards, the *Staphylococcus aureus* were diluted 1000x in TSB before seeding onto the silk samples in a non-treated 96 well-plate in 100 μl of solution (10^5 CFU/well). After 24 h., the BacTiter Glo assay (Promega), a luciferase based ATP assay was used to quantify the amount of ATP present on the electrospun silk samples. BacTiter Glo reagent was added at the same volume as the medium in each well, 100 μl, at room temperature. The samples were inoculated at room temperature for 5 min. while the BacTiter Glo reagents solubilized the bacterial membrane, after which, the luminescence was measured using the SpectraMax M3. A standard curve was constructed to equate the luminescence readings with known ATP amounts.

Statistics

All experiments were conducted in triplicate and repeated at least three times each. Analysis of variance and student's *t*-test were used to determine whether the differences in cellular activity over the different time periods were significant.

RESULTS AND DISCUSSION

To characterize the morphology of the electrospun silk scaffold, scanning electron microscope was used to visualize the surface of the nanocomposite. As shown in **Figures 1A,B**, the electrospun silk scaffolds contained fiber diameters ∼100–200 nm and pore sizes ∼2 μm. The silk scaffold contained unaligned fibers with very little beading and uniform thickness, demonstrating a morphology similar to those in the native extra-cellular matrix (ECM). The selenium nanoparticles (SeNP) were then reacted on the scaffold, causing a physisorption of the SeNP onto the silk scaffold. Two reaction conditions were chosen to deposit the SeNPs; SEM images showed that these produced two homogenous and distinct selenium nanoparticle populations: 40 (**Figures 1C,D**) and 70 nm (**Figures 1E,F**) nanoparticles.

First, *in vitro* viability tests were conducted using HDF cells. These cells were seeded onto the silk scaffold without selenium nanoparticles, the silk scaffolds containing the 40 and 70 nm selenium nanoparticles, and on regular polystyrene (PS) tissue culture plate to determine the change in growth of the HDF cells when grown on these substrates (**Figure 2**). Electrospun silk without addition of selenium nanoparticles produced statistically insignificant change ($p > 0.05$) in HDF activity as compared

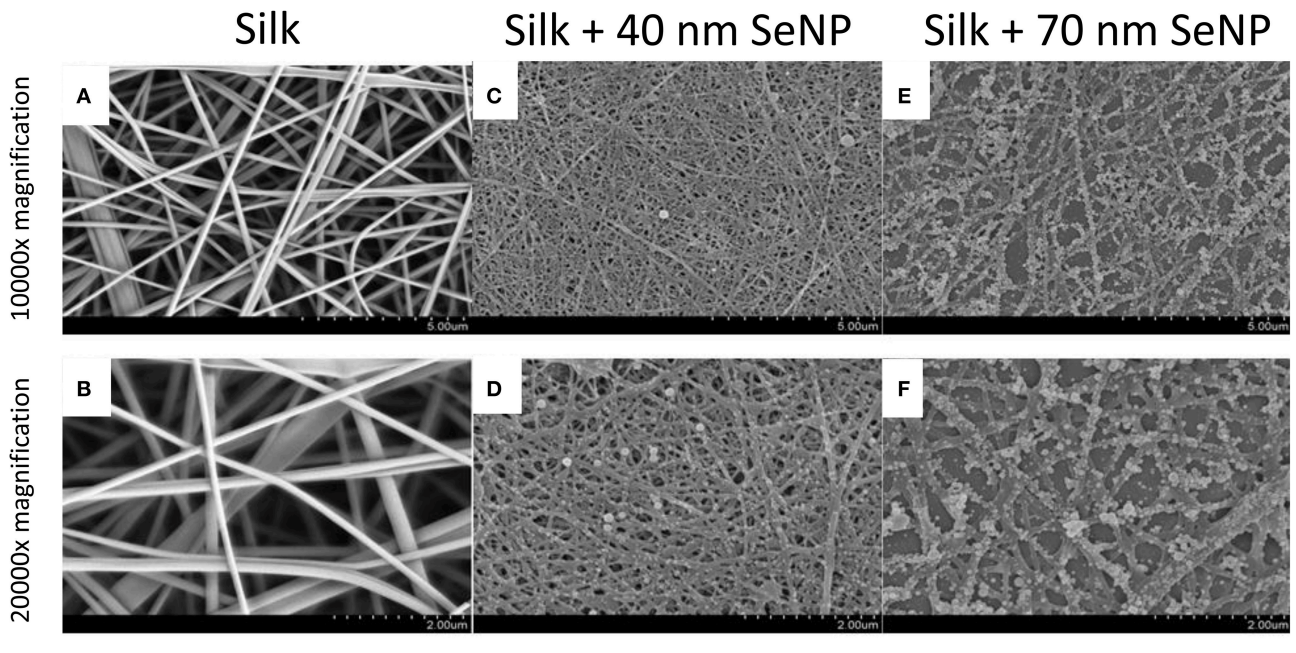

FIGURE 1 | Scanning electron microscopy (SEM) images of the electrospun silk scaffolds at 10,000x (A,C,E) and 20,000x (B,D,F) with 5 and 2 μm scale bars respectively. The silk scaffolds without selenium nanoparticles are shown in panels **(A,B)**; with 40 nm selenium nanoparticle in panels **(C,D)**; and with 70 nm selenium nanoparticles in panels **(E,F)**.

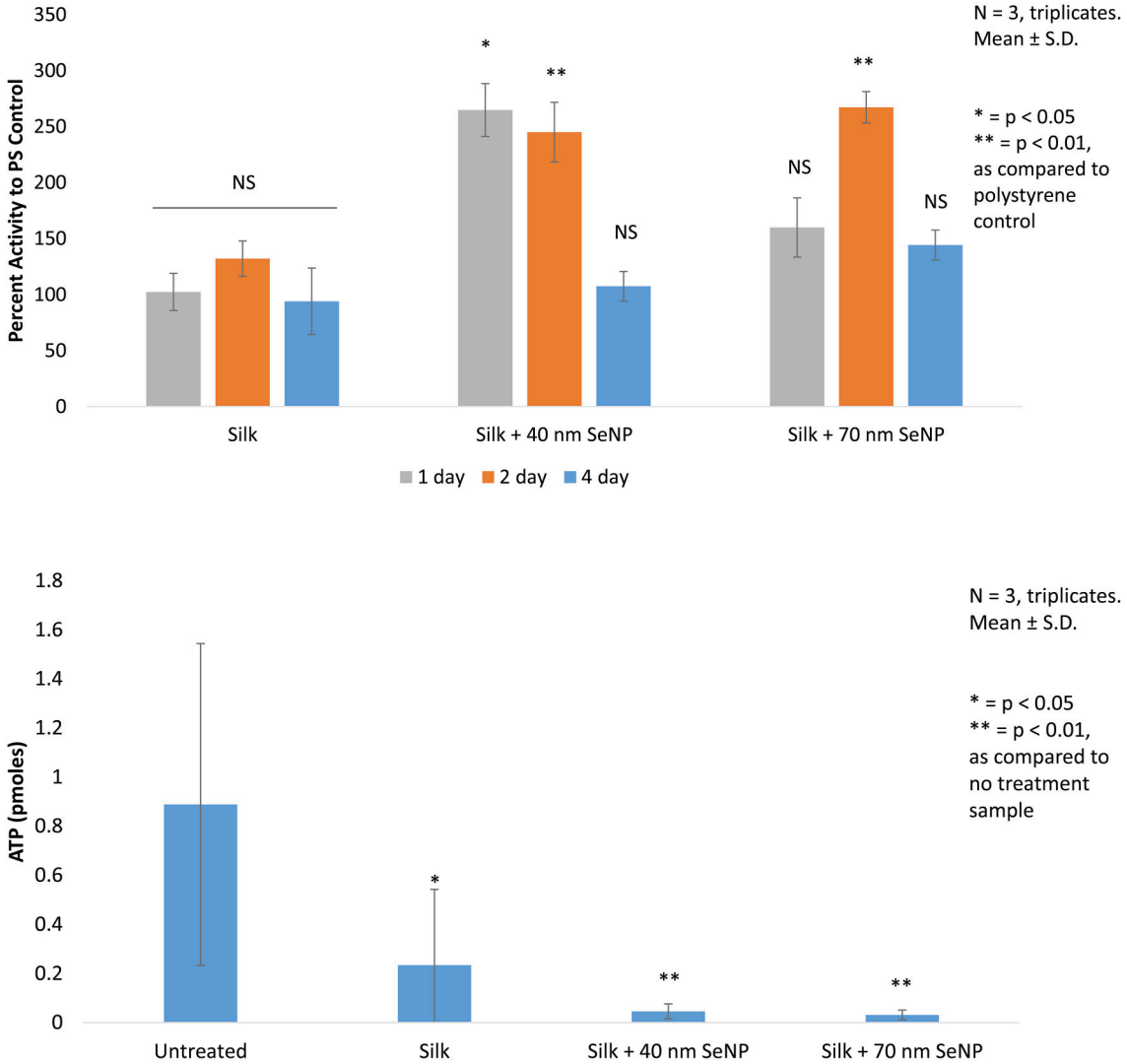

FIGURE 2 | *In vitro* cellular activity are depicted. (Top) The mitochondrial activity of human dermal fibroblast (HDF) grown on silk, silk +40 nm selenium nanoparticles, and silk +70 nm selenium nanoparticles are compared to activity of HDF grown on polystyrene tissue culture dish. All trials are conducted in triplicates, $N = 3$.*$p < 0.05$, **$p < 0.01$ as compared to polystyrene control. **(Bottom)** The ATP activity of *Staphylococcus aureus* grown on the same sample groups as tested for the HDF is depicted. All trials are conducted in triplicates, $N = 3$.*$p < 0.05$, **$p < 0.01$ as compared to no treatment sample.

activity when grown on normal tissue culture plate across all 3 days tested. The silk/selenium nanocomposites produced significantly higher metabolic activity for HDF as compared to HDF grown on tissue culture plate. The addition of selenium nanoparticles significantly improved the metabolic activity of HDF, especially at the shorter term time points. At 1 and 2 days, silk scaffold doped with 40 nm selenium nanoparticles produced greater than two fold increase in metabolic signal, 264 and 245% on day 1 and 2, respectively, as compared to the tissue culture plate control while the 70 nm scaffold produced 160 and 267% on day 1 and 2, respectively. The day 1 ($p < 0.05$) and day 2 signal ($p < 0.01$) from the silk+40 nm SeNP scaffolds and the day 2 signal ($p < 0.05$) from the silk+70 nm SeNP scaffolds were statistically significant from the signal produced at the same time points on the tissue culture plates. Surprisingly, the silk scaffolds without nanoparticle addition did not produce a statistically significant improvement in HDF growth despite the ECM like morphology. There was mild improvement on day 2 (132% compared to control), but overall, the presence of silk alone did not significant improve HDF response. The short term improvement in activity may have plateaued by day 4 compared to the control, because the HDF may have reached confluency on the silk/selenium nanocomposites.

Finally, the bacteria results were accessed by ATP assay. Here, the performance of the silk scaffolds were compared to *Staphylococcus aureus* grown in solution in the polystyrene plate. Bacterial growth across all silk samples showed statistically significant reduction as compared to untreated samples grown in

solution. Bacteria grown on silk without selenium nanoparticles showed a 74% reduction as compared with the control ($p < 0.05$). This was somewhat surprising, because this contradicted other reports found in literature (Kaur et al., 2014).

Addition of selenium nanoparticles significantly improved the bacterial load: the addition of the 40 nm selenium nanoparticles reduced bacterial load by 95% and the 70 nm selenium nanoparticles by 96% compared to the control ($p < 0.01$). The doping of selenium had achieved an additional reduction of 80% for the 40 nm selenium nanoparticle and 87% for the 70 nm selenium nanoparticle as compared to the silk samples. The 70 nm selenium nanoparticle produced an almost one log reduction in ATP content (0.88) as compared to the silk sample and an overall 1.4 log reduction compared to the control.

CONCLUSION

This study showed for the first time the efficacy of doping selenium nanoparticles with silk to improve bacterial efficacy. Reaction conditions successfully synthesized two different sized populations of selenium nanoparticles onto electrospun silk scaffolds. These nanocomposites were then compared to silk scaffolds and normal tissue culture plates and were found to significantly improve both the mammalian cell response while reducing bacterial cell activity. Addition of the selenium nanoparticles significantly improved the short term human dermal fibroblast metabolic activity while reducing the ATP content of *Staphylococcus aureus*. Together, these results suggest that selenium nanoparticle may selectively enhance mammalian cells functions while killing or reducing the bacterial load. In summary, this study provides evidence of the potential value of the use of selenium nanoparticles in skin applications due to their selective activity. Future works will focus on determining the mechanism by which selenium nanoparticles achieve this selectivity and the scope of the selenium nanoparticles for inhibiting bacteria in skin applications.

AUTHOR CONTRIBUTIONS

SC and BE made substantial contributions to conception and design, and acquisition of data, and nanalysis and interpretation of data. Equally contributed to planning and idea. AR participated in design of experiment/idea and revising the article. TW edited/revised it critically for important intellectual content and gave final approval of the version to be submitted and any revised version.

FUNDING

The authors would like to thank Northeastern University for funding and facilities.

ACKNOWLEDGMENTS

The authors thank Mr. William H. Fowle (Northeastern University) for help with the SEM and the Nanomedicine Laboratory.

REFERENCES

Andrews, P. J. D., Avenell, A., Noble, D. W., Campbell, M. K., Croal, B. L., Simpson, W. G., et al. (2011). Randomised trial of glutamine, selenium, or both, to supplement parenteral nutrition for critically ill patients. *BMJ* 342:d1542. doi: 10.1136/bmj.d1542

Baiguera, S., Del Gaudio, C., Lucatelli, E., Kuevda, E., Boieri, M., Mazzanti, B., et al. (2014). Electrospun gelatin scaffolds incorporating rat decellularized brain extracellular matrix for neural tissue engineering. *Biomaterials* 35, 1205–1214. doi: 10.1016/j.biomaterials.2013.10.060

Cai, Y.-Z., Zhang, G.-R., Wang, L.-L., Jiang, Y.-Z., Ouyang, H.-W., and Zou, X.-H. (2012). Novel biodegradable three-dimensional macroporous scaffold using aligned electrospun nanofibrous yarns for bone tissue engineering. *J. Biomed. Mater. Res. Part A*. 100A, 1187–1194. doi: 10.1002/jbm.a.34063

Cardwell, R. D., Dahlgren, L. A., and Goldstein, A. S. (2012). Electrospun fibre diameter, not alignment, affects mesenchymal stem cell differentiation into the tendon/ligament lineage. *J. Tissue Eng. Regen. Med.* 8, 937–945. doi: 10.1002/term.1589

Clark, L. C., Combs, G. F. Jr., Turnbull, B. W., Slate, E. H., Chalker, D. K., Chow, J., et al. (1996). Effects of selenium supplementation for cancer prevention in patients with carcinoma of the skin: a randomized controlled trial. *JAMA* 276, 1957–1963. doi: 10.1001/jama.1996.03540240035027

Dhandayuthapani, B., Krishnan, U. M., and Sethuraman, S. (2010). Fabrication and characterization of chitosan-gelatin blend nanofibers for skin tissue engineering. *J. Biomed. Mater. Res. Part B Appl. Biomater.* 94B, 264–272. doi: 10.1002/jbm.b.31651

Du, F., Wang, H., Zhao, W., Li, D., Kong, D., Yang, J., et al. (2012). Gradient nanofibrous chitosan/poly ε-caprolactone scaffolds as extracellular microenvironments for vascular tissue engineering. *Biomaterials* 33, 762–770. doi: 10.1016/j.biomaterials.2011.10.037

Fini, M., Motta, A., Torricelli, P., Giavaresi, G., Nicoli Aldini, N., Tschon, M., et al. (2005). The healing of confined critical size cancellous defects in the presence of silk fibroin hydrogel. *Biomaterials* 26, 3527–3536. doi: 10.1016/j.biomaterials.2004.09.040

Frohbergh, M. E., Katsman, A., Botta, G. P., Lazarovici, P., Schauer, C. L., Wegst, U. G., et al. (2012). Electrospun hydroxyapatite-containing chitosan nanofibers crosslinked with genipin for bone tissue engineering. *Biomaterials* 33, 9167–9178. doi: 10.1016/j.biomaterials.2012.09.009

Gil, E. S., Panilaitis, B., Bellas, E., and Kaplan, D. L. (2013). Functionalized silk biomaterials for wound healing. *Adv. Healthc. Mater.* 2, 206–217. doi: 10.1002/adhm.201200192

Guan, S., Zhang, X.-L., Lin, X.-M., Liu, T.-Q., Ma, X.-H., and Cui, Z.-F. (2013). Chitosan/gelatin porous scaffolds containing hyaluronic acid and heparan sulfate for neural tissue engineering. *J. Biomater. Sci.* 24, 999–1014. doi: 10.1080/09205063.2012.731374

Hajiali, H., Shahgasempour, S., Naimi-Jamal, M. R., and Peirovi, H. (2011). Electrospun PGA/gelatin nanofibrous scaffolds and their potential application in vascular tissue engineering. *Int. J. Nanomed.* 6, 2133–2141. doi: 10.2147/IJN.S24312

Howell, M. D., Jones, J. F., Kisich, K. O., Streib, J. E., Gallo, R. L., and Leung, D. Y. M. (2004). Selective killing of vaccinia virus by LL-37: implications for eczema vaccinatum. *J. Immunol.* 172, 1763–1767. doi: 10.4049/jimmunol.172.3.1763

Irani, S., Zandi, M., Salamian, N., Saeed, S. M., Daliri Joupari, M., and Atyabi, S. M. (2014). The study of P19 stem cell behavior on aligned oriented electrospun poly(lactic-co-glycolic acid) nano-fibers for neural tissue engineering. *Polym. Adv. Technol.* 25, 562–567. doi: 10.1002/pat.3280

James, R., Kumbar, S. G., Laurencin, C. T., Balian, G., and Chhabra, A. B. (2011). Tendon tissue engineering: adipose-derived stem cell and GDF-5 mediated regeneration using electrospun matrix systems. *Biomed. Mater.* 6:25011. doi: 10.1088/1748-6041/6/2/025011

Jin, G., Prabhakaran, M. P., and Ramakrishna, S. (2011). Stem cell differentiation to epidermal lineages on electrospun nanofibrous substrates for skin tissue engineering. *Acta Biomater.* 7, 3113–3122. doi: 10.1016/j.actbio.2011.04.017

Kador, K. E., Montero, R. B., Venugopalan, P., Hertz, J., Zindell, A. N., Valenzuela, D. A., et al. (2013). Tissue engineering the retinal ganglion cell nerve fiber layer. *Biomaterials* 34, 4242–4250. doi: 10.1016/j.biomaterials.2013.02.027

Kang, M., Jung, R., Kim, H.-S., Youk, J. H., and Jin, H.-J. (2007). Silver nanoparticles incorporated electrospun silk fibers. *J. Nanosci. Nanotechnol.* 7, 3888–3891. doi: 10.1166/jnn.2007.056

Kaur, J., Rajkhowa, R., Afrin, T., Tsuzuki, T., and Wang, X. (2014). Facts and myths of antibacterial properties of silk. *Biopolymers* 101, 237–245. doi: 10.1002/bip.22323

Kuppan, P., Vasanthan, K. S., Sundaramurthi, D., Krishnan, U. M., and Sethuraman, S. (2011). Development of Poly(3-hydroxybutyrate-co-3-hydroxyvalerate) fibers for skin tissue engineering: effects of topography, mechanical, and chemical stimuli. *Biomacromolecules* 12, 3156–3165. doi: 10.1021/bm200618w

Langer, R., and Vacanti, J. P. (1993). Tissue engineering. *Science* 260, 920–926. doi: 10.1126/science.8493529

Lee, O. J., Ju, H. W., Kim, J. H., Lee, J. M., Ki, C. S., Kim, J. H., et al. (2014). Development of artificial dermis using 3D electrospun silk fibroin nanofiber matrix. *J. Biomed. Nanotechnol.* 10, 1294–1303. doi: 10.1166/jbn.2014.1818

Liu, H., Li, X., Zhou, G., Fan, H., and Fan, Y. (2011). Electrospun sulfated silk fibroin nanofibrous scaffolds for vascular tissue engineering. *Biomaterials* 32, 3784–3793. doi: 10.1016/j.biomaterials.2011.02.002

Liu, Y., Cui, H., Zhuang, X., Wei, Y., and Chen, X. (2014). Electrospinning of aniline pentamer-graft-gelatin/PLLA nanofibers for bone tissue engineering. *Acta Biomater.* 10, 5074–5080. doi: 10.1016/j.actbio.2014.08.036

Okabayashi, R., Nakamura, M., Okabayashi, T., Tanaka, Y., Nagai, A., and Yamashita, K. (2009). Efficacy of polarized hydroxyapatite and silk fibroin composite dressing gel on epidermal recovery from full-thickness skin wounds. *J. Biomed. Mater. Res. Part B Appl. Biomater.* 90B, 641–646. doi: 10.1002/jbm.b.31329

Prabhakaran, M. P., Vatankhah, E., and Ramakrishna, S. (2013). Electrospun aligned PHBV/collagen nanofibers as substrates for nerve tissue engineering. *Biotechnol. Bioeng.* 110, 2775–2784. doi: 10.1002/bit.24937

Ricci, G., Patrizi, A., Bendandi, B., Menna, G., Varotti, E., and Masi, M. (2004). Clinical effectiveness of a silk fabric in the treatment of atopic dermatitis. *Br. J. Dermatol.* 150, 127–131. doi: 10.1111/j.1365-2133.2004.05705.x

Rnjak-Kovacina, J., Wise, S. G., Li, Z., Maitz, P. K. M., Young, C. J., Wang, Y., et al. (2011). Tailoring the porosity and pore size of electrospun synthetic human elastin scaffolds for dermal tissue engineering. *Biomaterials* 32, 6729–6736. doi: 10.1016/j.biomaterials.2011.05.065

Rockwood, D. N., Preda, R. C., Yucel, T., Wang, X., Lovett, M. L., and Kaplan, D. L. (2011). Materials fabrication from Bombyx mori silk fibroin. *Nat. Protocols* 6, 1612–1631. doi: 10.1038/nprot.2011.379

Roh, D.-H., Kang, S.-Y., Kim, J.-Y., Kwon, Y.-B., Young Kweon, H., Lee, K. G., et al. (2006). Wound healing effect of silk fibroin/alginate-blended sponge in full thickness skin defect of rat. *J. Mater. Sci. Mater. Med.* 17, 547–552. doi: 10.1007/s10856-006-8938-y

Sahoo, S., Ang, L. T., Goh, J. C.-H., and Toh, S.-L. (2010b). Growth factor delivery through electrospun nanofibers in scaffolds for tissue engineering applications. *J. Biomed. Mater. Res. Part A.* 93A, 1539–1550. doi: 10.1002/jbm.a.32645

Sahoo, S., Toh, S. L., and Goh, J. C. H. (2010a). A bFGF-releasing silk/PLGA-based biohybrid scaffold for ligament/tendon tissue engineering using mesenchymal progenitor cells. *Biomaterials* 31, 2990–2998. doi: 10.1016/j.biomaterials.2010.01.004

Santhosh Kumar, B., and Priyadarsini, K. I. (2014). Selenium nutrition: how important is it? *Biomed. Preventive Nutr.* 4, 333–341. doi: 10.1016/j.bionut.2014.01.006

Shakibaie, M., Forootanfar, H., Golkari, Y., Mohammadi-Khorsand, T., and Shakibaie, M. R. (2015). Anti-biofilm activity of biogenic selenium nanoparticles and selenium dioxide against clinical isolates of *Staphylococcus aureus*, Pseudomonas aeruginosa, and Proteus mirabilis. *J. Trace Elements Med. Biol.* 29, 235–241. doi: 10.1016/j.jtemb.2014.07.020

Shin, M., Yoshimoto, H., and Vacanti, J. P. (2010). "*In vivo* bone tissue engineering using mesenchymal stem cells on a novel electrospun nanofibrous scaffold," in *Advances in Tissue Engineering, Vol. 2,* eds P. C. Johnson and A. G. Mikos (Mary Ann Liebert), 205–213.

Sill, T. J., and von Recum, H. A. (2008). Electrospinning: applications in drug delivery and tissue engineering. *Biomaterials* 29, 1989–2006. doi: 10.1016/j.biomaterials.2008.01.011

Silver, S. (2003). Bacterial silver resistance: molecular biology and uses and misuses of silver compounds. *FEMS Microbiol. Rev.* 27, 341–353.

Tran, P. A., and Webster, T. J. (2011). Selenium nanoparticles inhibit *Staphylococcus aureus* growth. *Int. J. Nanomedicine.* 6:1553. doi: 10.2147/IJN.S21729

Tran, P. A., and Webster, T. J. (2013). Antimicrobial selenium nanoparticle coatings on polymeric medical devices. *Nanotechnology* 24, 155101. doi: 10.1088/0957-4484/24/15/155101

Wang, A., Tang, Z., Park, I.-H., Zhu, Y., Patel, S., Daley, G. Q., et al. (2011). Induced pluripotent stem cells for neural tissue engineering. *Biomaterials* 32, 5023–5032. doi: 10.1016/j.biomaterials.2011.03.070

Wang, Q., and Webster, T. J. (2012). Nanostructured selenium for preventing biofilm formation on polycarbonate medical devices. *J. Biomed. Mater. Res. Part A* 100A, 3205–3210. doi: 10.1002/jbm.a.34262

Wang, Q., and Webster, T. J. (2013). Short communication: inhibiting biofilm formation on paper towels through the use of selenium nanoparticles coatings. *Int. J. Nanomed.* 8:407. doi: 10.2147/IJN.S38777

Wharram, S. E., Zhang, X., Kaplan, D. L., and McCarthy, S. P. (2010). Electrospun silk material systems for wound healing. *Macromol. Biosci.* 10, 246–257. doi: 10.1002/mabi.200900274

Conflict of Interest Statement: The authors declare that the research was conducted in the absence of any commercial or financial relationships that could be construed as a potential conflict of interest.

frontiers in Physiology

REVIEW
published: 01 May 2018
doi: 10.3389/fphys.2018.00419

The Role of Macrophages in Acute and Chronic Wound Healing and Interventions to Promote Pro-wound Healing Phenotypes

*Paulina Krzyszczyk[1], Rene Schloss[1], Andre Palmer[2] and François Berthiaume[1]**

[1] Biomedical Engineering, Rutgers University, The State University of New Jersey, Piscataway, NJ, United States, [2] Chemical & Biomolecular Engineering, The Ohio State University, Columbus, OH, United States

OPEN ACCESS

Edited by:
Basak E. Uygun,
Harvard Medical School,
United States

Reviewed by:
Tarcio Teodoro Braga,
Universidade Federal do Paraná, Brazil
Luciola Silva Barcelos,
Universidade Federal de Minas Gerais, Brazil
Christophe Helary,
UMR7574 Chimie de la Matière Condensée de Paris (LCMCP), France

***Correspondence:**
François Berthiaume
fberthia@soe.rutgers.edu

Specialty section:
This article was submitted to Clinical and Translational Physiology, a section of the journal Frontiers in Physiology

Received: 16 January 2018
Accepted: 04 April 2018
Published: 01 May 2018

Citation:
Krzyszczyk P, Schloss R, Palmer A and Berthiaume F (2018) The Role of Macrophages in Acute and Chronic Wound Healing and Interventions to Promote Pro-wound Healing Phenotypes. Front. Physiol. 9:419. doi: 10.3389/fphys.2018.00419

Macrophages play key roles in all phases of adult wound healing, which are inflammation, proliferation, and remodeling. As wounds heal, the local macrophage population transitions from predominantly pro-inflammatory (M1-like phenotypes) to anti-inflammatory (M2-like phenotypes). Non-healing chronic wounds, such as pressure, arterial, venous, and diabetic ulcers indefinitely remain in inflammation—the first stage of wound healing. Thus, local macrophages retain pro-inflammatory characteristics. This review discusses the physiology of monocytes and macrophages in acute wound healing and the different phenotypes described in the literature for both *in vitro* and *in vivo* models. We also discuss aberrations that occur in macrophage populations in chronic wounds, and attempts to restore macrophage function by therapeutic approaches. These include endogenous M1 attenuation, exogenous M2 supplementation and endogenous macrophage modulation/M2 promotion via mesenchymal stem cells, growth factors, biomaterials, heme oxygenase-1 (HO-1) expression, and oxygen therapy. We recognize the challenges and controversies that exist in this field, such as standardization of macrophage phenotype nomenclature, definition of their distinct roles and understanding which phenotype is optimal in order to promote healing in chronic wounds.

Keywords: macrophages, chronic wounds, wound healing, inflammation, skin regeneration

CLINICAL AND ECONOMIC SIGNIFICANCE OF CHRONIC WOUNDS

Following surgical incisions and minor lacerations, diabetic, venous, and pressure ulcers are the most common wounds on a global scale (MedMarket Diligence, 2012, 2015). Whereas, a majority of surgical incisions and lacerations are categorized as acute wounds and often heal with minimal complications, ulcers are chronic wounds that resist healing and require expensive treatments. Furthermore, as surgical wounds become less of a problem due to the advances of minimally invasive surgery, chronic wounds are on the rise, as they often occur in growing populations, such as the elderly, obese, and diabetic. In recent years, there were ∼4.5, 9.7, and 10 million pressure, venous, and diabetic ulcer wound patients globally (MedMarket Diligence, 2012, 2015).

The numbers of pressure and venous ulcers are rising at rates of 6–7% annually, and growth is even larger for diabetic ulcers (9%) due to the increased incidence of diabetes in the developed world. Unfortunately, the staggering number of chronic, non-healing wounds is growing much faster than the emergence of new, effective therapies.

Standard wound care involves patient and wound assessments, offloading, debridement of necrotic and infected tissue, treatment with antibiotics, and regular wound dressing changes (Falanga, 2005; Frykberg and Banks, 2015). Advanced therapies are available for wounds that do not improve after several weeks of standard care. These include negative pressure wound therapy, topically applied platelet-derived growth factor (PDGF) (Regranex), acellular extracellular matrices (Integra, Matristem, Theraskin), and bioengineered cell-containing therapies (Apligraf, Dermagraft), to name a few. Other possible treatments include hyperbaric or topical oxygen treatment in order to restore oxygen to the wound. In the case of wounds in which infection and severe tissue damage cannot be controlled, the effects of which may otherwise be life-threatening, amputation is performed. In fact, two thirds of all lower-limb amputations are due to diabetic ulcers (Sen et al., 2009). Since many chronic wounds do not improve with standard care, treatment quickly becomes expensive with the introduction of advanced therapies, and sometimes amputation.

With so many people suffering from chronic wounds, and so many failed attempts at treating them, it is not surprising that wound care costs are also enormous. In the United States, over $25 billion dollars are spent annually on chronic wound care (Sen et al., 2009). In England, costs for pressure ulcer treatment can reach up to 6500 pounds per patient (>$8,000 U.S. dollars) (Posnett and Franks, 2008). Similarly, in the United States, the average cost of Medicare spending on pressure and arterial ulcers in 2014 was $3696 and $9015 per patient, respectively—the two most expensive of all types of wounds included in the study (Nussbaum et al., 2018). Furthermore, each amputation procedure can cost well over $35,000 (Gordois et al., 2003; Sen et al., 2009; Carls et al., 2011). Due to the increasing prevalence of diabetes in the U.S., the total cost of diabetic ulcer care has also drastically increased in the past 20 years (Nussbaum et al., 2018). There is an urgent need to understand the pathophysiology of non-healing wounds in order to develop effective therapies that restore their ability to resolve and heal.

Abbreviations: DAMPs, damage/danger-associated molecular patterns; ECM, extracellular matrix; EGF, epidermal growth factor; FGF, fibroblast growth factor; GC, gluococorticoid; GM-CSF, granulocyte-macrophage colony-stimulating factor; GT, granulation tissue; HA (in text), hyaluronan; HA (in table), hemorrhage-associated; HO-1, heme oxygenase-1; IFN-γ, interferon-gamma; IGF-1, insulin-like growth factor 1; IL-(1β, 6, 10, etc.), interleukins; iNOS, inducible nitric oxide synthase; LPS, lipopolysaccharide; M-CSF, macrophage colony-stimulating factor; MCP-1/5, monocyte chemoattractant protein-1/5 (CCL2/CCL12); MHCII, major histocompatibility complex class II; MIP-1α/β, macrophage inflammatory protein-1 alpha/beta (CCL3/CCL4); MNCs, mononuclear cells; MMPs, matrix metalloproteinases; MSCs, mesenchymal stromal cells; NF-κβ, nuclear factor kappa beta; PAMPs, pathogen-associated molecular patterns; PDGF, platelet-derived growth factor; PGE-2, prostaglandin E-2; ROS, reactive oxygen species; TAMs, tumor-associated macrophages; TGF-β1, transforming growth factor beta 1; TNF-α, tumor necrosis factor-alpha; VEGF, vascular endothelial growth factor.

THE WOUND HEALING PROCESS AND CHRONIC VS. ACUTE WOUNDS

Chronic wounds fail to heal, despite the use of current therapies, because they are stalled in the early inflammatory state within the wound healing stages (Zhao et al., 2016). In contrast, acute wounds progress through this process in a timely manner as they heal.

The wound healing process is composed of three overlapping phases: inflammation, proliferation and remodeling (Singer and Clark, 1999; Baum and Arpey, 2005; Liu and Velazquez, 2008). After skin injury occurs, platelets are activated at the site of blood vessel rupture and promote clot formation to stop blood loss. Platelets also release factors that attract immune cells from the circulation into the wound. This marks the beginning of the inflammatory phase. Polymorphonuclear neutrophils are first to arrive, followed by monocytes that quickly differentiate into macrophages (Sindrilaru and Scharffetter-Kochanek, 2013). Neutrophils produce high levels of reactive oxygen species (ROS), proteases and pro-inflammatory cytokines to sanitize the wound. When this process is complete, neutrophils apoptose and become phagocytosed by the newly arrived macrophages. Macrophages will also phagocytose bacteria and debris in order to clean the wound (Frykberg and Banks, 2015). During this time, the wound is sterilized and prepared for tissue regrowth, which occurs in the proliferative phase (Baum and Arpey, 2005). As the name indicates, wound cells proliferate and migrate during this phase, in order to regenerate the lost tissue. This includes endothelial cells, fibroblasts and keratinocytes. A preliminary, vascularized extracellular matrix (ECM), called the granulation tissue (GT), is laid down and keratinocytes migrate upon it to close the wound. During remodeling, the final phase of wound healing, ECM within the granulation tissue matures and increases in mechanical strength (Falanga, 2005). Wound healing is complete following apoptosis of myofibroblasts and vascular cells, leaving behind a collagen-rich scar (Zhao et al., 2016).

In chronic wounds, the proliferative and remodeling stages do not readily occur (Zhao et al., 2016). The wound remains in the inflammatory phase, which does not favor tissue regeneration, and therefore, the wound cannot heal (Frykberg and Banks, 2015). Targeting and correcting cellular and molecular causes of prolonged inflammation in chronic wounds may be an effective method to return them to healing states.

THE GENERAL ROLE OF MACROPHAGES IN WOUND HEALING

There is considerable evidence that macrophages are key regulators of the wound healing process, during which they take on distinct roles to ensure proper healing. It is well-established that the phenotype of macrophages evolves with the stages of wound healing (Mosser and Edwards, 2008; Ferrante

and Leibovich, 2012). Initially, pro-inflammatory macrophages, traditionally referred to as "M1" macrophages, infiltrate after injury in order to clean the wound of bacteria, foreign debris and dead cells. In acute wounds, as the tissue begins to repair, the overall macrophage population transitions to one that promotes anti-inflammatory effects (traditionally and collectively referred to as "M2" macrophages), and the migration and proliferation of fibroblasts, keratinocytes and endothelial cells to restore the dermis, epidermis and vasculature, respectively. This process will eventually close the wound and produce a scar. Macrophages also play particularly important roles in vascularization, by positioning themselves nearby newly forming blood vessels and aiding in their stabilization and fusion (Fantin et al., 2010; Ogle et al., 2016). In the beginning of the final remodeling phase, macrophages release matrix metalloproteinases (MMPs) to breakdown the provisional extracellular matrix, and then apoptose so that the skin can mature to its original, non-wounded state (Vannella and Wynn, 2017). In chronic wounds, pro-inflammatory macrophages persist without transitioning to anti-inflammatory phenotypes, which is believed to contribute to the impairment in tissue repair (Zhao et al., 2016; Hesketh et al., 2017).

Macrophage phenotype readily changes based on spatiotemporal cues during wound healing, and several different subsets of macrophages, beyond the limited confines of simply *M1* and *M2* (Martinez and Gordon, 2014), have been defined depending on their cell surface markers, cytokine/growth factor/chemokine production, and function (detailed in section Macrophage Phenotypes). The goal of this review is to highlight the importance of macrophages as they pertain to acute and chronic wound healing. The physiology of monocyte recruitment, macrophage differentiation, and their roles in wound healing are also discussed. Evidence toward a stalled pro-inflammatory macrophage phenotype in chronic wounds is also presented. Lastly, examples are provided of several different approaches that have been taken toward attenuating pro-inflammatory (M1-like) macrophages and promoting anti-inflammatory (M2-like) macrophages in order to heal chronic wounds. It is important to note that, due to the complexity of macrophages, there are several unanswered questions and controversial topics within the field. These are discussed throughout the text, and are also summarized in **Table 1**.

ORIGINS OF SKIN MACROPHAGES

Skin macrophages are derived from two different sources: (1) a resident macrophage population established before birth and (2) circulating monocytes that are recruited to areas of injury and differentiate into macrophages (Malissen et al., 2014; Vannella and Wynn, 2017). The first type consists of a self-renewing pool of cells derived from the embryonic yolk sack. These cells, called dermal macrophages, are permanent residents in healthy adult skin, often found in nearby skin appendages. In contrast, during injury, bone marrow-derived monocytes are recruited to the skin, locally differentiate into macrophages and play key roles in wound healing, as discussed previously (Malissen et al., 2014; Vannella and Wynn, 2017).

TABLE 1 | Guide to discussed macrophage questions/controversies.

Guide to Discussed Macrophage Questions/Controversies		
Topic	**Questions/Controversy in Literature**	**Related section**
Dermal Macrophages	• What is the contribution of tissue-resident, dermal macrophages to wound healing?	Sections Dermal Macrophages and Skin Appendages, Dermal Macrophages and Wound Healing
Monocyte Recruitment/ Macrophage Differentiation	• Are monocytes pre-programmed to becoming a specific macrophage phenotype prior to entering the wound and accordingly recruited when needed? • Or, does the wound microenvironment dictate monocyte differentiation/macrophage fate?	Section Monocyte Recruitment and Differentiation in Wound Healing; **Figure 1**
In Vitro vs. *In Vivo* Macrophages	• Do the phenotypes that are defined based on *in vitro* studies translate into *in vivo* wound macrophages?	Section Macrophage phenotypes
M1/M2 Macrophages	• Do macrophages possess distinct phenotypes with unique functions or do their characteristics form a spectrum? • Can all macrophages transition from one phenotype to another? • Can wound macrophages proliferate *in situ* or are they replenished by newly-infiltrated monocytes?	Section Macrophage Phenotypes; **Figure 2**; **Table 2**
Human vs. Murine Models	• How translatable are results obtained from murine models to human chronic wounds?	Section Human vs. Murine Models
Macrophages and Wound Healing	• Which macrophage phenotypes/characteristics are required, and at what time, to result in effective wound healing?	Sections Macrophage Phenotypes During Acute Wound Healing and Macrophage Dysregulation and Chronic Wounds; **Figure 2**
Targeting Macrophages to Promote Wound Healing	• Are M2-like macrophages the answer to promoting wound healing in all situations? If so, which specific phenotypes/characteristics? • What is the ideal treatment time for chronic wounds in order to promote desired wound macrophages and wound healing?	Section Experimental Therapies and Wound Macrophages; **Table 3**

Dermal Macrophages and Skin Appendages

There are several types of well-studied tissue-resident macrophages throughout the body, which play important roles in their respective organs. A few examples are microglia in the brain, Kupffer cells in the liver, and alveolar macrophages in the lungs (Davies et al., 2013). Their general roles include debris clearance (e.g., surfactant in alveolar macrophages and red blood cells in Kupffer cells), initiation of the inflammatory response and the return to homeostasis. Due to these general functions of tissue-resident macrophages, it is not surprising that tissue-resident macrophages in skin (dermal macrophages) contribute to the maintenance and renewal of skin appendages during homeostasis, and wound healing.

Dermal macrophages are located in close proximity to hair follicles, in the surrounding connective tissue sheath and help regulate the hair growth cycle (Eichmuller et al., 1998; Christoph et al., 2000; Castellana et al., 2014). One of the activities of macrophages during hair growth is phagocytosis of collagen, to allow for matrix remodeling (Parakkal, 1969). In a murine model, Castellana et al. (2014) found that apoptosis of skin-resident macrophages activated epithelial hair follicle stem cells, which contribute to hair regeneration (Castellana et al., 2014). Macrophage-specific Wnt-signaling was shown to be central to this process; when it was inhibited, hair follicle growth was delayed. Apoptosis of macrophages occurred immediately prior to hair follicles' transition from telogen to anagen—the hair cycle's resting and growth phases, respectively. Although the study did not use a wound healing model, the results have potential implications in regenerating hair in healing skin. In contrast, Osaka et al. 2007 used a wound model (full-thickness murine wounds) to study signaling pathways and macrophage activation during subsequent hair growth (Osaka et al., 2007). They found that apoptosis signal-regulating kinase 1 (ASK1) is important for efficient hair regrowth; ASK1-deficient mice exhibited delayed hair regeneration following wounding. ASK1 has previously been shown to be increased in the epithelial layer of wound peripheries in rats (Funato et al., 1998). ASK1-deficient mice also had dysregulated macrophage function; less macrophages were recruited to the wound site and several chemotactic and activating factors (IL-1β, TNF-α) were downregulated (Osaka et al., 2007). When bone-marrow derived, cytokine-stimulated macrophages were introduced to the wounds via intracutaneous injection in both ASK1+ and ASK1- mice, hair growth was stimulated.

These studies highlight the importance of dermal macrophages in hair growth, which can have many implications in the development of future therapies that promote wound healing along with hair regeneration. Although there is more research linking macrophages to hair follicles rather than sweat or sebaceous glands, there is still evidence that macrophages can also respond to cues in the microenvironment created by these appendages. For example, the type of lipids produced by sebocytes can impact whether local macrophages take on pro- or anti-inflammatory characteristics, which could potentially impede or promote healing in that area (Lovaszi et al., 2017). Overall, appendage regeneration remains one of the biggest challenges in wound repair (Takeo et al., 2015). Large wounds that are able to heal have a lack of hair and are unable to produce sweat and oil, which leads to cosmetic deficiencies and discomfort to patients. In general, the relationship between macrophages and skin appendages warrants attention, specifically in the context of wound healing.

Dermal Macrophages and Wound Healing

A proposed role for tissue-resident macrophages during injury is that they serve as early indicators of injury or invading pathogens. Some of these macrophages express CD4 and are located near capillaries (Malissen et al., 2014). They are first-responders to injury by recognizing damage-associated molecular patterns (DAMPs; e.g., free heme, ATP) and releasing hydrogen peroxide, which initiates a powerful pro-inflammatory cascade (Minutti et al., 2017). In the case of infection, tissue-resident macrophages recognize pathogen-associated molecular patterns (PAMPs; e.g., lipopolysachharide, LPS). Responses to DAMPs and PAMPs result in the recruitment of neutrophils to help fight early infection (Malissen et al., 2014; Minutti et al., 2017). Monocyte-derived macrophages are also recruited to the wounded area to further amplify the inflammatory response (Davies et al., 2013). Although tissue-resident macrophages aid in the recruitment of immune cells, they are not the only cells in the wound (e.g., platelets) that produce chemokines and signals that have this effect. In general, dermal macrophages can be identified by several surface markers, such as CD64+, MERTK+, and CCR2-/low. They are also highly phagocytic and have a slow turnover (Malissen et al., 2014). Near the end of wound healing, during resolution, dermal macrophages self-renew, and clear apoptotic cells as the tissue returns to homeostasis (Davies et al., 2013).

In addition to macrophages, there are also dendritic cells in the skin that are derived from monocytes (e.g., Langerhans cells). These cells share many surface markers with macrophages, including MHCII, F4/80, CD14, and IL-10, which can make it difficult to distinguish them from each other (Malissen et al., 2014; Minutti et al., 2017). Some even consider Langerhans cells as a type of tissue-resident macrophage, as they have a similar gene expression profile (Satpathy et al., 2012; Davies et al., 2013; Doebel et al., 2017; Minutti et al., 2017), and interestingly, a correlation between healing diabetic foot ulcers and increased numbers of Langerhans cells has been reported (Stojadinovic et al., 2013; Doebel et al., 2017). The specific role of Langerhans cells in wound healing—particularly chronic—has yet to be defined, however, they do repopulate the epidermis during re-epithelialization in acute wound models (Stojadinovic et al., 2013).

Monocyte Recruitment and Differentiation in Wound Healing

Whereas dermal macrophages initiate the local inflammatory response and have relatively short-term effects, monocyte-derived macrophages are systemically recruited ∼24 h post-wounding (in mice) in order to heighten the inflammatory response and protect the tissue from further damage (Italiani and Boraschi, 2014; Minutti et al., 2017). Monocyte-derived macrophages are initially recruited to the wound by signals

from damaged tissue via DAMPs or PAMPs (Sindrilaru and Scharffetter-Kochanek, 2013; Ogle et al., 2016; Vishwakarma et al., 2016). For example, lipopolysaccharide (LPS), a component of the outer membrane of Gram-negative bacteria, is a PAMP that macrophages recognize via binding with toll-like receptor 4 (Bianchi and Manfredi, 2009). This signaling pathway activates the transcription factor, NF-κB, which leads to expression of pro-inflammatory genes. Extracellular DNA, RNA, and ATP, released due to cell death, are examples of DAMPs that signal immune cells and attract them to injury sites (Gallucci, 2016). Monocytes can also be recruited to the wound by chemokines and cytokines downstream of DAMPs/PAMPs, such as IL-1, IL-6, TNF-α, and CCL2 (MCP-1), although in mice, CCL3(MIP-1α) and CCL4(MIP-1β) play this role (Evans et al., 2013).

Multiple monocyte types, categorized as pro-inflammatory and anti-inflammatory, are attracted to the wound site (Ogle et al., 2016). The former, sometimes defined as "classical" monocytes, are derived from the bone marrow and spleen, increase in concentration in the bloodstream following injury, and are $CD14^{+}CD16^{-}$ (human) or $Ly6C^{+/high}$ (mice) (Ogle et al., 2016; Boyette et al., 2017). Surface cell adhesion molecules, such as the $\alpha_4\beta_1$ integrin and CD62L, are responsible for recruiting these cells from the circulation to the blood vessel wall. When there is no injury, pro-inflammatory monocytes do not tightly adhere. However, in the vicinity of the wound, the local presence of inflammatory chemokines and cytokines, such as CCL2(MCP-1), TNF-α, and IFN-γ, promotes expression of cell adhesion molecules. This facilitates the firm adhesion of pro-inflammatory monocytes to the endothelium and subsequent translocation into the tissue space. In addition to extravasation, another mechanism of monocyte recruitment to wounds is by entering through micro-hemorrhages in damaged blood vessels (Rodero et al., 2014; Minutti et al., 2017). With a half-life of only 20 h (in mice), the numbers of pro-inflammatory monocytes fluctuate with the supply of new cells recruited from the bone marrow and circulation, but reach a peak ∼48 h after injury (Yona et al., 2013; Ogle et al., 2016). The second type of recruited monocytes consists of anti-inflammatory monocytes, which have a longer half-life (>2 days, in mice). Human markers include $CD14^{low/-}CD16^{+}$ and for mice, $Ly6^{-/low}$. These cells attach to the blood vessel wall via $\alpha_L\beta_2$ integrin (LFA-1) and L-selection (CD62L). The expression of CD62L enables anti-inflammatory monocytes to crawl on the endothelium even during homeostasis, so that they are nearby to aid in tissue and vascular repair when needed (Auffray et al., 2007; Ogle et al., 2016; Boyette et al., 2017). This suggests that, in addition to tissue-resident macrophages, "resident" monocytes may exist as well. Interestingly, pro- and anti-inflammatory monocytes in mice are attracted to areas of inflammation via different signals: CCR2 vs. CX3CR1-dependent pathways, respectively (Italiani and Boraschi, 2014; Ogle et al., 2016).

Others have used a different nomenclature to group human monocytes into classical ($CD14^{++}CD16^{-}$), intermediate ($CD14^{dim}CD16^{++}$) and non-classical ($CD14^{++}$, $CD16^{+}$) phenotypes. The classical phenotype is analogous to the pro-inflammatory phenotype previously described, whereas the non-classical phenotype is analogous to anti-inflammatory monocytes (Boyette et al., 2017). Each subset exhibits a different morphology following tissue culture, with classical being the largest and roundest, and non-classical being the smallest and having poor attachment. They each have distinct secretomes and respond to different stimuli to varying degrees. For example, classical and intermediate monocytes readily respond to bacteria-associated signals, whereas non-classical monocytes are much less responsive (Cros et al., 2010). All monocyte subsets are capable of differentiating into M1 and M2 macrophages *in vitro*, however M1 macrophages derived from classical monocytes are the most phagocytic and hence, the "most M1-like" (Boyette et al., 2017). Interestingly, non-classical monocytes can differentiate into macrophages even in the absence of differentiation media. This may support one of the proposed models that monocytes themselves transition from classical to non-classical, before differentiating into macrophages (Ogle et al., 2016; Boyette et al., 2017). So, in addition to the existence of several monocyte phenotypes, each possesses varying potentials to differentiate into different macrophage phenotypes as shown through these *in vitro* studies. This adds further complexity in understanding monocyte recruitment/macrophage differentiation in *in vivo* wound healing, where this process is also not entirely clear.

In humans, at homeostasis, ∼85% of blood monocytes are classical, 5% are intermediate and 10% are non-classical (Italiani and Boraschi, 2014). In inflammatory conditions, classical monocytes differentiate into M1-like macrophages whereas non-classical monocytes aid in tissue repair and differentiate into M2-like macrophages (**Figure 1**, Process 1). Accordingly, classical monocytes are recruited to wounds to a higher extent following injury compared to non-classical monocytes. There is also evidence that classical monocytes are recruited to the skin for their pro-inflammatory effects, can become non-classical monocytes and eventually differentiate into M2-like macrophages (Crane et al., 2014; Ogle et al., 2016). With several different monocyte and macrophage phenotypes, the recruitment and differentiation processes are complex, especially within dynamic wound microenvironments. It is not surprising that several models of monocyte recruitment and macrophage differentiation during injury have arisen. Although not exhaustive, a few widely discussed models are depicted in **Figure 1**.

MACROPHAGE PHENOTYPES

General markers for wound macrophages include $CD14^{+}$, $FXIIIA^{+}$, F4/80 (in mice), CD68 (macrosialin), and lysozyme M (LYZ2). Macrophages can also be identified by their relatively strong autofluorescence, which differentiates them from similar $CD14^{+}$ monocyte-derived dendritic cells (Njoroge et al., 2001; Malissen et al., 2014). In general, primary macrophages have limited proliferative capabilities *in vitro*, although there is evidence that dermal macrophages can self-renew *in vivo* (Davies et al., 2013). In contrast, it is not clear whether monocyte-derived macrophages proliferate *in vivo*, or if they are simply recruited to the site of injury as needed, and apoptose following healing (Murray and Wynn, 2011; Italiani and Boraschi, 2014).

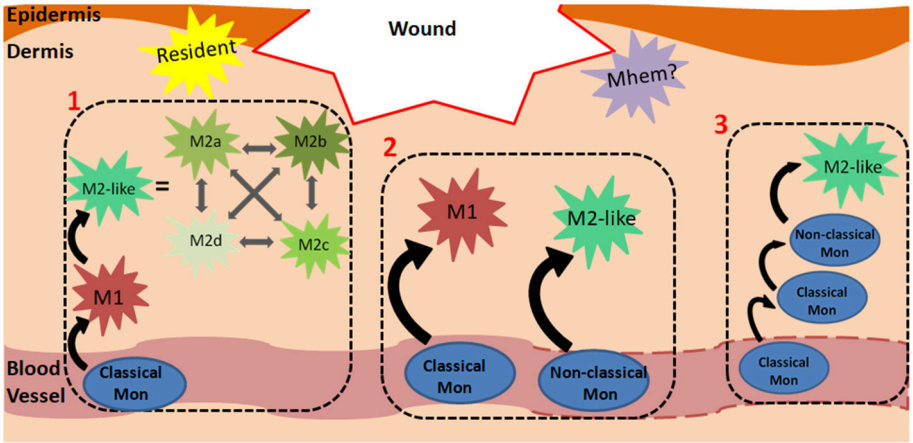

FIGURE 1 | Monocyte-Macrophage Recruitment and Differentiation in Wounds. The mechanism of monocyte recruitment and macrophage differentiation during dermal wound healing can vary depending on spatiotemporal cues. A few models are presented: (1) Classical monocytes in the circulation are primed to differentiate into M1 macrophages following extravasation. In the wound microenvironment, they respond to spatiotemporal cues and can differentiate into any of the M2-like phenotypes, which can transdifferentiate into one another. For brevity, M2a, b, c and d phenotypes are also categorized as M2-like in the remaining processes. (2) Classical monocytes can differentiate into M1 macrophages in the wound. In contrast to the first model, in this panel, macrophages retain the M1 phenotype without further differentiating to M2-like macrophages. Similarly, non-classical monocytes are primed to differentiate into M2-like macrophages and can retain this phenotype. This panel suggests that the final macrophage phenotype is predetermined by the starting monocyte phenotype, and an M1/M2 transition does not occur. (3) This model shows that classical monocytes, rather than macrophages, can also persist in the wound environment for several days, and at a later time, differentiate into non-classical monocytes and then M2-like macrophages. Dashes on the blood vessel indicate that monocytes can exit damaged vasculature via micro-hemorrhages. The yellow star-shape represents resident macrophages, which are established during embryonic development. The purple star-shape represents a possible Mhem phenotype in wounds (analogous to that found in atherosclerotic plaques) which breakdowns hemoglobin and releases anti-inflammatory factors.

Furthermore, their proliferative capability may depend on the particular microenvironment or stage of healing (Italiani and Boraschi, 2014; Murray, 2017).

As described in section The General Role of Macrophages in Wound Healing, two categories of macrophages have been traditionally defined—classically activated, *M1 macrophages* and alternatively activated, *M2 macrophages*. M1 macrophages are typically associated with pro-inflammatory events, whereas M2 macrophages are recognized as anti-inflammatory and pro-regenerative. However, accumulating data suggest that this bipolar M1/M2 definition is grossly oversimplified. It is important to note that M1 and M2 macrophages are not distinct categories, however they form a spectrum in which cells possess varying degrees of M1- or M2-like qualities (Martinez and Gordon, 2014). In support of this view, *in vivo* studies suggest that a heterogeneous population of macrophages exists, with each cell exhibiting a variety of M1 and M2 characteristics (Ogle et al., 2016). Some have even described macrophage activation as a "color wheel," with classically-activated, wound healing and regulatory macrophages as the primary colors, and the secondary colors representing intermediate macrophage phenotypes (Mosser and Edwards, 2008). As a result, many additional subpopulations of macrophage phenotypes have been described and defined in the literature.

Before discussing the specifics of M1- and M2-like macrophages, a different categorization will be presented in section Pro-inflammatory, pro-wound Healing and pro-resolving Macrophages—one that separates macrophage phenotype based on their role within the wound healing process. In regards to this review, this categorization is more relevant and intuitive, although it is not as widely accepted as the M1/M2 spectrum (section M1/M2 Macrophage Spectrum). Discrete M1/M2 phenotypes are useful *in vitro* when the stimulating molecule is known and experimentally introduced to the system, however this nomenclature is less applicable when discussing *in vivo* macrophages in a wound healing context (Novak and Koh, 2013). All of the macrophages associated with wound healing across both *in vitro* and *in vivo* classification systems are presented in **Figure 2**, along with their respective roles.

Pro-inflammatory, Pro-wound Healing, and Pro-resolving Macrophages

In agreement with the phases of wound healing, pro-inflammatory macrophages are present shortly after a wound is formed, followed by pro-wound healing macrophages that support cellular growth and proliferation, and finally pro-resolving macrophages that drastically down-regulate the immune response and aid in collagen reorganization and maturation (Murray and Wynn, 2011; Vannella and Wynn, 2017). Pro-inflammatory macrophages produce nitric oxide, ROS, IL-1, IL-6, and TNF-α. They also secrete MMP-2 and MMP-9 in order to break down the extracellular matrix and make room for infiltrating inflammatory cells (Murray and Wynn, 2011). Pro-wound healing macrophages produce elevated levels of growth factors such as PDGF, insulin-like growth factor 1 (IGF-1), VEGF and TGF-β1 (Murray and Wynn, 2011; Vannella and Wynn, 2017), which aid in cellular proliferation, granulation tissue formation, and angiogenesis. They also produce tissue

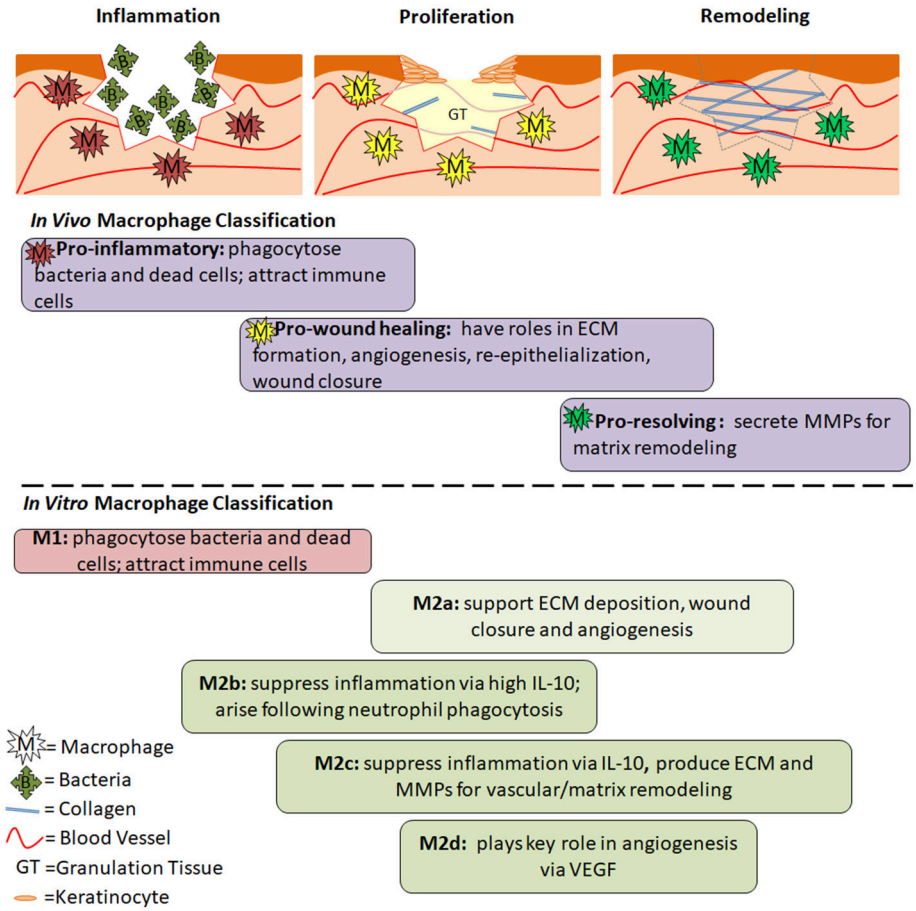

FIGURE 2 | The Role of Macrophage Phenotypes in Wound Healing. Acute wounds progress through the phases of inflammation, proliferation and remodeling as they heal. In **inflammation**, pro-inflammatory macrophages are present. Their role is to phagocytose dead cells and bacteria and prepare the wound for healing. In **proliferation**, pro-wound healing macrophages are present. They secrete factors that aid in angiogenesis, formation of granulation tissue, collagen deposition, and reepithelialization. In **remodeling**, pro-resolving macrophages aid in breakdown of the provisional granulation tissue to allow for maturation of collagen and strengthening of the newly regenerated skin. Below the diagrams are the general roles and timing of different macrophage phenotypes during the wound healing process. Differences between *in vivo* and *in vitro* classifications are separated by the dashed line, however similar roles can be seen between many of the phenotypes. The timing is an estimate based on the role of each phenotype, and has not been experimentally confirmed.

inhibitor of metalloproteinases 1 (TIMP1) in order to counteract MMPs and allow for ECM formation (Murray and Wynn, 2011). Pro-resolving macrophages (aka regulatory macrophages) suppress inflammation via upregulation of IL-10. They also express arginase 1, resistin-like molecule-α (RELMα) programmed death ligand 2 (PDL2) and TGF-β1. MMPs (some evidence pointing toward MMP-12 and MMP-13 specifically) are produced to remodel and strengthen the ECM (Hesketh et al., 2017; Vannella and Wynn, 2017). The function of pro-resolving macrophages is to restore homeostasis while minimizing fibrosis via apoptosis of myofibroblasts, suppression of T cell proliferation and a return to balanced MMP/TIMP levels (Murray and Wynn, 2011). Just as wound healing phases overlap, these different macrophages also share some characteristics with one another. This is especially true for pro-wound healing macrophages which fall between the early and late phases of wound healing, and therefore exhibit characteristics similar to both pro-inflammatory and pro-resolving macrophages.

M1/M2 Macrophage Spectrum

Analogous to pro-inflammatory macrophages, M1 macrophages dominate during the pro-inflammatory phase of wound healing, and through their highly phagocytic behavior, serve the role of sanitizing the wound and clearing it of dead tissue. M1 macrophages also activate other immune cells during the early phase of the wound healing process. *In vitro*, M1 macrophages are stimulated by intracellular proteins and nucleic acids released from lysed cells (e.g., IFN- γ), and bacterial components, such as LPS and peptidoglycan (Ferrante and Leibovich, 2012). M1 macrophages express CD86, and produce high levels of (ROS) and pro-inflammatory cytokines, such as interleukins 1 and 6 (IL-1, IL-6), TNF- α, and IFN-γ.

Traditionally defined *M2 macrophages* serve a regenerative role. M2 macrophages are stimulated by IL-4 and IL-13 and express high levels of the mannose receptor (CD206), dectin, interleukin 10 (IL-10), and transforming growth factor β (TGF-β). They produce low levels of pro-inflammatory cytokines such

as TNF-α, IL-12, and CXCL8(IL-8) (Ferrante and Leibovich, 2012). It has also been found that interferon regulator factors (IRF4/IRF5) are transcriptional regulators that play a role in differential signaling seen between M2 and M1 macrophages, respectively.

M2 macrophages have been divided into different subtypes according to differential expression of surface markers. These subtypes have been traditionally used and identified *in vitro* to study M2-like macrophages with different characteristics. In *in vivo* studies, this nomenclature is not as widely used to identify macrophages, potentially due to the heterogeneous populations present, which are generated from a variety of stimuli within wounds (Novak and Koh, 2013). **Table 2** identifies the different names and markers for each macrophage phenotype. The table is not comprehensive, and it is important to note that marker expression for each phenotype can vary from study to study, hence adding to the complexity and difficulty of defining macrophages.

The previously described M2 macrophages, also known as wound healing macrophages, align with what is now defined as the *M2a subset* (Ogle et al., 2016). M2a macrophages are stimulated by IL-4/IL-13 and exhibit IL-4 receptor α (IL-4Rα) signaling (Ferrante and Leibovich, 2012). CD206 is a distinguishing surface marker and they produce high levels of arginase-1 (in mice), PDGF-BB, IGF-1, and several chemokines (CCL17, CCL18, CCL22; Ogle et al., 2016). M2a macrophages produce collagen precursors and factors that stimulate fibroblasts. Thus, M2a macrophages play a key role in ECM formation, which is required during the proliferative phase of wound healing. They also secrete high levels of PDGF, which is involved in angiogenesis (Spiller et al., 2014).

M2b macrophages, which express CD86, CD68, and MHCII, are stimulated by immune complexes and TLF/Il-1 agonists (Ogle et al., 2016; Hesketh et al., 2017). They are also known as type 2 macrophages. M2b macrophages suppress inflammation by increasing IL-10 production, although they also secrete IL-6, IL-β, and TNF, and express high levels of iNOS. M2b macrophages also produce several different MMPs. *In vitro*, macrophages take on an M2b phenotype following phagocytosis of apoptotic neutrophils (Filardy et al., 2010).

M2c macrophages are stimulated by glucocorticoids, IL-10 and TGF-β (Roszer, 2015; Garash et al., 2016). They express CD206 and MERTK. M2c macrophages produce high levels of IL-10, MMP-9, IL-1β, and TGF-β, and low levels

TABLE 2 | Macrophage phenotypes and characteristics.

Phenotype	Other nomenclature	Nomenclature by activation molecule	Markers	Other notes
M1	classically activated; pro-inflammatory	–	Surface: CD86, CD68, CD80, MHC-II Secreted: TNF-α, IL-6, IL-12, IL-1β	abundant and persistent in chronic wounds; activated *in vitro* by LPS, peptidoglycans and pro-inflammatory cytokines
M2	all M2-phenotypes collectively: alternatively activated; anti-inflammatory	–	–	–
M2a	alternatively activated; wound healing	M(IL-4)	Surface: CD206, arginase (mice), Ym1 (mice) CD163, MHC-II, CD209 Secreted: TGF-β, IL-10, IL-1RA	aid in ECM formation, angiogenesis
M2b	type 2; regulatory	M(Ic)	Surface: CD86, MHC-II Secreted: TNF-α, IL-1, IL-6, IL-10	similar to M1 macrophages, but dampen inflammation
M2c	deactivated; pro-resolving?	M(IL-10), M(GC), M(GC+TGF-β)	Surface: CD86, CD163, CD206 Secreted: IL-10, CD206, TGF-β, MMP-9	involved in vascular and matrix remodeling; some shared characteristics with Mhem
M2d	–	–	Secreted: VEGF, IL-10, IL-12, TNF-α, TGF-β	pro-angiogenic; activated *in vitro* by stimulating adenosine and toll-like receptors
Mhem	HA-Mac; Heme-directed macrophage	M(Hb)	Surface: CD163, CD206 Secreted: IL-10 Internal: HMOX-1 gene, activating transcription factor (ATF)	found near hemmorrhaged vessels in atherosclerotic plaques; anti-inflammatory effects
M4	CXCL4 derived macrophage	–	Surface: CD206, CD86, Lack CD163 Secreted: IL-6, TNF-α	associated with atherosclerosis in human models; M1-like; low phagocytosis
Mox	Oxidized phospholipid derived macrophages	–	Surface: ↓arginase-1 Secreted: ↓MCP-1, ↓TNF-α Internal: HMOX-1 gene, HO-1, sulfiridoxin 1, theoredoxin reductase-1	associated with atherosclerosis in murine models; low phagocytosis; antioxidant properties
TAMs	tumor-associated macrophages	–	Surface: CD163, CD206, CD204 Secreted: IL-10, MIF, CXCL12, VEGF, IL-6, IL-23, TGF-β Internal: HIF-1α	located nearby tumors; promote angiogenesis and cell proliferation; M2-like

of IL-12. M2c macrophages also express CD163, which is the hemoglobin receptor. This is important to note, as there exists another macrophage phenotype, called Mhem, that is similarly characterized by high CD163 expression and IL-10 production, albeit stimulated by hemoglobin and typically identified in atherosclerotic plaques (Boyle, 2012). These shared features may indicate that different stimuli can elicit the same, or very similar, macrophage phenotypes that are nevertheless referred to by different names (M2c vs. Mhem). Furthermore, due to their production of ECM and MMPs and hence, their matrix remodeling capability, M2c macrophages may be analogous to the aforementioned pro-resolving macrophages. M2c macrophages are also sometimes referred to as deactivated macrophages as they can arise from M1 macrophages that have "deactivated" the M1 gene profile to become M2c macrophages. M2 macrophages can shift between *a, b* and *c* phenotypes (Ogle et al., 2016).

In contrast to *M2a* macrophages, *M2d* macrophages do not have either elevated mannose receptor (CD206) or dectin-1 expression (Ferrante and Leibovich, 2012). M2d macrophages arise from stimulation by IL-6 and adenosine. They produce high levels of vascular endothelial growth factor (VEGF) as well as IL-10 and TGF-β. They also down-regulate pro-inflammatory TNF-α and IL-12. M2d macrophages are activated by concurrent stimulation of toll-like receptor (via IL-6) and adenosine A_{2A} receptors (Ferrante and Leibovich, 2012; Roszer, 2015).

Several other macrophage types have been defined, however, they tend to be associated with specific diseases, such as atherosclerosis or cancer (Colin et al., 2014; Medbury et al., 2014). For example, Mox, M4 and Mhem arise from macrophages stimulated by oxidated phospholipids, CXCL4 and hemoglobin-haptoglobin complexes, respectively. Although these phenotypes are not typically associated with chronic wounds, it is possible that some wound macrophages have some shared characteristics, especially in regards to Mhem, as hemoglobin-haptoglobin receptor (CD163) expression and cellular regulation of iron are associated with wound healing (Cairo et al., 2011; Sindrilaru et al., 2011; Evans et al., 2013). There also exist cancer-specific macrophages, called tumor-associated macrophages (TAMs), which support tumors by stimulating angiogenesis, aiding in metastasis and inhibiting T-cell anti-tumor responses (Yang and Zhang, 2017). They can differentiate from resident progenitor cells, but are more often derived from recruited monocytes from the blood stream. TAMs are more similar to M2 macrophages, as they produce anti-inflammatory cytokines and promote proliferation and growth to support the tumor microenvironment. These additional, disease-specific macrophages underline the unique plasticity and range of phenotypes and functions that macrophages possess and can exhibit in different microenvironments.

Overall, macrophage nomenclature within this vast spectrum is not yet agreed upon and it is unclear whether the phenotypes are distinct, or even applicable to *in vivo* wound healing (Martinez and Gordon, 2014). It is important to remember that the macrophage population during wound healing is complex; wound macrophages can take on a different phenotype depending on several factors, such as the anatomical location of the wound (foot, lower back), the specific region within the wound (center/edge), the environment (moist, dry) and whether or not the wound is infected (Ferrante and Leibovich, 2012). Unsurprisingly, it is still unclear the exact signals and differentiation cascade required to produce a specific macrophage phenotype (M2a vs. M2b vs. M2c, etc., see **Figure 1**). Adding further complexity to this question is the fact that these phenotypes exist on a spectrum, and macrophages can easily transition from M1-like to M2-like (and M2a-like, M2b-like etc.). Furthermore, wound macrophage populations are heterogenous, as it is possible for pro- and anti-inflammatory cytokines to be present simultaneously (Novak and Koh, 2013; Martinez and Gordon, 2014). Interestingly, although differentiation of M2a macrophages is stimulated by IL-4 and IL-13 *in vitro*, these cytokines are not present in healing murine wounds that contain M2-like macrophages (Daley et al., 2010), further underlining the disconnect between *in vitro* and *in vivo* models. Although the defined macrophage definitions are useful *in vitro*, they must be regarded with caution when considering macrophage phenotypes in the *in vivo* wound healing process.

Macrophage Standardization Efforts

Murray et al. (2014) acknowledge the complexity of the current macrophage nomenclature and provide suggestions for improvement moving forward (Murray et al., 2014). The authors met to attempt to set a foundation toward consolidating and standardizing the wealth of macrophage activation terms and methods that have arisen throughout the years.

Their recommendations include:

1. differentiating murine or human bone marrow/peripheral blood monocytes with CSF-1 or GM-CSF to generate macrophages, and using post-differentiation stimuli IFN-γ and IL-4 to obtain M1 and M2 macrophages, respectively;
2. reporting defined metrics such as tissue culture conditions, media, time, etc., to characterize *in vitro* macrophage cultures;
3. defining the activator for *in vitro* macrophages using the following notation: M(LPS), M(IFN-γ), M (IL-10), etc. and referencing a provided spectrum of M1/M2-like characteristics;
4. the avoidance of the term "regulatory macrophages", as well as the use of GM-CSF to create M1 macrophages and CSF for M2 macrophages; and
5. use of a combination of markers (cytokines, chemokines, scavenger receptors and more) to describe macrophage state.

The authors not only discussed how to define *in vitro* macrophages, but also macrophages isolated from *in vivo* models. A main point includes encouraging scientists to detail the isolation process in publications. Researchers should also characterize *ex vivo* macrophages and attempt to fit them within the *in vitro* macrophage spectrum defined in the article, in a manner similar to that depicted in **Figure 2** in this review. They also acknowledge the differences between interspecies macrophages, and suggest thorough side-by-side comparisons in order to glean information about human macrophage behavior. With more characterization and understanding, scientists will

begin to bridge the gap between macrophages from different sources and species.

These guidelines were a vital starting point to tackling the complex challenge of streamlining macrophage nomenclature and research/reporting practices. These standards should be broadly distributed, and scientists should regularly meet to update them. As a result, understanding of macrophage function and behavior will improve across the entire field. This may prime faster advancement in the development of therapies that target macrophages, within chronic wound healing applications and many others.

HUMAN VS. MURINE MODELS

Mice are commonly-used animal models for wound healing studies due to their affordability and ease-of-use, however, it is important to acknowledge differences between human and murine skin anatomies, wound healing processes, and immune systems (and hence, macrophage behaviors) (Murray, 2017). In terms of anatomy, mice have more densely-packed hair follicles and thinner epidermal and dermal layers compared to human skin (Pasparakis et al., 2014). It is also generally believed that murine skin heals by contraction—that is, the edges of the wound pull in toward each other, like a drawstring bag, in order to quickly close. In contrast, human skin heals by re-epithelialization, during which keratinocytes crawl over the granulation tissue in order to close the wound. This assumption has recently been revisited, to argue that mice heal both by contraction and re-epithelialization, making them better models for wound healing than previously assumed (Chen et al., 2015).

Diabetic mice are used as *in vivo* chronic wound models, as they exhibit delayed wound healing. Mice are either bred to contain a genetic mutation which results in a diabetes-like phenotype, or it is induced via chemical means, for example, injection with streptozocin (Nunan et al., 2014). Diabetic mouse wounds share several key characteristics in common with chronic wounds in diabetic patients (Blakytny and Jude, 2006). These include decreased nerve count, angiogenesis, granulation tissue formation, and collagen content compared to acute wounds. They both contain higher levels of MMPs and lower levels of TGF-β1, IGF-1, and PDGF. More is actually known about diabetic mouse wounds compared to human diabetic ulcers, due to an increased number of studies and an increased ability to probe and measure tissue characteristics (particularly *ex vivo*). So, whereas there are several studies showing decreased VEGF, FGF, and KGF in diabetic mouse wounds, in human diabetic ulcers, there is both an incomplete panel of measured cytokines and growth factors, as well as less significant trends due to large biological variability.

One discrepancy between murine and human macrophages is their expression of inducible nitric oxide synthase (iNOS) (Mestas and Hughes, 2004). Mouse macrophages readily express iNOS in response to LPS or IFN-γ, and for this reason, it is recognized as an M1 marker in mice. Human macrophages, however, do not over-express iNOS in response to these same stimuli. General markers to identify murine and human macrophages differ as well. In humans, they are CD14 and CD33, and in mice, they are F4/80 and CD11b. Other murine-specific M2 markers include Ym1, FIZZ1, and arginase-1 (Roszer, 2015). Human and mouse macrophages also express different FcR and IgG receptors, which play a bigger role in the immune system as a whole, by linking the adaptive and innate immune systems (Mestas and Hughes, 2004).

The function of specific receptors can also differ between species (Mestas and Hughes, 2004). For example, CD163 is a common M2-like macrophage marker that functions as the hemoglobin-haptoglobin receptor (Etzerodt et al., 2013). In humans, the binding of hemoglobin and haptoglobin significantly increases endocytosis of hemoglobin and activation of downstream signaling pathways. In mice however, haptoglobin does not promote binding of hemoglobin to CD163. Although this may seem insignificant, it is just one specific example of how human and murine macrophages have different mechanisms and behaviors. To overcome these discrepancies, there is a need to conduct thorough, side-by-side experiments (e.g., single-cell and bioinformatics approaches) using monocytes and macrophages from different species and sources (Murray, 2017). Through these efforts, well-informed comparisons can be made across models while taking advantage of their other benefits (affordability, ease-of-use, etc.).

In addition to specific differences between human and murine skin and macrophages, on a whole, it is important to remember that, although diabetic mice are slower to heal than wild type mice, they do eventually heal. Diabetic mice are not an ideal model for non-healing, chronic wound studies, but they do have many fundamental similarities on the tissue and cellular levels, making them a widely-accepted model in current wound healing research (Nunan et al., 2014).

MACROPHAGE PHENOTYPES DURING ACUTE WOUND HEALING

Except for fetal wounds, which have the capacity to regenerate in the absence of inflammatory response, macrophages are vital for successful adult wound healing (Leibovich and Ross, 1975; Mackool et al., 1998). Studies have shown that the depletion of macrophages in wounded mice results in delayed re-epithelialization, reduced collagen formation and impaired angiogenesis (Goren et al., 2009; Mirza et al., 2009). These effects occurred along with increased levels of TNF-α and decreased VEGF and TGF-β1. Furthermore, in the absence of macrophages, there was a prolonged neutrophil presence and reduced wound contraction (Goren et al., 2009).

Although the general importance of macrophages in wound healing is known, there is still much to learn about the details regarding timing, relative proportion and specific role of each phenotype. Mirza and Koh (2011) isolated macrophages during the wound healing process in mice at Days 5, 10, and 20 post-injury in order to study the temporal phenotype change (Mirza and Koh, 2011). In wild type mice, pro-inflammatory macrophages were detected on Day 5. These macrophages expressed high levels of IL-1β, MMP-9, and nitric oxide synthase

(NOS). By Day 10, the expression of these pro-inflammatory factors decreased, concurrent with an increase in expression of anti-inflammatory markers CD206 and CD36 and growth factors IGF-1, TGF-β, and VEGF. Non-diabetic mice had efficient wound repair, achieving wound closure after 20 days, at which elevated expression remained for CD206, CD36, and TGF-β, but not for IGF-1 or VEGF.

Evans et al. (2013) used an acute wound model in humans to better understand the pro- to anti- inflammatory macrophage transition in blisters (Evans et al., 2013). Wounds were chemically induced by application of cantharidin, a topical treatment for warts. Blister fluid was collected 16 and 40 h after injury, to represent the inflammatory and resolving phases of wound healing, respectively. Cell counts from the fluid yielded more monocytes/macrophages at the 40 h time point compared to 16 h. Furthermore, the proportion of CD163+ macrophages increased over 10 fold at the later time point (3.4 vs. 47.6%), indicating that CD163 is strongly associated with the resolution phase of healing. Amounts of inflammatory mediators were also measured in the wound fluid. At the 16 h "inflammatory" time point, there were significantly higher levels of CCL2(MCP-1), CXCL8(IL-8), TNF-α, CCL3(MIP-1α), CCL4(MIP-1β), and CCL11(eotaxin). At the 40 h "resolution" time point, there was significantly more macrophage-derived chemokine (MDC) and TGF-β in the wound fluid. Interestingly, this study reported undetectable levels of IL-10 at either time point, which is surprising, as it is recognized as a cytokine produced at high levels by anti-inflammatory macrophages.

MACROPHAGE DYSREGULATION AND CHRONIC WOUNDS

When macrophages become dysregulated, several wound healing complications can arise, such as the formation of chronic wounds or excessive scarring (Vannella and Wynn, 2017).

Macrophages in chronic wounds have a reduced capability to phagocytose dead neutrophils, which, as a result, accumulate and promote a strong inflammatory environment. Diabetic patients have macrophages with reduced apoptotic clearance activity because of the effects of hyperglycemia and advanced glycation endproducts (Khanna et al., 2010; Hesketh et al., 2017). The act of neutrophil clearance by macrophages can induce the phenotypic switch of M1 macrophages to M2b, and lead to the resolution of inflammation (Filardy et al., 2010; Hesketh et al., 2017). This is one of many reasons as to why chronic wounds may have an abundance of M1 macrophages.

Significantly higher numbers of macrophages are found in the peripheries of venous and diabetic ulcers compared to acute wounds (Loots et al., 1998). In this study, CD68 was used as a general marker to detect macrophages (although other studies define it as an M1 marker, this study did not make that clear). In acute wounds, the number of macrophages was highest at the first time point, and decreased as healing progressed. In contrast, venous and diabetic ulcers had the highest number of macrophages compared to acute wounds. The results of this study also suggested that macrophages are not the only immune cell that is dysregulated in chronic wound healing, as lower numbers of T-cells and higher numbers of B-cells were also observed. Another study also detected high levels of CD68 macrophages in the dermis and wound edges in chronic leg ulcers (Moore et al., 1997). CD16 and CD35 were also measured and defined as "activation-associated markers," with positive staining denoting the presence of mature macrophages (rather than monocytes) in inflammatory environments. Most of the wounds studied had low expression of these markers (<12%), and the few areas that were positive were near the vasculature, suggesting that other microenvironments in the wound suppress or prevent macrophage activation. Although this study provided information about macrophage presence and marker expression in chronic wounds, particularly in different locations of a single wound, a low patient number (12 patients) was evaluated and results were not compared relative to patients with acute wounds. These early studies provided important histological data on macrophages in human wounds, but did not explicitly discriminate between pro- or anti-inflammatory phenotypes, nor did they measure cytokines or growth factors in the wound environment.

Most *in vivo* studies, especially in humans, do not tend to study macrophages directly via detection of cell markers, but rather indirectly through the cytokines and proteins present in the wound tissue or fluid. Macrophages are major producers of cytokines and growth factors during wound healing, so, based on the identities and amounts measured, a determination can be made on whether the local macrophage population is more pro- or anti-inflammatory (M1/M2-like).

Accordingly, studies show that chronic wound fluid contains high levels of pro-inflammatory cytokines, particularly TNF-α and IL-1β, which were measured to be 100-fold higher compared to acute wounds fluids (mastectomy drain fluids; Tarnuzzer and Schultz, 1996). IL-6 was also elevated, but only 2–4 fold. In contrast, mastectomy fluid had the highest levels IL-1β and IL-6 on Day 1 post-surgery and thereby steadily decreased to Day 7. Interestingly, TNF-α levels remained constant during this time period. This is in agreement with observations by Wallace and Stacey, who also observed higher levels of total TNF-α in chronic wounds (Wallace and Stacey, 1998). Interestingly, the amount of bioactive TNF-α in both healing and non-healing wounds was not significantly different. The amount of bioactive TNF-α did not change as acute wounds closed, suggesting that the regulation of other cytokines may be more important in progressing wound healing. Chronic wound fluid also contains high levels of MMPs, specifically MMP-2 and MMP-9 (Wysocki et al., 1993). MMPs degrade proteins and extracellular matrix and are not favorable for extended periods, as they do not support tissue regrowth in the proliferative phase of wound healing. Macrophages produce MMPs, so they may be responsible for maintaining elevated levels in chronic wounds (Newby, 2008). Specifically, human blood monocytes are stimulated to produce MMP-2 and MMP-9 in the presence of pro-inflammatory signals, such as LPS, IFN-γ, IL-1β, and TNF-α (Zhou et al., 2003; Newby, 2008). Furthermore, the proteases degrade and decrease the bioactivity of growth factors that may be present, hence canceling out their pro-healing benefits as inflammation prevails (Tarnuzzer and Schultz, 1996).

Since there are no non-healing animal models of chronic wounds, diabetic mice are often used as they exhibit delayed wound healing and share several characteristics with human chronic wounds (Blakytny and Jude, 2006; Nunan et al., 2014). Studies investigating wound macrophages show that their function is not properly regulated in diabetic vs. wild type mice, with a prolonged M1 macrophage presence and hence, inefficient transition to the M2 phenotype (Mirza and Koh, 2011). Mirza and Koh found that, although macrophages from non-diabetic mouse wounds had transitioned from a pro- to anti-inflammatory phenotype by Day 10, macrophages from diabetic mice retained pro-inflammatory characteristics. This included two-fold higher levels of pro-inflammatory factors IL-1β and IFN-γ, and ∼two-fold lower anti-inflammatory IL-10 in the general wound environment. More specifically, isolated macrophages from Day 10 wounds in diabetic vs. non-diabetic mice had significantly higher mRNA expression of IL-1β and MMP-9 and significantly lower expression of CD206 and CD36. At the same time, they have reduced growth factor production (IGF-1, TGF-β1, VEGF, and IL-10). In non-diabetic wounds, these factors are already present and contributing to key events in wound healing such as cell proliferation and migration, ECM formation, and angiogenesis. Most of the aforementioned cytokine and growth factor trends were retained until Day 20, which is in stark contrast to non-diabetic wounds, which had already healed by this point and long-completed the M1-to-M2 transition. Also interesting to note, is the fact that diabetic wounds contained fewer mature macrophages (more Ly6C expression v. F4/80) even at Day 10, suggesting that the monocyte-to-macrophage transition is impaired and may contribute to delayed wound healing. Overall, diabetic and non-diabetic wound macrophages only started to exhibit significantly different cytokine/growth factor differences by Day 10; at Day 5, they had similar levels. This suggests that between Day 5 and Day 10, non-diabetic mouse wounds are transitioning to the proliferative phase, in accordance with the M1 to M2-like macrophage phenotype change. Diabetic mouse wounds remain highly inflammatory, guided by persistent pro-inflammatory macrophages. Overall, this study provided key evidence of delayed macrophage phenotype transition concurrent with delayed wound healing in diabetic mice.

Other studies have shown prolonged presence of other pro-inflammatory cytokines in diabetic mouse wounds, much longer than seen in wild type mice. One study compared the expression of IL-1β and TNF-α in three different mouse strains: Balb/c, C57BLKS, and db/db (Wetzler et al., 2000). No IL-1β was detected after Day 7 in the first two strains, whereas high levels persisted into Day 13 in diabetic mouse wounds. Similarly, TNF-α was detected at the highest levels in db/db mouse wounds at Day 13, and was completely absent or present at very low levels in the wild type groups at the same time. The diabetic group also retained elevated levels of MIP-2 and CCL2(MCP-1) mRNA and protein into Day 13, whereas both strains of wild type mice had stopped producing those factors by Day 13 or even earlier. MIP-2 and CCL2(MCP-1) are chemoattractants, so their presence continually attracted more macrophages, which was detrimental to healing, as the macrophages that were recruited maintained an M1 phenotype. Again, the prolonged presence of pro-inflammatory/M1 macrophages is a hallmark of delayed wound healing in diabetic mice.

Differential iron regulation by macrophages is another factor that can promote M1/M2 phenotypes (Cairo et al., 2011). M1-like cells store the majority of the iron intracellularly as ferritin, whereas, M2-like macrophages release it to the extracellular environment via the transmembrane channel, ferroportin. Sindrilaru et al. (2011) identified the role of high intracellular iron stores in maintaining M1 macrophages in chronic wounds, particularly chronic venous ulcers (Sindrilaru et al., 2011). The source of iron was hemoglobin from erythrocytes that escape from damaged blood vessels and enter the wound environment. In a corresponding wounded murine model with iron delivered intravenously, wound macrophages produced high levels of TNF and hydroxyl radical, and a senescence program was induced in nearby fibroblasts. As a result, wound closure was delayed.

The prolonged presence of the M1 phenotype is not the only macrophage-related problem that can contribute to wound healing disruption. In fact, if M2-like macrophages remain for too long, there may be excessive collagen formation, resulting in scarring (Sindrilaru and Scharffetter-Kochanek, 2013; Vannella and Wynn, 2017). It is interesting to note that fetal wound healing is scarless, with virtually no infiltrating macrophages, and many have attempted to mimic this model to improve wound healing outcomes in adults (Mackool et al., 1998). These examples suggest that an overabundance or prolonged presence of macrophages, regardless of the phenotype, can lead to wound healing complications.

EXPERIMENTAL THERAPIES AND WOUND MACROPHAGES

Based on the role played by the different types of macrophages in the wound healing response, it has been hypothesized that interventions that dampen the M1 macrophage phenotype and promote M2-like characteristics may help the healing of chronic wounds. Some have even delivered exogenous macrophages as cell therapies for chronic wounds. A few of these approaches are highlighted below and summarized in **Table 3**. Note that the table focuses on key *in vivo* studies, whereas the text in the following subsections includes both *in vivo* and *in vitro* results.

Endogenous M1 Macrophage Attenuation

Goren et al. (2007) aimed to silence M1 macrophages in obese/obese (ob/ob) mouse wounds (Goren et al., 2007). These animals have diabetes and hence, exhibit impaired wound healing. In the study, anti-TNF-α or anti-F4/80 antibodies were systemically administered beginning 7 days post-wounding, concurrent with the end of the inflammatory phase. These treatments resulted in wound closure and re-epithelialization while control wounds treated with a non-specific antibody remained unhealed with scabs. There were fewer total macrophages and decreased levels of TNF-α, IL-1β, and

TABLE 3 | Experimental approaches to modulate macrophages in wound healing.

Method	Wound model	Treatment details	Conclusion	References
ENDOGENOUS M1 ATTENUATION				
Neutralizing Monoclonal antibodies: • anti-TNF-α • anti-F4/80 • control: non-specific, rat IgG	• ob/ob mice • Full-thickness excisional wounds (5 mm diameter)	• Systemic administration • 1 μg/g body weight • Day 7, 9 and 11 post-wounding (End of inflammatory phase)	• TNF-α and F4/80 antibodies effectively target and kill pro-inflammatory wound macrophages, resulting in accelerated healing	Goren et al., 2007
EXOGENOUS M2 SUPPLEMENTATION				
Injection of *in vitro* polarized: • M2a macrophages (by IL-4) • M2c macrophages (by-IL-10) • control: non-polarized macrophages (M0) • control: saline	• db/db mice • full-thickness excisional wounds (4 mm diameter)	• intradermal injection (0.5×10^6 cells) • Day 1 and 3 post-wounding	• *In vitro*-polarized M2 macrophage supplementation immediately after wounding did not accelerate healing	Jetten et al., 2014
Ulcers treated with: • macrophages from blood of young, healthy donors, stimulated by hypo-osmotic shock ($n = 72$ ulcer patients) • conventional wound care ($n = 127$)	• human pressure ulcers in elderly patients • range of sizes (not indicated)	• intradermal injections near ulcer periphery and topically on ulcer • 0.05 mL/injection; 1 cm between injections along periphery • 2×10^6 cells/mL • majority of ulcers treated 1 time; rare case of reinjection occurred 2 months after initial	• Injection of blood-derived macrophages to pressure ulcers resulted in healing of 27% of those treated vs. 6% in controls	Danon et al., 1997
Ulcers treated with: • macrophages from blood of young, healthy donors, stimulated by hypo-osmotic shock ($n = 141$ ulcers) • conventional wound care ($n = 75$)	• human pressure ulcers • human diabetic ulcers • large range in wound sizes; average ∼30 cm^2	• intradermal injections near ulcer periphery and topically on ulcer • 0.1 mL/injection; 1 cm between injections along periphery • 15–40 mL total depending on size • $2–4 \times 10^6$ cells/mL • re-injection depending on wound condition ∼4 weeks after initial treatment	• Injection of blood-derived macrophages lead to healing of a majority (69.5%) of pressure and diabetic ulcers compared to only 13.3% healed with standard treatment	Zuloff-Shani et al., 2010
ENDOGENOUS MACROPHAGE MODULATION/M2 PROMOTION				
MSCs				
Conditioned media from: • bone-marrow derived MSCS • control: fibroblasts	• healthy mice (Balb/C) • full-thickness excisional wounds (6 mm diameter)	• 100 μL total administered • subcutaneous (80 μL) and topical injections (20 μL)	• MSC-conditioned media resulted in increased numbers of macrophages and endothelial progenitor cells in the wound. Wound closure was significantly accelerated.	Chen et al., 2008
• human gingiva-derived MSCs (in PBS) • control: PBS	• healthy mice (C57BL/6J) • full-thickness excisional wounds (6 mm diameter)	• intravenous injection (2×10^6 cells) • one time, on Day 1 after wounding	• Wound closure with MSC treatment was significantly accelerated. This occurred with a decrease in TNF-α and IL-6 and an increase in IL-10 and arginase-1	Zhang et al., 2010
Autologous bone-marrow derived: • MSCs • mononuclear cells • control: saline and standard care	• human diabetic ulcers • average size ∼4 cm^2	• intramuscular injection • 20 separate sites all on Day 1 • many cells used (exact number not clear)	• Ulcers treated with MSCs had accelerated healing compared to MNCs. Patients in this group also had better outcomes in terms of time to painless-walking, transcutaneous oxygen pressure and blood vessel formation	Lu et al., 2011

(Continued)

TABLE 3 | Continued

Method	Wound model	Treatment details	Conclusion	References
Growth factors				
• PDGF-BB • control: collagen-vehicle • control: non-irradiated	• healthy rats (Sprague-Dawley) • linear surgical incisions (6 cm long) • irradiated (whole-body or topically) to depress wound healing	• topical (2 μg and 10 μg/wound) • single dose	• Wounds treated with PDGF had higher cellularity scores and breaking strength. Effect of PDGF-BB was only seen in rats containing wound macrophages (topical irradiation vs. whole-body irradiation)	Mustoe et al., 1989
• recombinant human GM-CSF	• human chronic venous leg ulcers • range of sizes (not indicated)	• intradermal injection at 4 corners of wound • 150 μg	• GM-CSF causes wound macrophages to increase VEGF production, which results in improved vascularization in wounds	Cianfarani et al., 2006
Biomaterials and macrophages				
PEG-RGD hydrogels of varying stiffnesses: • 130 kPa • 240 kPa • 840 kPa	• healthy mice (C57BL/6)	• subcutaneous implantation • 5 mm diameter hydrogels	• Macrophage infiltration was the greatest in the stiffest hydrogels (840 kDa). Generally, stiffer hydrogels resulted in more severe foreign body responses.	Blakney et al., 2012
HO-1 expression				
Hemin (in diabetic rats) controls: • vehicle (in diabetic rats) • non-diabetic rats	• diabetic rats (streptozotocin-induced) • full-thickness excisional wounds	• topical 10% hemin ointment • daily	• HO-1 was induced in wounds of diabetic rats receiving hemin treatment. These wounds healed significantly faster than vehicle controls, at rates similar to non-diabetic rats. Hemin treatment led to decreased levels of TNF-α and IL-6 in wound tissue	Chen et al., 2016
• Hemin injection • topical povidone-iodine (positive control) • Saline injection	• healthy rats (Wistar) • full-thickness excisional wounds (2 × 2 cm^2)	• hemin solution (diluted in saline) • intraperitoneal injection (30 mg/kg) • daily	• Hemin treatment increased wound closure and collagen synthesis. mRNA of pro-inflammatory cytokines ICAM-1 and TNF-α were decreased whereas anti-inflammatory IL-10 was increased. In some cases, the effect of hemin was greater than the positive control.	Ahanger et al., 2010
Oxygen therapy				
Hyperbaric Oxygen (HBO) Therapy • controls: normoxia hyperoxia increased pressure only	• *in vitro* human macrophage culture • cells stimulated with LPS, PHA, TNF-α, or Lipid A	• cells cultured in HBO, normoxia, hyperoxia, or increased pressure for up to 12 h	• Short-term (30 min) hyperbaric oxygen therapy (both increased pressure *and* oxygenation) has immunosuppressive effects on macrophages	Benson et al., 2003

CCL2(MCP-1) proteins in wounds with anti-TNF-α and anti-F4/80. Furthermore, a greater proportion of wound macrophages were apoptotic compared to control groups. Overall, anti-TNFα and anti-F4/80 therapies reduced the impact of M1 macrophages, and accelerated the healing of diabetic wounds. It is noteworthy that by choosing Day 7 post-injury as the time point to begin treatment, necessary early inflammatory events in M1 macrophages were not disrupted. Treatment timing was strategically chosen to rescue the wound healing response during late-stage inflammation, during which the macrophage population should begin transitioning to M2.

Exogenous M2 Macrophage Supplementation

Since the appearance of M2 macrophages correlates with a desirable progression in the wound healing response, direct

addition of isolated M2 macrophages has been attempted to stimulate healing. However, as reported by Jetten et al. (2014), who used macrophages that were polarized into M2a and M2c phenotypes *in vitro* and then injected them into mouse wounds, this approach did not accelerate healing in wild type mice and even delayed healing in diabetic mice (Jetten et al., 2014). The M2 macrophages were introduced to the wounds during early inflammation (post-injury Days 1 and 3), and they continued to express M2 markers 15 days post-wounding. The lack of improvement in wound healing may be attributed to the timing of the treatment, which may have disrupted the function of M1 macrophages at a stage when they are presumably still needed. This study exemplifies the need to have an adequately-timed therapeutic approach.

In contrast, in Israel, treatment of chronic ulcers with blood-derived macrophages is an approved procedure, and it has been used successfully in over 1,000 patients (Zuloff-Shani et al., 2004). Danon et al. (1997), treated pressure ulcers in elderly patients with macrophages derived from blood units of young, healthy donors (Danon et al., 1997). The macrophage isolation method is completely sterile, using a closed system of interconnected bags containing the various reagents needed for the process. In order to stimulate isolated macrophages to produce factors beneficial for wound healing, they were activated by hypo-osmotic shock for 45 s (Zuloff-Shani et al., 2004). Related studies characterized these cells by measuring mRNA expression in over 72 genes (Frenkel et al., 2002). The results revealed that expression of several genes related to wound healing (IL-1, IL-6, TGF-β, FGF-8, TNF receptors, VEGF, and GM-CSF, to name a few) dramatically increased due to hypo-osmotic shock. Protein measurements revealed that hypo-osmotic shock could increase production up to 123- and 175-fold, in the case of IL-1 and IL-6, respectively, although donor-to-donor variability does exist. Hence, although this study did not utilize a traditional M2a/b/c/d-polarization method, macrophages were stimulated to be more anti-inflammatory via hypo-osmotic shock prior to wound application. However, the induced cell population was not completely characterized, particularly on the protein level.

In the clinical study, patients' ulcers were injected with the isolated macrophages near the wound periphery (Danon et al., 1997). A portion of the cell suspension was also deposited on top of the wound, which was then covered with dressings. Macrophage treatment was performed a single time in most patients, unless they still exhibited delayed healing about 1 month later, in which case a second treatment was performed. The effects of the treated ulcers were compared with other patient ulcers at the same hospital treated with conventional methods, including debridement, antibiotics and wound dressings. Results revealed that 27% of ulcers treated with macrophages healed, whereas only 6% of controls did, and that there were no adverse reactions to treatment.

The same group later published results of a more comprehensive study, including randomization of patients between macrophage-treated and standard-of-care groups (Zuloff-Shani et al., 2010). In addition to providing more data, including healing time, etiology, and size of the wounds in this study, subsets of patients with diabetic ulcers were also included and analyzed separately. The overall results for all ulcers demonstrated improved statistics compared to the previous study: 69% of macrophage-treated patients healed in an average of 86.7 days, whereas control groups had only 13.3% full-closure wounds in 117.7 days. Similarly, in the diabetes groups, 65.5% of wounds with the macrophage treatment and only 15.4% of controls healed. Again, wounds in the treatment group healed in a faster time compared to controls.

These studies provided an interesting strategy of using exogenous macrophages from healthy individuals, stimulated by hypo-osmotic shock, without the use of LPS, IFN-γ, or any other stimulus, to aid in the healing of chronic ulcers. The success of the treatments in both pressure and diabetic ulcer patients is promising, however more work must be done to determine the reason why some wounds do not respond to treatment, and investigate ways to improve these outcomes. Additionally, isolation and purification of macrophage populations was not extensive in these studies, and therefore cell types other than monocytes/macrophages may be contributing to this therapy.

Endogenous Macrophage Modulation/M2 Phenotype Promotion

Several different approaches have been taken to modulate wound macrophages with the goal of promoting M2-like characteristics, which often simultaneously attenuate M1 characteristics. Although not a comprehensive list, methods using mesenchymal stromal cells (MSCs), growth factors, biomaterials, heme oxygenase-1 (HO-1) induction, and oxygen therapy are discussed.

Mesenchymal Stromal Cells

Mesenchymal stromal cells (MSCs) secrete many growth factors that are required for wound healing, and have therefore been explored as cell therapies. Their use in animal and human studies has been successful, resulting in accelerated wound closure and more mature angiogenesis and granulation tissue (Nuschke, 2014). Evidence shows that MSCs and their secreted products affect a variety of skin and immune cells. Of particular interest to this review are MSC interactions with macrophages. MSCs have such powerful modulating effects on macrophages, that some have defined yet another phenotype of macrophages based on this interaction (Kim and Hematti, 2009). These MSC-educated macrophages exhibit M2-like characteristics (IL-10 high, IL-12 low, IL-6 high, TNF-α low) and hence possess a secretome that can have powerful benefits in wound healing.

One of the mechanisms of MSC action on wounds is via recruitment of macrophages. Chen et al. (2008) used MSC-conditioned media *in vitro* and found that it accelerated migration of macrophages, in addition to keratinocytes and endothelial cells (Chen et al., 2008). In a murine excisional wound model, subcutaneous injection and topical application of the MSC-conditioned media also led to increased presence of macrophages and endothelial progenitor cells. Macrophage recruitment by MSCs may be attributed to high levels of secreted chemoattractants CCL3(MIP-1α), MIP-2, and CCL12(MCP-5).

MSCs also secrete an important regulator, prostaglandin E-2 (PGE-2), that has a direct effect on macrophages, by

reprogramming them to up-regulate the M2-like marker, IL-10 (Nemeth et al., 2009; Barminko et al., 2014). In a murine sepsis model, Nemeth et al. (2009) showed that systemic MSC administration reduced mortality and improved organ function, but only in the presence of macrophages (Nemeth et al., 2009). When macrophages were depleted, the benefits of the MSC-treatment were eliminated. In response to the MSC-treatment, extracted lung macrophages produced significantly higher IL-10 (an M2-like marker) compared to those from control groups. As a result, neutrophil tissue infiltration was decreased, which has a protective effect due to lower levels of local oxidative tissue damage. The group also performed *in vitro* studies to determine the molecular interaction between MSCs and macrophages that leads to IL-10 upregulation. Results suggested that PGE-2 from MSCs stimulates macrophages to produce IL-10. Similar findings were confirmed *in vitro* by Barminko et al. (2014), showing that MSCs, via PGE-2, reduced TNF-α and increased IL-10 secretion from macrophages, hence attenuating M1, and promoting M2, characteristics (Barminko et al., 2014). Although these studies were not performed in a chronic wound model, they reveal relevant interactions between MSCs and macrophages, which may partially explain the success of MSC therapy in wound healing studies.

In a wound healing context, MSCs have a similar effect on macrophages. Zhang et al. (2010) studied the effect of human gingival-derived MSCs on macrophage phenotype and found that *in vitro*, they increased expression of M2-like markers IL-10, IL-6, and CD206, decreased expression of TNF-α (M1-like marker) and decreased induction of Th-17 cell expansion (Zhang et al., 2010). In an *in vivo* murine wound healing model, systemically-administered MSCs accumulated near the wound area, and induced M2 characteristics in surrounding macrophages, such as increased IL-10 and decreased TNF-α and IL-6. Wound healing was accelerated with MSC-treatment.

Several clinical studies have also investigated the potential of MSCs as a treatment for chronic wounds. As discussed in the previous section, exogenous monocyte/macrophage cell therapies have also been tested in human wounds (Danon et al., 1997; Zuloff-Shani et al., 2010). One interesting clinical study compared the effects of MSCs vs. mononuclear cells (MNCs) in diabetic ulcers (Lu et al., 2011). Both cell sources were autologous and bone-marrow derived. MSCs were expanded *in vitro*, whereas the mononuclear fraction—containing a variety of hematopoietic cell types including monocytes— was isolated from bone marrow aspirate. Prior to administration to ulcers, MSCs and MNCs were analyzed for levels of angiogenic factors. Interestingly, MSCs produced significantly higher levels of VEGF, FGF-2, and angiopoeitin-1 than MNCs in both hypoxic and normoxic conditions. In the clinical study, ulcers treated with MSCs healed significantly faster, and were fully closed 4 weeks earlier than treatment with MNCs. The MSC-group also had the best outcomes in terms of pain-free walking time, transcutaneous oxygen pressure, and blood vessel formation, followed by the MNC-group and, lastly, the saline controls. These results showed that MSCs had more potent effects on diabetic wounds compared to MNCs. This suggests that MSCs, rather than a monocyte-based treatment, may have more potent effects in a wound environment. Another possibility is that the MNC group may have performed better if it was stimulated, for example by hypo-osmotic shock, or pre-polarized into an M2-like phenotype via biochemical stimulation. Regardless, MSCs are known to have powerful modulating effects on macrophages, therefore this approach may be better-suited for wound healing compared to monocyte/macrophage supplementation, as suggested by these results.

In developing new therapies, it is pertinent to consider the special characteristics of chronic wound environments, such as low oxygen tension, and how they may affect macrophage function. Through *in vitro* studies, Faulknor et al. (2017) demonstrated that a hypoxic environment lessened macrophage plasticity in response to MSCs (Faulknor et al., 2017). Macrophages cultured in normoxic conditions (20% O_2) with MSCs produced high levels of the M2 marker, IL-10, however, in hypoxic conditions (1% O_2), secretion was significantly lower. As macrophages possess a high degree of phenotypic plasticity, they react not only to the treatments that are introduced, but also to the existing microenvironment, which may affect their ability to respond to treatment. This is an important consideration that emerging chronic wound therapies should address.

Growth Factors

Cell therapies provide wounds with numerous cytokines and growth factors, which in sum affect local cells and enhance the coordinated wound healing process. Another approach to treating chronic wounds is through the application of a single growth factor, which can elicit cellular responses. As advertised on their website, Regranex is the, "first and only FDA-approved recombinant PDGF therapy for diabetic neuropathic ulcers" (Smith, 2018). The mechanism of action involves macrophages as a key player. During hemostasis, PDGF recruits macrophages to the wound in order to initiate inflammation. In the next phase, macrophages are stimulated by Regranex to produce more PDGF, as well as TGF-β, to stimulate extracellular tissue formation by fibroblasts. An early study on surgical incisions in rats investigated the mechanism of PDGF therapy by studying its effects in rats receiving either surface irradiation or total body irradiation (Mustoe et al., 1989). Whereas, surface-irradiated rats retain bone marrow elements and wound monocytes/macrophages, total body irradiated rats are depleted of them. Hence, this approach was used to determine the importance of macrophages in the efficacy of PDGF in wound healing. The results revealed that PDGF therapy was ineffective in aiding wound healing in rats depleted of monocytes/macrophages (total body irradiation). In contrast, in rats that were surface-irradiated, macrophages were able to migrate into the wounds and PDGF treatment successfully aided healing. The number of wound fibroblasts increased, as well as wound strength, presumably by the formation of more collagen. Interestingly, in wounds that contained fibroblasts but no macrophages (total body-irradiated rats), PDGF did not stimulate collagen synthesis. This suggests that macrophages are the first-responders to PDGF treatment, and in response, they must activate fibroblasts, via TGF-β, to proliferate and synthesize collagen, which contributes to granulation tissue formation and

wound closure. Overall, wound macrophages are a vital part in the mechanism of action of Regranex.

Interestingly, granulocyte macrophage-colony stimulating factor (GM-CSF) has also shown benefits in chronic wound healing (Da Costa et al., 1999), despite the fact that it is used *in vitro* to promote the M1 phenotype. In cell culture, GM-CSF induces macrophages to produce more pro-inflammatory factors (TNF, IL-23) and less anti-inflammatory factors (IL-10) compared to baseline levels, however, LPS and IFN-γ are often used as more potent M1-stimuli that activate different signaling pathways (Lacey et al., 2012). In contrast, *in vivo* effects of GM-CSF, particularly in a chronic wound healing environment, can promote healing. Cianfarani et al. (2006) demonstrated that GM-CSF injections to non-healing venous leg ulcers induced VEGF transcription in the wound bed, primarily within macrophages (Cianfarani et al., 2006). As PDGF, in the previous example, stimulates macrophages to produce TGF-β, GM-CSF stimulates macrophages to produce VEGF. This finding was corroborated with *in vitro* results showing the same effect of GM-CSF on VEGF production in a differentiated monocytic cell line but not in keratinocytes. In patient ulcers, increased VEGF transcription by GM-CSF lead to improved vascularization and healing. GM-CSF also acts on other skin cells, which further explains its pro-wound healing effects. In addition to macrophages, GM-CSF also has chemotactic effects on fibroblasts, endothelial cells and keratinocytes. Accordingly, formation of granulation tissue, blood vessels and the epidermal layer are improved with exogenous GM-CSF (Mann et al., 2001).

A potential explanation of the pro-wound healing effect of GM-CSF *in vivo* vs. its perceived pro-inflammatory role *in vitro* is that, within the complex chronic wound environment, which contains several interacting cell types and signaling pathways, an intermediate macrophage phenotype is formed. A combination of M1-like and M2-like factors, such as IFN-γ, IL-6 and TGF-β are increased upon upregulation of GM-CSF *in vivo*, all of which have distinct roles in the wound healing process (Mann et al., 2001). Interestingly, evidence shows that GM-CSF is more effective in accelerating chronic wound healing rather than acute (Barrientos et al., 2014). This discrepancy further underlines the complex role of macrophages within the intricate, multi-cellular wound healing environment.

Many other growth factors (i.e., VEGF, FGF, EGF) have shown potential in aiding in wound healing (Barrientos et al., 2014), however less work has been published showing their direct effect on macrophages, as they primarily act on other cells such as endothelial cells, fibroblasts, and keratinocytes. Regardless, FGF and EGF are approved wound care therapies in Japan and Cuba, respectively (Frykberg and Banks, 2015).

Immunomodulatory Biomaterials

Any material that comes in contact with the body has the potential to elicit an immune response and affect surrounding cells and tissue. The body's response to the material is not always harmful, and can be tuned to promote healing if the material possesses the right characteristics. Immunomodulatory materials are being developed with the goal of limiting negative reactions to implants and instead, promoting their integration into the body (Vishwakarma et al., 2016). General approaches when designing immunomodulatory materials include (1) carefully selecting physical properties, (2) altering chemistry, (3) incorporating therapeutic molecules for controlled release and, (4) combination with cell therapies. As the last two points were discussed in previous sections, the following discussion is focused on physical and chemical properties of biomaterials that modulate macrophage behavior. The discussion includes examples of both currently used wound healing materials, and those under development for potential future applications.

One chemical approach involves modifying native extracellular matrix molecules. Hyaluronan (HA), a glycosaminoglycan (GAG), is one such ECM component that can cause macrophages to take on pro- or anti-inflammatory characteristics depending on certain chemical modifications (Stern and Maibach, 2008; Vishwakarma et al., 2016). For example, sulfated GAGs can bind and interact with growth factors and cytokines, thereby preventing them from affecting macrophage behavior. Kajahn et al. (2012) tested the *in vitro* response of monocytes to biomaterials composed of collagen and HA, or sulfated HA derivatives (made by simultaneously degrading and sulfating native HA), within an inflammatory environment created by exogenous IL-6, IFN-γ, and MCP-1 (Kajahn et al., 2012). In the presence of collagen with highly-sulfated HA derivatives, monocytes resisted an M1 phenotype transition [via lower levels of IL-1β, CXCL8(IL-8), IL-12 and TNF-α], and instead differentiated into M2-like macrophages with increased IL-10 production and CD163 expression. Other experimental conditions, including collagen only, collagen + non-sulfated HA, and collagen + lowly-sulfated HA derivatives, promoted macrophages with more M1 characteristics. The results of this study are interesting in regards to wound healing, as several wound-care products are based on ECM proteins.

Chitosan is another material that is in found in several FDA-approved wound products (Dai et al., 2011). It is known for its antimicrobial effects and also acts on skin cells to aid in wound healing. Researchers have also investigated its effect on macrophages (Ueno et al., 2001). In response to culturing with chitosan, macrophages increased production of TGF-β1, which stimulates ECM formation. In contrast, chitosan did not stimulate direct ECM formation by fibroblasts. This result highlights the importance of macrophage subset modulation as they produce many growth factors that can affect other local wound cells. Additionally, chitosan also stimulated macrophages to produce high levels of PDGF, which is important in angiogenesis. Other studies have shown that chitosan promotes nitric oxide production and chemotaxis in macrophages (Peluso et al., 1994). It is believed that the cellular interaction occurs via N-acetylglucosamine on chitosan and corresponding receptors on macrophages.

Physical cues on biomaterials can also affect macrophages by causing them to take on rounded vs. elongated shapes, which are likely to exhibit M1- or M2-like characteristics, respectively (McWhorter et al., 2013). One approach to achieving M2-like macrophages on biomaterials is by micropatterning ECM molecules or integrins that promote cell attachment and spreading (McWhorter et al., 2013; Cha et al., 2017).

Modifications like these can also alter the stiffness of the cell/biomaterial interface. Blakney et al. (2012) investigated the effect of hydrogel stiffness and macrophage adhesion in an *in vivo*, subcutaneous implantation murine study (Blakney et al., 2012). All hydrogels (130, 240, and 840 kPa moduli) were composed of polyethylene glycol and RGD, to allow for cell attachment. Hydrogels were implanted into mice, and 28 days later, were removed for histological analysis. Staining with a macrophage-specific cell-surface marker, Mac3 (CD107b), revealed that the softest hydrogels had significantly lower macrophage infiltration compared to the other two groups. These results suggest that stiffness of wound care products may be important in directing macrophage fate, and overall wound healing success.

In some cases, a combination of chemical and physical cues and an understanding of which has the greater effect, can further promote differentiation of the desired macrophage phenotype (McWhorter et al., 2013; Cha et al., 2017). This can be optimized by intentional selection of material properties to achieve successful immunomodulatory biomaterials. Surprisingly, many studies in the literature seem to consider immunomodulatory properties of wound dressings and therapies as an afterthought with their experimental treatment or product. Recognizing the importance of macrophages in the wound healing process, it is pertinent to ensure that a material that is introduced to chronic wounds does not further promote a pro-inflammatory environment, but rather attenuates M1 macrophages and promotes the transition to M2-like phenotypes. Moving forward, immunomodulatory properties of materials should be a key design factor for new wound healing therapies.

Heme Oxygenase-1 Induction

Heme oxygenase-1 (HO-1) is an inducible enzyme that catalyzes heme breakdown and releases anti-inflammatory factors. When hemoglobin is endocytosed by macrophages, the HO-1 pathway breaks it down into iron, carbon monoxide and biliverdin, which is converted to bilirubin.

The three products of HO-1 activity can individually affect wound healing responses. Carbon monoxide and bilirubin can exert anti-inflammatory properties to help wound healing (Kapitulnik, 2004; Ryter et al., 2006) however, differential regulation of the iron product can promote M1- or M2-like macrophages (Cairo et al., 2011). M1-like cells store the majority of the iron intracellularly as ferritin, whereas, M2-like macrophages release it to the extracellular environment via the transmembrane channel, ferroportin. Likewise, M2-like macrophages express higher levels of ferroportin compared to M1. M2-like cells have a higher number of hemoglobin-binding receptors (specifically CD163). Thus, the HO-1 signaling pathway is more active. Perhaps the downstream effects of this process, such as higher HO-1 activity, carbon monoxide and bilirubin production, and iron release in M2 macrophages contributes to their pro-regenerative properties.

The HO-1 pathway is important in wound healing, as it plays roles in angiogenesis and re-epithelialization (Grochot-Przeczek et al., 2009). Mice with inhibited or deleted HO-1 exhibit delayed wound healing, and diabetic mice inherently have lower levels of HO-1, which may partially explain their challenges with wound healing. Restoring HO-1 expression in wild type and diabetic mice resulted in improved and accelerated wound healing, which suggests an important role of hemoglobin breakdown in the wound healing process. HO-1 is also expressed in fibroblasts and keratinocytes, which underlines its role in dermal wound healing (Lundvig et al., 2012).

During acute wound healing, HO-1 protein was expressed at high levels in a murine model 3 days after creation of full-thickness excisional wounds, before returning to basal levels (Hanselmann et al., 2001). HO-1 mRNA levels continued to be high until Day 7. Macrophages and proliferating keratinocytes along the wound edge were the primary cell types that overexpressed HO-1. Interestingly, it was also found that patients with psoriatic skin constitutively overexpress HO-1, as well as HO-2. *In vitro* studies found that ROS, rather than growth factors or cytokines (KGF, EGF, TNF-α), directly stimulated HO-1 expression.

HO-1 has also been targeted in models of delayed wound healing. In a wounded diabetic rat model, HO-1 expression was induced using topical, 10% hemin ointment (Chen et al., 2016). Wound TNF-α and IL-6 levels, as measured by Western blot, were significantly decreased compared to rats treated with vehicle controls. VEGF and intercellular adhesion molecule (ICAM) serum levels were increased, and accordingly, so was blood vessel density. Induction of HO-1 in diabetic rats brought levels of several measured biomolecules, as well as wound healing rates, back to those seen in non-diabetic controls. Even in non-diabetic rats, studies have shown that hemin accelerates healing, concurrently with decreased levels of pro-inflammatory proteins ICAM-1 and TNF-α and increased IL-10 (Ahanger et al., 2010). The involvement of these prototypical M1/M2 markers suggests the involvement of macrophages in the enhancement of wound healing.

In fact, there is evidence that HO-1 expression in macrophages promotes an M2-like phenotype (Mhem) (Naito et al., 2014). Several animal studies in different disease models, have induced HO-1 expression and measured subsequent macrophage markers. Resulting M2-like markers include arginase-1, mannose receptor, and CD163, among others. HO-1 has demonstrated potential as a method to promote M2-like characteristics in macrophages to aid in healing, however, as with many macrophage-targeted therapies, timing must be well-suited in order to successfully resolve inflammation (Lundvig et al., 2012).

Hemoglobin-based substances (polymerized hemoglobin, PEG-encapsulated hemoglobin, etc.) may be interesting approaches to activate the HO-1 pathway, while simultaneously delivering oxygen (Palmer et al., 2009; Palmer and Intaglietta, 2014). This method would elicit anti-inflammatory effects from local macrophages, and restore oxygen levels, thereby targeting two major deficiencies of chronic wounds with one therapy.

Oxygen Therapy

Chronic wounds are hypoxic, as blood flow and, hence, oxygen delivery to the tissues are disrupted (Sen, 2009). Direct delivery of oxygen to skin wounds, such as by exposing patients to 100% oxygen at 2–3 atm pressure in hyperbaric chambers, has been

shown to enhance wound healing. The effect of increasing oxygen levels in the wound are multifaceted, but evidence suggests that one of the targets may be the wound macrophages. One study investigated the direct effects of hyperbaric oxygen and hyperoxia (without increased pressure) on the cytokine profiles of cultured macrophages (Benson et al., 2003). Hyperbaric oxygen dampened IL-1β and TNF-α secretion by ∼40%, while hyperoxia alone had no effect. However, when hyperbaric oxygen exposure exceeded 6 h, an increase, rather than a decrease, in the production of these pro-inflammatory mediators was observed. This study did not investigate any M2-like macrophage functional parameters.

CONCLUSIONS AND FUTURE DIRECTIONS

It is clear that macrophages play an important role in wound healing, and that anti-inflammatory, M2-like phenotypes are desirable for efficient healing. Questions remain regarding the details behind monocyte recruitment and macrophage differentiation, specifically whether monocytes are predestined to become one particular phenotype (M1/M2-like) or if macrophages themselves change from M1 to M2 phenotypes (or vice versa) within the tissue (**Figure 1**; Vannella and Wynn, 2017). More thorough histological studies on *in vivo* wound environments (both acute and chronic) would lead to a better understanding of macrophage phenotypes and their spatiotemporal and functional contributions during healing. This information could help identify macrophage phenotypes needed to promote healing in chronic wounds. Another challenge in this field is that the definition of each macrophage sub-phenotype is neither clear, nor agreed upon. There are also inconsistencies between *in vitro* and *in vivo* macrophage phenotypes, especially in chronic wound models, which further confuse this area of research. There is a need for a more thorough characterization of macrophage phenotypes and a definition of their respective roles (**Table 2** and **Figure 2**). Novel technologies and tools that can quickly and thoroughly define macrophage phenotypes, even within heterogeneous populations, would advance research (Ginhoux et al., 2016; Murray, 2017). In the midst of this work, it is also important to recognize differences between murine and human wound healing processes and roles of immune cells (Pasparakis et al., 2014).

Current experimental therapies that are being investigated for their potential to promote wound healing macrophages include mesenchymal stem cells, growth factors, biomaterials, and more (**Table 3**). Up-and-coming methods to control macrophage fate include microRNA therapies to affect macrophage transcriptome and function (Self-Fordham et al., 2017). Delivery time for novel therapies, in regards to current macrophage phenotype and the needs of the particular wound, should not be overlooked, as it can make the difference between an effective and an ineffective therapy. Another question is whether or not directly promoting M2-like phenotypes is entirely necessary, or, is it possible that by only attenuating M1 macrophages, the wound environment will be reprogrammed to successfully heal? Furthermore, is targeting macrophages alone enough to promote healing, within the complex, multi-cellular chronic wound environment? Hence, an effective treatment may need to address multiple deficiencies of chronic wounds. As macrophages are involved in all phases of wound healing, and their dysregulation in chronic wounds leads to a stalled and heightened inflammatory state, an improved understanding of these key regulators will ultimately lead to advancements in wound healing therapies.

AUTHOR CONTRIBUTIONS

PK wrote the majority of the review text and generated the figures. AP, RS, and FB read and edited several drafts, provided valuable feedback and suggested ideas and broad perspectives to address in the review.

FUNDING

This work was partially supported by grants from the National Institutes of Health (R01EB021926 and T32GM008339). PK was supported by a Graduate Assistance in Areas of National Need (GAANN) fellowship from the US Department of Education.

REFERENCES

Ahanger, A. A., Prawez, S., Leo, M. D., Kathirvel, K., Kumar, D., Tandan, S. K., et al. (2010). Pro-healing potential of hemin: an inducer of heme oxygenase-1. *Eur. J. Pharmacol.* 645, 165–170. doi: 10.1016/j.ejphar.2010.06.048

Auffray, C., Fogg, D., Garfa, M., Elain, G., Join-Lambert, O., Kayal, S., et al. (2007). Monitoring of blood vessels and tissues by a population of monocytes with patrolling behavior. *Science* 317, 666–670. doi: 10.1126/science.1142883

Barminko, J. A., Nativ, N. I., Schloss, R., and Yarmush, M. L. (2014). Fractional factorial design to investigate stromal cell regulation of macrophage plasticity. *Biotechnol. Bioeng.* 111, 2239–2251. doi: 10.1002/bit.25282

Barrientos, S., Brem, H., Stojadinovic, O., and Tomic-Canic, M. (2014). Clinical application of growth factors and cytokines in wound healing. *Wound Repair Regen.* 22, 569–578. doi: 10.1111/wrr.12205

Baum, C. L., and Arpey, C. J. (2005). Normal cutaneous wound healing: clinical correlation with cellular and molecular events. *Dermatol Surg.* 31, 674–686. discussion: 86. doi: 10.1097/00042728-200506000-00011

Benson, R. M., Minter, L. M., Osborne, B. A., and Granowitz, E. V. (2003). Hyperbaric oxygen inhibits stimulus-induced proinflammatory cytokine synthesis by human blood-derived monocyte-macrophages. *Clin. Exp. Immunol.* 134, 57–62. doi: 10.1046/j.1365-2249.2003.02248.x

Bianchi, M. E., and Manfredi, A. A. (2009). Immunology. Dangers in and out. *Science* 323, 1683–1684. doi: 10.1126/science.1172794

Blakney, A. K., Swartzlander, M. D., and Bryant, S. J. (2012). The effects of substrate stiffness on the *in vitro* activation of macrophages and *in vivo* host response to poly(ethylene glycol)-based hydrogels. *J. Biomed. Mater. Res. A* 100, 1375–1386. doi: 10.1002/jbm.a.34104

Blakytny, R., and Jude, E. (2006). The molecular biology of chronic wounds and delayed healing in diabetes. *Diabet. Med.* 23, 594–608. doi: 10.1111/j.1464-5491.2006.01773.x

Boyette, L. B., Macedo, C., Hadi, K., Elinoff, B. D., Walters, J. T., Ramaswami, B., et al. (2017). Phenotype, function, and differentiation potential of human monocyte subsets. *PLoS ONE* 12:e0176460. doi: 10.1371/journal.pone.0176460

Boyle, J. J. (2012). Heme and haemoglobin direct macrophage Mhem phenotype and counter foam cell formation in areas of intraplaque haemorrhage. *Curr. Opin. Lipidol.* 23, 453–461. doi: 10.1097/MOL.0b013e328356b145

Cairo, G., Recalcati, S., Mantovani, A., and Locati, M. (2011). Iron trafficking and metabolism in macrophages: contribution to the polarized phenotype. *Trends Immunol.* 32, 241–247. doi: 10.1016/j.it.2011.03.007

Carls, G. S., Gibson, T. B., Driver, V. R., Wrobel, J. S., Garoufalis, M. G., Defrancis, R. R., et al. (2011). The economic value of specialized lower-extremity medical care by podiatric physicians in the treatment of diabetic foot ulcers. *J. Am. Podiatr. Med. Assoc.* 101, 93–115. doi: 10.7547/1010093

Castellana, D., Paus, R., and Perez-Moreno, M. (2014). Macrophages contribute to the cyclic activation of adult hair follicle stem cells. *PLoS Biol.* 12:e1002002. doi: 10.1371/journal.pbio.1002002

Cha, B. H., Shin, S. R., Leijten, J., Li, Y. C., Singh, S., Liu, J. C., et al. (2017). Integrin-mediated interactions control macrophage polarization in 3D hydrogels. *Adv. Healthc. Mater.* 6, 1–12. doi: 10.1002/adhm.201700289

Chen, L., Mirza, R., Kwon, Y., DiPietro, L. A., and Koh, T. J. (2015). The murine excisional wound model: contraction revisited. *Wound Repair Regen.* 23, 874–877. doi: 10.1111/wrr.12338

Chen, L., Tredget, E. E., Wu, P. Y., and Wu, Y. (2008). Paracrine factors of mesenchymal stem cells recruit macrophages and endothelial lineage cells and enhance wound healing. *PLoS ONE* 3:e1886. doi: 10.1371/journal.pone.0001886

Chen, Q. Y., Wang, G. G., Li, W., Jiang, Y. X., Lu, X. H., and Zhou, P. P. (2016). Heme oxygenase-1 promotes delayed wound healing in diabetic rats. *J. Diabetes Res.* 2016:9726503. doi: 10.1155/2016/9726503

Christoph, T., Müller-Röver, S., Audring, H., Tobin, D. J., Hermes, B., Cotsarelis, G., et al. (2000). The human hair follicle immune system: cellular composition and immune privilege. *Br. J. Dermatol.* 142, 862–873. doi: 10.1046/j.1365-2133.2000.03464.x

Cianfarani, F., Tommasi, R., Failla, C. M., Viviano, M. T., Annessi, G., Papi, M., et al. (2006). Granulocyte/macrophage colony-stimulating factor treatment of human chronic ulcers promotes angiogenesis associated with de novo vascular endothelial growth factor transcription in the ulcer bed. *Br. J. Dermatol.* 154, 34–41. doi: 10.1111/j.1365-2133.2005.06925.x

Colin, S., Chinetti-Gbaguidi, G., and Staels, B. (2014). Macrophage phenotypes in atherosclerosis. *Immunol. Rev.* 262, 153–166. doi: 10.1111/imr.12218

Crane, M. J., Daley, J. M., van Houtte, O., Brancato, S. K., Henry, W. L. Jr., and Albina, J. E. (2014). The monocyte to macrophage transition in the murine sterile wound. *PLoS ONE* 9:e86660. doi: 10.1371/journal.pone.0086660

Cros, J., Cagnard, N., Woollard, K., Patey, N., Zhang, S. Y., Senechal, B., et al. (2010). Human CD14dim monocytes patrol and sense nucleic acids and viruses via TLR7 and TLR8 receptors. *Immunity* 33, 375–386. doi: 10.1016/j.immuni.2010.08.012

Da Costa, R. M., Ribeiro Jesus, F. M., Aniceto, C., and Mendes, M. (1999). Randomized, double-blind, placebo-controlled, dose- ranging study of granulocyte-macrophage colony stimulating factor in patients with chronic venous leg ulcers. *Wound Repair Regen.* 7, 17–25. doi: 10.1046/j.1524-475X.1999.00017.x

Dai, T., Tanaka, M., Huang, Y. Y., and Hamblin, M. R. (2011). Chitosan preparations for wounds and burns: antimicrobial and wound-healing effects. *Expert Rev. Anti Infect. Ther.* 9, 857–879. doi: 10.1586/eri.11.59

Daley, J. M., Brancato, S. K., Thomay, A. A., Reichner, J. S., and Albina, J. E. (2010). The phenotype of murine wound macrophages. *J. Leukoc. Biol.* 87, 59–67. doi: 10.1189/jlb.0409236

Danon, D., Madjar, J., Edinov, E., Knyszynski, A., Brill, S., Diamantshtein, L., et al. (1997). Treatment of human ulcers by application of macrophages prepared from a blood unit. *Exp. Gerontol.* 32, 633–641. doi: 10.1016/S0531-5565(97)00094-6

Davies, L. C., Jenkins, S. J., Allen, J. E., and Taylor, P. R. (2013). Tissue-resident macrophages. *Nat. Immunol.* 14, 986–995. doi: 10.1038/ni.2705

Doebel, T., Voisin, B., and Nagao, K. (2017). Langerhans cells - the macrophage in dendritic cell clothing. *Trends Immunol.* 38, 817–828. doi: 10.1016/j.it.2017.06.008

Eichmüller, S., van der Veen, C., Moll, I., Hermes, B., Hofmann, U., Müller-Röver, S., et al. (1998). Clusters of perifollicular macrophages in normal murine skin: physiological degeneration of selected hair follicles by programmed organ deletion. *J. Histochem. Cytochem.* 46, 361–370. doi: 10.1177/002215549804600310

Etzerodt, A., Kjolby, M., Nielsen, M. J., Maniecki, M., Svendsen, P., and Moestrup, S. K. (2013). Plasma clearance of hemoglobin and haptoglobin in mice and effect of CD163 gene targeting disruption. *Antioxid. Redox Signal.* 18, 2254–2263. doi: 10.1089/ars.2012.4605

Evans, B. J., Haskard, D. O., Sempowksi, G., and Landis, R. C. (2013). Evolution of the macrophage CD163 phenotype and cytokine profiles in a human model of resolving inflammation. *Int. J. Inflam.* 2013:780502. doi: 10.1155/2013/780502

Falanga, V. (2005). Wound healing and its impairment in the diabetic foot. *Lancet* 366, 1736–1743. doi: 10.1016/S0140-6736(05)67700-8

Fantin, A., Vieira, J. M., Gestri, G., Denti, L., Schwarz, Q., Prykhozhij, S., et al. (2010). Tissue macrophages act as cellular chaperones for vascular anastomosis downstream of VEGF-mediated endothelial tip cell induction. *Blood* 116, 829–840. doi: 10.1182/blood-2009-12-257832

Faulknor, R. A., Olekson, M. A., Ekwueme, E. C., Krzyszczyk, P., Freeman, J. W., and Berthiaume, F. (2017). Hypoxia impairs mesenchymal stromal cell-induced macrophage M1 to M2 transition Technology. 5, 81–86. doi: 10.1142/S2339547817500042

Ferrante, C. J., and Leibovich, S. J. (2012). Regulation of macrophage polarization and wound healing. *Adv. Wound Care* 1, 10–16. doi: 10.1089/wound.2011.0307

Filardy, A. A., Pires, D. R., Nunes, M. P., Takiya, C. M., Freire-de-Lima, C. G., Ribeiro-Gomes, F. L., et al. (2010). Proinflammatory clearance of apoptotic neutrophils induces an IL-12(low)IL-10(high) regulatory phenotype in macrophages. *J. Immunol.* 185, 2044–2050. doi: 10.4049/jimmunol.1000017

Frenkel, O., Shani, E., Ben-Bassat, I., Brok-Simoni, F., Rozenfeld-Granot, G., Kajakaro, G., et al. (2002). Activated macrophages for treating skin ulceration: gene expression in human monocytes after hypo-osmotic shock. *Clin. Exp. Immunol.* 128, 59–66. doi: 10.1046/j.1365-2249.2002.01630.x

Frykberg, R. G., and Banks, J. (2015). Challenges in the treatment of chronic wounds. *Adv Wound Care* 4, 560–582. doi: 10.1089/wound.2015.0635

Funato, N., Moriyama, K., Saitoh, M., Baba, Y., Ichijo, H., and Kuroda, T. (1998). Evidence for apoptosis signal-regulating kinase 1 in the regenerating palatal epithelium upon acute injury. *Lab. Invest.* 78, 477–483.

Gallucci, S. (2016). *Chapter 1 - An Overview of the Innate Immune Response to Infectious and Noninfectious Stressors A2 - Amadori, Massimo*. (San Diego, CA: The Innate Immune Response to Noninfectious Stressors, Academic Press), 1–24.

Garash, R., Bajpai, A., Marcinkiewicz, B. M., and Spiller, K. L. (2016). Drug delivery strategies to control macrophages for tissue repair and regeneration. *Exp. Biol. Med.* 241, 1054–1063. doi: 10.1177/1535370216649444

Ginhoux, F., Schultze, J. L., Murray, P. J., Ochando, J., and Biswas, S. K. (2016). New insights into the multidimensional concept of macrophage ontogeny, activation and function. *Nat. Immunol.* 17, 34–40. doi: 10.1038/ni.3324

Gordois, A., Scuffham, P., Shearer, A., Oglesby, A., and Tobian, J. A. (2003). The health care costs of diabetic peripheral neuropathy in the US. *Diabetes Care* 26, 1790–1795. doi: 10.2337/diacare.26.6.1790

Goren, I., Allmann, N., Yogev, N., Schürmann, C., Linke, A., Holdener, M., et al. (2009). A transgenic mouse model of inducible macrophage depletion: effects of diphtheria toxin-driven lysozyme M-specific cell lineage ablation on wound inflammatory, angiogenic, and contractive processes. *Am. J. Pathol.* 175, 132–147. doi: 10.2353/ajpath.2009.081002

Goren, I., Müller, E., Schiefelbein, D., Christen, U., Pfeilschifter, J., Muhl, H., et al. (2007). Systemic anti-TNFalpha treatment restores diabetes-impaired skin repair in ob/ob mice by inactivation of macrophages. *J. Invest. Dermatol.* 127, 2259–2267. doi: 10.1038/sj.jid.5700842

Grochot-Przeczek, A., Lach, R., Mis, J., Skrzypek, K., Gozdecka, M., Sroczynska, P., et al. (2009). Heme oxygenase-1 accelerates cutaneous wound healing in mice. *PLoS ONE* 4:e5803. doi: 10.1371/journal.pone.0005803

Hanselmann, C., Mauch, C., and Werner, S. (2001). Haem oxygenase-1: a novel player in cutaneous wound repair and psoriasis? *Biochem. J.* 353(Pt 3), 459–466. doi: 10.1042/bj3530459

Hesketh, M., Sahin, K. B., West, Z. E., and Murray, R. Z. (2017). Macrophage phenotypes regulate scar formation and chronic wound healing. *Int. J. Mol. Sci.* 18:E1545. doi: 10.3390/ijms18071545

Italiani, P., and Boraschi, D. (2014). From monocytes to M1/M2 macrophages: phenotypical vs. Functional differentiation. *Front Immunol.* 5:514. doi: 10.3389/fimmu.2014.00514

Jetten, N., Roumans, N., Gijbels, M. J., Romano, A., Post, M. J., de Winther, M. P., et al. (2014). Wound administration of M2-polarized macrophages does not improve murine cutaneous healing responses. *PLoS ONE* 9:e102994. doi: 10.1371/journal.pone.0102994

Kajahn, J., Franz, S., Rueckert, E., Forstreuter, I., Hintze, V., Moeller, S., et al. (2012). Artificial extracellular matrices composed of collagen I and high sulfated hyaluronan modulate monocyte to macrophage differentiation under conditions of sterile inflammation. *Biomatter* 2, 226–236. doi: 10.4161/biom.22855

Kapitulnik, J. (2004). Bilirubin: an endogenous product of heme degradation with both cytotoxic and cytoprotective properties. *Mol. Pharmacol.* 66, 773–779. doi: 10.1124/mol.104.002832

Khanna, S., Biswas, S., Shang, Y., Collard, E., Azad, A., Kauh, C., et al. (2010). Macrophage dysfunction impairs resolution of inflammation in the wounds of diabetic mice. *PLoS ONE* 5:e9539. doi: 10.1371/journal.pone.0009539

Kim, J., and Hematti, P. (2009). Mesenchymal stem cell-educated macrophages: a novel type of alternatively activated macrophages. *Exp. Hematol.* 37, 1445–1453. doi: 10.1016/j.exphem.2009.09.004

Lacey, D. C., Achuthan, A., Fleetwood, A. J., Dinh, H., Roiniotis, J., Scholz, G. M., et al. (2012). Defining GM-CSF- and macrophage-CSF-dependent macrophage responses by *in vitro* models. *J. Immunol.* 188, 5752–5765. doi: 10.4049/jimmunol.1103426

Leibovich, S. J., and Ross, R. (1975). The role of the macrophage in wound repair. A study with hydrocortisone and antimacrophage serum. *Am. J. Pathol.* 78, 71–100.

Liu, Z. J., and Velazquez, O. C. (2008). Hyperoxia, endothelial progenitor cell mobilization, and diabetic wound healing. *Antioxid. Redox Signal.* 10, 1869–1882. doi: 10.1089/ars.2008.2121

Loots, M. A., Lamme, E. N., Zeegelaar, J., Mekkes, J. R., Bos, J. D., and Middelkoop, E. (1998). Differences in cellular infiltrate and extracellular matrix of chronic diabetic and venous ulcers versus acute wounds. *J. Invest. Dermatol.* 111, 850–857. doi: 10.1046/j.1523-1747.1998.00381.x

Lovászi, M., Mattii, M., Eyerich, K., Gácsi, A., Csányi, E., Kovács, D., et al. (2017). Sebum lipids influence macrophage polarization and activation. *Br. J. Dermatol.* 177, 1671–1682. doi: 10.1111/bjd.15754

Lu, D., Chen, B., Liang, Z., Deng, W., Jiang, Y., Li, S., et al. (2011). Comparison of bone marrow mesenchymal stem cells with bone marrow-derived mononuclear cells for treatment of diabetic critical limb ischemia and foot ulcer: a double-blind, randomized, controlled trial. *Diabetes Res. Clin. Pract.* 92, 26–36. doi: 10.1016/j.diabres.2010.12.010

Lundvig, D. M., Immenschuh, S., and Wagener, F. A. (2012). Heme oxygenase, inflammation, and fibrosis: the good, the bad, and the ugly? *Front. Pharmacol.* 3:81. doi: 10.3389/fphar.2012.00081

Mackool, R. J., Gittes, G. K., and Longaker, M. T. (1998). Scarless healing. The fetal wound. *Clin. Plast. Surg.* 25, 357–365.

Malissen, B., Tamoutounour, S., and Henri, S. (2014). The origins and functions of dendritic cells and macrophages in the skin. *Nat. Rev. Immunol.* 14, 417–428. doi: 10.1038/nri3683

Mann, A., Breuhahn, K., Schirmacher, P., and Blessing, M. (2001). Keratinocyte-derived granulocyte-macrophage colony stimulating factor accelerates wound healing: stimulation of keratinocyte proliferation, granulation tissue formation, and vascularization. *J. Invest. Dermatol.* 117, 1382–1390. doi: 10.1046/j.0022-202x.2001.01600.x

Martinez, F. O., and Gordon, S. (2014). The M1 and M2 paradigm of macrophage activation: time for reassessment. *F1000Prime Rep.* 6:13. doi: 10.12703/P6-13

McWhorter, F. Y., Wang, T., Nguyen, P., Chung, T., and Liu, W. F. (2013). Modulation of macrophage phenotype by cell shape. *Proc. Natl. Acad. Sci. U.S.A.* 110, 17253–17258. doi: 10.1073/pnas.1308887110

Medbury, H. J., Williams, H., and Fletcher, J. P. (2014). Clinical significance of macrophage phenotypes in cardiovascular disease. *Clin. Transl. Med.* 3:63. doi: 10.1186/s40169-014-0042-1

MedMarket Diligence (2012). *Worldwide Market for Surgical Sealants, Glues, Wound Closure and Anti-Adhesion 2010–2017.*

MedMarket Diligence (2015). *Wound Management to 2024.* Contract No. S251.

Mestas, J., and Hughes, C. C. (2004). Of mice and not men: differences between mouse and human immunology. *J. Immunol.* 172, 2731–2738. doi: 10.4049/jimmunol.172.5.2731

Minutti, C. M., Knipper, J. A., Allen, J. E., and Zaiss, D. M. (2017). Tissue-specific contribution of macrophages to wound healing. *Semin. Cell Dev. Biol.* 61, 3–11. doi: 10.1016/j.semcdb.2016.08.006

Mirza, R., and Koh, T. J. (2011). Dysregulation of monocyte/macrophage phenotype in wounds of diabetic mice. *Cytokine* 56, 256–264. doi: 10.1016/j.cyto.2011.06.016

Mirza, R., DiPietro, L. A., and Koh, T. J. (2009). Selective and specific macrophage ablation is detrimental to wound healing in mice. *Am. J. Pathol.* 175, 2454–2462. doi: 10.2353/ajpath.2009.090248

Moore, K., Ruge, F., and Harding, K. G. (1997). T lymphocytes and the lack of activated macrophages in wound margin biopsies from chronic leg ulcers. *Br. J. Dermatol.* 137, 188–194. doi: 10.1046/j.1365-2133.1997.1804 1895.x

Mosser, D. M., and Edwards, J. P. (2008). Exploring the full spectrum of macrophage activation. *Nat. Rev. Immunol.* 8, 958–969. doi: 10.1038/nri2448

Murray, P. J., and Wynn, T. A. (2011). Protective and pathogenic functions of macrophage subsets. *Nat. Rev. Immunol.* 11, 723–737. doi: 10.1038/nri3073

Murray, P. J., Allen, J. E., Biswas, S. K., Fisher, E. A., Gilroy, D. W., Goerdt, S., et al. (2014). Macrophage activation and polarization: nomenclature and experimental guidelines. *Immunity* 41, 14–20. doi: 10.1016/j.immuni.2014.06.008

Murray, P. J. (2017). Macrophage polarization. *Annu. Rev. Physiol.* 79, 541–566. doi: 10.1146/annurev-physiol-022516-034339

Mustoe, T. A., Purdy, J., Gramates, P., Deuel, T. F., Thomason, A., and Pierce, G. F. (1989). Reversal of impaired wound healing in irradiated rats by platelet-derived growth factor-BB. *Am. J. Surg.* 158, 345–350. doi: 10.1016/0002-9610(89)90131-1

Naito, Y., Takagi, T., and Higashimura, Y. (2014). Heme oxygenase-1 and anti-inflammatory M2 macrophages. *Arch. Biochem. Biophys.* 564, 83–88. doi: 10.1016/j.abb.2014.09.005

Newby, A. C. (2008). Metalloproteinase expression in monocytes and macrophages and its relationship to atherosclerotic plaque instability. *Arterioscler. Thromb. Vasc. Biol.* 28, 2108–2114. doi: 10.1161/ATVBAHA.108.173898

Njoroge, J. M., Mitchell, L. B., Centola, M., Kastner, D., Raffeld, M., and Miller, J. L. (2001). Characterization of viable autofluorescent macrophages among cultured peripheral blood mononuclear cells. *Cytometry* 44, 38–44. doi: 10.1002/1097-0320(20010501)44:1<38::AID-CYTO1080>3.0.CO;2-T

Novak, M. L., and Koh, T. J. (2013). Macrophage phenotypes during tissue repair. *J. Leukoc. Biol.* 93, 875–881. doi: 10.1189/jlb.1012512

Nunan, R., Harding, K. G., and Martin, P. (2014). Clinical challenges of chronic wounds: searching for an optimal animal model to recapitulate their complexity. *Dis. Model. Mech.* 7, 1205–1213. doi: 10.1242/dmm.016782

Nuschke, A. (2014). Activity of mesenchymal stem cells in therapies for chronic skin wound healing. *Organogenesis* 10, 29–37. doi: 10.4161/org.27405

Nussbaum, S. R., Carter, M. J., Fife, C. E., DaVanzo, J., Haught, R., Nusgart, M., et al. (2018). An economic evaluation of the impact, cost, and medicare policy implications of chronic nonhealing wounds. *Value Health* 21, 27–32. doi: 10.1016/j.jval.2017.07.007

Németh, K., Leelahavanichkul, A., Yuen, P. S., Mayer, B., Parmelee, A., Doi, K., et al. (2009). Bone marrow stromal cells attenuate sepsis via prostaglandin E(2)-dependent reprogramming of host macrophages to increase their interleukin-10 production. *Nat. Med.* 15, 42–49. doi: 10.1038/nm.1905

Ogle, M. E., Segar, C. E., Sridhar, S., and Botchwey, E. A. (2016). Monocytes and macrophages in tissue repair: implications for immunoregenerative biomaterial design. *Exp. Biol. Med.* 241, 1084–1097. doi: 10.1177/1535370216650293

Osaka, N., Takahashi, T., Murakami, S., Matsuzawa, A., Noguchi, T., Fujiwara, T., et al. (2007). ASK1-dependent recruitment and activation of macrophages induce hair growth in skin wounds. *J. Cell Biol.* 176, 903–909. doi: 10.1083/jcb.200611015

Palmer, A. F., and Intaglietta, M. (2014). Blood substitutes. *Annu. Rev. Biomed. Eng.* 16, 77–101. doi: 10.1146/annurev-bioeng-071813-104950

Palmer, A. F., Sun, G., and Harris, D. R. (2009). The quaternary structure of tetrameric hemoglobin regulates the oxygen affinity of polymerized hemoglobin. *Biotechnol. Prog.* 25, 1803–1809. doi: 10.1002/btpr.265

Parakkal, P. F. (1969). Role of macrophages in collagen resorption during hair growth cycle. *J. Ultrastruct. Res.* 29, 210–217. doi: 10.1016/S0022-5320(69)90101-4

Pasparakis, M., Haase, I., and Nestle, F. O. (2014). Mechanisms regulating skin immunity and inflammation. *Nat. Rev. Immunol.* 14, 289–301. doi: 10.1038/nri3646

Peluso, G., Petillo, O., Ranieri, M., Santin, M., Ambrosio, L., Calabro, D., et al. (1994). Chitosan-mediated stimulation of macrophage function. *Biomaterials* 15, 1215–1220. doi: 10.1016/0142-9612(94)90272-0

Posnett, J., and Franks, P. J. (2008). The burden of chronic wounds in the UK. *Nurs. Times* 104, 44–45.

Rodero, M. P., Licata, F., Poupel, L., Hamon, P., Khosrotehrani, K., Combadiere, C., et al. (2014). *In vivo* imaging reveals a pioneer wave of monocyte recruitment into mouse skin wounds. *PLoS ONE* 9:e108212. doi: 10.1371/journal.pone.0108212

Roszer, T. (2015). Understanding the mysterious M2 macrophage through activation markers and effector mechanisms. *Mediators Inflamm.* 2015:816460. doi: 10.1155/2015/816460

Ryter, S. W., Alam, J., and Choi, A. M. (2006). Heme oxygenase-1/carbon monoxide: from basic science to therapeutic applications. *Physiol. Rev.* 86, 583–650. doi: 10.1152/physrev.00011.2005

Satpathy, A. T., Wu, X., Albring, J. C., and Murphy, K. M. (2012). Re(de)fining the dendritic cell lineage. *Nat. Immunol.* 13, 1145–1154. doi: 10.1038/ni.2467

Self-Fordham, J. B., Naqvi, A. R., Uttamani, J. R., Kulkarni, V., and Nares, S. (2017). MicroRNA: dynamic regulators of macrophage polarization and plasticity. *Front. Immunol.* 8:1062. doi: 10.3389/fimmu.2017.01062

Sen, C. K., Gordillo, G. M., Roy, S., Kirsner, R., Lambert, L., Hunt, T. K., et al. (2009). Human skin wounds: a major and snowballing threat to public health and the economy. *Wound Repair Regen.* 17, 763–771. doi: 10.1111/j.1524-475X.2009.00543.x

Sen, C. K. (2009). Wound healing essentials: let there be oxygen. *Wound Repair Regen.* 17, 1–18. doi: 10.1111/j.1524-475X.2008.00436.x

Sindrilaru, A., and Scharffetter-Kochanek, K. (2013). Disclosure of the culprits: macrophages-versatile regulators of wound healing. *Adv. Wound Care* 2, 357–368. doi: 10.1089/wound.2012.0407

Sindrilaru, A., Peters, T., Wieschalka, S., Baican, C., Baican, A., Peter, H., et al. (2011). An unrestrained proinflammatory M1 macrophage population induced by iron impairs wound healing in humans and mice. *J. Clin. Invest.* 121, 985–997. doi: 10.1172/JCI44490

Singer, A. J., and Clark, R. A. (1999). Cutaneous wound healing. *N. Engl. J. Med.* 341, 738–746. doi: 10.1056/NEJM199909023411006

Smith and Nephew (2018). *Mechanism of Action –Regranex (becaplermin) Gel.* Available online at: https://regranex.com/mechanism-of-action

Spiller, K. L., Anfang, R. R., Spiller, K. J., Ng, J., Nakazawa, K. R., Daulton, J. W., et al. (2014). The role of macrophage phenotype in vascularization of tissue engineering scaffolds. *Biomaterials* 35, 4477–4488. doi: 10.1016/j.biomaterials.2014.02.012

Stern, R., and Maibach, H. I. (2008). Hyaluronan in skin: aspects of aging and its pharmacologic modulation. *Clin. Dermatol.* 26, 106–122. doi: 10.1016/j.clindermatol.2007.09.013

Stojadinovic, O., Yin, N., Lehmann, J., Pastar, I., Kirsner, R. S., and Tomic-Canic, M. (2013). Increased number of Langerhans cells in the epidermis of diabetic foot ulcers correlates with healing outcome. *Immunol. Res.* 57, 222–228. doi: 10.1007/s12026-013-8474-z

Takeo, M., Lee, W., and Ito, M. (2015). Wound healing and skin regeneration. *Cold Spring Harb. Perspect. Med.* 5:a023267. doi: 10.1101/cshperspect.a023267

Tarnuzzer, R. W., and Schultz, G. S. (1996). Biochemical analysis of acute and chronic wound environments. *Wound Repair Regen.* 4, 321–325. doi: 10.1046/j.1524-475X.1996.40307.x

Ueno, H., Nakamura, F., Murakami, M., Okumura, M., Kadosawa, T., and Fujinag, T. (2001). Evaluation effects of chitosan for the extracellular matrix production by fibroblasts and the growth factors production by macrophages. *Biomaterials* 22, 2125–2130. doi: 10.1016/S0142-9612(00)00401-4

Vannella, K. M., and Wynn, T. A. (2017). Mechanisms of organ injury and repair by macrophages. *Annu. Rev. Physiol.* 79, 593–617. doi: 10.1146/annurev-physiol-022516-034356

Vishwakarma, A., Bhise, N. S., Evangelista, M. B., Rouwkema, J., Dokmeci, M. R., Ghaemmaghami, A. M., et al. (2016). Engineering immunomodulatory biomaterials to tune the inflammatory response. *Trends Biotechnol.* 4, 470–482. doi: 10.1016/j.tibtech.2016.03.009

Wallace, H. J., and Stacey, M. C. (1998). Levels of tumor necrosis factor-alpha (TNF-alpha) and soluble TNF receptors in chronic venous leg ulcers–correlations to healing status. *J. Invest. Dermatol.* 110, 292–296. doi: 10.1046/j.1523-1747.1998.00113.x

Wetzler, C., Kämpfer, H., Stallmeyer, B., Pfeilschifter, J., and Frank, S. (2000). Large and sustained induction of chemokines during impaired wound healing in the genetically diabetic mouse: prolonged persistence of neutrophils and macrophages during the late phase of repair. *J. Invest. Dermatol.* 115, 245–253. doi: 10.1046/j.1523-1747.2000.00029.x

Wysocki, A. B., Staiano-Coico, L., and Grinnell, F. (1993). Wound fluid from chronic leg ulcers contains elevated levels of metalloproteinases MMP-2 and MMP-9. *J. Invest. Dermatol.* 101, 64–68. doi: 10.1111/1523-1747.ep12359590

Yang, L., and Zhang, Y. (2017). Tumor-associated macrophages: from basic research to clinical application. *J. Hematol. Oncol.* 10:58. doi: 10.1186/s13045-017-0430-2

Yona, S., Kim, K. W., Wolf, Y., Mildner, A., Varol, D., Breker, M., et al. (2013). Fate mapping reveals origins and dynamics of monocytes and tissue macrophages under homeostasis. *Immunity* 38, 79–91. doi: 10.1016/j.immuni.2012.12.001

Zhang, Q. Z., Su, W. R., Shi, S. H., Wilder-Smith, P., Xiang, A. P., Wong, A., et al. (2010). Human gingiva-derived mesenchymal stem cells elicit polarization of m2 macrophages and enhance cutaneous wound healing. *Stem Cells* 28, 1856–1868. doi: 10.1002/stem.503

Zhao, R., Liang, H., Clarke, E., Jackson, C., and Xue, M. (2016). Inflammation in chronic wounds. *Int. J. Mol. Sci.* 17:2085. doi: 10.3390/ijms17122085

Zhou, M., Zhang, Y., Ardans, J. A., and Wahl, L. M. (2003). Interferon-gamma differentially regulates monocyte matrix metalloproteinase-1 and−9 through tumor necrosis factor-α and caspase 8. *J. Biol. Chem.* 278, 45406–45413. doi: 10.1074/jbc.M309075200

Zuloff-Shani, A., Adunsky, A., Even-Zahav, A., Semo, H., Orenstein, A., Tamir, J., et al. (2010). Hard to heal pressure ulcers (stage III-IV): efficacy of injected activated macrophage suspension (AMS) as compared with standard of care (SOC) treatment controlled trial. *Arch. Gerontol Geriatr.* 51, 268–272. doi: 10.1016/j.archger.2009.11.015

Zuloff-Shani, A., Kachel, E., Frenkel, O., Orenstein, A., Shinar, E., and Danon, D. (2004). Macrophage suspensions prepared from a blood unit for treatment of refractory human ulcers. *Transfus. Apher. Sci.* 30, 163–167. doi: 10.1016/j.transci.2003.11.007

Conflict of Interest Statement: The authors declare that the research was conducted in the absence of any commercial or financial relationships that could be construed as a potential conflict of interest.

frontiers in Physiology

REVIEW
published: 05 August 2016
doi: 10.3389/fphys.2016.00341

Engineered Biopolymeric Scaffolds for Chronic Wound Healing

Laura E. Dickinson[1] *and Sharon Gerecht*[2]*

[1] Gemstone Biotherapeutics, Baltimore, MD, USA, [2] Department of Chemical and Biomolecular Engineering, Institute for NanoBioTechnology, Johns Hopkins University, Baltimore, MD, USA

Skin regeneration requires the coordinated integration of concomitant biological and molecular events in the extracellular wound environment during overlapping phases of inflammation, proliferation, and matrix remodeling. This process is highly efficient during normal wound healing. However, chronic wounds fail to progress through the ordered and reparative wound healing process and are unable to heal, requiring long-term treatment at high costs. There are many advanced skin substitutes, which mostly comprise bioactive dressings containing mammalian derived matrix components, and/or human cells, in clinical use. However, it is presently hypothesized that no treatment significantly outperforms the others. To address this unmet challenge, recent research has focused on developing innovative acellular biopolymeric scaffolds as more efficacious wound healing therapies. These biomaterial-based skin substitutes are precisely engineered and fine-tuned to recapitulate aspects of the wound healing milieu and target specific events in the wound healing cascade to facilitate complete skin repair with restored function and tissue integrity. This mini-review will provide a brief overview of chronic wound healing and current skin substitute treatment strategies while focusing on recent engineering approaches that regenerate skin using synthetic, biopolymeric scaffolds. We discuss key polymeric scaffold design criteria, including degradation, biocompatibility, and microstructure, and how they translate to inductive microenvironments that stimulate cell infiltration and vascularization to enhance chronic wound healing. As healthcare moves toward precision medicine-based strategies, the potential and therapeutic implications of synthetic, biopolymeric scaffolds as tunable treatment modalities for chronic wounds will be considered.

Keywords: chronic wounds, biopolymeric scaffolds, skin substitutes, acellular matrices, matrix remodeling, skin regeneration, inflammatory

OPEN ACCESS

Edited by:
Basak E. Uygun, Massachusetts General Hospital, USA

Reviewed by:
Miriam Wittmann, University of Leeds, UK
Julie Devalliere, Massachusetts General Hospital/Harvard Medical School, USA

***Correspondence:**
Sharon Gerecht
gerecht@jhu.edu

Specialty section:
This article was submitted to Clinical and Translational Physiology, a section of the journal Frontiers in Physiology

Received: *03 June 2016*
Accepted: *22 July 2016*
Published: *05 August 2016*

Citation:
Dickinson LE and Gerecht S (2016) Engineered Biopolymeric Scaffolds for Chronic Wound Healing. Front. Physiol. 7:341. doi: 10.3389/fphys.2016.00341

INTRODUCTION

In the United States and other developed countries, aging populations coupled with escalating rates of diabetes, and obesity have significantly contributed to the increased prevalence of chronic wounds. Chronic wounds fail to progress through the systematic and reparative wound healing process and instead remain unhealed for >12 weeks (Shultz et al., 2003). Most chronic wounds can be classified into three major wound types [diabetic foot ulcers (DFUs), leg ulcers and pressure ulcers] based on their underlying pathogenesis, i.e., diabetes mellitus, venous deficiencies, arterial perfusion, or unrelieved pressure (local tissue hypoxia) (Mustoe et al., 2006) However, factors such as advanced age, poor nutrition, and immunosuppression plague the patient demographic suffering

with non-healing, chronic wounds. These factors cause additional cellular and systemic stress that further contribute to wound chronicity and delay healing.

Chronic wounds are estimated to affect more than 6.5 million patients in the United States alone, and the annual healthcare burden associated with their treatment is estimated to be in excess of $25 billion (Sen et al., 2009). Not only are chronic wounds incredibly painful for patients, significantly diminishing their quality of life, but they also require long-term treatment at high costs. Despite these high costs, reported recurrence rates for chronic ulcers remain extremely high, ranging from 23 to 40% for pressure ulcers, 24–57% for most chronic venous ulcers, and upward of 60% for diabetic ulcers (Werdin et al., 2009). One reason for their recurrence is because chronic wounds do not progress through the stages of normal wound healing. Even with current treatment modalities, chronic wounds are unable to regenerate tissue of complete functional integrity. The current standard of care currently focuses on compression, infection control, debridement, and selecting an appropriate dressing that maintains a moist wound healing environment. Complete wound closure is the primary clinical outcome for chronic wounds, however, successful wound closure does not necessarily correlate to regenerated tissue of a higher quality, which is desired because it is more resistant to wound dehiscence and recurrence.

WOUND HEALING

Classic wound healing is a dynamic yet well-orchestrated and highly efficient process that requires the interaction of numerous cell types, soluble mediators, and the extracellular milieu to proceed linearly through the wound healing cascade: inflammation, re-epithelialization, angiogenesis, granulation tissue formation, wound contraction, and tissue maturation (Singer and Clark, 1999; Blakytny and Jude, 2006). During inflammation, aggregated platelets release growth factors, and pro-inflammatory chemokines to recruit neutrophils and macrophages to the local wound site. These inflammatory cell types phagocytose debris and bacteria and secrete mediators to stimulate the chemotaxis of cell types necessary for the proliferative phase. During the proliferative phase, fibroblasts, keratinocytes, endothelial and smooth muscle cells migrate through the wound, and proliferate to re-epithelialize the denuded surface, synthesize and deposit a provisional extracellular matrix, form new blood vessels, and contract the wound size. During the final stage, the newly formed granulation tissue is remodeled by the activity of matrix metalloproteinases (MMPs) balanced with tissue inhibitors of metalloproteinases (TIMPs), which rearranges the loose, regenerated dermis, and strengthens the repaired tissue (Gurtner et al., 2008).

Disruption of this normal wound healing cascade results in the development of non-healing chronic wounds. There is a perpetual antagonism between pro- and anti-inflammatory cytokines and an excess of oxygen free radicals and proteases, which creates a hostile microenvironment, and maintains chronic wounds in a prolonged state of inflammation that is unable to progress through later phases of wound healing. Indeed, chronic wounds display a myriad of cellular, and molecular abnormalities, many of which are attributed to dysregulated, and dysfunctional interactions between cellular constituents and the ECM (Schultz and Wysocki, 2009).

ABERRANT MICROENVIRONMENT OF CHRONIC WOUNDS

The wound microenvironment presents a myriad of instructive biochemical cues, cell adhesive sites and molecules within a structural framework of essential matrix proteins—the ECM. The ECM provides structural support and tensile strength, attachment sites for cell surface receptors, and a reservoir for signaling factors that regulate cell migration, proliferation, and angiogenesis. The ECM has a complex 3D architecture of fibrous proteins, polysaccharides and proteoglycans that are secreted by fibroblast and epidermal cells, and it plays a significant and dynamic role in wound healing (Badylak, 2002; Tracy et al., 2016).

Classic wound healing is a cascade of overlapping events through bidirectional interaction between various cell types and the ECM. For instance, fibroblasts synthesize and secrete collagen and ECM components, which in turn concomitantly regulates fibroblast function, such as migration, collagen synthesis, and myofibroblast differentiation (Bainbridge, 2013). Chronic wounds exhibit a host of aberrant cellular and biochemical elements that contributes to their state of persistent inflammation and significantly impairs healing. Fibroblasts from chronic wounds are phenotypically different from those in acute wounds; they are senescent and exhibit diminished migration, reduced proliferation, and decreased collagen synthesis (Lerman et al., 2003). Coupled with inhibited ECM deposition is elevated protease activity, including upregulated and amplified activity of MMPs, collagenase, elastase, and serine proteases (Vaalamo et al., 1996; McCarty and Percival, 2013). The excess of proteases degrade fibrillar collagen I to non-bioactive gelatin, cleave signaling sequences from proteins, and inactivate growth factors (Eming et al., 2007). Indeed, fluid from chronic wounds, but not acute wounds, has been found to rapidly degrade platelet derived growth factor (PDGF), transforming growth factor (TGF-β1), and angiogenic vascular endothelial growth factor (VEGF) (Lauer et al., 2000). The excessive degradation of the ECM, proteins and growth factors deprives cells of attachment sites and vital signals, subsequently disrupting the progression of wound healing (Shultz et al., 2012).

Keratinocytes are also dysfunctional in chronic wounds. In normal wound repair, keratinocytes migrate as a cell sheet over the granulation tissue, and differentiate to re-epithelialize the skin via integrin mediated binding interactions with ECM molecules (Santoro and Gaudino, 2005). However, in chronic wounds, although keratinocytes are hyperproliferative, they are unable to migrate and close the wound (Pastar et al., 2008). This poor migratory ability is concomitantly attributed to altered integrin expression (Hakkinen et al., 2004) and the degraded

ECM components. Instead, keratinocytes at the non-healing edges of chronic wounds continuously proliferate, forming a thick, hyperkeratotic layer. Contributing to poor epithelialization is the overall excessive inflammatory tissue microenvironment, which inhibits the migration of fibroblasts and the synthesis of new ECM, and the loss of epidermal stem cell (ESC) populations. ESC populations reside in distinct compartments or niches that regulate their self-renewal and lineage fate (Braun and Prowse, 2006); in response to tissue injury, the ESCs proliferate, differentiate, and migrate to re-epithelialize the wounded area (Cha and Falanga, 2007). However, in chronic venous ulcers, it has been shown that there is a loss of SC niche signaling and subsequent deregulation and depletion of ESCs that possibly contributes to the hyperpoliferative epidermis of a non-healing venous ulcer wound edge (Stojadinovic et al., 2014).

Although far from an exhaustive summary, the discussion above emphasizes the biological complexity of chronic wounds. Indeed, the impairment of the ECM in chronic wounds has long been identified as a key target for wound healing strategies. Within the last 20 years, substantial emphasis has been directed toward the development of bioengineered skin substitutes, such as living skin equivalents, acellular matrices, and polymeric scaffolds, that recapitulate multiple features of the native ECM that are so necessary in regulating the wound healing cascade (Rennert et al., 2013). Several bioengineered scaffolds that are FDA approved and commercially available will be discussed in this review. All of the wound healing skin substitutes discussed in this mini-review provide an ECM, whether natural or synthetic, that supports the infiltration of cells, tissue regeneration, and ultimately wound closure. These skin substitutes are designed to provide a bio-inductive and vulnerary environment by modulating the proteolytic climate and/or supplementing the wound bed with exogenous, bioactive factors that stimulate innate tissue repair mechanisms. However, to date, there have been limited head-to-head comparative clinical studies evaluating the performance of the plethora of advanced wound care products, which are required to guide clinical practice and payer determinations (Valle et al., 2014).

BIOENGINEERED SKIN SUBSTITUTES

The optimal bioengineered scaffold for skin regeneration of chronic wounds should (1) be non-immunogenic; (2) modulate proteolytic activity to reset the wound to an acute state; (3) provide a bio-resorbable scaffold that facilitates cellular migration and promotes cellular proliferation and matrix deposition; (4) recruit angiogenic and fibroblast cell types to synthesize granulation tissue; and (5) absorb and neutralize free radicals (Gould, 2015). In the following sections, we will describe the various types of bioengineered skin substitutes, including those that contain natural ECM components harvested from human tissue or animal sources and synthesized, ECM-mimetic biopolymeric scaffolds. All scaffolds detailed in this review are listed in **Table 1**.

Living Skin Equivalents: Human-Derived Technologies

Living skin equivalents comprise scaffolds, either natural, or synthetic, seeded with allogenic fibroblasts, and/or keratinocytes. There are several iterations of products that have been developed using this approach, which essentially provide cellular, and structural components for wound healing. Apligraf® (Organogenesis, Inc.) is composed of a bovine type I collagen matrix seeded with neonatal fibroblasts to produce a neodermal layer. Human neonatal epidermal keratinocytes are subsequently added on top of this dermal component as a monolayer to approximate the epidermis and form a differentiated stratum corneum (Zaulyanov and Kirsner, 2007). This results in a metabolically active bilayered skin substitute providing both a dermal and epidermal layer with living cells. Although the fibroblasts and keratinocytes in Apligraf do not persist beyond 6 weeks in patients (Hu et al., 2006), they are thought to be responsible for stimulating differentiation and proliferation via secretion of essential cytokines and growth factors (Falanga et al., 2002). Apligraf was the first allogeneic cell-based product to be approved by the FDA in 1998 for the treatment of DFUs and venous leg ulcers. Large multicenter randomized clinical trials demonstrated a significantly higher rate of wound closure compared with conventional standard of care (Veves et al., 2001; Edmonds and European and Australian Apligraf Diabetic Foot Ulcer Study Group, 2009).

Dermagraft® (Organogenesis, Inc.) was approved by the FDA in 2001 for the treatment of non-healing DFUs. Although it also contains neonatal dermal fibroblasts, it differs from Apligraf in that the fibroblasts are cultured onto a bioresorbable polyglactin mesh scaffold; polyglactin is a standard suture material. The metabolically active fibroblasts proliferate within the interstices of the synthetic scaffold, secreting collagens, growth factors, cytokines, proteoglycans, and other key regulatory molecules, to create a 3-D bioactive matrix, which is then cryopreserved for storage (Naughton et al., 1997). When applied to DFUs, Dermagraft significantly increased the rate of wound closure compared to the control (Marston et al., 2003).

Another biologically active human skin allograft is TheraSkin® (Soluble Systems), which is harvested within 24 h post-mortem and cryogenically processed to preserve the viable fibroblasts, keratinocytes, and fully developed ECM sequestered with essential growth factors and cytokines. It has been reported that Theraskin, which was found to be effective in the treatment of DFUs and venous stasis ulcers (Landsman et al., 2011), contains a greater quantity of the key collagens critical to wound healing compared to Apligraf (DiDomenico et al., 2011). This may be attributed to the manufacturing process of Apligraf in which a bovine collagen substrate is used to culture neonatal cells that deposit the ECM *in vitro*. The application of a living human dermal skin substitute delivers a smorgasbord of vital key regulatory proteins and cytokines that stimulate angiogenesis, fibroblast migration, and keratinocyte proliferation to accelerate wound healing. However, there is an absence of head-to-head studies that compare the clinical and cost efficacy advanced wound care products to inform clinical practice and payer determination. Indeed this stems also from the variety of

TABLE 1 | Summary of scaffolds for chronic wound healing.

Product	Composition	Properties/Mechanism of action	FDA
LIVING SKIN SUBSTITUTES			
Apligraf®	Bovine type I collagen seeded with human neonatal fibroblasts and keratinocytes	Metabolically active cells secrete cytokines and growth factors to stimulate differentiation and proliferation	PMA (1998)
Dermagraft®	Human neonatal fibroblasts seeded on bioabsorbable polyglactin scaffold—cryopreserved	Metabolically active fibroblasts secrete collagen, matrix proteins, growth factors and cytokines	PMA (2001)
TheraSkin®	Cryopreserved skin allograft harvested from cadavers	Biologically active scaffold providing cellular and extracellular components Natural barrier to infection	HCT/Ps
ACELLULAR NATURALLY DERIVED POLYMERIC SCAFFOLDS			
Oasis®	Minimally processed ECM derived from porcine small-intestine submucosa	Provides structural matrix and delivers growth factors to stimulate angiogenesis and cell migration	510 K (1998)
GraftJacket®	Processed (crosslinked and cryopreserved) human dermal matrix	Fenestrated acellular matrix that acts as a foundation for revascularization and cellular repopulation Reduces inflammation	HCT/Ps
DermACELL®	Decellularized human dermis allograft	Unique anionic detergent and endonuclease-based process to decellularize tissue Scaffold supports cell ingrowth	HCT/Ps
EpiFix®	Dehydrated allograft: amnion and chorion membranes derived from donated human placenta	Composed of a single layer of epithelial cells, a basement membrane and an avascular connective tissue matrix Retains soluble biological molecules and growth factors that stimulate human dermal fibroblast proliferation and the migration of human mesenchymal stem cells	HCT/Ps
Integra™	Cross-linked bovine collagen and chondroitin 6-sulfate with a silicone membrane	Biodegradable matrix provides a scaffold for cellular invasion and capillary growth	PMA (1996) 510 K (2002)
Promogran™	Freeze-dried composite of 55% collagen and 45% oxidized regenerated cellulose	Composite matrix absorbs wound exudate to form a biodegradable gel Provides a scaffold for cellular migration	510 K (2002)
Tegagen™, Algisite™, Algi-Fiber, etc.	Dressings of calcium alginate fibers	Form gelatinous mass upon contact with wound exudate Extremely absorbent (10×) Controls mild hemorrhages	510 K
BIOPOLYMERIC SCAFFOLDS			
Talymed®	Shortened fibers of N-acetyl glucosamine isolated from microalgae	Material interacts with fibroblasts and endothelial cells to stimulate cell migration	510 K (2010)
Hyalomatrix®	Non-woven pad of benzyl ester of hyaluronic acid and a semipermeable silicone membrane	Biodegradable scaffold for cellular invasion and capillary growth. Contains a semipermeable silicone membrane to prevent water loss	510 K (2007)
Dextran	Crosslinked modified dextran and PEG diacrylate	Biodegradable matrix fills wound defect and provides a scaffold for cellular infiltration	N/A

Pre-market approval (PMA); Human cells, tissues, or cellular-based products (HCT/Ps).

chronic wound types with various etiologies—there is no single wound care product to treat and manage all wound types. Most comparative studies are either retrospective analyses or funded by the company. In a retrospective study evaluating the efficacy of EpiFix compared to Apligraf in treating DFUs, it was reported that patients treated with EpiFix required more applications compared to patients treated with Apligraf, and that the median time to wound closure using Apligraf was 13.3 weeks compared to 26 weeks for EpiFix (Kirsner et al., 2015b). However, in a prospective study, 97% of lower extremity diabetic ulcers healed when treated with EpiFix compared to only 73% of wounds treated with Apligraf, suggesting that patients treated with EpiFix experienced a shorter time to wound closure (Zelen et al., 2016). The median graft cost was $8,918 (range $1,486–19,323) per healed wound for the Apligraf group and $1517 (range $434–25,710) per healed wound in the EpiFix group (Zelen et al., 2016). In a separate retrospective analysis, treatment using the bilayered living cell construct Apligraf reduced the median time to wound closure of venous leg ulcers by 44% compared to treatment using a naturally derived, acellular porcine dressing (Oasis®; to be discussed below) (Kirsner et al., 2015b).

Acellular Naturally Derived Polymeric Scaffolds

Acellular matrices are characterized as nonviable biomaterials. They may be animal- or human-derived, with all cells removed during manufacture, or they may be synthetic or a composite, where cells are simply not present from the outset. Natural polymers are commonly utilized in the development of acellular matrices for chronic wound treatments because of their inherent biocompatibility and bioactivity as well as their ability to mimic the structural, biomechanical, and biochemical functions of the ECM. There are cost advantages to using naturally derived ECM-based polymeric scaffolds. Using a Markov model to estimate the comparative cost effectiveness of Apligraf, Dermagraft, and an ECM-based therapy, the ECM-based therapy

was economically dominant and determined to be the most cost effective for the management of venous leg ulcers as an adjunct therapy to standard of care (Carter et al., 2014). The expected costs for a naturally derived ECM-based scaffold (Oasis®), Apligraf and Dermagraft were $6732, $10, 638, and $11, 237, for 31, 29, and 17 ulcer free weeks, respectively, suggesting that naturally derived ECM-based therapies yield potential savings compared to other cell or tissue-derived products (Carter et al., 2014). The most common, bioactive natural polymers utilized in the development of acellular matrices for wound healing are collagen, hyaluronic acid, chitosan, and alginate.

Collagens are the most abundant ECM macromolecule and are the main component in human skin that provides structural integrity (Singer and Clark, 1999). In addition to its structural function, collagen I governs many cellular functions of fibroblasts and keratinocytes, including cell adhesion, differentiation, migration, ECM deposition, and angiogenesis (Heino, 2000; Gelse et al., 2003; Whelan and Senger, 2003). Collagen I is also able to bind excess proteases, inflammatory cytokines, and free radicals that are rampant in the chronic wound bed (Wiegand et al., 2010). The role of collagen in tissue repair and wound healing are multifactorial, which supports the extensive use of exogenous collagen-based scaffolds for chronic wound applications. Generally speaking, collagen-based scaffolds are classified as either decellularized matrices, derived from a variety of mammalian sources, and anatomical locations, including porcine small-intestine submucosa, or urinary bladder matrix, human cadavers, placental tissue, or they are synthesized via extraction and chemical crosslinking. There are many products that are currently used in the treatment of chronic wounds and several of them are briefly described below as representative examples.

Oasis® Wound Matrix (Healthpoint) is a naturally occurring ECM graft (>90% collagen) derived from porcine SIS, which is a thin, approximately 0.15 mm thick translucent layer of porcine intestine that is predominately type 1 collagen. Porcine SIS possesses a porous microstructure, with pores ranging in size from 20–30 μm that enables oxygen diffusion and promotes cell viability (Nihsen et al., 2008). Porcine SIS also retains the active forms of other biologically relevant components that provide cell and growth factor binding sites, sequester matrix-degrading enzymes, and enhance cellular infiltration into injured tissue. It is also embedded with glycosaminoglycans, proteoglycans, fibronectin, and various growth factors that imparts significant bioactivity (Hodde et al., 1996, 2001; Shi and Ronfard, 2013). In this way, the SIS not only provides a structural matrix and delivers growth factors to stimulate angiogenesis and cell migration but also regulates proteolytic activity and dampens the inhibitory effects of MMP-1, MMP-2, and MMP-9 on keratinocyte migration (Shi et al., 2012).

There are myriad acellular wound matrices available for clinical use that are processed, decellularized dermal constructs derived from donated human tissue. They are all designed to provide a scaffold for wound repair, however, each acellular dermal wound matrix differs by the way in which it is processed. For GraftJacket® (Wright Medical Technology), donated human tissue is treated to remove the epidermis and cellular components, but it retains collagen, elastin, proteoglycans, and the internal matrix of the dermis, which remains intact and is chemically crosslinked to maintain the collagen architecture before cryopreservation (Turner and Badylak, 2015). DermACELL® (LifeNet Health) is a human tissue matrix allograft that employs a unique, proprietary MATRACELL® technology (Moore et al., 2015) that uses anionic detergents and an endonuclease to achieve >97% nucleic acid removal while retaining biomechanical strength. This allows DermACELL to be preserved at ambient temperature and offer a >3 year shelf-life. Both of these products have been indicated for the treatment of non-healing ulcers and dermal wounds and have demonstrated the ability to reduce time to complete wound closure and increase healing rates compared to conventional care (Reyzelman et al., 2009; Yonehiro et al., 2013; Walters et al., 2016). In these processed acellular dermal matrices, the removal of the cellular components reduces the risk of rejection, and the critical dermal proteins that remain minimize inflammation and facilitate cell infiltration and tissue revascularization. In contrast to xenogeneic ECM allografts, minimally manipulated human tissue products are classified as human cell, tissues, and cellular and tissue-based products (HCT/Ps) by the FDA. As a result, there are fewer restrictions on the applications for which these devices can be used; they are viewed as tissue transplants and manufacturers are only required to follow manipulation guidelines to ensure materials are free from transmissible pathogens (**Table 2**).

The use of placental membranes for wound healing has been reported for over 100 years, which can be attributed to its collagen-rich ECM presenting biologically active components, such as developmental cytokines and elevated concentrations of regenerative growth factors (Silini et al., 2015). Placental membranes contain a plethora of multifunctional growth factors, including, but not limited to, epidermal growth factor, basic fibroblast growth factor, PDGF, VEGF, TGF-β1, and keratinocyte growth factor, as well as MMPs and TIMPs (Fortunato et al., 1998; Koizumi et al., 2000; Lopez-Valladares et al., 2010) that support critical cell behavior and wound healing events. Also expressed in placental membranes are immunosuppressive factors and antibacterial peptides that contribute to the reduced risk of rejection of placental membranes (Park et al., 2008; Mamede et al., 2010). Large amounts of the ECM glycosaminoglycan hyaluronan (HA) are also present in placental membranes, which has been shown to function as a free radical scavenger to remove reactive oxygen species (Trabucchi et al., 2002; Lockington et al., 2014). However, different processing methods impact the composition and functionality of these materials (von Versen-Hoeynck et al., 2008). There are more than 25 commercially available placental membrane products, yet most contain no viable cells because they are either dehydrated or are cryopreserved devitalized or decellularized tissue. One such product, EpiFix® (MiMedx), is a dehydrated human tissue allograft comprising laminated amnion and chorion membranes derived from donated human placenta. During processing, the amnion and chorion tissue layers are isolated from the placenta and washed. The two layers are then laminated to form the graft, which is subsequently dehydrated and sterilized. EpiFix

TABLE 2 | Brief overview of United States FDA pathways for wound healing products (medical devices).

Device classification/ Risk	**PHS 361: HCT/Ps low**	**510 K Class II/moderate**	**PMA Class III/high**
Review standard	No pre-market review Not required to demonstrate safety or effectiveness	Substantial equivalence in safety and effectiveness to a legally marketed predicate device	Approval requires that the safety and effectiveness of the device be established with valid scientific evidence, i.e., high-quality clinical data
Requirements	Minimally manipulated Intended for homologous use No systemic effect/not dependent on metabolic activity of cells Manufacturers follow good tissue practice to prevent the introduction, transmission, and spread of communicable diseases	Non-clinical laboratory studies for safety (performed under GLP conditions) *Clinical investigations not typically required* *Quality Systems in place prior to interstate commerce* *Manufacturing not reviewed pre-approval*	Non-clinical laboratory studies for safety (performed under GLP conditions) Clinical investigations (such as performed under an Investigational Device Exemption) Detailed Quality Systems in place Pre-approval of manufacturing facility with inspection
Regulatory burden	**Low**	**Medium**	**High**
Wound healing products	TheraSkin® GraftJacket® DermACELL® EpiFix®	Oasis® Integra®* Promogran™ Tegagen™, Algisite™ Algi-Fiber Talymed® Hyalomatrix®	Apligraf® Dermagraft® Integra™*

Pre-market approval (PMA); Human cells, tissues, or cellular-based products (HCT/Ps).
**Although initial PMA was received in 1996, in April 2001, the FDA approved Integra™ Dermal Regeneration Template for marketing in the treatment of life-threatening full-thickness and/or deep partial thickness thermal injuries. Because the treatment of thermal injuries poses a significant risk, medical devices developed to treat burns are considered Class III devices that support of sustain human life. These products require a PMA submission accompanied with clinical data demonstrating safety and effectiveness. A separate 510(k) submission was filed for Integra™ Bilayer Matrix Wound Dressing, which was cleared for marketing in August 2002 for the management of a broad range of wound types, including partial, and full-thickness chronic wounds, surgical wounds (donor sites/grafts, post-Mohs surgery, post-laser surgery, podiatric, wound dehiscence), trauma wounds (abrasions, lacerations, second-degree burns, and skin tears) and draining wounds. Both Integra LifeSciences products are composed of cross-linked bovine tendon collagen with glycosaminoglycan and a semi-permeable polysiloxane membrane. With the 510(k) clearance, the Bilayer Matrix Wound Dressing is marketed to manage a broad range of wound indications, whereas the PMA limits indications to thermal injuries. However, as recently as January 2016, the Integra™ Dermal Regeneration Template was approved for indications including partial and full thickness neuropathic DFUs based on submitted clinical data.*
www.FDA.gov.

contains a single layer of epithelial cells, a basement membrane, and an avascular connective tissue matrix. After processing, EpiFix retains soluble biological molecules and growth factors that stimulate human dermal fibroblast proliferation and the migration of human mesenchymal stem cells (Koob et al., 2013). When evaluated in the treatment of DFUs and venous leg ulcers, EpiFix promoted complete epithelialization and reduced the wound size in patients compared to standard treatment (Zelen et al., 2013).

Integra™ (Integra Life Sciences) and Promogran™ (Systagenix Wound Management) are two wound healing products synthesized using extracted and polymerized collagen. Integra is a bilayer composite matrix of crosslinked collagen type I from bovine sources and a glycosaminoglycan (chondroitin 6-sulfate) isolated from shark skin. It has a semipermeable silicone membrane that functions as a temporary epidermal layer by controlling water vapor loss and providing structural integrity. The bilayer matrix recruits dermal fibroblasts to the wound, which then synthesize, and secrete new ECM to the wound bed to facilitate healing (Burke et al., 1982). Although initially indicated for third degree burns via an FDA pre-market approval (PMA; to be discussed below), a 300 subject clinical trial demonstrated that the non-healing DFUs treated with Integra had a more rapid time to complete wound closure and increased rate of wound closure compared to standard of care treatment (Driver et al., 2015). Promogran is a combination matrix composed of 55% bovine type I collagen and 45% oxidized regenerated cellulose (ORC) that is freeze dried and formed into a 3 mm thick sheet that is applied directly to the wound bed. Upon application, the composite matrix absorbs wound exudate to form a biodegradable gel that enhances fibroblast migration and proliferation (Hart et al., 2002). The composite matrix binds and stabilizes growth factors and physically sequesters and inactivates excessive MMPs while providing a scaffold for cellular migration (Cullen et al., 2002). Clinical studies demonstrate a significant reduction in the concentration and activity of proteases in the wound exudate of DFUs treated with Promogran and a greater reduction in wound size (Ulrich et al., 2011).

Other natural polymers used as wound dressings are alginate and chitosan. Alginate is a polysaccharide with homopolymeric blocks of 1,4-linked β-D-mannuronic and α-L-guluronic residues that is isolated from the cell walls of a variety of species of brown seaweed. Alginate exhibits unique gelation properties and ionically crosslinks in the presence of divalent ions to form a biocompatible 3D polymeric crosslinked scaffold for tissue engineering applications (Augst et al., 2006). Alginate wound dressings are used in wound management because they provide a moist environment, are highly absorbent, and function as a hemostat. When an alginate dressing comes into contact with wound exudate there is an ion exchange between the calcium

ions in the mannuronic and gluronic groups of the alginate dressing and the sodium ions in blood or exudate (Segal et al., 1998). As sufficient calcium ions are replaced by sodium ions, the alginate fibers swell, partially dissolve, and form a gel that maintains a moist environment for autolytic debridement and reduces pain during dressing changes (Pirone et al., 1992). Alginate dressings have also been shown to minimize microbial bioburden and sequester proteinases (Sweeney et al., 2012). There are numerous alginate-based wound dressings approved for use in managing variety of wound types in which exudate is present, such as chronic wounds, including Tegagen™ (3M), Algisite™ (Smith and Nephew), and Algi-Fiber (CoreLeader Biotech) to name a few (Dumville et al., 2015; O'Meara et al., 2015).

Chitosan is a linear polysaccharide composed of randomly distributed β-(1–4)-linked D-glucosamine and N-acetyl-D-glucosamine that is predominately used as a hemostat but is currently being evaluated as a wound dressing for chronic wounds because of its ability to modulate the wound environment (Sandoval et al., 2011; Mayol et al., 2014). Chitosan is prepared by deacetylating chitin, the principle component in the exoskeleton of crustaceans, via enzymatic or alkaline hydrolysis before being processed into various fibrous, scaffold, and hydrogel biomaterials (Azuma et al., 2015). Chitosan contributes to wound healing by stimulating the rapid mobilization, adhesion, and aggregation of platelets and red blood cells to the wound site to facilitate rapid clotting (Chou et al., 2003; Okamotoa et al., 2003). Post-hemostasis, chitosan also accelerates granulation tissue and matrix formation (Biagini et al., 1992; Ueno et al., 2001). Lysozymes gradually depolymerize chitosan via hydrolysis to release N-acetyl-D-glucosamine, which stimulates fibroblast proliferation and collagen deposition and remodeling (Kojima et al., 2004). Chitosan has also been shown to stimulate inflammatory cells migration (Peluso et al., 1994). As a wound dressing biomaterial, chitosan exhibits several unique advantages, including non-toxicity, physiological inertness, antibacterial properties, biocompatibility, and an affinity to proteins (Dai et al., 2012). Chitosan's antimicrobial properties are attributed to the presence of primary amine groups that confer an overall cationic charge, which destabilizes, and permeabilizes microbial membranes (Rabea et al., 2003).

Acellular Matrices-Biosynthetic Polymeric Scaffolds

Acellular synthetic matrices offer several advantages over naturally derived polymeric and cellular based scaffolds, including longer shelf-life, cost efficacy, and limited risk of rejection. In a retrospective study, the number of applications needed to treat (NNT) was used to model the comparative clinical and cost efficacy of currently available advanced wound care matrices as adjuncts to compression therapy for the treatment of venous leg ulcers. It was found that fewer applications of an acellular biosynthetic scaffold was required to achieve closure compared to a human skin equivalent (Apligraf) and biologically derived polymeric scaffold (Oasis) at a significantly lower cost. The incremental costs per additional successfully treated patient were $1600 for the acellular biosynthetic scaffold (Talymed®), $3150 for Oasis, and $29,952 for Apligraf (Hankin et al., 2012).

To design an efficacious biosynthetic polymeric scaffold that achieves wound closure and skin regeneration, several parameters, and criteria need to be considered in addition to those listed in the above section. Scaffolds that are chemically synthetized or modified not only need to be easily manufacturable but also biocompatible, biodegradable, and non-toxic while exhibiting optimal biomechanical properties, including ideal porosity, and morphology to modulate the transport cells, metabolites, and signaling molecules. Most importantly, cells must be able to appropriately respond to and infiltrate the scaffold to facilitate degradation and support a regenerative healing process (Kirsner et al., 2015a). Therefore, the fundamental design strategy in developing biosynthetic scaffolds is to recapitulate structural and molecular aspects of the ECM using tunable polymeric materials that simulate the elasticity and porosity of dermis. Polysaccharides possess reactive functional groups that can be modified to form non-toxic and bioactive wound healing biomaterials with optimized and tailorable characteristics, such as pore size and degradation rate, which elicit the appropriate biological response, and stimulate tissue regeneration. To date, there are few FDA cleared, commercially available biosynthetic scaffolds indicated for the use in managing chronic wounds. Two FDA cleared scaffolds, both of which are polysaccharide-based, will be discussed below. A brief overview of FDA device classification for wound healing scaffolds is also provided.

The United States FDA predominately regulates wound healing products as medical devices based on their composition and device classification, which depends on the intended use of the device. Devices that present relatively low risk are generally categorized as Class I or Class II devices, and higher risk devices are Class III. Minimally manipulated human-derived products, such as placental membrane-derived products, are regulated as human cells, tissues, and cellular and tissue-based products (HCT/Ps) and only require manufacturers to follow good tissue practices and manipulation guidelines. Class III human/animal-derived products, such as cellular wound matrices, are approved through a pre-market approval (PMA). Devices that present relatively low or moderate risk (Class II), such as animal-derived and synthetic products, require the manufacturer to seek 510(k) clearance, which is generally granted when submitted information establishes that a new device is "substantially equivalent" to an already approved and legally marketed "predicate" device in terms of technological characteristics, such as design, mode of action and composition, and performance. Many biosynthetic scaffolds are cleared through the 510(k) pathway (**Table 2**). In the European Union there are directives that outline requirements under which a medical device could be marketed across all E.U. member states after earning a Conformité Européenne (CE) mark in any one member country. These directives similarly categorize devices into four classes (I, IIa, IIb, and III) on the basis of associated risks. Approval and CE marks for medical devices are directly managed by designated Notified Bodies and are subject to performance and reliability testing. Approval is generally

granted if the device successfully performs as intended in a manner in which the benefits outweigh expected risks. The specific requirements for pre-marketing clinical studies are vague, and the guidelines for the nature of these studies are not binding on manufacturers or Notified Bodies (Kramer et al., 2012).

Talymed® (Marine Polymer Technologies) is a biodegradable, wafer-thin wound matrix that was cleared in 2010 for the management of full and partial-thickness wounds, including chronic wounds. Talymed is a bioactive scaffold composed of shortened fibers of poly-N-acetyl glucosamine derived from diatom algae. Native poly-N-acetyl glucosamine fibers are shortened to ∼4–7 μm using gamma radiation, which retains the unique 3D polymeric structure and enables the nanofibers to form a thin, biodegradable scaffold membrane (Scherer et al., 2009). Pre-clinical animal studies demonstrated that a nanofibrous scaffold composed of shortened poly-N-acetyl glucosamine fibers initiated wound healing through material-facilitated interactions with fibroblast and endothelial cells that stimulated re-epithelization via increased keratinocyte migration, granulation tissue formation, cell proliferation and vascularization (Scherer et al., 2009). The shortened fibers of poly-N-acetyl glucosamine become completely integrated into the wound bed and upregulate the integrin-dependent Ets1 transcription factor, which regulates genes involved in cell migration, proliferation and survival. The shortened fibers of poly-N-acetyl glucosamine stimulate endothelial cells and the increased secretion of several cytokines and growth factors, including IL-1 and VEGF, that are imperative for proper wound healing (Vournakis et al., 2008). In a pilot study, 86% of patients with venous leg ulcers that were treated with Talymed biweekly achieved complete wound healing within 5 months compared to patients only receiving standard of care (45%) (Kelechi et al., 2012).

Hyaluronan or hyaluronic acid (HA) is a linear glycosaminoglycan composed of alternating units of D-glucuronic acid and D-*N*-acetyl-d-glucosamine that is ubiquitously distributed within the ECM and specifically in connective tissue. HA is a well-established co-regulator for gene expression, proliferation, motility, adhesion, signaling, and morphogenesis (Toole, 2004). In wound healing, HA plays a key role in modulating inflammation, stimulating cell migration, and promoting angiogenesis through interactions with 2 cellular receptors: RHAMM and CD44 (Chen and Abatangelo, 1999). However, the role of HA in tissue repair is largely dependent on molecular size (Litwiniuk et al., 2016). High molecular weight HA exhibits anti-inflammatory, immunosuppressive, and anti-angiogenic effects by inhibiting EC proliferation, migration, and capillary formation, whereas short chain, low molecular weight degradation products of HA, namely oligosaccharides of 3–10 disaccharide units, are potent pro-inflammatory molecules that induce angiogenesis by stimulating EC proliferation, migration, and angiogenic sprouting (West and Fan, 2002). *In vivo,* native HA is subject to rapid enzymatic degradation by hyaluronidases and, in wounded tissue, further fragmentation by free radicals (Stern, 2004). Fortunately, HA is amenable to chemical modifications due to the presence of carboxyl and hydroxyl groups on its repeating disaccharide units. The functional groups allow HA-based biomaterials to be tailored to retard and control degradation for tissue regeneration and wound healing applications. Indeed, synthetic HA derivatives have been chemically modified by esterification of the carboxylic group of glucuronic acid with benzyl groups (Benedetti et al., 1993). This modification imparts higher resistance to hyaluronidase enzymatic activity and degradation. Hyalomatrix® (Anika Therapeutics) is a bilayered wound device composed of a wound contact layer containing fibers of esterified HA and an outer semipermeable silicone membrane that acts as

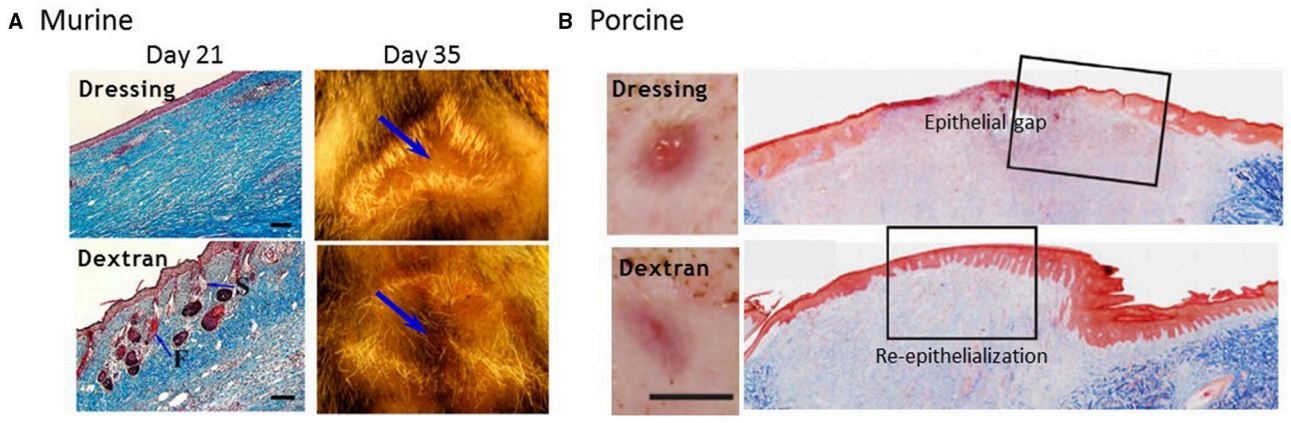

FIGURE 1 | Biopolymeric dextran scaffold facilitates wound healing in murine and porcine burn models. (A) Complete healing was observed in mice by day 21. Dextran treated wounds exhibited mature epithelial structures, including hair follicles (F) and sebaceous glands in the dermal layer as indicated by Masson trichrome staining (left panel; scale bar = 100 μm). By day 35, new hair growth was observed in the center of dextran treated wounds, as shown by photos, compared to wounds treated with dressing only; arrows indicate center of wound. **(B)** Wound closure was observed by day 14 in a porcine model as shown by representative macroscopic and immunohistological images. Identification of neoepithelium using Masson's trichrome-stained sections (right panel) confirmed that wounds treated with dressing-only had an epithelial gap, whereas dextran-treated wounds were completely re-epithelialized with a thick reticulated epithelium. Scale bar = 1 cm. Modified from Sun et al. (2011b), and modified and reprinted from Shen et al. (2015). Copyright (2015), with permission from Elsevier.

a barrier to prevent vapor loss and reduce bacterial colonization. Hyalomatrix acts as a regenerative matrix by providing HA in the form of a 3D scaffold. The scaffold enables rapid fibroblast and endothelial cell infiltration and modulates ECM deposition (Galassi et al., 2000; Turner et al., 2004). In slow-healing wounds, as the matrix degrades, a high concentration of HA is locally released to the wound site that stimulates a regenerative response. When evaluated in wounds of different etiologies, including vascular, DFUs, traumatic wounds, and pressure ulcers, 83% of Hyalomatrix treated wounds achieved some degree of re-epithelialization ($\geq$10%) within 16 days (Caravaggi et al., 2011).

Among the natural polymers, dextran is a hydrophilic, non-toxic polysaccharide composed of linear a-1,6-linked D-glucopyranose residues with a low fraction of branches extending from α-1,2, α-1,3, and α-1,4 linked side chains. Dextran is synthesized by bacteria, *Leuconostoc mesenteroide*, and is naturally resistant to protein adsorption and cell adhesion, and modification of its polymer backbone allows the development of biomaterials with specific properties. Dextran is also highly water soluble and easily functionalized through its reactive hydroxyl groups. For instance, modifying dextran polymers with polymerizable vinyl groups creates functionalized dextran macromers that present available C = C groups for crosslinking. These modified dextran macromers are then combined with PEG-diacrylate and photopolymerized to produce a hybrid crosslinked scaffold (Sun et al., 2010). The biosynthetic scaffold technology was developed in Dr. Gerecht's laboratory at Johns Hopkins University. The physical properties of the biosynthetic dextran scaffold can be tuned to facilitate cell infiltration and scaffold degradation by modifying the degree of substitution of crosslinking groups and ratio of polymeric components, modified dextran and PEG-diacrylate (Sun et al., 2011a). The degree of substitution, or the number of functionalized hydroxyl groups on the dextran anhydroglucose units, and dextran content combinatorially affect the crosslinking density and, therefore, the porosity, elasticity, and degradation of the scaffold. Tissue ingrowth and regeneration is largely dependent on these physical properties. A reduced degree of substitution of crosslinking groups affects degradation and generates a scaffold with a more porous architecture ($\sim$10 μm) that facilitates cell infiltration and migration as well as the diffusion of oxygen and nutrients. Increased dextran content generates a less rigid scaffold but retains structural integrity to enable handling and interface with the wound bed. When applied to 3rd degree burns in murine and porcine models, the dextran scaffold is quickly penetrated, and degraded by early inflammatory cells, promoting the infiltration of necessary cells to re-epithelialize the wound and facilitate skin regeneration. Third degree burns were selected to evaluate the wound healing potential of the dextran scaffold because in preliminary studies, the dextran scaffold demonstrated rapid vascularization when implanted subcutaneously (Sun et al., 2011a). Thermal injuries display increased capillary permeability and thrombosis, so wound healing outcomes are dependent on neovascularization (Rowan et al., 2015). In mice, complete epithelial repair with mature epithelial morphologies was observed, including hair follicles and sebaceous glands, after application of the dextran scaffold, see **Figure 1A** (Sun et al., 2011b). Accelerated wound closure was also observed in a porcine model after treatment with the dextran scaffold, in which a thick reticulated neoepithelium was regenerated, see **Figure 1B** (Shen et al., 2015). This is particularly exciting, because the ability to regenerate skin with functional epidermal appendages, such as hair follicles, and sebaceous and sweat glands, has long been and still is a major clinical objective, and challenge, particularly in the healing of chronic wounds in which obtaining wound closure is the primary objective.

CONCLUSIONS

Chronic wounds are characterized by an extremely complex pathophysiology arising from varied etiologies and combined comorbidities including diabetes, immunosuppression, vascular deficiencies, and increased bacterial load that disrupt healing. These wounds suffer from severe molecular and cellular deficiencies and are, unfortunately, heterogeneous across the patient population. This has contributed to the lack of clinical studies directly comparing the efficacy of available products for the treatment of chronic wounds. Performing controlled comparative trials that evaluate the efficacy of advanced wound care products in healing difficult-to-to heal chronic wounds are necessary. Because of the heterogeneity and lack of clinical evidence demonstrating significantly greater performance of specific products, there is currently no single wound dressing or scaffold that is exclusively used for the treatment and healing of all chronic wound types. The treatment paradigm for chronic wounds must shift toward precision medicine strategies that provide personalized therapy based on individual patient need. The development of novel polymers that mimic the ECM and can be modified to incorporate therapeutics, growth factors, antimicrobials, or cells ushers in a new era of customized platform technologies that deliver bioactive components for the treatment of chronic wounds. As chronic wound healing is multifactorial, biopolymeric scaffolds will be designed based on specific patient need to alter the wound bed and provide the optimal wound healing microenvironment. This personalized approach begins with the identification of therapeutic targets and the development of quantitative biomarker assays to allow physicians to stratify patient populations and guide interventional treatments. This may include delivering bioactive VEGF to stimulate vascularization, releasing antimicrobials to control infection, and/or supplying protease inhibitors to mitigate proteolytic activity and stimulate regenerative wound healing.

AUTHOR CONTRIBUTIONS

LD and SG contributed to writing and revising the manuscript. Both authors approved the final version of this manuscript.

ACKNOWLEDGMENTS

The authors acknowledge the research work completed by members of Dr. SG's laboratory that is cited in this review and the funding resources used to support that work.

REFERENCES

Augst, A., Kong, H., and Mooney, D. (2006). Alginate hydrogels as biomaterials. *Macromol. Biosci.* 6, 623–633. doi: 10.1002/mabi.200600069

Azuma, K., Izumi, R., Osaki, T., Ifuku, S., Morimoto, M., Saimoto, H., et al. (2015). Chitin, Chitosan, and its derivatives for wound healing: old and new materials. *J. Funct. Biomater* 6, 104–142. doi: 10.3390/jfb6010104

Badylak, S. F. (2002). The extracellular matrix as a scaffold for tissue reconstruction. *Semin. Cell Dev. Biol.* 13, 377–383. doi: 10.1016/S1084952102000940

Bainbridge, P. (2013). Wound healing and the role of fibroblasts. *J. Wound Care* 22:407. doi: 10.12968/jowc.2013.22.8.407

Benedetti, L., Cortivo, R., Berti, T., Berti, A., Pea, F., Mazzo, M., et al. (1993). Biocompatibility and biodegradation of different hyaluronan derivatives (Hyaff) implanted in rats. *Biomaterials* 14, 1154–1163. doi: 10.1016/0142-9612(93)90160-4

Biagini, G., Muzzarelli, R., Giardino, R., and Castaldini, C. (1992). "Biological materials for wound healing," in *Advances in Chitan and Chitosan*, eds C. J. Brine, P. A. Sandford, and J. P. Zikakis (New York, NY: Elsevier Appl. Sci.), 16–24.

Blakytny, R., and Jude, E. (2006). The molecular biology of chronic wounds and delayed healing in diabetes. *Diabet. Med.* 23, 594–608. doi: 10.1111/j.1464-5491.2006.01773.x

Braun, K., and Prowse, D. (2006). Distinct epidermal stem cell compartments are maintained by independent niche microenvironments. *Stem Cell Rev.* 2, 221–231. doi: 10.1007/s12015-006-0050-7

Burke, J., Yannas, I., Quinby, W., Bondoc, C., and Jung, W. (1982). Successful use of a physiologically acceptable artificial skin in the treatment of extensive burn injury. *Ann. Surg.* 194, 413–428. doi: 10.1097/00000658-198110000-00005

Caravaggi, C., Grigoletto, F., and Scuderi, N. (2011). Wound bed preparation with a dermal substitute (Hyalomatrix® PA) facilitates Re-epithelialization and healing: results of a multicenter, prospective, observational study on complex chronic ulcers (The Fast Study). *Wounds* 23, 228–235.

Carter, M., Waycaster, C., Schaum, K., and Gilligan, A. (2014). Cost-effectiveness of three adjunct cellular/tissue derived products used in the management of chronic venous leg ulcers. *Value Heal.* 17, 801–813. doi: 10.1016/j.jval.2014.08.001

Cha, J., and Falanga, V. (2007). Stem cells in cutaneous wound healing. *Clin. Dermatol.* 25, 73–78. doi: 10.1016/j.clindermatol.2006.10.002

Chen, W., and Abatangelo, G. (1999). Function of hyaluronan in wound repair. *Wound Repair Regen.* 7, 79–89. doi: 10.1046/j.1524-475X.1999.00079.x

Chou, T., Fu, E., Wu, C., and Yeh, J. (2003). Chitosan enhances platelet adhesion and aggregation. *Biochem. Biophys. Res. Comm.* 302, 480–483. doi: 10.1016/S0006-291X(03)00173-6

Cullen, B., Smith, R., and McCullogh, E. (2002). Mechanism of action of PROMOGRAN, a protease modulating matrix, for the treatment of diabetic foot ulcers. *Wound Repair Regen.* 10, 16–25. doi: 10.1046/j.1524-475X.2002.10703.x

Dai, T., Tanaka, M., Huang, Y., and Hamblin, M. (2012). Chitosan preparations for wounds and burns: antimicrobial and wound-healing effects. *Expert. Rev. Anti. Infect. Ther.* 9, 857–879. doi: 10.1586/eri.11.59

DiDomenico, L., Landsman, A. R., Emch, K. J., and Landsman, A. (2011). A prospective comparison of diabetic foot ulcers treated with either cryopreserved skin allograft or bioengineered skin substitute. *Wounds* 23, 184–189.

Driver, V., Lavery, L., Reyzelman, A., Dutra, T., Dove, C., Kotsis, S., et al. (2015). A clinical trial of Integra Template for diabetic foot ulcer treatment. *Wound Repair Regen.* 23, 891–900. doi: 10.1111/wrr.12357

Dumville, J. C., Keogh, S. J., Liu, Z., Stubbs, N., Walker, R. M., and Fortnam, M. (2015). Alginate dressings for treating pressure ulcers. *Cochrane Database Syst. Rev.* 5:CD011277. doi: 10.1002/14651858.cd011277

Edmonds, M., and European and Australian Apligraf Diabetic Foot Ulcer Study Group (2009). Apligraf in the treatment of neuropathic diabetic foot ulcers. *Int. J. Low. Extrem. Wounds* 8, 11–18. doi: 10.1177/1534734609331597

Eming, S., Krieg, T., and Davidson, J. (2007). Inflammation in wound repair: molecular and cellular mechanisms. *J. Invest. Dermatol.* 127, 514–523. doi: 10.1038/sj.jid.5700701

Falanga, V., Isaacs, C., Paquette, D., Downing, G., Kouttab, N., Butmarc, J., et al. (2002). Wounding of bioengineered skin: cellular and molecular aspects after injury. *J. Invest. Dermatol.* 119, 653–660. doi: 10.1046/j.1523-1747.2002.01865.x

Fortunato, S., Menon, R., and Lombardi, S. (1998). Presence of four tissue inhibitors of matrix metalloproteinases (TIMP-1, -2, -3 and -4) in human fetal membranes. *Am. J. Reprod. Immunol.* 40, 395–400. doi: 10.1111/j.1600-0897.1998.tb00424.x

Galassi, G., Brun, P., Radice, M., Cortivo, R., Zanon, G., Genovese, P., et al. (2000). *In vitro* reconstructed dermis implanted in human wounds: degradation studies of the HA-based supporting scaffold. *Biomaterials* 21, 2183–2191. doi: 10.1016/S0142-9612(00)00147-2

Gelse, K., Poschl, E., and Aigner, T. (2003). Collagens–structure, function, and biosynthesis. *Adv. Drug Deliv. Rev.* 55, 1531–1546. doi: 10.1016/j.addr.2003.08.002

Gould, L. J. (2015). Topical Collagen-based biomaterials for chronic wounds: rationale and clinical application. *Adv. Wound Care* 5, 19–31. doi: 10.1089/wound.2014.0595

Gurtner, G. C., Werner, S., Barrandon, Y., and Longaker, M. T. (2008). Wound repair and regeneration. *Nature* 453, 314–321. doi: 10.1038/nature07039

Hakkinen, L., Koivisto, L., Gardner, H., Saarialho-Kere, U., Carroll, J., Lakso, M., et al. (2004). Increased expression of beta6-integrin in skin leads to spontaneous development of chronic wounds. *Am. J. Pathol.* 164, 229–242. doi: 10.1016/S0002-9440(10)63113-6

Hankin, C. S., Knispel, J., Lopes, M., Bronstone, A., and Maus, E. (2012). Clinical and cost efficacy of advanced wound care matrices for venous leg ulcers. *J. Manag. Care Spec. Pharm.* 18, 375. doi: 10.18553/jmcp.2012

Hart, J., Silcock, D., Gunnigle, S., Cullen, B., Light, N., and Watt, P. (2002). The role of oxidised regenerated cellulose/collagen in wound repair: effects *in vitro* on fibroblast biology and *in vivo* in a model of compromised healing. *Int. J. Biochem. Cell Biol.* 34, 1557–1570. doi: 10.1016/S1357-2725(02)00062-6

Heino, J. (2000). The collagen receptor integrins have distinct ligand recognition and signaling functions. *Matrix Biol.* 19, 319–323. doi: 10.1016/S0945-053X(00)00076-7

Hodde, J., Badylak, S., Brightman, A., and Voytik-Harbin, S. (1996). Glycosaminoglycan content of small intestinal submucosa: a bioscaffold for tissue replacement. *Tissue Eng.* 2, 209–217. doi: 10.1089/ten.1996.2.209

Hodde, J., Record, R., Liang, H., and Badylak, S. F. (2001). Vascular endothelial growth factor in porcine-derived extracellular matrix. *Endothelium* 8, 11–24. doi: 10.3109/10623320109063154

Hu, S., Kirsner, R. S., Falanga, V., Phillips, T., and Eaglstein, W. H. (2006). Evaluation of Apligraf® persistence and basement membrane restoration in donor site wounds: a pilot study. *Wound Repair Regen.* 14, 427–433. doi: 10.1111/j.1743-6109.2006.00148.x

Kelechi, T., Mueller, M., Hankin, C., Bronstone, A., Samies, J., and Bonham, P. (2012). A randomized, investigator-blinded, controlled pilot study to evaluate the safety and efficacy of a poly-N-acetyl glucosamine-derived membran material in patients with venous leg ulcers. *J. Am. Acad. Dermatol.* 66, e209–e215. doi: 10.1016/j.jaad.2011.01.031

Kirsner, R., Bohn, G., Driver, V., Mills, J., Nanney, L., Williams, M., et al. (2015a). Human acellular dermal wound matrix:evidence and experience. *Int. Wound J.* 12, 646–654. doi: 10.1111/iwj.12185

Kirsner, R. S., Sabolinski, M. L., Parsons, N. B., Skornicki, M., and Marston, W. A. (2015b). Comparative effectiveness of a bioengineered living cellular construct vs. a dehydrated human amniotic membrane allograft for the treatment of diabetic foot ulcers in a real world setting. *Wound Repair Regen.* 23, 737–744. doi: 10.1111/wrr.12332

Koizumi, N., Inatomi, T., Sotozono, C., Fullwood, N., Quantock, A., and Kinoshita, S. (2000). Growth factor mRNA and protein in preserved human amniotic membrane. *Curr. Eye Res.* 20, 173–177. doi: 10.1076/0271-3683(200003)2031-9FT173

Kojima, K., Okamoto, Y., Kojima, K., Miyatake, K., Fujise, H., Shigemasa, Y., et al. (2004). Effects of chitin and chitosan on collagen synthesis in wound healing. *J. Vet. Med. Sci.* 66, 1595–1598. doi: 10.1292/jvms.66.1595

Koob, T., Rennert, R., Zabek, N., Massee, M., Lim, J., Temenoff, J., et al. (2013). Biological properties of dehydrated human amnion/chorion composite graft: implications for chronic wound healing. *Int. Wound J.* 10, 493–500. doi: 10.1111/iwj.12140

Kramer, D. B., Xu, S., and Kesselheim, A. S. (2012). Regulation of medical devices in the united states and european union. *N.Engl. J. Med.* 366, 848–855. doi: 10.1056/NEJMhle1113918

Landsman, A., Cook, J., Landsman, A., Garrett, P., Yoon, J., Kirkwood, A., et al. (2011). A retrospective clinical study of 188 consectuvie patients to examine the effectiveness of a biologically active cryopreserved human skin allograft (Theraskin) on the treatement of diabetic foot ulcers and venous leg ulcers. *Foot Ankle Spec.* 4, 29–41. doi: 10.1177/1938640010387417

Lauer, G., Sollberg, S., Cole, M., Kreig, T., and Eming, S. (2000). Expression and proteolysis of vascular endothelial growth factor is increased in chronic wounds. *J. Invest. Dermatol.* 115, 12–18. doi: 10.1046/j.1523-1747.2000.00036.x

Lerman, O., Galiano, R., Armour, M., Levine, J., and Gurtner, G. (2003). Cellular dysfunction in the diabetic fibroblast: impairment in migration, vascular endothelial growth factor production, and response to hypoxia. *Am. J. Pathol.* 162, 303–312. doi: 10.1016/S0002-9440(10)63821-7

Litwiniuk, M., Krejner, A., and Grzela, T. (2016). Hyaluronic acid in inflammation and tissue regeneration. *Wounds* 28, 78–88.

Lockington, D., Agarwal, P., Young, D., Caslake, M., and Ramaesh, K. (2014). Antioxidant properties of amniotic membrane: novel observations from a pilot study. *Can. J. Opthalmol.* 49, 426–430. doi: 10.1016/j.jcjo.2014.07.005

Lopez-Valladares, M., Rodriguez-Ares, M., Tourino, R., Gude, F., Silva, M., and Couceiro, J. (2010). Donor age and gestational age influence on growth factor levels in human amniotic membrane. *Acta Opthamol.* 88, 211–216. doi: 10.1111/j.1755-3768.2010.01908.x

Mamede, A., Carvalho, M., Abrantes, A., Laranjo, M., Maia, C., and Botelho, M. (2010). Amniotic membrane: from structure and functions to clinical applications. *Cell Tissue Res.* 349, 447–458. doi: 10.1007/s00441-012-1424-6

Marston, W. A., Hanft, J., Norwood, P., and Pollak, R. (2003). The efficacy and safety of dermagraft in improving the healing of chronic diabetic foot ulcers: results of a prospective randomized trial. *Diabetes Care* 26, 1701–1705. doi: 10.2337/diacare.26.6.1701

Mayol, L., De Stefano, D., Campani, V., De Falco, F., Ferrari, E., Cencetti, C., et al. (2014). Design and characterization of a chitosan physical gel promoting wound healing in mice. *J. Mater Sci.* 25, 1483–1493. doi: 10.1007/s10856-014-5175-7

McCarty, S., and Percival, S. (2013). Proteases and delayed wound healing. *Adv. Wound Care* 2, 438–447. doi: 10.1089/wound.2012.0370

Moore, M., Samsell, B., Wallis, G., Triplett, S., Chen, S., Linthurst Jones, A., et al. (2015). Decellularization of human dermis using non-denaturing anionic detergent and endonuclease: a review. *Cell Tissue Bank* 16, 249–259. doi: 10.1007/s10561-014-9467-4

Mustoe, T. A., O'Shaughnessy, K., and Kloeters, O. (2006). Chronic wound pathogenesis and current treatment strategies: a unifying hypothesis. *Plast. Reconstr. Surg.* 117, 35s–41s. doi: 10.1097/01.prs.0000225431.63010.1b

Naughton, G., Mansbridge, J., and Gentzkow, G. (1997). A metabolically active human dermal replacement for the treatment of diabetic foot Ulcers. *Artif. Organs* 21, 1203–1210. doi: 10.1111/j.1525-1594.1997.tb00476.x

Nihsen, E., Johnson, C., and Hiles, M. (2008). Bioactivity of small intestinal submucosa and oxidized regenerated cellulose/collagen. *Adv. Ski. Wound Care* 21, 479–486. doi: 10.1097/01.ASW.0000323561.14144.19

O'Meara, S., Martyn-St James, M., and Adderley, U. J. (2015). Alginate dressings for venous leg ulcers. *Cochrane Database Syst. Rev.* 19:CD010182. doi: 10.1002/14651858.CD010182.pub3

Okamotoa, Y., Yanoa, R., Miyatakea, K., Tomohirob, I., Shigemasac, Y., and Minamia, S. (2003). Effects of chitin and chitosan on blood coagulation. *Carbohydr. Polym.* 53, 337–342. doi: 10.1016/S0144-8617(03)00076-6

Park, C., Kohanim, S., Zhu, L., Gehlbach, P., and Chuck, R. (2008). Immunosuppressive property of dried human amniotic membrane. *Ophthalmic Res.* 41, 112–113. doi: 10.1159/000187629

Pastar, I., Stojadinovic, O., and Tomic-Canic, M. (2008). Role of keratinocytes in healing of chronic wounds. *Surg. Technol. Int.* 17, 105–112.

Peluso, G., Petillo, O., Ranieri, M., Santin, M., Ambrosio, L., Calabró, D., et al. (1994). Chitosan-mediated stimulation of macrophage function. *Biomaterials* 15, 1215–1220. doi: 10.1016/0142-9612(94)90272-0

Pirone, L. A., Bolton, L. L., Monte, K. A., and Shannon, R. J. (1992). Effect of calcium alginate dressings on partial-thickness wounds in swine. *J. Invest. Surg.* 5, 149–153. doi: 10.3109/08941939209012431

Rabea, E., Badawy, M., Stevens, C., Smagghe, G., and Steurbaut, W. (2003). Chitosan as antimicrobial agent: applications and mode of action. *Biomacromolecules* 4, 1457–1465. doi: 10.1021/bm034130m

Rennert, R. C., Rodrigues, M., Wong, V. W., Duscher, D., Hu, M., Maan, Z., et al. (2013). Biological therapies for the treatment of cutaneous wounds: phase III and launched therapies. *Expert Opin. Biol. Ther.* 13, 1523–1541. doi: 10.1517/14712598.2013.842972

Reyzelman, A., Crews, R., Moore, J., Moore, L., Mukker, J., Offutt, S., et al. (2009). Clinical effectiveness of an acellular dermal regenerative tissue matrix compared to standard wound management in healing diabetic foot ulcers: a prospective, randomised, multicentre study. *Int. Wound J.* 6, 196–208. doi: 10.1111/j.1742-481X.2009.00585.x

Rowan, M. P., Cancio, L. C., Elster, E. A., Burmeister, D. M., Rose, L. F., Natesan, S., et al. (2015). Burn wound healing and treatment: review and advancements. *Crit. Care* 19, 243. doi: 10.1186/s13054-015-0961-2

Sandoval, M., Albornoz, C., Muñoz, S., Fica, M., García-Huidobro, I., Mertens, R., et al. (2011). Addition of chitosan may improve the treatment efficacy of triple bandage and compression in the treatment of venous leg ulcers. *J. Drugs Dermatol.* 10, 75–79.

Santoro, M., and Gaudino, G. (2005). Cellular and molecular facets of keratinocyte reepithelization during wound healing. *Exp. Cell Res.* 304, 274–286. doi: 10.1016/j.yexcr.2004.10.033

Scherer, S., Pietramaggiori, G., Matthews, J., Perry, S., Assmann, A., Carothers, A., et al. (2009). Poly-N-acetyl glucosamine nanofibers: a new bioactive material to enhance diabetic wound healing by cell migration and angiogenesis. *Ann. Surg.* 250, 322–330. doi: 10.1097/SLA.0b013e3181ae9d45

Schultz, G. S., and Wysocki, A. (2009). Interactions between extracellular matrix and growth factors in wound healing. *Wound Repair Regen.* 17, 153–162. doi: 10.1111/j.1524-475X.2009.00466.x

Segal, H., Hunt, B., and Gilding, K. (1998). The effects of alginate and non-alginate wound dressings on blood coagulation and platelet activation. *J. Biomater. Appl.* 12, 249–257.

Sen, C. K., Gordillo, G. M., Roy, S., Kirsner, R. S., Lambert, L., Hunt, T. K., et al. (2009). Human skin wounds: a major and snowballing threat to public health and the economy. *Wound Repair Regen.* 17, 763–771. doi: 10.1111/j.1524-475X.2009.00543.x

Shen, Y.-I., Song, H.-H. G., Papa, A. E., Burke, J. A., Volk, S. W., and Gerecht, S. (2015). Acellular hydrogels for regenerative burn wound healing: translation from a porcine model. *J. Invest. Dermatol.* 135, 2519–2529. doi: 10.1038/jid.2015.182

Shi, L., Ramsay, S., Ermis, R., and Carson, D. (2012). *In vitro* and *in vivo* studies on matrix metalloproteinases interacting with small intestine submucosa wound matrix. *Int. Wound J.* 9, 44–53. doi: 10.1111/j.1742-481X.2011.00843.x

Shi, L., and Ronfard, V. (2013). Biochemical and biomechanical characterization of porcine small intestinal submucosa (SIS): a mini review. *Int. J. Burn. Trauma* 3, 173–179.

Shultz, G., Davidson, J., Kirsner, R. S., Bornstein, P., and Herman, I. (2012). Dynamic reciprocity in the wound microenvironment. *Wound Repair Regen.* 19, 134–148. doi: 10.1111/j.1524-475X.2011.00673.x

Shultz, G., Sibbald, R., Falanga, V., Ayello, E., Dowsett, C., Harding, K., et al. (2003). Wound bed preparation: a systematic approach to wound management. *Wound Repair Regen.* 11, S1–S28. doi: 10.1046/j.1524-475X.11.s2.1.x

Silini, A., Cargnoni, A., Magatti, M., Pianta, S., and Parolini, O. (2015). The long path of human placenta, and its derivatives, in regenerative medicine. *Front. Physiol.* 3:162. doi: 10.3389/fbioe.2015.00162

Singer, A. J., and Clark, R. A. F. (1999). Cutaneous wound healing. *N.Engl. J. Med.* 341, 738–746. doi: 10.1056/NEJM199909023411006

Stern, R. (2004). Hyaluronan catabolism: a new metablolic pathway. *Eur. J. Cell Biol.* 83, 317–325. doi: 10.1078/0171-9335-00392

Stojadinovic, O., Pastar, I., Nusbaum, A. G., Vukelic, S., Krzyzanowska, A., and Tomic-Canic, M. (2014). Deregulation of epidermal stem cell niche contributes to pathogenesis of non-healing venous ulcers. *Wound Repair Regen.* 22, 220–227. doi: 10.1111/wrr.12142

Sun, G., Shen, Y.-I., Ho, C. C., Kusuma, S., and Gerecht, S. (2010). Functional groups affect physical and biological properties of dextran-based hydrogels. *J. Biomed. Mater. Res. A* 93, 1080–1090. doi: 10.1002/jbm.a.32604

Sun, G., Shen, Y.-I., Kusuma, S., Fox-Talbot, K., Steenbergen, C. J., and Gerecht, S. (2011a). Functional neovascularization of biodegradable dextran

hydrogels with multiple angiogenic growth factors. *Biomaterials* 32, 95–106. doi: 10.1016/j.biomaterials.2010.08.091

Sun, G., Zhang, X., Shen, Y.-I., Sebastian, R., Dickinson, L. E., Fox-Talbot, K., et al. (2011b). Dextran hydrogel scaffolds enhance angiogenic responses and promote complete skin regeneration during burn wound healing. *Proc. Natl. Acad. Sci. U.S.A.* 108, 20976–20981. doi: 10.1073/pnas.1115973108

Sweeney, I., Miraftab, M., and Collyer, G. (2012). A critical review of modern and emerging absorbent dressings used to treat exuding wounds. *Int. Wound J.* 9, 601–612. doi: 10.1111/j.1742-481X.2011.00923.x

Toole, B. P. (2004). Hyaluronan: from extracellular glue to pericellular cue. *Nat Rev. Cancer* 4, 528–529. doi: 10.1038/nrc1391

Trabucchi, E., Pallotta, S., Morini, M., Corsi, F., Franceschini, R., Casiraghi, A., et al. (2002). Low molecular weight hyaluronic acid prevents oxygen free radical damage to granulation tissue during wound healing. *Int. J. Tissue React.* 24, 65–71. doi: 10.4049/jimmunol.181.3.2103

Tracy, L. E., Minasian, R. A., and Caterson, E. J. (2016). Extracellular matrix and dermal fibroblast function in the healing wound. *Adv. Wound Care* 5, 119–136. doi: 10.1089/wound.2014.0561

Turner, N., and Badylak, S. (2015). The use of biologic scaffolds in the treatment of chronic nonhealing wounds. *Adv. Wound Care* 4, 490–500. doi: 10.1089/wound.2014.0604

Turner, N., Kielty, C., Walker, M., and Canfield, A. (2004). A novel hyaluronan-based biomaterial (Hyaff-11) as a scaffold for endothelial cells in tissue engineered vascular grafts. *Biomaterials* 25, 5955–5964. doi: 10.1016/j.biomaterials.2004.02.002

Ueno, H., Mori, T., and Fujinaga, T. (2001). Topical formulations and wound healing applications of chitosan. *Adv. Drug Deliv. Rev.* 52, 105–115. doi: 10.1016/S0169-409X(01)00189-2

Ulrich, D., Smeets, R., Unglaub, F., Wöltje, M., and Pallua, N. (2011). Effect of oxidized regenerated cellulose/collagen matrix on proteases in wound exudate of patients with diabetic foot ulcers. *J. Wound Ostomy Continence Nurs.* 38, 522–528. doi: 10.1097/WON.0b013e31822ad290

Vaalamo, M., Weckroth, M., Puolakkainen, P., Kere, J., Saarinen, P., Lauharanta, J., et al. (1996). Patterns of matrix metalloproteinase and TIMP-1 expression in chronic and normally healing human cutaneous wounds. *Br. J. Dermatol.* 135, 52–59. doi: 10.1111/j.1365-2133.1996.tb03607.x

Valle, M., Maruthur, N., Wilson, L., Malas, M., Qazi, U., Haberl, E., et al. (2014). Comparative effectiveness of advanced wound dressings for patients with chronic venous leg ulcers: a systematic review. *Wound Repair Regen.* 22, 193–204. doi: 10.1111/wrr.12151

Veves, A., Falanga, V., Armstrong, D. G., and Sabolinski, M. L. (2001). Graftskin, a human skin equivalent, is effective in the management of noninfected neuropathic diabetic foot ulcers: a prospective randomized multicenter clinical trial. *Diabetes Care* 24, 290–295. doi: 10.2337/diacare.24.2.290

von Versen-Hoeynck, F., Steinfeld, A., Becker, J., Hermel, M., Rath, W., and Hesselbarth, U. (2008). Sterilization and preservation influence the biophysical properties of human amnion grafts. *Biologicals* 36, 248–255. doi: 10.1016/j.biologicals.2008.02.001

Vournakis, J., Eldridge, J., Demcheva, M., and Muise-Helmericks, R. (2008). Poly-N-acetyl glucosamine nanofibers regulate endothelial cell movement and angiogenesis: dependency on integrin activation of Ets1. *J. Vasc. Res.* 45, 222–232. doi: 10.1159/000112544

Walters, J., Cazzell, S., Pham, H., Vayser, D., and Reyzelman, A. (2016). Healing rates in a multicenter assessment of a sterile, room temperature, acellular dermal matrix versus conventional care wound management and an active comparator in the treatment of full-thickness diabetic foot ulcers. *Eplasty* 16:e10.

Werdin, F., Tennenhaus, M., Schaller, H.-E., and Rennekampff, H.-O. (2009). Evidence-based management strategies for treatment of chronic wounds. *Eplasty* 9:e19.

West, D., and Fan, T.-P. (2002). "Hyaluronan oligosaccharides promote wound repair: It's size dependent regulation of angiogenesis," in *The New Angiotherapy*, eds T.-P. D. Fan and E. C. Kohn (New York, NY: Humana Press), 177–188.

Whelan, M., and Senger, D. (2003). Collagen I initiates endothelial cell morphogenesis by inducing actin polymerization through suppression of cyclic AMP and Protein Kinase A. *J. Biol. Chem.* 278, 327–334. doi: 10.1074/jbc.M207554200

Wiegand, C., Schönfelder, U., Abel, M., Ruth, P., Kaatz, M., and Hipler, U. (2010). Protease and pro-inflammatory cytokine concentrations are elevated in chronic compared to acute wounds and can be modulated by collagen type I *in vitro*. *Arch. Dermatol. Res.* 302, 419–428. doi: 10.1007/s00403-009-1011-1

Yonehiro, L., Burleson, G., and Sauer, V. (2013). Use of a new acellular dermal matrix for treatment of nonhealing wounds in the lower extremities of patients with diabetes. *Wounds* 25, 340–344.

Zaulyanov, L., and Kirsner, R. S. (2007). A review of a bi-layered living cell treatment (Apligraf (®)) in the treatment of venous leg ulcers and diabetic foot ulcers. *Clin. Interv. Aging* 2, 93–98. doi: 10.2147/ciia.2007.2.1.93

Zelen, C., Serena, T., Denoziere, G., and Fetterolf, D. (2013). A prospective randomised comparative parallel study of amniotic membrane wound graft in the management of diabetic foot ulcers. *Int. Wound J.* 10, 502–507. doi: 10.1111/iwj.12097

Zelen, C., Serena, T., Gould, L., Le, L., Carter, M., Keller, J., et al. (2016). Treatment of chronic diabetic lower extremity ulcers with advanced therapies: a prospective, randomised, controlled, multi-centre comparative study examining clinical efficacy and cost. *Int. Wound J.* 13, 272–282. doi: 10.1111/iwj.12566

Conflict of Interest Statement: Intellectual property related to the biosynthetic dextran scaffold is owned by Johns Hopkins University and licensed to Gemstone Biotherapeutics LLC, of which SG is a cofounder and consultant. SG has a financial interest in Gemstone Biotherapeutics LLC, which is subject to certain restrictions under University policy. The terms of this arrangement are being managed by the Johns Hopkins University in accordance with its conflict of interest policies. Gemstone Biotherapeutics, LLC, partially supported the research work cited in the manuscript; Gemstone Biotherapeutics LLC did not affect the design, interpretation, or reporting of any of the experiments herein. LD is currently an employee of Gemstone Biotherapeutics. All research described in this review of which LD is a contributing author was completed prior to her employment with Gemstone and was therefore conducted in the absence of any commercial or financial relationships that could be construed as a potential conflict of interest.

The reviewer JD and handling Editor declared their shared affiliation, and the handling Editor states that the process nevertheless met the standards of a fair and objective review.

Advantages of publishing in Frontiers

OPEN ACCESS
Articles are free to read for greatest visibility and readership

FAST PUBLICATION
Around 90 days from submission to decision

HIGH QUALITY PEER-REVIEW
Rigorous, collaborative, and constructive peer-review

TRANSPARENT PEER-REVIEW
Editors and reviewers acknowledged by name on published articles

Frontiers
Avenue du Tribunal-Fédéral 34
1005 Lausanne | Switzerland

Visit us: www.frontiersin.org
Contact us: info@frontiersin.org | +41 21 510 17 00

REPRODUCIBILITY OF RESEARCH
Support open data and methods to enhance research reproducibility

DIGITAL PUBLISHING
Articles designed for optimal readership across devices

FOLLOW US
@frontiersin

IMPACT METRICS
Advanced article metrics track visibility across digital media

EXTENSIVE PROMOTION
Marketing and promotion of impactful research

LOOP RESEARCH NETWORK
Our network increases your article's readership